Introduction to Thermodynamics

Training Objectives

The participant will be introduced to:
1.1   basic concepts and definitions.
1.2   the properties of a pure substance.
1.3   work and heat.
1.4   the fist law of thermodynamics.
1.5   the second law of thermodynamics.
1.6   the steam cycle.

Introduction to Thermodynamics

Table of Contents

1.0   Introduction

Thermodynamics is the science that deals with heat and work and these properties of substances that bear a relation to heat and work. Like all sciences, the basis of thermodynamics is experimental observation. In thermodynamics these findings have been formalized into certain basic laws, which are known as the first, second, and third law of thermodynamics. In addition to these laws, the zeroth law of thermodynamics, which in the logical development of thermodynamics precedes the first law, has been set forth.

In what follows, we will present the basic thermodynamics laws, and apply them to a number of representative examples.

Before, a brief description of a CANDU nuclear plant will be presented to illustrate the actual thermodynamics processes and the required equipment.

CANDU 600 Primary (Heat Transport) Circuit: 380 reactor channels are distributed in four groups of 95 pressure tubes. Each group is connected to a single inlet and outlet header via individual feeders. The core is cooled by heavy water coolant circulating in two distinct circuits, each one including two main coolant pumps and two steam generators (see Fig. 1.1). Each circuit is designed as a figure of 8 loop with two reactor passes (95 channels per pass).

CANDU 600 Secondary (Conventional) Side: the secondary side uses light water as coolant in the liquid-vapour cycle. The circuit starts at the upper part of the four steam generators which are connected to a steam header. Through the governor valve, the steam main feeds the two stages (low and high pressure stages) of the turbine. The turbine is connected to the condenser where liquid water is recovered. Through the feedwater pumps and control valves, the cold water is then supplied to the preheater (lower part) of the steam generators (see Fig. 1.1)

Fig. 1.1:
CANDU reactor simplified flow diagram; primary and secondary circuits.
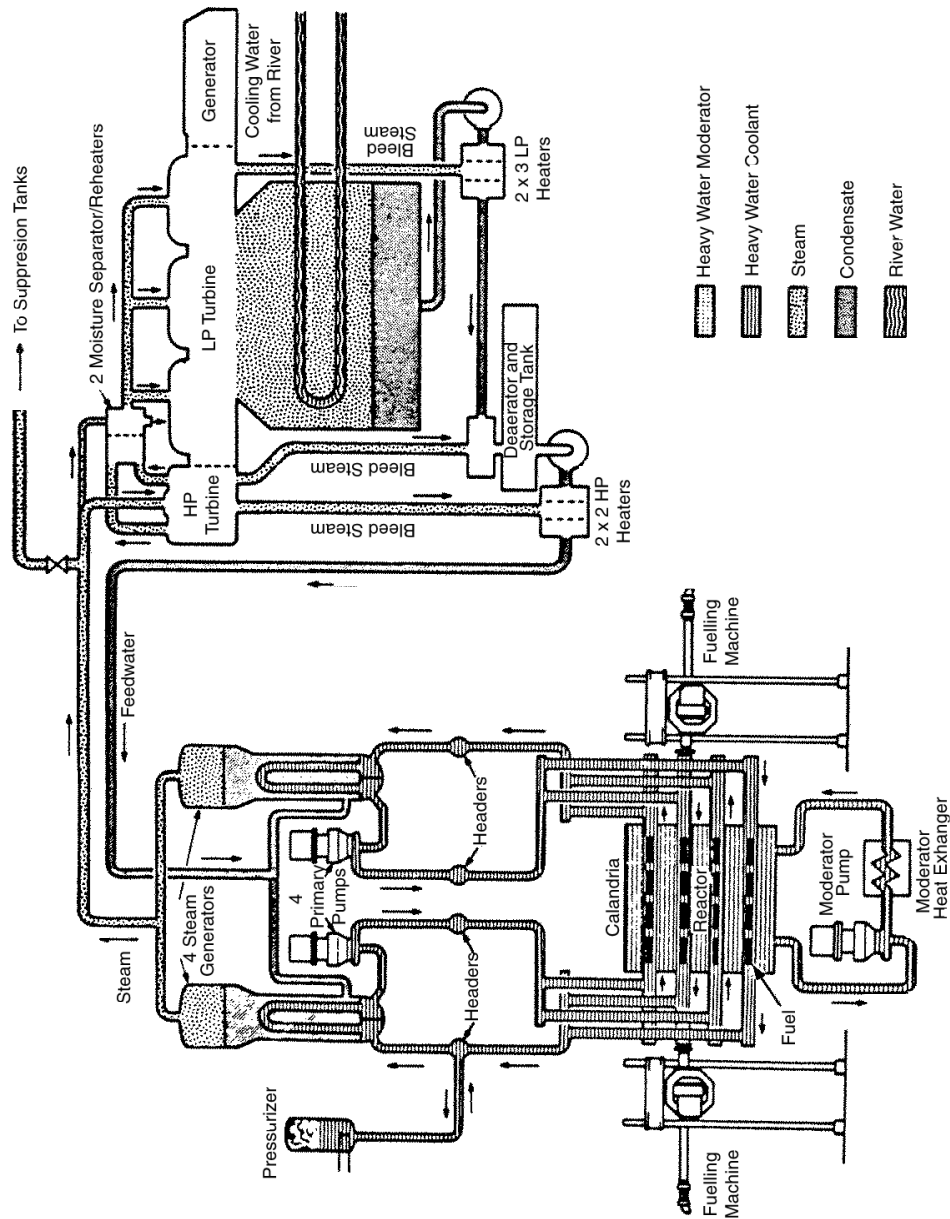
2.0   Basic Concepts and Definitions

2.1   Thermodynamic system

A thermodynamic system is defined as a quantity of matter of fixed mass and identity on which attention is focused for study. Everything external to the system is the surroundings, and the system is separated from the surroundings by the system boundaries. These boundaries may be either movable or fixed.

Example:

In Fig. 2.1 the gas in the cylinder is considered to be the system. When the cylinder is heated from below, the temperature of the gas will increase and the piston will rise. As the piston rises, the boundary of the system moves. Heat and work cross the boundary of the system during this thermodynamic process, but the matter that comprises the system can always be identified.

Fig. 2.1:

Example of a thermodynamic system.
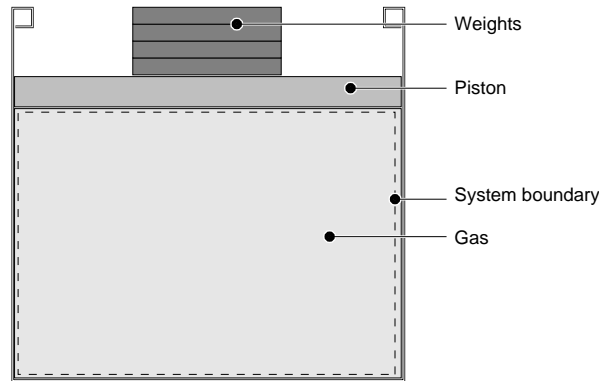
2.2 Control volume

Mass, as well as heat and work (and momentum), can flow across the control surface. Example: air compressor (see Fig. 2.2).

Fig. 2.2:

Example of a control volume.
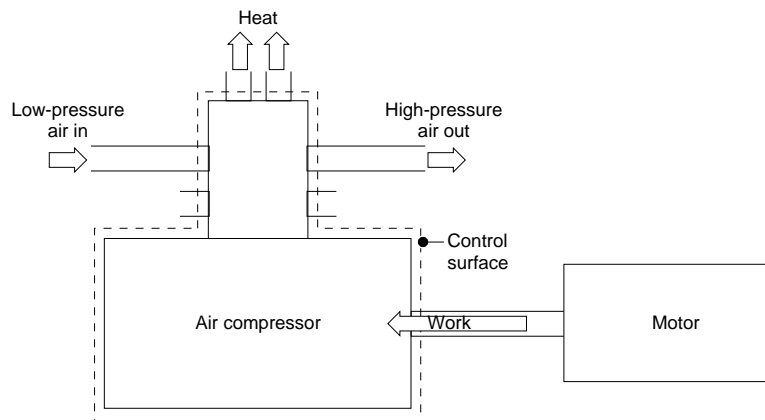
2.3 Properties and state of a substance

A given mass of water can exist in various forms. If it is liquid, it may become vapour when heated or solid when cooled. Thus, we talk about the different Phases of a substance. A phase is defined as a quantity of matter that is homogeneous throughout. When more than one phase is present, the phases are separated from each other by the phases boundaries. In each phase the substance may exist at various pressures and temperatures or, to use the thermodynamic term, in various states. The State may be identified or described

by certain observable, macroscopic properties; some familiar ones are temperature, pressure, and density.

2.4 Process and cycles

Whenever one or more of the properties of a system change, a Change in State has occurred. For example, when one of the weights on the piston in Fig. 2.3 is removed, the piston rises and a change in state occurs, for the pressure decreases and the specific volume increases. The path of the succession of states through which the system passes is called the process.

When a system in a given initial state goes through a number of different changes of state or processes and finally returns to its initial state, the system has undergone a Cycle. Therefore, at the conclusion of a cycle, all the properties have the same value they had at the beginning. Steam (water) that circulates through a steam power plant (like the conventional side of a nuclear reactor) undergoes a cycle.

Fig. 2.3:
Example of a thermodynamic system that may undergo a process

- Weights
- Piston
- System boundary
- Gas
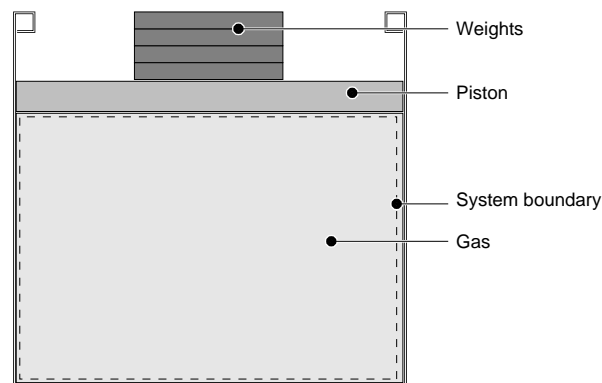
2.5 Energy

One of the very important concepts in a study of thermodynamics is the concept of energy. Energy is a fundamental concept, such as mass or force and, as is often the case with such concepts, is very difficult to define. Energy is defined as the capability to produce an effect. It is important to note that energy can be stored within a system and can be transferred (as heat, for example) from one system to another.

2.6 Specific volume

The specific volume of a substance is defined as the volume per unit mass, and is given the symbol *v*.

$$v = \frac{\delta V}{\delta m} \left[\frac{m^3}{kg} \right]$$

The density of a substance (ρ) is defined as the mass per unit volume, and is therefore the reciprocal of the specific volume.

$$\rho = \frac{1}{v}\left[\frac{\text{kg}}{\text{m}^3}\right]$$

2.7 Pressure

Pressure is defined as the normal component of force per unit area.

$$p = \frac{\delta F_n}{\delta A} \quad \left[\frac{N}{m^2} \text{ or } Pa\right]$$

Most thermodynamics investigations are concerned with absolute pressure. Most pressure and vacuum gauges, however, read the difference between the absolute pressure and the atmospheric pressure existing at the gauge. This is referred to as gauge pressure (see Fig. 2.4).

Fig. 2.4:
Illustration of terms used in pressure measurement, and examples in a nuclear reactor.
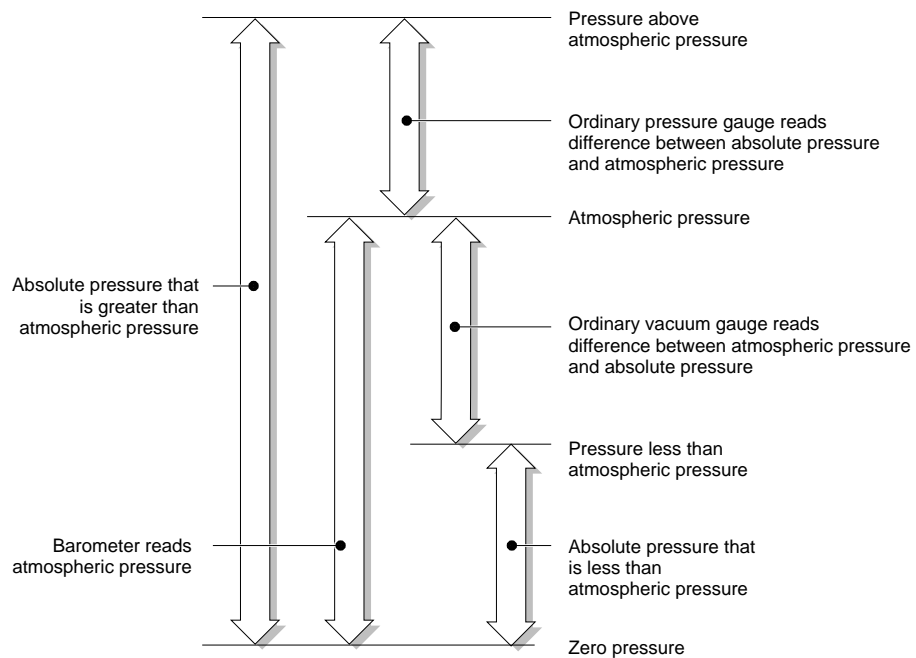
2.8 Temperature

Although temperature is a familiar property, an exact definition of it is difficult. Thus, we define equality of temperatures. Two bodies have equality of temperatures if, when they are in thermal communication, no change in observable property occurs.

2.9 The zeroth law of thermodynamics

The zeroth law of thermodynamics states that when two bodies have equality of temperatures with a third body, they in turn have equality of temperatures with each other.

3.0   The Properties of a Pure Substance

3.1   The pure substance

A pure substance is one that has a homogeneous and invariable chemical composition. It may exist in more than one phase, but the chemical composition is the same in all phases. Thus, liquid water, a mixture of liquid water and water vapour (steam), and a mixture of ice and liquid water are all pure substances; every phase has the same chemical composition.

3.2   Vapour-liquid-solid-phase equilibrium

As an example consider a system of 1 kg of water contained in the piston-cylinder arrangement shown in Fig. 3.1. Suppose that the piston and weight maintain a pressure of 0.1 MPa in the cylinder, and that the initial temperature is 20 °C. As heat is transferred to the water, the temperature increases appreciably, the specific volume increases slightly, and the pressure remains constant. When the temperature reaches 99.6 °C, additional heat transfer results in change of phase, as indicated in Fig. 3.1. That is, some of the liquid becomes vapour, and during this process both the temperature and pressure remain constant, but the specific volume increases considerably. When the last drop of liquid has vaporized, further transfer of heat results in an increase in both temperature and specific volume of vapour, as shown in Fig. 3.1.

Fig. 3.1:
Constant-pressure change from liquid to vapour phase for a pure substance.
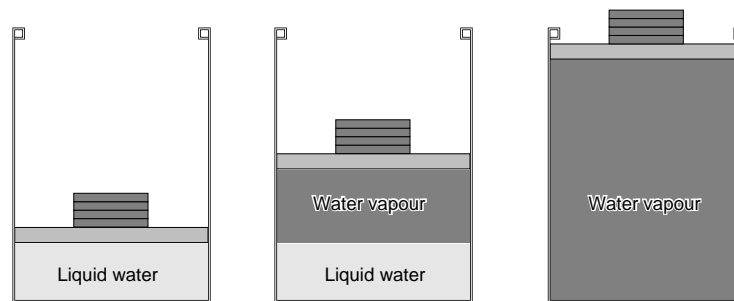
The term **Saturation Temperature** designates the temperature at which vaporization takes place at a given pressure. This pressure is called the **Saturation Pressure** for the given temperature. Thus, for water at 99.6 °C the saturation pressure is 0.1 MPa, and for water at 0.1 MPa the saturation temperature is 99.6 °C. For a pure substance there is a definite relation between saturation pressure and saturation temperature. A typical curve, called Vapour-Pressure curve, is shown in Figure 3.2.

Fig. 3.2:
Vapour-pressure curve of a pure substance.
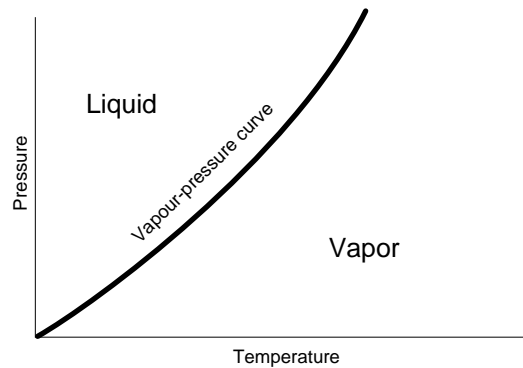
If a substance exists as liquid at the saturation temperature and pressure, it is called saturated liquid. If the temperature of the liquid is lower than the saturation temperature for the existing pressure, it is called either a **Subcooled Liquid** (implying that the temperature is lower than the saturation temperature for the given pressure) or a **Compressed Liquid** (implying that the pressure is greater than the saturation pressure for the given temperature).

When a substance exists as part liquid and part vapour at the saturation temperature, its **QUALITY** is defined as the ratio of the mass of vapour to the total mass. Thus, in Fig. 3.3, if the mass of the vapour is 0.2 kg and the mass of the liquid is 0.8 kg, the quality x is 0.2 or 20 %. Quality has meaning only when the substance is in a saturated state, that is, at saturation pressure and temperature.

Fig. 3.3:
Constant-pressure change from liquid to vapour change.
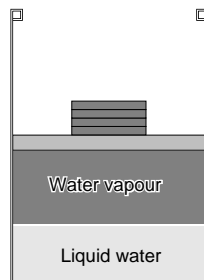
If a substance exists as vapour at the saturation temperature it is called **Saturated Vapour**. When the vapour is at a temperature greater than the saturation temperature, it is said to exist as superheated vapour. The pressure and temperature of **Superheated Vapour** are independent properties, since the temperature may increase while the pressure remains constant.
Let us plot on the **Temperature-Volume Diagram** in Fig. 3.4 the constant-pressure line that represents the states through which the water passes as it is

heated from the initial state of 0.1 MPa and 20 °C. Let state A represent the initial state, B the saturated-liquid state of 0.1 MPa and 20 °C. Let state A represent the initial state, B the saturated-liquid state (100 °C), and line AB the process in which the liquid is heated from the initial temperature to the saturation temperature. Point C is the saturated-vapour state, and line BC is the constant-temperature process in which the change of phase from liquid to vapour occurs. Line CD represents the process in which the steam is superheated at constant pressure.

At a pressure of 22.09 MPa, represented by line MNO, we find, however, that there is no constant-temperature vaporization process. Instead, point N is a point of inflection with a zero slope. This point is called the **Critical Point.** At the critical point the saturated-liquid and saturated-vapour states are identical. The temperature, pressure, and specific volume at the critical point are called the critical temperature, critical pressure, and critical volume.

Fig. 3.4:
Temperature-volume diagram for water showing liquid and vapour phases.
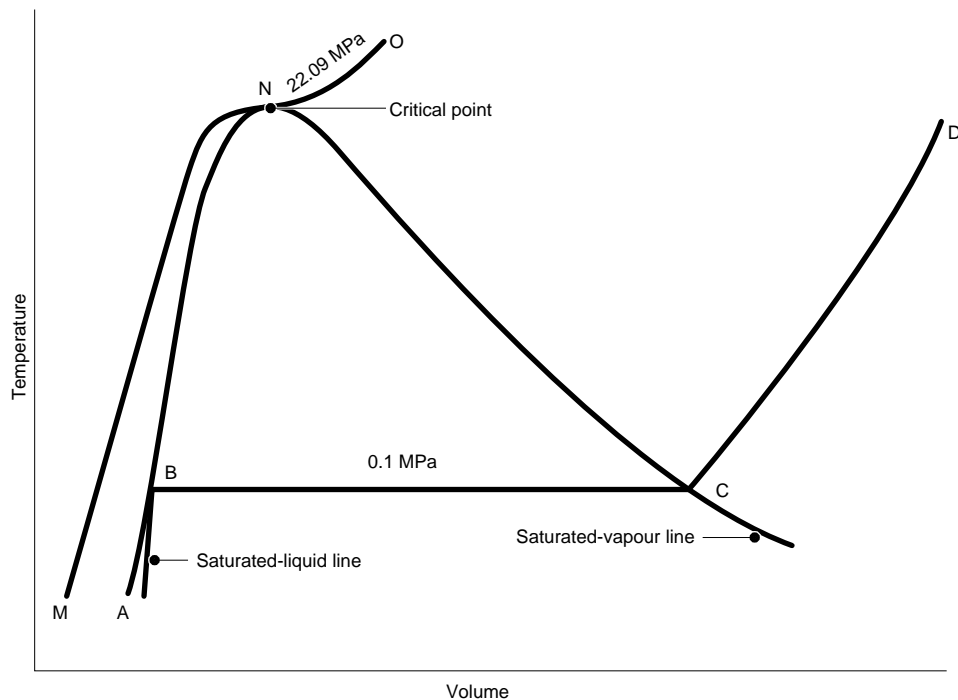
3.3   Independent properties of a pure substance

The state of a simple compressible pure substance is defined by two independent properties. For example, if the specific volume and temperature of superheated steam are specified, the state of the steam is determined.

3.4 Equation of state for the vapour phase of a simple compressible substance

From experimental observations it has been established that the P-v-T behaviour of gases at low density is closely given by the following equation of state:

$$P\bar{v} = \bar{R}T$$

where

$$\bar{R} = 8.3144 \ \frac{kN \ m}{kmol \ K}$$

is the universal gas constant.

Dividing by M, the molecular weight, we have the equation of state on a unit mass basis,

$$Pv = RT$$

This equation of state can be written in terms of the total volume:

$$PV = n\bar{R}T$$

$$PV = mRT$$

for mass m occupying volume V

The equation of state given above is referred to as the ideal-gas equation of state. At very low density all gases and vapours approach ideal-gas behaviour, with the P-v-T relationship being given by the ideal-gas equation of state.

3.5 Numerical example

A tank has a volume of 0.5 m^3 and contains 10 kg of an ideal gas having a molecular weight of 24. The temperature is 25 °C. What is the pressure?
The gas constant is determined first:

$$R = \frac{\bar{R}}{M} = \frac{8.3144 \ kN \ m \ / \ kmol \ K}{24 \ kg \ / \ kmol}$$

We now solve for P:

$$P = \frac{mRT}{V} = \frac{10 \ kg \times 0.34643 \ kNm \ / \ kgK \times 298.2K}{0.5 \ m^3}$$

$$= 2066 \ kPa$$

4.0 Work and Heat

It is essential to understand clearly the definitions of both work and heat, because the correct analysis of many thermodynamic problems depends on distinguishing between them.

4.1 Definition of work

Work is defined as a force F acting through a displacement x, the displacement being in the direction of the force.

$$W = \int_1^2 F dx$$

Thermodynamics defines work as follows: work is done by a system if the sole effect on the surroundings (everything external to the system) could be the raising of a weight. Work done by a system is considered positive and work done to a system is considered negative.

Example:

Consider as a system the battery and motor of Fig. 4.1 and let the motor drive a fan. Does work cross the boundary of the system? If the fan is replaced with the pulley and weight arrangement shown in Fig. 4.1, as the motor turns, the weight is raised, and the sole effect external to the system is the raising of a weight.

Fig. 4.1:
Example of work crossing the boundary of a system.
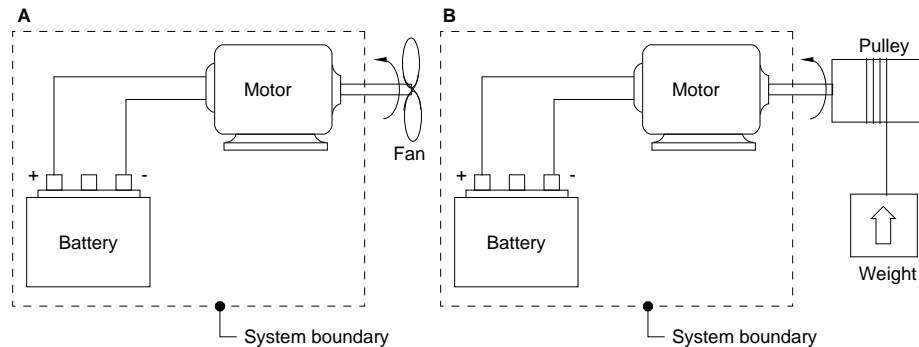
4.2   Units for work

The unit for work in SI units is called the joule (J).

   $1J = 1 \text{ N} \bullet \text{m}$

4.3   Numerical example

Consider as a system the gas in the cylinder in Fig. 4.2; the cylinder is fitted with a piston on which a number of small weights are placed. The initial pressure is 200 kPa and the initial volume of the gas is 0.04 m^3.

Fig. 4.2:
Example of work done by a thermodynamic process.
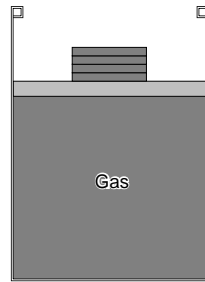
1. Let a Bunsen burner be placed under the cylinder, and let the volume of the gas increase to 0.1 m^3 while the pressure remains constant. Calculate the work done by the system during the process.

$$W = \int_1^2 PdV$$

Since the pressure is constant,

$$W = P\int_1^2 dV = P(V_2 - V_1)$$

$$W = 200kPa \times (0.1 - 0.04)\, m^3 = 12 \ kJ$$

2. Consider the same system and initial conditions, but at the same time the Bunsen burner is under the cylinder and the piston is rising, let weights be removed from the piston at such a rate that, during the process, the temperature of the gas remains constant. If we assume that the ideal-gas model is valid, and that is a polytropic process with exponent n = 1. Therefore,

$$W = \int_1^2 PdV = P_1V_1\ln\frac{V_2}{V_1}$$

$$W = 200 \ kPa \times 0.04 m^3 \times \ln\frac{0.10}{0.04} = 7.33 \ kJ$$

4.4 Definition of heat

Heat is defined as the form of energy that is transferred across the boundary of a system at a given temperature to another system (or the surroundings) at a lower temperature by virtue of the temperature difference between the two systems. Another aspect of this definition of heat is that a body never contains heat. Rather, heat can be identified only as it crosses the boundary. Thus, heat is a transient phenomenon.

Example:
If we consider a hot block of copper as one system and cold water in a beaker as another system, we recognize that originally neither system contains any heat (they do contain energy, of course). When the copper block is placed in the

water and the two are in thermal communication, heat is transferred from the copper to the water until equilibrium of temperature is established. At this point we no longer have heat transfer, because there is no temperature difference. Heat is identified at the boundary of the system.

Heat transferred to a system is considered positive, and heat transferred from a system is negative. The symbol Q represents heat.

4.5 Units of heat

Heat, like work, is a form of energy transfer to or from a system. Therefore, the units for heat are the same as the units for work. In the International System the unit for heat (energy) is the joule.

5.0 The First Law of Thermodynamics

This law is also called the law of conservation of energy.

5.1 The first law of thermodynamics for a system undergoing a cycle

The first law of thermodynamics states that during any cycle a system undergoes, the cyclic integral of the heat is equal to the cyclic integral of the work. To illustrate this law, consider as a system the gas in the container shown in Fig. 5.1. Let this system go through a cycle that is made up of two processes. In the first process work is done on the system by the paddle that turns as the weight is lowered. Let this system return to its initial state by transferring heat from the system until the cycle has been completed. When the amounts of work and heat are compared it is found that they are equal.

$$\oint \delta Q = \oint \delta W$$

Fig. 5.1:
Example of a system undergoing a cycle.
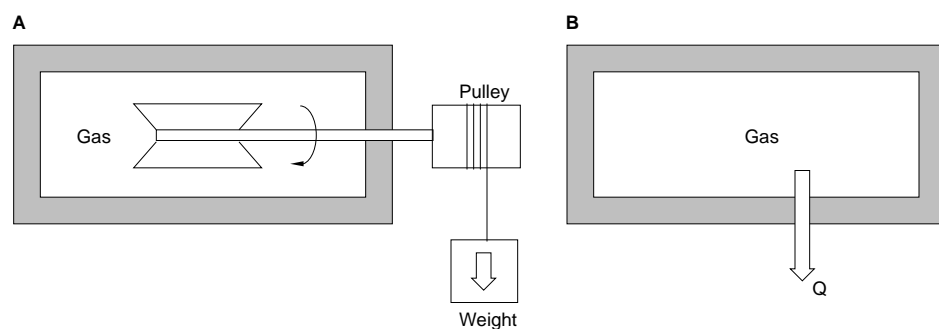
5.2 The first law of thermodynamics for a change in state of a system

We now consider the first law of thermodynamics for a system that undergoes a change of state. We begin by introducing a new property, the energy, which is given the symbol E. Consider a system that undergoes a cycle, in which it changes from state 1 to state 2 by process A, and returns from state 2 to state 1 by process B. This cycle is shown in Fig. 5.2 on a pressure-volume diagram.

Fig. 5.2:
Demonstration of the existence of thermodynamic property E.
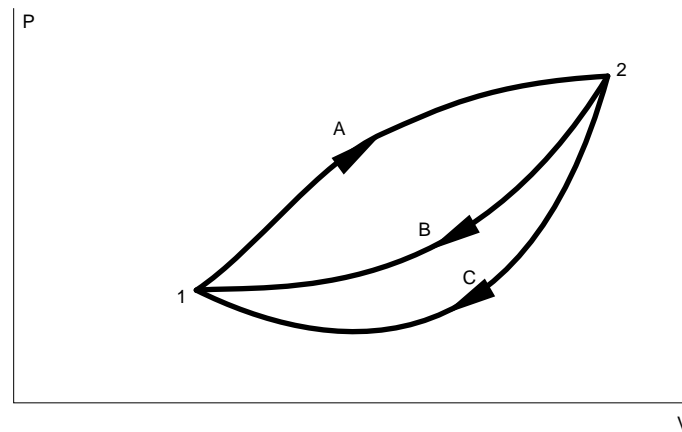
From the first law of thermodynamics,

$$\oint \delta Q = \oint \delta W$$

Considering the two separate processes, we have

$$\int_1^2 \delta Q_A + \int_2^1 \delta Q_B = \int_1^2 \delta W_A + \int_2^1 \delta W_B$$

Now consider another cycle in which the system changes from state 1 to state 2 by process A, as before, and returns to state 1 by process C. For this cycle we can write.

$$\int_1^2 \delta Q_A + \int_2^1 \delta Q_C = \int_1^2 \delta W_A + \int_2^1 \delta W_C$$

Subtracting the second of these equations from the first, we have

$$\int_2^1 \delta Q_B + \int_2^1 \delta Q_C = \int_2^1 \delta W_B - \int_2^1 \delta W_C$$

or, by rearranging

$$\int_2^1 (\delta Q - \delta W)_B = \int_2^1 (\delta Q - \delta W)_C$$

Since B and C represent arbitrary processes between states 1 and 2, the quantity $\delta Q - \delta W$ is the same for all processes between state 1 and state 2. This property is the energy of the system and is given the symbol E.

$$\delta Q = dE + \delta W$$

The physical significance of the property E is that it represents all the energy of the system in the given state. Usually we consider the bulk kinetic and potential energy separately and then consider all the other energy of the system in a single property that we call the internal energy, U.

E = Internal Energy + Kinetic Energy + Potential Energy

5.3   The thermodynamic property enthalpy

The enthalpy is defined as follow:

$H = U + pV$ **[kJ]**

or, per unit mass,

$h = u + pv$ **[kJ/kg]**

5.4   The constant-volume and constant-pressure specific heats

The constant-volume specific heat is

$$C_v = \frac{1}{m}\left(\frac{\delta Q}{\delta T}\right)_v = \frac{1}{m}\left(\frac{\partial U}{\partial T}\right)_v = \left(\frac{\partial u}{\partial T}\right)_v \left[\frac{kJ}{kg\;°C}\right]$$

The constant-pressure specific heat is

$$C_p = \frac{1}{m}\left(\frac{\delta Q}{\delta T}\right)_p = \frac{1}{m}\left(\frac{\partial H}{\partial T}\right)_p = \left(\frac{\partial h}{\partial T}\right)_p \left[\frac{kJ}{kg\;°C}\right]$$

5.5   First-law analysis for a control volume

5.5.1   Conservation of mass

A control volume is a volume in space that has interest for a particular study or analysis. The surface of this control volume is referred to as a control surface and is always a closed surface. Mass, heat, and work can cross the control surface. The mass in the control volume, as well as the properties of this mass can change with time (Fig. 5.3).

Fig. 5.3:

Schematic diagram of a control volume showing mass and energy transfers and accumulation.
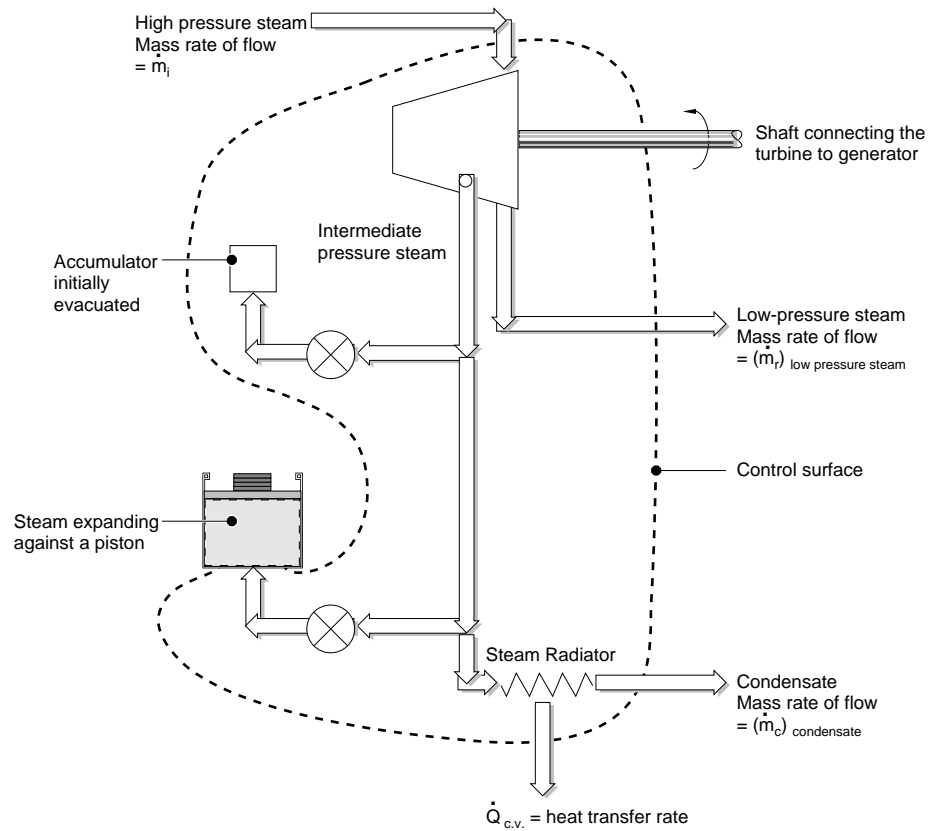
Let us consider the law of the conservation of mass as it relates to the control volume (Fig. 5.4).

Fig. 5.4:

Schematic diagram of a control volume for analysis of the continuity equation as applied to a control volume. (a) System and control volume at time t. (b) System and control volume at time t+δt.
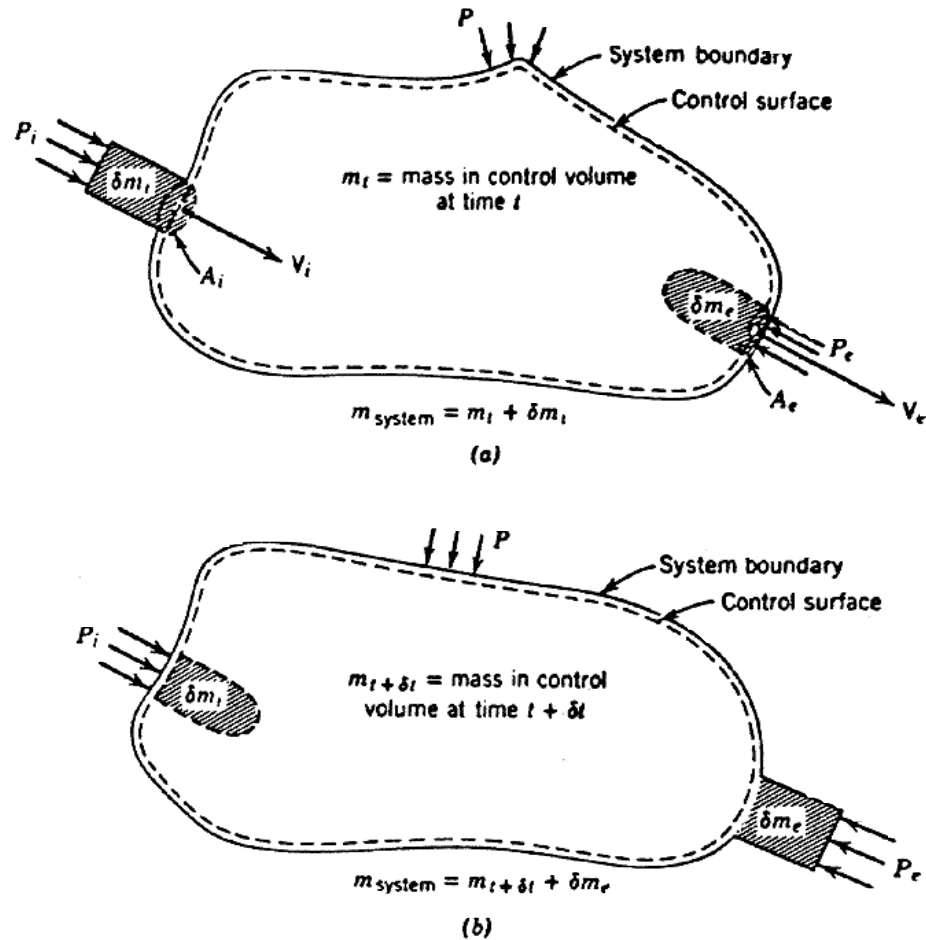
During a time interval δt, let the mass δm_i enter the control volume, and the mass δm_e leave the control volume. From the law of the conservation of mass,

$$m_t + \delta m_i = m_{t+\delta t} + \delta m_e$$

and the rate equation for the control volume is:

$$\frac{dm_{c.v.}}{dt} + \dot{m}_e + \dot{m}_i = 0$$

The conservation of mass is commonly termed the continuity equation.

5.5.2   The first law of thermodynamics

Let consider each of the terms of the first law as it is written for the system and transform each term into an equivalent form that applies to the control volume (Fig. 5.5).

Fig. 5.5:

Schematic for a first law analysis of a control volume, showing heat and work as well as mass crossing the control surface

δQ = heat transfer to system during δt

$\delta W_{c.v.}$ = work (such as that associated with a rotating shaft, shearing forces, displacement of the control surface, and electrical or magnetic effects) that crosses the control surface during δt

System boundary

Control surface

m_t = mass in control volume at time t

E_t = energy in control volume at time t

time = t

$m_t + \delta m_i$ = mass of system

$E_t + e_i \delta m_i$ = energy of system at time t

$W_{c.v.}$ includes the work associated with a displacement of the control surface

$m_{t+\delta t}$ = mass in control volume at time $t + \delta t$

$E_{t+\delta t}$ = energy in control volume at time $t + \delta t$

time = $t + \delta t$

$m_{t+\delta t} + \delta m_e$ = mass of system

$E_{t+\delta t} + e_e \delta m_e$ = energy of system at time $t + \delta t$

$$Q_1|^2 = E_2 - E_1 + w_1|^2$$

Consider first the term $E_2 - E_1$. Let

$\quad E_t$ = the energy in the control volume at t

$\quad E_{t+\delta t}$ = the energy in the control volume at t+δt.

Then

$\quad E_1 = E_t + e_i \delta m_i$ = energy of the system at t

$\quad E_2 = E_{t+\delta t} + e_e \delta m_e$ = energy of the system at t+δt

Therefore,

$\quad E_2 - E_1 = (E_{t+\delta t} - E_t) + (e_e \delta m_e - e_i \delta m_i)$

The total work associated with the masses δm_i and δm_e during δt is

$$\delta W = \delta W_{c.v.} + (P_e \, v_e \delta m_e - P_i \, v_i \delta m_i)$$

After dividing by δt, substituting into the first law, combining and rearranging, we have

$$\dot{Q}_{c.v.} + \Sigma \dot{m}_i \left(h_i + \frac{V_i^2}{2} + gZ_i \right) = \frac{dE_{c.v.}}{dt} + \Sigma \dot{m}_e \left(h_e + \frac{V_e^2}{2} + gZ_e \right) + \dot{W}_{c.v.}$$

6.0 The Second and Third Laws of Thermodynamics

The Second Law acknowledges that processes proceed in a certain direction but not in the opposite direction. A hot cup of coffee cools by virtue of heat transfer to the surroundings, but heat will not flow from the cooler surroundings to the hotter cup of coffee.

6.1 Heat engines and thermal efficiencies

A **Heat Engine** may be defined as a device that operates in a thermodynamics cycle and does a certain amount of net positive work through the transfer of heat from a high-temperature and to a low-temperature body. A simple steam power plant is an example of a heat engine (Fig. 6.1).

Fig. 6.1:
A heat engine involving steady-state, steady-flow processes.
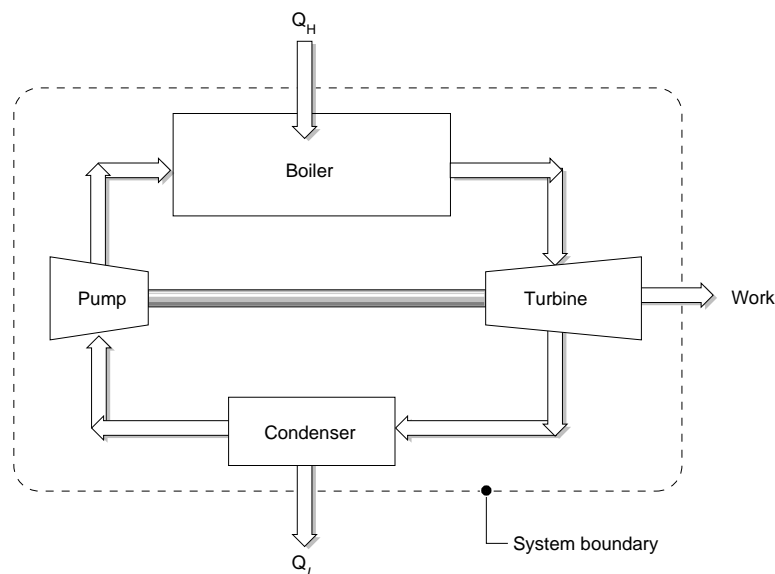
An amount of heat, Q_H, is transferred from a high-temperature body. In Fig. 6.1 the turbine is shown as driving the pump. What is significant, however, is the net work that is delivered during the cycle. The quantity of heat Q_L is rejected to a low-temperature body. Thus, the simple steam power plant is a heat engine, for it has a working fluid, to which and from which heat is transferred, and which does a certain amount of work as it undergoes a cycle.

At this point it is appropriate to introduce the concept of Thermal Efficiency of a heat engine. Thermal efficiency is the ratio of output, the energy sought, to input, the energy that costs. **Thermal efficiency** is defined as

$$\eta_{thermal} = \frac{W(energy\ sought)}{Q_H(energy\ that\ costs)} = \frac{Q_H - Q_L}{Q_H} = 1 - \frac{Q_L}{Q_H}$$

6.2   Introduction of entropy

In our consideration of the first law, we initially stated the law in terms of a cycle, but then defined a property, the internal energy, which enabled us to use the first law quantitatively for processes. Similarly, we have stated the second law for a cycle, and we now find that the second law leads to a property, entropy, which enables us to treat the second law quantitatively for processes.

6.3   Inequality of Clausius

For all reversible cycle we can write,

$$\oint \frac{\delta Q}{T} = 0$$

Where T is absolute temperature (°K)

For all irreversible cycles

$$\oint \frac{\delta Q}{T} < 0$$

Thus, for all cycles we can write

$$\oint \frac{\delta Q}{T} \leq 0$$

Example

The significance of the Inequality Of Clausius may be illustrated by considering the simple steam power plant cycle shown in Fig. 6.2.

Fig 6.2:

A simple steam power plant that demonstrates the inequality of Clausius.
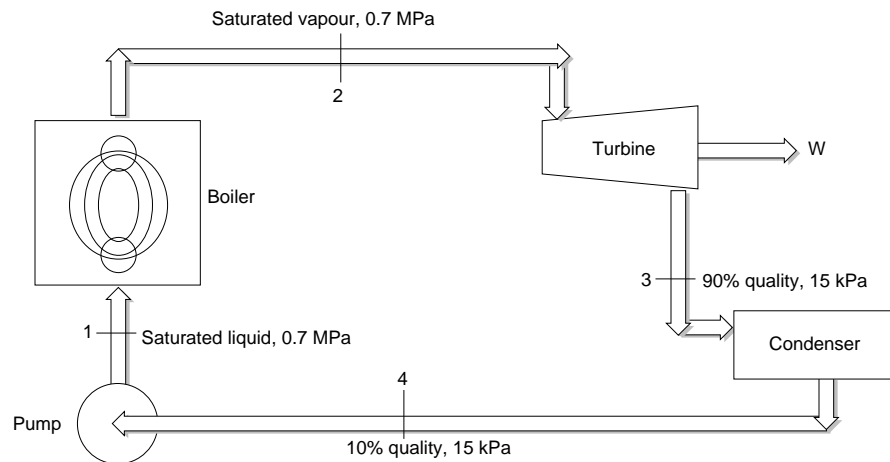
This cycle is slightly different from the usual cycle from steam power plants in that the pump handles a mixture of liquid and vapour in such proportions that saturated liquid leaves the pump and enters the boiler. Does this cycle satisfy the inequality of Clausius?

Heat is transferred in two places, the boiler and the condenser. Therefore,

$$\oint \frac{\delta Q}{T} = \oint \left(\frac{\delta Q}{T}\right)_{boiler} + \oint \left(\frac{\delta Q}{T}\right)_{condenser}$$

Since the temperature remains constant in both the boiler and condenser, this may be integrated as follows:

$$\oint \frac{\delta Q}{T} = \frac{1}{T_1}\int_1^2 \delta Q + \frac{1}{T_3}\int_3^4 \delta Q = \frac{Q\Big|_1^2}{T_1} + \frac{Q\Big|_3^4}{T_3}$$

Let us consider a 1-kg mass as the working fluid.

$q_1^2 = h_2 - h_1 = 2066.3 \text{ kJ/kg}, T_1 = 164.97 \text{ °C}$

$q_3^4 = h_4 - h_3 = 463.4 - 2361.8 = -1898.4 \text{ kJ/kg}, T_3 = 53.97 \text{ °C}, \text{Therefore,}$

$$\oint \frac{\delta Q}{T} = \frac{2066.3}{164.97 + 273.15} - \frac{1898.4}{53.97 + 273.15} = -1.087 \text{ kJ / kg K}$$

The cycle satisfies the inequality of Clausius.

6.4   Entropy

For a system which undergoes a reversible process, the second law of thermodynamics leads to a property of a system that we call **Entropy**.

$$dS \equiv \left(\frac{\delta Q}{T}\right)_{rev}$$

The change in entropy of a system as it undergoes a change of state may be

found by integrating the previous equation. Thus,

$$S_2 - S_1 = \int_1^2 \left(\frac{\delta Q}{T} \right)_{rev}$$

The important point is that since entropy is a property, the change in the entropy of a substance in going from one state to another is the same for all processes, both reversible and irreversible, between these two states. The previous equation enables us to find the change in entropy only along a reversible path. However, once the change has been evaluated, this value is the magnitude of the entropy change for all processes between these two states.

6.5   The third law of thermodynamics
The entropy of all pure substances can be assigned the value of zero at the absolute zero of temperature.

6.6   Entropy change of a system during an irreversible process
Consider a system that undergoes the cycles shown in Fig. 6.3. The cycle made up of the reversible processes A and B is a reversible cycle.

Fig. 6.3
Entropy change of a system during an irreversible process.
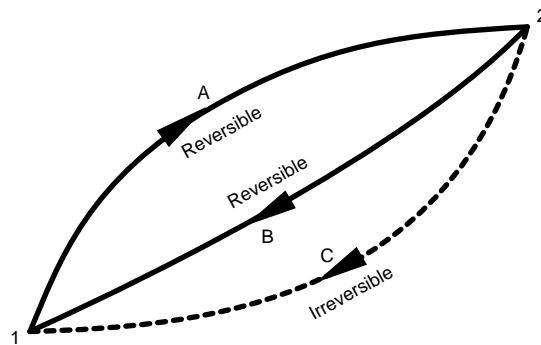
Therefore, we can write

$$\oint \frac{\delta Q}{T} = \oint_1^2 \left(\frac{\delta Q}{T} \right)_A + \oint_2^1 \left(\frac{\delta Q}{T} \right)_B = 0$$

The cycle made up of the reversible process A and the irreversible process C is an irreversible cycle. Therefore, for this cycle the inequality of Clausius may be applied, giving the result

$$\oint \frac{\delta Q}{T} = \oint_1^2 \left(\frac{\delta Q}{T} \right)_A + \oint_2^1 \left(\frac{\delta Q}{T} \right)_C < 0$$

Subtracting the second equation from the first and rearranging, we have

$$\oint_2^1 \left(\frac{\delta Q}{T} \right)_B > \oint_2^1 \left(\frac{\delta Q}{T} \right)_C$$

Since path B is reversible, and since entropy is a property,

$$\oint_2^1 \left(\frac{\delta Q}{T}\right)_B = \oint_2^1 dS_B = \oint_2^1 dS_C$$

Therefore,

$$\oint_2^1 dS_C > \oint_2^1 \left(\frac{\delta Q}{T}\right)_C$$

For the general case we can write

$$dS \geq \frac{\delta Q}{T}$$

$$S_2 - S_1 \geq \int_1^2 \frac{\delta Q}{T}$$

In these equation the equality holds for a reversible process and the inequality for an irreversible process.

6.7　Principle of the increase of entropy

In an isolated system, the only processes that can occur are those that have an associated increase in entropy.

6.8　Second-law analysis for a control volume

The second law of thermodynamics can be applied to a control volume by a procedure similar to that used for writing the first law for a control volume. The second law can be written

$$dS \geq \frac{\delta Q}{T}$$

For a change in entropy, S_2 - S_1, that occurs during a time interval δt, we can write

$$\frac{S_2 - S_1}{\delta t} \geq \frac{1}{\delta t}\frac{\delta Q}{T}$$

Consider the system and control volume shown in Fig. 6.4. During time δt let the mass δm_i enter the control volume, and the mass δm_e leave the control volume. An amount of heat δQ is transferred to the system across an element of area where the surface temperature is T, and work δW is done by the system.

Fig 6.4:

Schematic diagram for a second law analysis of a control volume.

(a)

(b)
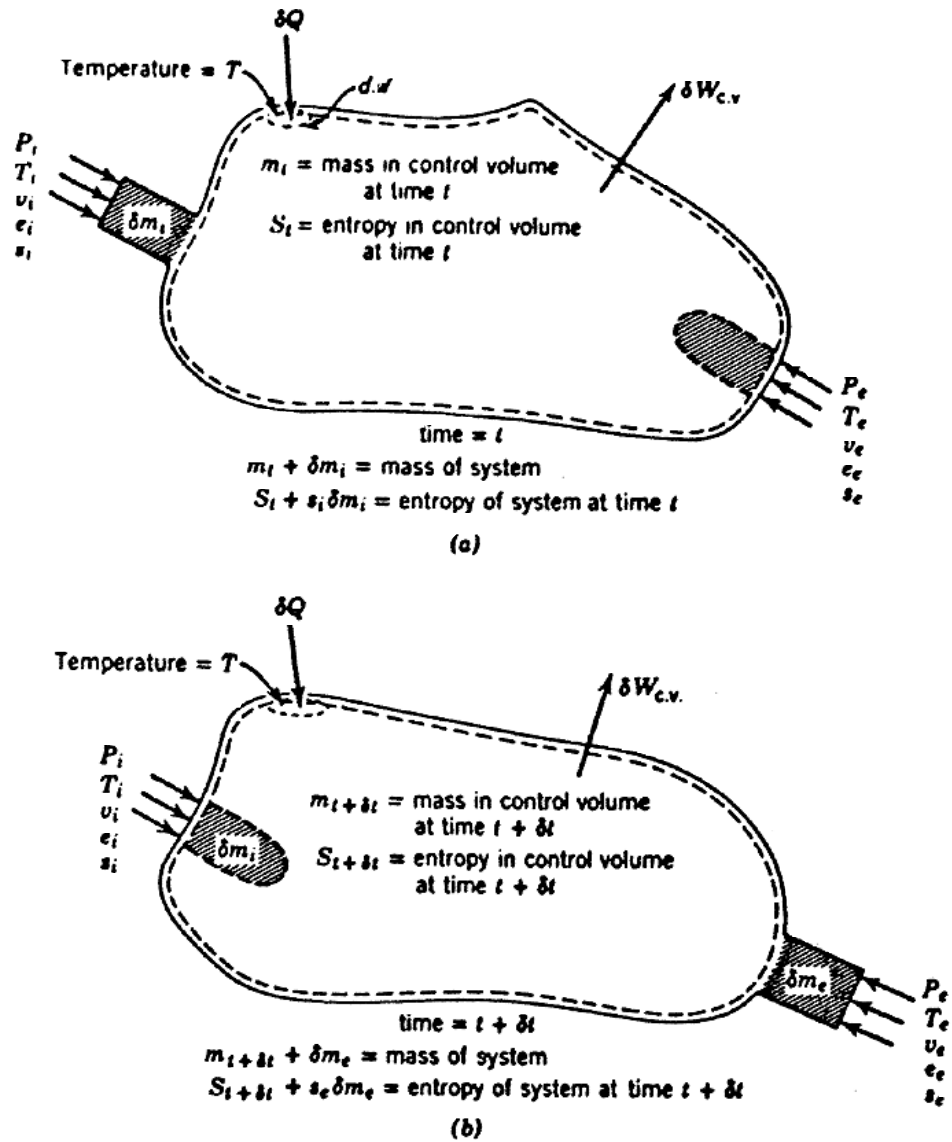
Let

S_t = the entropy in the control volume at t

$S_{t+\delta t}$ = the entropy in the control volume at t+δt.

Then

$S_1 = S_t + s_i\delta m_i$ = entropy of the system at t

$S_2 = S_{t+\delta t} + s_e\delta m_e$ = entropy of the system at t+ δt

Therefore,

$S_2 - S_1 = (S_{t+\delta t} - S_t) + (s_e\delta m_e - s_i\delta m_i)$

After writing the heat transfer term as the summation of all local δQ/T terms throughout the interior of the control volume, and after reducing this equation to a rate equation the resulting expression is

$$\frac{dS_{c.v.}}{dt} + \Sigma \ \dot{m}_e s_e - \Sigma \ \dot{m}_i s_i \geq \Sigma_{c.v.} \frac{Q_{c.v.}}{T}$$

where the equality applies to internally reversible processes and the inequality to internally irreversible processes.

7.0   The Steam Cycle

The ideal cycle for a simple steam power plant is the Rankine cycle, shown in Fig. 7.1.

Fig. 7.1:
Simple steam power plant which operates on the Rankine cycle.
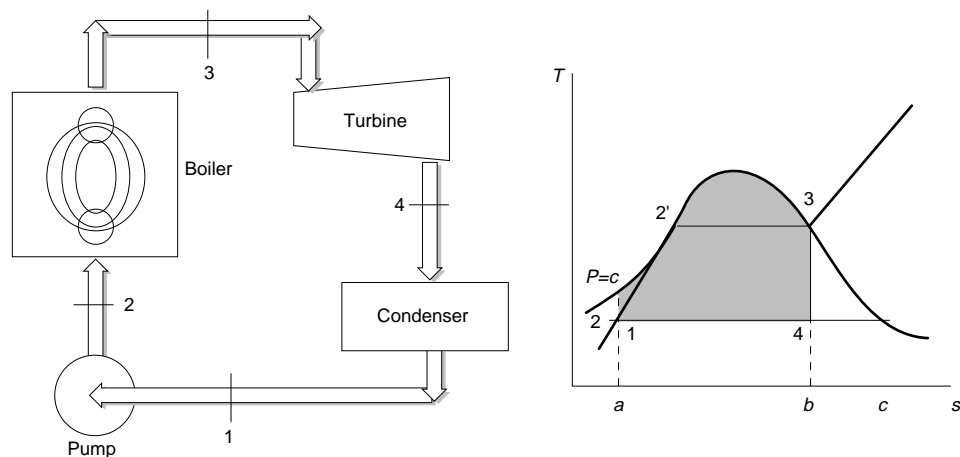
The processes that comprise the cycle are.

1-2: Reversible adiabatic pumping process in the pump.
2-3: Constant-pressure transfer of heat in the boiler.
3-4: Reversible adiabatic expansion in the turbine
4-1: Constant-pressure transfer of heat in the condenser.

If changes of kinetic and potential energy are neglected, heat transfer and work may be represented by various areas on the T-S diagram. The heat transferred to the working fluid is represented by area a-1-2-2'-3-b-a, and the heat transferred from the working fluid by area a-1-4-b-a. From the first law we conclude that the area representing the work is the difference between these two areas, area 1-2-2'-3-4-1. The thermal efficiency is defined by the relation

$$\eta_{th} = \frac{w_{net}}{q_H} = \frac{\text{area } 1-2-2'-3-4-1}{\text{area } a-2-2'-3-b-a}$$

7.1   Exercise
Determine the efficiency of a Rankine cycle using steam as the working fluid in which the condenser pressure is 10 kPa. The boiler pressure is 2 MPa. The steam leaves the boiler as saturated vapour. In solving Rankine-cycle problems,

we will let w_p denote the work into the pump per kilogram of fluid flowing, and q_L the heat rejected from the working fluid per kilogram of fluid flowing.
To solve this problem we consider, in succession, a control surface around the pump, the boiler, the turbine and the condenser. For each, the thermodynamic model is the steam tables (Table 7.1), and the process is a steady-state, steady-flow process with negligible changes in kinetic and potential energies.

Control volume: Pump.
Inlet state: P_1 known, saturated liquid.
Exit state: P_2 known.
Analysis:
    First law: $w_p = h_2 - h_1$
    Second law: $s_2 = s_1$
Because

$$s_2 = s_1 \qquad h_2 - h_1 = \int_1^2 v dP$$

Solution.
Assuming the liquid to be incompressible, we have
    $w_p = v(P_2 - P_1) = (0.00101)(2000 - 10) = 2.0 \text{ kJ/kg}$
    $h_2 = h_1 + w_p = 191.8 + 2.0 = 193.8 \text{ kJ/kg}$

Control volume: Boiler.
Inlet state: P_2, h_2 known; state fixed.
Exit state: P_3 known, saturated vapour.
Analysis:
    First law: $q_h = h_3 - h_2$
Solution
    $q_H = h_3 - h_2 = 2799.5 - 193.8 = 2605.7 \text{ kJ/kg}$

Control volume: Turbine.
Inlet state: State 3 known (above).
Exit state: P_4 known.
Analysis:
First law: $w_t = h_3 - h_4$
Second law: $s_3 = s_4$
Solution
We can determine the quality at state as follows:
    $s_3 = s_4 = 6.3409 = 0.6493 + x_4 7.5009$, $x_4 = 0.7588$
    $h_4 = 191.8 + 0.7588 (2392.8) = 2007.5 \text{ kJ/kg}$
    $w_t = 2799.5 - 2007.5 = 792.0 \text{ kj/kg}$

Control volume: Condenser.
Inlet state: State 4 known (as given).
Exit state: State 1 known (as given).

Analysis:

First law: $q_L = h_4 - h_1$

Solution

$q_L = h_4 - h_1 = 2007.5 - 191.8 = 1815.7 \text{ kJ/kg}$

We can now calculate the thermal efficiency:

$$\eta_{th} = \frac{w_{net}}{q_H} = \frac{q_H - q_L}{q_H} = \frac{w_t - w_p}{q_H} = \frac{792.0 - 2.0}{2605.7} = 30.3\%$$

We could also write an expression for thermal efficiency in terms of properties at various points in the cycle.

$$\eta_{th} = \frac{(h_3 - h_2) - (h_4 - h_1)}{h_3 - h_2} = \frac{(h_3 - h_4) - (h_2 - h_1)}{h_3 - h_2}$$

$$= \frac{2605.7 - 1815.7}{2605.7} = \frac{792.0 - 2.0}{2605.7} = 30.3\%$$

Table 7.1:
Steam tables.

Press. kPa p	Temp. °C T	Specific Volume Sat. Liquid v_f	Sat. Vapor v_g	Internal Energy Sat. Liquid u_f	Evap. u_{fg}	Sat. Vapor u_g	Enthalpy Sat. Liquid h_f	Evap. h_{fg}	Sat. Vapor h_g	Entropy Sat. Liquid s_f	Evap. s_{fg}	Sat. Vapor s_g
0.6113	0.01	0.001 000	206.14	.00	2375.3	2375.3	.01	2501.3	2501.4	.0000	9.1562	9.1562
1.0	6.98	0.001 000	129.21	29.30	2355.7	2385.0	29.30	2484.9	2514.2	.1059	8.8697	8.9756
1.5	13.03	0.001 001	87.98	54.71	2338.6	2393.3	54.71	2470.6	2525.3	.1957	8.6322	8.8279
2.0	17.50	0.001 001	67.00	73.48	2326.0	2399.5	73.48	2460.0	2533.5	.2607	8.4629	8.7237
2.5	21.08	0.001 002	54.25	88.48	2315.9	2404.4	88.49	2451.6	2540.0	.3120	8.3311	8.6432
3.0	24.08	0.001 003	45.67	101.04	2307.5	2408.5	101.05	2444.5	2545.5	.3545	8.2231	8.5776
4.0	28.96	0.001 004	34.80	121.45	2293.7	2415.2	121.46	2432.9	2554.4	.4226	8.0520	8.4746
5.0	32.88	0.001 005	28.19	137.81	2282.7	2420.5	137.82	2423.7	2561.5	.4764	7.9187	8.3951
7.5	40.29	0.001 008	19.24	168.78	2261.7	2430.5	168.79	2406.0	2574.8	.5764	7.6750	8.2515
10	45.81	0.001 010	14.67	191.82	2246.1	2437.9	191.83	2392.8	2584.7	.6493	7.5009	8.1502
15	53.97	0.001 014	10.02	225.92	2222.8	2448.7	225.94	2373.1	2599.1	.7549	7.2536	8.0085
20	60.06	0.001 017	7.649	251.38	2205.4	2456.7	251.40	2358.3	2609.7	.8320	7.0766	7.9085
25	64.97	0.001 020	6.204	271.90	2191.2	2463.1	271.93	2346.3	2618.2	.8931	6.9383	7.8314
30	69.10	0.001 022	5.229	289.20	2179.2	2468.4	289.23	2336.1	2625.3	.9439	6.8247	7.7686
40	75.87	0.001 027	3.993	317.53	2159.5	2477.0	317.58	2319.2	2636.8	1.0259	6.6441	7.6700
50	81.33	0.001 030	3.240	340.44	2143.4	2483.9	340.49	2305.4	2645.9	1.0910	6.5029	7.5939
75	91.78	0.001 037	2.217	384.31	2112.4	2496.7	384.39	2278.6	2653.0	1.2130	6.2434	7.4564

Table 7.1:
Steam tables.

Press. MPa P	Temp. °C T	Specific Volume		Internal Energy			Enthalpy			Entropy		
		Sat. Liquid v_f	Sat. Vapor v_g	Sat. Liquid u_f	Evap. u_{fg}	Sat. Vapor u_g	Sat. Liquid h_f	Evap. h_{fg}	Sat. Vapor h_g	Sat. Liquid s_f	Evap. s_{fg}	Sat. Vapor s_g
0.100	99.63	0.001 043	1.6940	417.36	2088.7	2506.1	417.46	2258.0	2675.5	1.3026	6.0568	7.3594
0.125	105.99	0.001 048	1.3749	444.19	2069.3	2513.5	444.32	2241.0	2685.4	1.3740	5.9104	7.2844
0.150	111.37	0.001 053	1.1593	466.94	2052.7	2519.7	467.11	2226.5	2693.6	1.4336	5.7897	7.2233
0.175	116.06	0.001 057	1.0036	486.80	2038.1	2524.9	486.99	2213.6	2700.6	1.4849	5.6868	7.1717
0.225	124.00	0.001 064	0.7933	520.47	2013.1	2533.6	520.72	2191.3	2712.1	1.5706	5.5173	7.0878
0.250	127.44	0.001 067	0.7187	535.10	2002.1	2537.2	535.37	2181.5	2716.9	1.6072	5.4455	7.0527
0.275	130.60	0.001 070	0.6573	548.59	1991.9	2540.5	548.89	2172.4	2721.3	1.6408	5.3801	7.0209
0.300	133.55	0.001 073	0.6058	561.15	1982.4	2543.6	561.47	2163.8	2725.3	1.6718	5.3201	6.9919
0.325	136.30	0.001 076	0.5620	572.90	1973.5	2546.4	573.25	2155.8	2729.0	1.7006	5.2646	6.9652
0.350	138.88	0.001 079	0.5243	583.95	1965.0	2548.9	584.33	2148.1	2732.4	1.7275	5.2130	6.9405
0.375	141.32	0.001 081	0.4914	594.40	1956.9	2551.3	594.81	2140.8	2735.6	1.7528	5.1647	6.9175
0.40	143.63	0.001 084	0.4625	604.31	1949.3	2553.6	604.74	2133.8	2738.6	1.7766	5.1193	6.8959
0.45	147.93	0.001 088	0.4140	622.77	1934.9	2557.6	623.25	2120.7	2743.9	1.8207	5.0359	6.8565
0.50	151.86	0.001 093	0.3749	639.68	1921.6	2561.2	640.23	2108.5	2748.7	1.8607	4.9606	6.8213
0.55	155.48	0.001 097	0.3427	655.32	1909.2	2564.5	655.93	2097.0	2753.0	1.8973	4.8920	6.7893
0.60	158.85	0.001 101	0.3157	669.90	1897.5	2567.4	670.56	2086.3	2756.8	1.9312	4.8288	6.7600
0.65	162.01	0.001 104	0.2927	683.56	1886.5	2570.1	684.28	2076.0	2760.3	1.9627	4.7703	6.7331
0.70	164.97	0.001 108	0.2729	696.44	1876.1	2572.5	697.22	2066.3	2763.5	1.9922	4.7158	6.7080
0.75	167.78	0.001 112	0.2556	708.64	1866.1	2574.7	709.47	2057.0	2766.4	2.0200	4.6647	6.6847
0.80	170.43	0.001 115	0.2404	720.22	1856.6	2576.8	721.11	2048.0	2769.1	2.0462	4.6166	6.6628
0.85	172.96	0.001 118	0.2270	731.27	1847.4	2578.7	732.22	2039.4	2771.6	2.0710	4.5711	6.6421
0.90	175.38	0.001 121	0.2150	741.83	1838.6	2580.5	742.83	2031.1	2773.9	2.0946	4.5280	6.6226
0.95	177.69	0.001 124	0.2042	751.95	1830.2	2582.1	753.02	2023.1	2776.1	2.1172	4.4869	6.6041
1.00	179.91	0.001 127	0.194 44	761.68	1822.0	2583.6	762.81	2015.3	2778.1	2.1387	4.4478	6.5865
1.10	184.09	0.001 133	0.177 53	780.09	1806.3	2586.4	781.34	2000.4	2781.7	2.1792	4.3744	6.5536
1.20	187.99	0.001 139	0.163 33	797.29	1791.5	2588.8	798.65	1986.2	2784.8	2.2166	4.3067	6.5233
1.30	191.64	0.001 144	0.151 25	813.44	1777.5	2591.0	814.93	1972.7	2787.6	2.2515	4.2438	6.4953
1.40	195.07	0.001 149	0.140 84	828.70	1764.1	2592.8	830.30	1959.7	2790.0	2.2842	4.1850	6.4693
1.50	198.32	0.001 154	0.131 77	843.16	1751.3	2594.5	844.89	1947.3	2792.2	2.3150	4.1298	6.4448
1.75	205.76	0.001 166	0.113 49	876.46	1721.4	2597.8	878.50	1917.9	2796.4	2.3851	4.0044	6.3896
2.00	212.42	0.001 177	0.099 63	906.44	1693.8	2600.3	908.79	1890.7	2799.5	2.4474	3.8935	6.3409
2.25	218.45	0.001 187	0.088 75	933.83	1668.2	2602.0	936.49	1865.2	2801.7	2.5035	3.7937	6.2972
2.5	223.99	0.001 197	0.079 98	959.11	1644.0	2603.1	962.11	1841.0	2803.1	2.5547	3.7028	6.2575
3.0	233.90	0.001 217	0.066 68	1004.78	1599.3	2604.1	1008.42	1795.7	2804.2	2.6457	3.5412	6.1869

Table 7.1:
Steam tables.

Press. MPa P	Temp. °C T	Specific Volume		Internal Energy			Enthalpy			Entropy		
		Sat. Liquid v_f	Sat. Vapor v_g	Sat. Liquid u_f	Evap. u_{fg}	Sat. Vapor u_g	Sat. Liquid h_f	Evap. h_{fg}	Sat. Vapor h_g	Sat. Liquid s_f	Evap. s_{fg}	Sat. Vapor s_g
3.5	242.60	0.001 235	0.057 707	1045.43	1558.3	2603.7	1049.75	1753.7	2803.4	2.7253	3.4000	6.1253
4	250.40	0.001 252	0.049 978	1082.31	1520.0	2602.3	1087.31	1714.1	2801.4	2.7964	3.2737	6.0701
5	263.99	0.001 286	0.039 44	1147.81	1449.3	2597.1	1154.23	1640.1	2794.3	2.9202	3.0532	5.9734
6	275.64	0.001 319	0.032 44	1205.44	1384.3	2589.7	1213.35	1571.0	2784.3	3.0267	2.8625	5.8892
7	285.88	0.001 351	0.027 37	1257.55	1323.0	2580.5	1267.00	1505.1	2772.1	3.1211	2.6922	5.8133
8	295.06	0.001 384	0.023 52	1305.57	1264.2	2569.8	1316.64	1441.3	2758.0	3.2068	2.5364	5.7432
9	303.40	0.001 418	0.020 48	1350.51	1207.3	2557.8	1363.26	1378.9	2742.1	3.2858	2.3915	5.6772
10	311.06	0.001 452	0.018 026	1393.04	1151.4	2544.4	1407.56	1317.1	2724.7	3.3596	2.2544	5.6141
11	318.15	0.001 489	0.015 987	1433.7	1096.0	2529.8	1450.1	1255.5	2705.6	3.4295	2.1233	5.5527
12	324.75	0.001 527	0.014 263	1473.0	1040.7	2513.7	1491.3	1193.6	2684.9	3.4962	1.9962	5.4924
13	330.93	0.001 567	0.012 780	1511.1	985.0	2496.1	1531.5	1130.7	2662.2	3.5606	1.8718	5.4323
14	336.75	0.001 611	0.011 485	1548.6	928.2	2476.8	1571.1	1066.5	2637.6	3.6232	1.7485	5.3717
15	342.24	0.001 658	0.010 337	1585.6	869.8	2455.5	1610.5	1000.0	2610.5	3.6848	1.6249	5.3098
16	347.44	0.001 711	0.009 306	1622.7	809.0	2431.7	1650.1	930.6	2580.6	3.7461	1.4994	5.2455
17	352.37	0.001 770	0.008 364	1660.2	744.8	2405.0	1690.3	856.9	2547.2	3.8079	1.3698	5.1777
18	357.06	0.001 840	0.007 489	1698.9	675.4	2374.3	1732.0	777.1	2509.1	3.8715	1.2329	5.1044
19	361.54	0.001 924	0.006 657	1739.9	598.1	2338.1	1776.5	688.0	2464.5	3.9388	1.0839	5.0228
20	365.81	0.002 036	0.005 834	1785.6	507.5	2293.0	1826.3	583.4	2409.7	4.0139	.9130	4.9269
21	369.89	0.002 207	0.004 952	1842.1	388.5	2230.6	1888.4	446.2	2334.6	4.1075	.6938	4.8013
22	373.80	0.002 742	0.003 568	1961.9	125.2	2087.1	2022.2	143.4	2165.6	4.3110	.2216	4.5327
22.09	374.14	0.003 155	0.003 155	2029.6	0	2029.6	2099.3	0	2099.3	4.4298	0	4.4298

December 1995

Single Phase Flow: Part 1

Training Objectives

The participant will be introduced to:
1   fluids and the continuum hypothesis.
2   fluid properties.
3   mechanics of nonflowing fluids.
4   the finite control volume approach to flow analysis.

# Single Phase Flow: Part 1

Table of Contents

1 Introduction

Fluid mechanics is the branch of engineering science that is concerned with forces and energies generated by fluids at rest and in motion. The study of fluid mechanics involves applying the fundamental principles of mechanics and thermodynamics to develop physical understanding and analytic tools that engineers can use to design and evaluate equipment and processes involving fluids. The fundamentals of fluid mechanics include a knowledge of the nature of fluids and the properties used to describe them, the physical laws that govern fluid behaviour, the ways in which these laws may be cast into mathematical form, and the various methodologies that may be used to solve engineering problems.

1.1   Fluids and the continuum hypothesis

All matter exists in one of two states: solid or fluid. A solid does not easily change its shape, but a fluid changes shape with relative ease. To develop a formal definition of a fluid, consider imaginary chunks of both a solid and a fluid (Fig. 1.1).

Fig. 1.1:

Response of samples of solid and fluid to applied shear force.
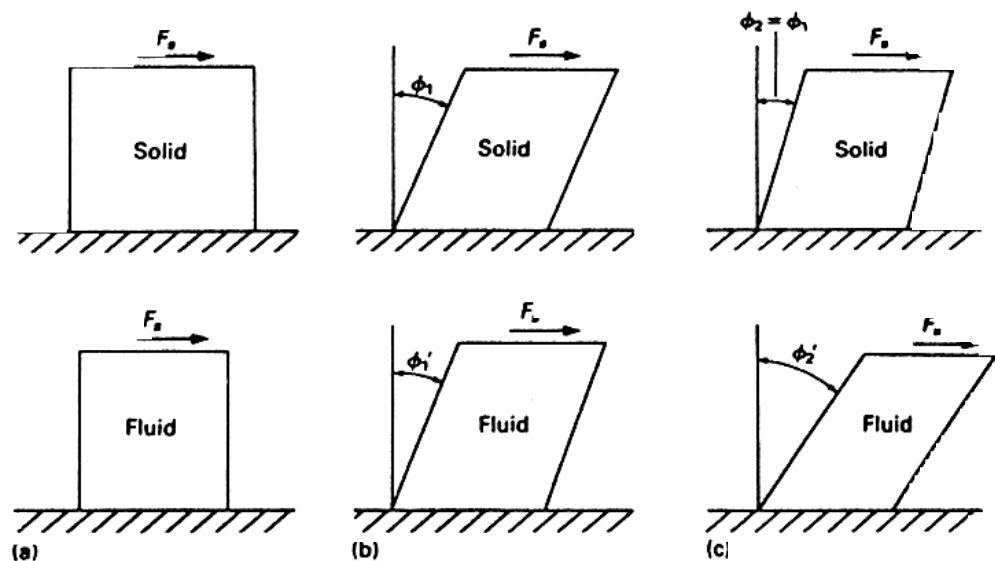
The chunks are fixed along one edge, and a shear force is applied at the opposite edge. A short time after application of the force, the solid assumes a deformed shape, which can be measured by the angle ϕ_1. If we maintain this force and examine the solid at a later time, we find that the deformation is exactly the same, that is, $\phi_2 = \phi_1$. Consider the response of the fluid to the applied shear force. A short time after application of the force, the fluid assumes a deformed

shape, as indicated by the angle ϕ_1'. At a later time, the deformation is greater, $\phi_2' > \phi_1'$; in fact, the fluid continues to deform as long as the force is applied. Thus, we can define a fluid:

A fluid is a substance that deforms continuously under the action of an applied shear force or stress.

Because a fluid will always flow if a shear stress is applied, it is necessary to consider the relation between stress and the time rate of deformation. A fluid deforms at a rate related to the applied stress. The fluid attains a state of "dynamic equilibrium" in which the applied stress is balanced by the resisting stress. Thus an alternative definition of a fluid is:

A fluid is a substance that can resist shear only when moving.

1.1.1 The continuum model

All substances are composed of an extremely large number of discrete particles called molecules. In principle it would be possible to describe a sample of fluid in terms of the dynamics of its individual molecules; in practice it is impossible because of the extremely large numbers of molecules involved. For most cases of practical interest, it is possible to ignore the molecular nature of matter and to assume that matter is continuous. This assumption is called the continuum model and may be applied to both solids and fluids. The continuum model assumes that molecular structure is so small relative to the dimensions involved in problems of practical interest that we may ignore it.

2 Fluid Properties

Fluid properties characterize the state or condition of the fluid and macroscopically represent microscopic (molecular) structure and motion.

2.1 Density, specific volume, specific weight, specific gravity.

The density of a fluid is its mass per unit volume. Density has a value at each point in a continuum and may vary from one point to another. The smallest volume (δV) for which the density variation is smooth is the limit of the continuum hypothesis.

$$\rho \equiv \lim_{\Delta V \to \delta V} \frac{\Delta m}{\Delta V} \quad \left[\frac{\text{kg}}{\text{m}^3}\right]$$

The small volume δV represents the size of a typical "point" in the continuum.

For fluids near atmospheric pressure and temperature, δV is of order of 10^{-9} mm^3. We interpret all fluid properties as representing an average of the fluid molecular structure over this small volume.

Several other fluid properties are directly related to density. The specific volume (v), define by

$$v \equiv \frac{1}{\rho} \quad \left[\frac{m^3}{kg}\right]$$

The specific weight (γ) is the weight of the fluid per unit volume; thus

$$\gamma \equiv \rho g \quad \left[\frac{N}{m^3}\right]$$

where g is the local acceleration of gravity.

The specific gravity of a fluid is the ratio of the density of the fluid to the density of reference fluid. The defining equation is

$$S \equiv \frac{\rho}{\rho_{REF}}$$

For liquids, the reference fluid is pure water at 4°C and 101,330 N/m², ρ_{REF} = 1000 kg/m³. Specific gravity of gases is usually based on dry air as the reference fluid.

2.2 Pressure
We define pressure as follows:

Pressure is the normal compressive force per unit area acting on a real or imaginary surface in fluid.

Consider a small surface area ΔA within a fluid (Fig. 2.1).

Fig. 2.1:
Illustration for definition of pressure.
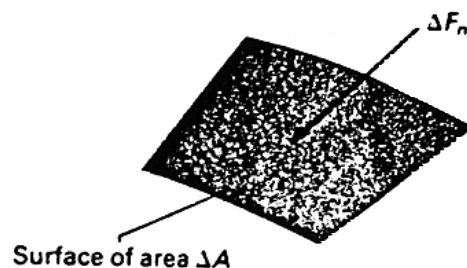
A force ΔF_n acts normal to the surface. The pressure is defined by

$$p \equiv \lim_{\Delta A \to \delta A} \frac{\Delta F_n}{\Delta A} \quad \left[\frac{N}{m^2}\right]$$

The limiting value δA represents the lower bound of the continuum assumption.

2.3   Viscosity

Fluid is a substance that undergoes continuous deformation when subjected to a shear stress and that the shear stress is a function of the rate of the deformation. For many common fluids, the shear stress is proportional to the rate of deformation. The constant of proportionality, called the viscosity, is a fluid property.

If the shear stress (τ) in the fluid is proportional to the strain rate, we can write

$$\tau = \mu \frac{du}{dy}$$

The coefficient μ is the viscosity. This is called Newton's law of viscosity. Fluids that obey this particular law and its generalization to multidimensional flow are called Newtonian fluids. The viscosity of Newtonian fluids varies considerably from fluid to fluid. For a particular fluid, viscosity varies rather strongly with temperature but only slightly with pressure. We usually neglect viscosity variation with pressure in practical calculations.

The ratio of viscosity to density often appears in the equations describing fluid motion. This ratio is given the name kinematic viscosity and is usually denoted by the symbol ν:

$$\nu = \frac{\mu}{\rho}$$

An effect usually associated with fluid viscosity is the no-slip condition. Whenever a fluid is in contact with a solid surface, the velocity of the fluid at the surface is equal to the velocity of the surface (Fig. 2.2). A velocity gradient always occurs near a surface when a fluid flows over the surface, and according to Newton's law of viscosity, shear stress always acts on the fluid in this region.

To simplify the equations of motion we introduce the assumption of zero shear stress by pretending that the fluid has zero viscosity ($\mu = 0$ gives $\tau = 0$). A fluid with zero viscosity is called an inviscid fluid. Although no real fluid has zero viscosity, the viscosity of many fluids is small, so shear stresses in these fluids are small if du/dy is not large. This relation is often true, except in the immediate vicinity of solid boundaries (as in Fig. 2.2). The assumption of an inviscid fluid is often useful for analyzing flow away from solid boundaries.

Fig. 2.2
Variation of fluid velocity relative to a wall;
note $u_{rel} = 0$ at the wall.
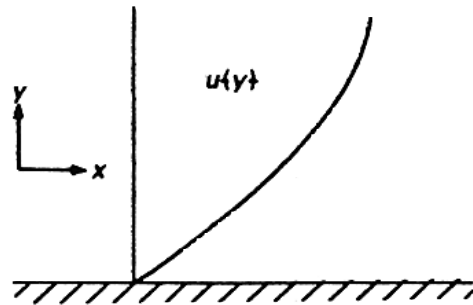
The incompressible fluid and inviscid fluid models are combined in the so-called ideal fluid. The ideal fluid has $\mu \equiv 0$ and $\rho \equiv$ constant.

2.4   Calculation of shear stress from a velocity profile

Figure 2.3 shows a liquid film flowing down an inclined surface. The liquid is a Newtonian fluid with viscosity μ. The velocity profile is given by

$$u(y) = U\left[2\left(\frac{y}{Y}\right) - \left(\frac{y}{Y}\right)^2\right]$$

where U is a constant and Y is the thickness of the liquid layer. Find the shear stress at the fluid-solid interface (y = 0), at y = Y/2, and at the "free surface" (y = Y).

Fig. 2.3
Liquid film flowing down an inclined surface.
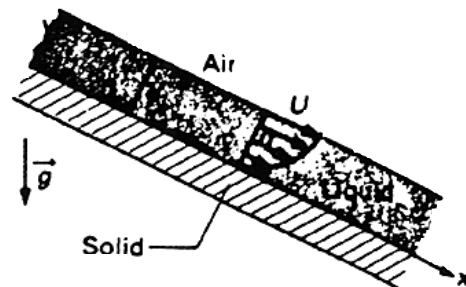
For a Newtonian fluid,

$$\tau = \mu\,\frac{du}{dy}$$

Substituting the velocity u gives

$$\tau = \mu\,U\,\frac{d}{dy}\left[2\left(\frac{y}{Y}\right) - \left(\frac{y}{Y}\right)^2\right]$$

$$= \mu\,\frac{U}{Y}\left[2 - 2\left(\frac{y}{Y}\right)\right]$$

The shear stresses at the various y locations are

$$\tau)_{y=0} = 2\mu\frac{U}{Y}$$

$$\tau)_{y=Y/2} = \mu\frac{U}{Y}$$

$$\tau)_{y=Y} = 0$$

3   Mechanics of Nonflowing Fluids

The mechanics of fluids that are not flowing means that the particles of the fluid are not experiencing any deformation.

3.1   Pressure at a point: Pascal' s law

If there is no deformation, there are no shear stresses acting on the fluid; the forces on any fluid particle are the result of gravity and pressure only. In a nonflowing fluid, the pressure is a scalar quantity; that is:

    The pressure at any point in a nonflowing fluid has a single value, independent of direction.

In a fluid with shear stresses, the pressure is not necessarily independent of direction.
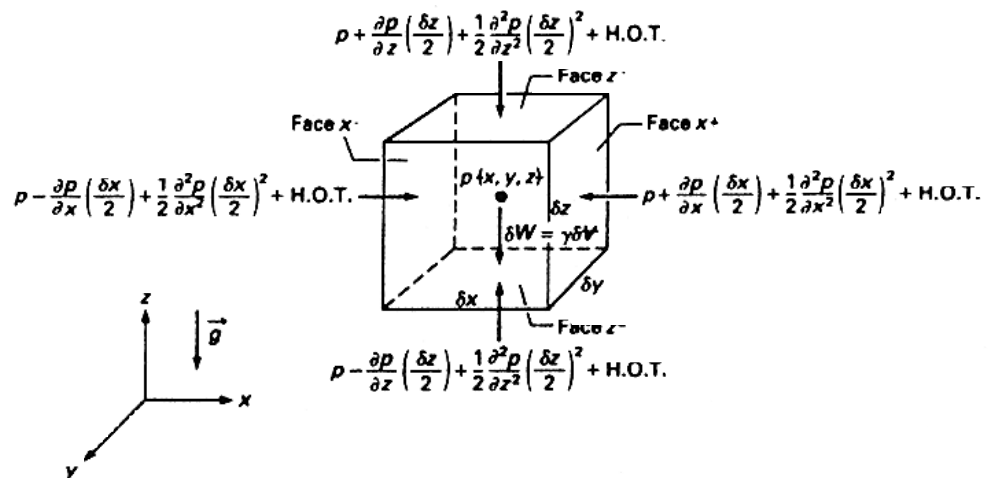
3.2   Pressure variation in a static fluid

Even though the pressure at a point is the same in all directions in a static fluid, the pressure may vary from point to point. To evaluate the pressure variation let's examine a cubical fluid element at rest (Fig. 3.1) of volume

$$\delta V = \delta x \delta y \delta z$$

Fig 3.1:
Cubic fluid element in a static fluid

The pressure at the centre of the element is p. We assume that the pressure does not vary in y direction. As the fluid is continuous, we can express the pressure at the faces of the element $\pm\delta x/2$ and $\pm\delta z/2$ from the centre by Taylor series:

$$P_{z+} = p \ + \frac{\partial p}{\partial z}\left(\frac{\delta z}{2}\right) + \frac{1}{2}\frac{\partial^2 p}{\partial z^2}\left(\frac{\delta z}{2}\right)^2 + \text{H.O.T.}$$

$$P_{z-} = p \ - \frac{\partial p}{\partial z}\left(\frac{\delta z}{2}\right) + \frac{1}{2}\frac{\partial^2 p}{\partial z^2}\left(\frac{\delta z}{2}\right)^2 + \text{H.O.T.}$$

$$P_{x+} = p \ + \frac{\partial p}{\partial x}\left(\frac{\delta x}{2}\right) + \frac{1}{2}\frac{\partial^2 p}{\partial x^2}\left(\frac{\delta x}{2}\right)^2 + \text{H.O.T.}$$

$$P_{x-} = p \ - \frac{\partial p}{\partial x}\left(\frac{\delta x}{2}\right) + \frac{1}{2}\frac{\partial^2 p}{\partial x^2}\left(\frac{\delta x}{2}\right)^2 + \text{H.O.T.}$$

H.O.T. represents "high order terms" involving δz and δx. The fluid element is at rest, so

$$\Sigma\ F_x = p_{x-}\delta z\delta y - p_{x+}\delta z\delta y = 0$$
$$\Sigma\ F_z = p_{z-}\delta z\delta y - p_{z+}\delta z\delta y - \gamma\,\delta x\delta z\delta y = 0$$

Substituting the series expressions for the pressures and combining and cancelling terms where possible, we get

$$\left(-\frac{\partial p}{\partial x} + \text{H.O.T.}\right)\delta x\delta z\delta y = 0$$

$$\left(-\frac{\partial p}{\partial x} - \gamma + \text{H.O.T.}\right)\delta x\delta z\delta y = 0$$

We now divide by $\delta x\delta z\delta y$, and then take the limit as δx, δy, and δz approach zero. The higher order terms contain positive powers of δx and δz, so they vanish as we pass to the limit. Our equations become

$$\frac{\partial p}{\partial x} = 0$$

$$\frac{\partial p}{\partial z} + \gamma\ = 0$$

The first equation shows that the pressure does not vary in a horizontal plane. The second equation shows that the pressure increases if we go "down" and decreases if we go "up". Because the pressure changes in only one direction, we can replace the partial derivative with an ordinary derivative:

$$\frac{dp}{dz} = -\gamma$$

This is the basic equation of fluid statics.

3.2.1   Pressure variation in a constant-density fluid

If the specific weight of the fluid is constant (as in a liquid), we can easily integrate the above equation

$p\ (z) = -\gamma z + p_0$

where p_0 is the pressure at $z = 0$. Consider a body of liquid with a free surface, as shown in Fig. 3.2. The free surface is at constant pressure, so it is horizontal.

We introduce the depth of the liquid, h, measured downward from the free surface. As z = -h, we can write

$$p(h) = p_0 + \gamma h$$

The pressure distribution implied by this equation is called a hydrostatic pressure distribution. The term γh is called the hydrostatic pressure.

Fig. 3.2:

Body of liquid with a free surface.
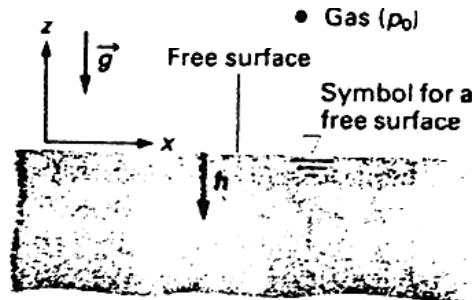
Example:

Calculation of pressure in a static liquid

The tank of water shown in Fig. 3.3 has a 3-m column of gasoline (S = 0.73) above it. Find the pressure on the bottom of the tank. The atmospheric pressure is 101 kPa.

Fig. 3.3:

Tank of water with column of gasoline.
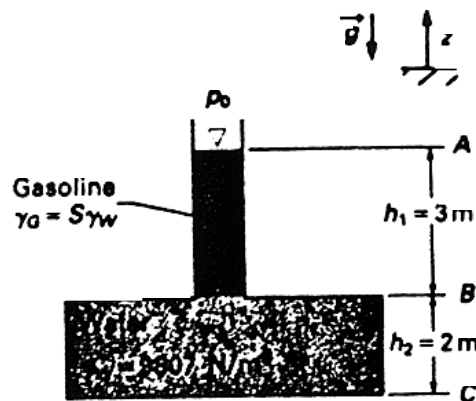
We use the letters A, B, and C to represent the top of the gasoline, the interface between the gasoline and the water, and the bottom of the tank, respectively.

$$p_B = p_A + \gamma_G h_1 \quad \text{and} \quad p_C = p_B + \gamma_W h_2$$

Substituting the first equation into the second and setting $p_A = p_0$, we have

$$p_C = p_0 + \gamma_G h_1 + \gamma_W h_2$$

The specific weight of gasoline is $\gamma_G = S\gamma_W$, so
$$p_C = p_0 + \gamma_W (Sh_1 + h_2)$$
Substituting numerical values, we obtain
$$p_C = 101\ kPa + 9807\ N/m^3\ [0.73\ (3) + 2\ ]\ m = 142\ kPa$$

3.3 Pressure forces on surfaces

When a surface is in contact with a fluid, fluid pressure exerts a force on the surface. This force is distributed over the surface; it is often helpful to replace the distributed force by a single resultant. To completely specify the resultant force, we must determine its magnitude, direction, and point of application. As

$$p = \frac{dF_n}{dA}$$

we can find the resultant force by integration:

$$F_n = \int pdA$$

In general, we have to overcome two difficulties in performing this calculation.

1   The pressure and area must be expressed in terms of a common variable to permit integration.
2   If the surface is curved, the normal direction varies from point to point on the surface, and F_n is meaningless because no single "normal" direction characterizes the entire surface. In this case, the force at each point on the surface must be resolved into components and then each component integrated.

3.4 Buoyancy

When a body is either fully or partially submerged in a fluid, a net upward force called the buoyant force acts on the body. This force is caused by the imbalance of pressures on the upper and lower surfaces. Figure 3.4 shows a body submerged in a fluid.

Fig. 3.4:
Arbitrary closed body submerged in fluid.
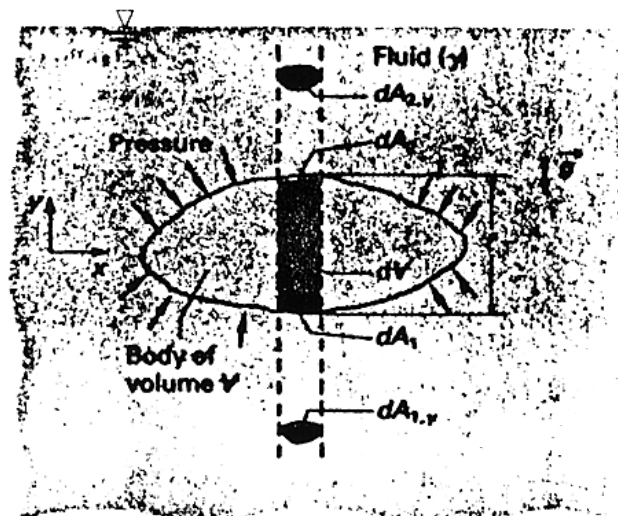
The net pressure force on the lower (dA_1) and upper (dA_2) area is

$dF = p_1 d A_{1,y} - p_2 d A_{2,y}$

The vertical projections of dA1 and dA2 are equal, so

$dF =(p_1 - p_2) d A_y = \gamma l d A_{2,y}$

Integrating, we obtain

$$F = \int \gamma l dA_y = \gamma V$$

This equation shows that:

The buoyant force on a body submerged in a fluid is equal to the weight of the fluid displaced by the body.

We can also show that:

The line of action of the buoyant force passes through the centroid of the displaced volume. This centroid is called the centre of buoyancy.

This is Archimedes' first principle of buoyancy.

These principles also apply if the body is only partly submerged. A body will float if its average density is less than the density of the fluid in which it is placed. For a floating body (Fig. 3.5), the weight is

$W = \gamma_f V_s$

where γ_f is the specific weight of the fluid and V_s is the submerged volume. That is:

A floating body displaces a volume of fluid equivalent to its own weight.

This is Archimedes' second principle of buoyancy.

Fig. 3.5:
Floating body.
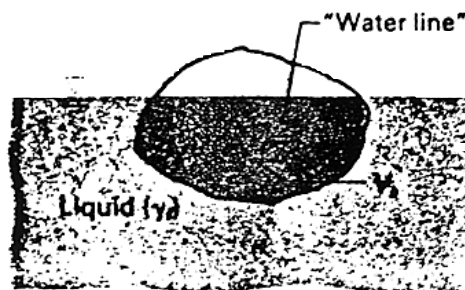
An application of the principles of buoyancy is the use of a hydrometer to measure the specific gravity of a liquid. Figure 3.6 illustrates a hydrometer floating in pure water (S = 1.0) and in another liquid (S > 1.0).

Fig. 3.6:
Hydrometer in two liquids:
(a) water, S=1.0; (b) other liquid S>0.
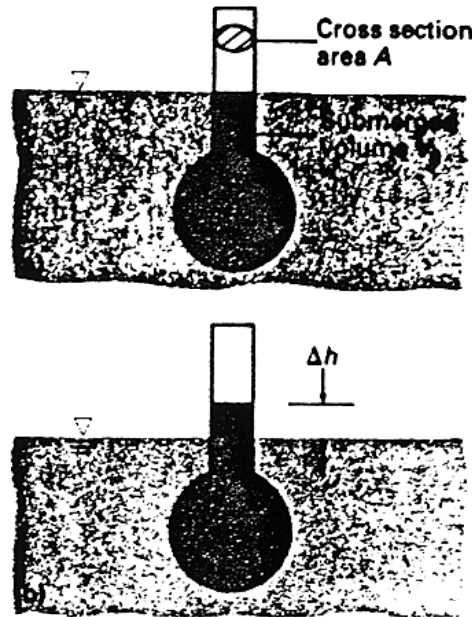
If S > 1.0, the buoyant force per unit of submerged volume is greater, so less volume of submergence is necessary to balance the hydrometer's weight. In water,

$$W = \gamma_{H2O} V_0$$

but in the other fluid,

$$W = S\gamma_{H2O} (V_0 - Ah)$$

Therefore

$$h = \frac{V_0}{A}\left(1 - \frac{1}{S}\right)$$

4 The Finite Control Volume Approach to Flow Analysis

4.1 The field concept: Lagrangian versus Eulerian descriptions

Let's consider two of the flows illustrated in Figs. 4.1 and 4.2: the flow of water in a pipe and the flow of air around a moving automobile. In the pipe flow, the fluid is confined within the pipe; in the flow around the automobile, the entire atmosphere is the fluid of interest. In both cases, however, the fluid is continuous. A tiny mass, which we call a fluid particle, exists at each point in the fluid region.

Fig. 4.1:

Typical examples of internal flows.
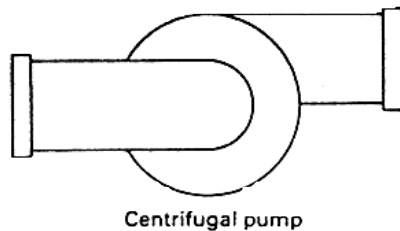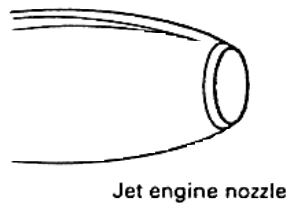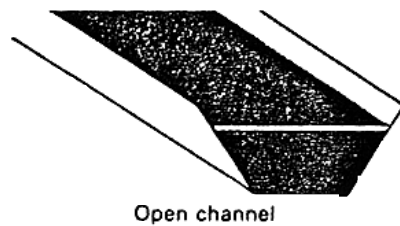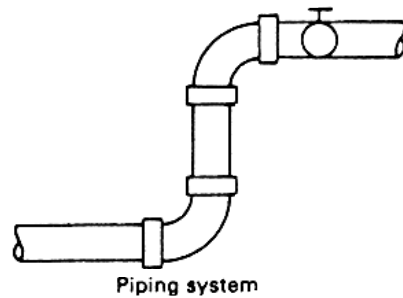
Fig. 4.2:

Typical examples of external flows.

Piping system

Open channel

Jet engine nozzle

Centrifugal pump

Wind blowing over building

Flying airplane

Sailboat

Moving automobile
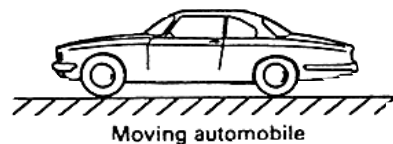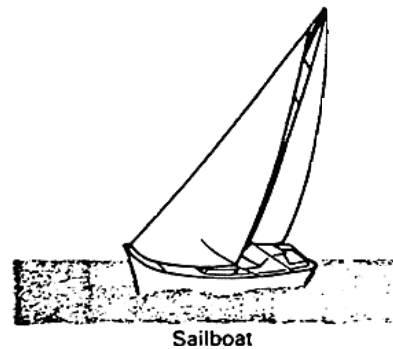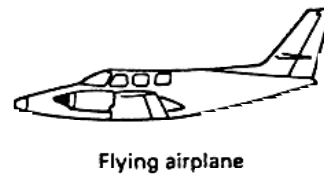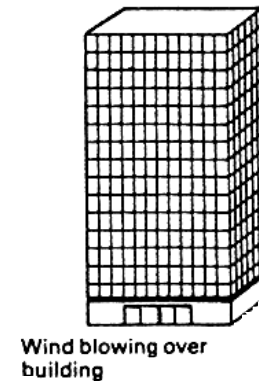
We define the velocity of a fluid particle as the velocity of the particle's centre of mass.

$$\vec{v} = u\vec{i} + v\vec{j} + w\vec{k}$$

A complete description of fluid motion requires specification of the velocity, pressure, and so on of all particles at all times. As a fluid is continuous, we can specify those characteristics only by mathematical functions that express the velocity and fluid properties for all particles at all times. Such a representation is called a **field representation**, and the dependent variables (such as velocity and pressure) are called **field variables**. The fluid region of interest (the water in the pipe or the air around the automobile) is called the **flow field**.

To describe a flow field, we can adopt either of two approaches. The first approach, called the **Lagrangian description**, identifies each particle and describes what happens to it over time. Mathematically we write fluid velocity as

$$\overrightarrow{v} = \overrightarrow{v} \text{ (particle identity, t)}$$

The second approach, called Eulerian description, focuses attention on a particular point (or region) in space and describes happenings at that point (or within and on the boundaries of the region) over time. The properties of a fluid particle depend on the location of the particle in space and time. Mathematically, we express the velocity field as

$$\overrightarrow{v} = \overrightarrow{v} \text{ (x, y, z, t)}$$

In this section, we develop the finite control volume approach. It ignores the details of a particular flow and gives relations between various gross features of the flow such as flow rate and force. The finite control volume approach is a very important tool for flow analysis. Like any other single tool, it will not solve every flow problem, but it is frequently the best tool available.

4.2   The fundamental laws

Experience has shown that all fluid motion must be consistent with the following fundamental laws of nature.

- **The law of conservation of mass**. Mass can be neither created nor destroyed; it can only be transported or stored.
- **Newton's three laws of motion**.
1. A mass remains in a state of equilibrium, that is, at rest or moving at constant velocity, unless acted on by an unbalanced force. (First law)
2. The rate of change of momentum of a mass is proportional to the net force acting on the mass. (Second law)
3. Any force action has an equal (in magnitude) and opposite (in direction) force reaction. (Third law)

- **The first law of thermodynamics** (law of conservation of energy). Energy, like mass, can be neither created nor destroyed. Energy can be transported, changed in form, or stored.
- **The second law of thermodynamics.** The second law deals with the availability of energy to perform useful work. The only possible natural processes are those that either decrease or, in the ideal case, maintain, the availability of the energy of the universe. The science of thermodynamics defines a material property called entropy, which quantifies the second law. The entropy of the universe must increase or, in the ideal case, remain constant in all natural processes.
- **The state postulate (law of property relations)**. The various properties of a fluid are related. If a certain minimum number (usually two) of a fluid's properties are specified, the remainder of the properties can be determined.

The important thing to remember about these laws is that they apply to all flows. In addition to these universal laws, several less fundamental "laws" apply in

restricted circumstances. An example is Newton's law of viscosity.

The shear stress in a fluid is proportional to the rate of deformation of the fluid.

This "law" is true only for some fluids and does not apply at all to solids. Such "laws" are better termed constitutive relations.

4.3 The transport theorem

The transport theorem is a mathematical expression that connects the system and control volume points of view for a global or finite control volume approach to flow analysis. It provides a way to identify a finite system and to evaluate the rate of change of any property or characteristic of that system by examining the flow through a control volume.

The fundamental laws deal with rates of change of certain properties of the system to which they are applied. In order to apply these laws, we have to figure out how to identify a specific system in a moving, deforming fluid and how to calculate the rate of change of this system's properties. This is where a control volume comes in. We designate our system as **the fluid mass that instantaneously occupies the control volume**. Figure 4.3 shows a three-dimensional, three-directional flow field with a control volume superimposed. The mass contained in the control volume at the instant that the figure represents is chosen as a system.

Fig. 4.3:
Control volume and enclosed system in a flow field.
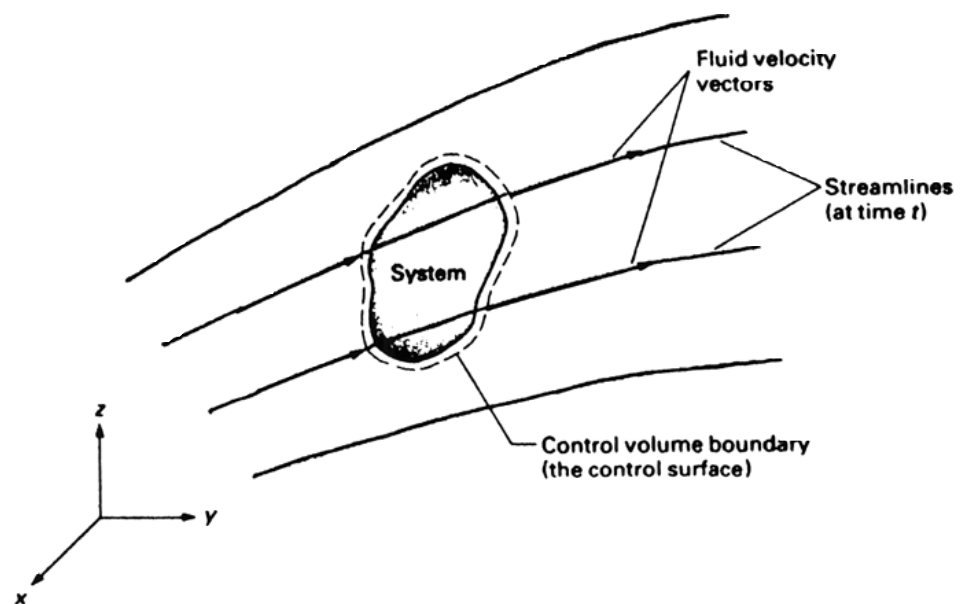
Figure 4.4 shows the passage of that system out of the control volume over time.

Fig. 4.4:
A system flows through a control volume.
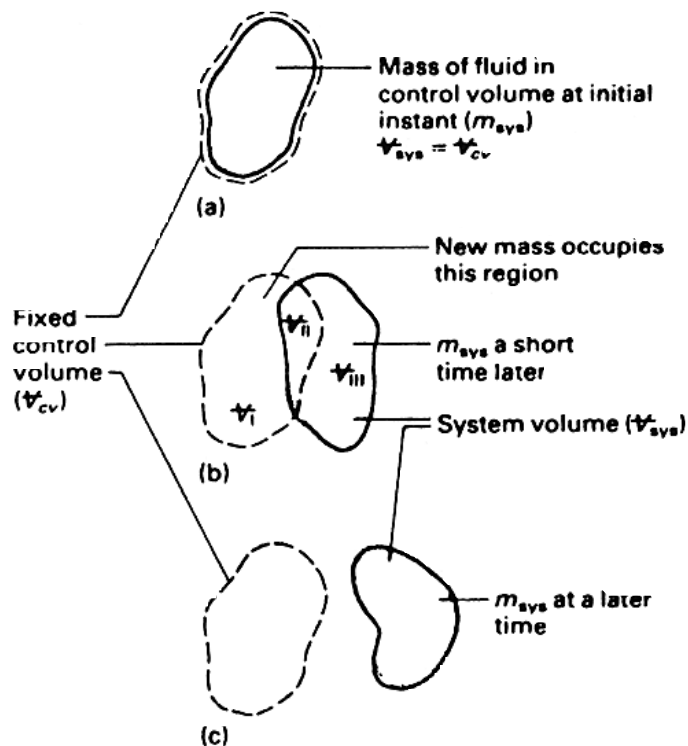
Figure 4.4(a) shows the situation at time t, when the system exactly fills the control volume. Figure 4.4(b) shows the situation at a later time, $t + \delta t$, when a portion of the system has left the control volume: V_I is the portion of the control volume that has been vacated by the system in time δt; V_{II} is the portion of the control volume that contained part of the system at time t and still contains part of the system at time $t + \delta t$; and V_{III} lies outside the control volume and contains the portion of the system that has left the control volume in time δt.

We can calculate the rate of change of an arbitrary property B of this system; B could be momentum, energy, or any other property. Property B may be non-uniformly distributed throughout the system, so we let b be the specific (per-unit-mass) property.

$$\frac{dB_{sys}}{dt} = \frac{d}{dt} \int_{V_{cv}} \rho \, b \, d V \; + \dot{B}_{out} - \dot{B}_{in}$$

In words:
> The rate of change of any property of the system that occupies a control volume at any particular instant is equal to the instantaneous rate of accumulation of the property inside the control volume plus the difference between the instantaneous rates of outflow and inflow of the property. This latter term is the net rate of outflow of the property across the control surface.

The transport theorem can also be written in the following vector form. Figure 4.5 illustrates a portion of the control surface through which mass enters the control volume. Figure 4.5(a) shows the velocity vector $\vec{v}$ and the unit outward normal vector n at the area dA at time t. Figure 4.5(b) shows the situation at time t + δt.

Fig. 4.5:
Details of inflow through a small piece of control surface.
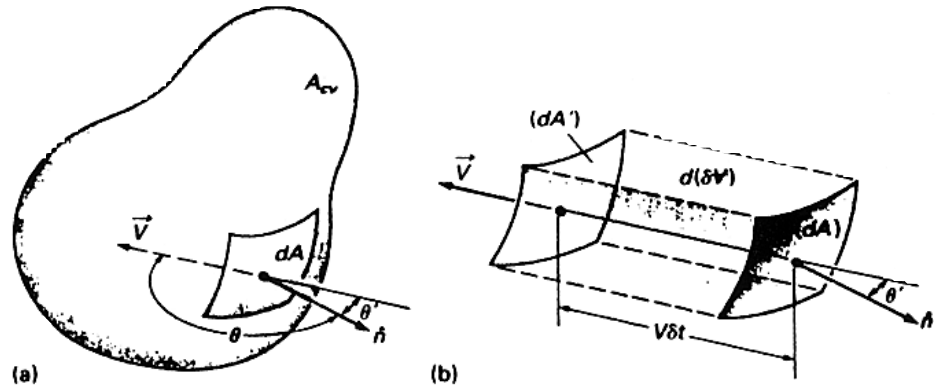
$$\frac{dB_{sys}}{dt} = \frac{d}{dt}\int_{V_{cv}} \rho\, b\, dV + \int_{A_{out}} \rho\, b\, v\cos\theta\, dA + \int_{A_{in}} \rho\, b\, v\cos\theta\, dA$$

$$\frac{dB_{sys}}{dt} = \frac{d}{dt}\int_{V_{cv}} \rho\, b\, dV + \int_{A_{out}} \rho\, b\, v_n\, dA - \int_{A_{in}} \rho\, b\, v_n\, dA$$

and

$$\frac{dB_{sys}}{dt} = \frac{d}{dt}\int_{V_{cv}} \rho\, b\, dV + \oint_{A_{cv}} \rho\, b\left(\vec{v}\hat{n}\right) dA$$

$\vec{v}\hat{n}$ represents the velocity component normal to the control surface. Each of the fundamental laws, when combined with the transport theorem, produces a specific equation. The law of conservation of mass produces the **continuity equation**, the law of conservation of energy produces the **energy equation**, and Newton's second law of motion produces the **momentum equation**.

4.4 The continuity equation

For generality, we consider a three-dimensional, three directional, unsteady flow field. A control volume is superimposed on the flow as shown in Fig. 4.6.

Fig. 4.6:
Flow field with control volume for continuity equation.
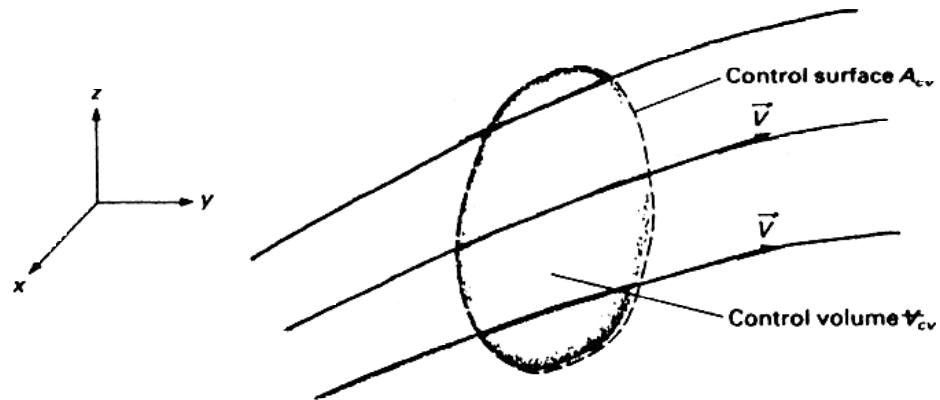
Combining the law of conservation of mass with the transport theorem, we get the continuity equation:

$$\frac{d}{dt} \int_{V_{cv}} \rho \, dV + \oint_{A_{cv}} \rho \left(\vec{v}_r \cdot \hat{n} \right) dA = 0$$

This equation expresses the principle of conservation of mass for a control volume. Recalling that the first term of the transport theorem represents accumulation (storage) of a quantity within the control volume and that the remaining terms represent outflow and inflow of the quantity, we write the continuity equation in words as follows:

$$\begin{bmatrix} \text{Rate of Accumulation} \\ \text{of mass inside} \\ \text{the control volume} \end{bmatrix} + \begin{bmatrix} \text{Rate of mass flow} \\ \text{leaving the} \\ \text{control volume} \end{bmatrix} - \begin{bmatrix} \text{Rate of mass flow} \\ \text{entering the} \\ \text{control volume} \end{bmatrix} = 0$$

In symbolic terms,

$$\frac{dm_{cv}}{dt} + \Sigma \dot{m}_{out} - \Sigma \dot{m}_{in} = 0$$

where m_{cv} is the mass contained in the control volume and $\dot{m}$ is the mass flow rate crossing the control surface.

Example:
Illustration of the continuity equation
A constant-density fluid flows in the converging, two dimensional channel shown in Fig. 4.7. Show that the flow field satisfies the continuity equation.

Fig. 4.7:
Control volume for converging two-dimensional channel.
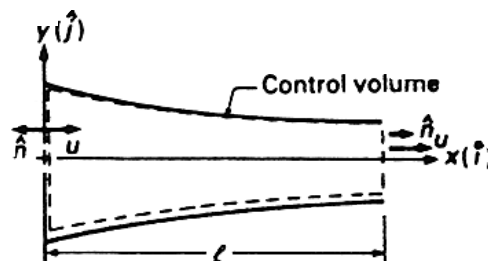
$$Y = \frac{Y_0}{1 + \frac{x}{l}} \quad \text{and} \quad u = u_0 \left(1 + \frac{x}{l}\right)\left[1 - \left(\frac{y}{Y}\right)^2\right]$$

Because the flow is steady and ρ is constant we have to show that

$$\oint_{A_{cv}} \left(\vec{v}_r \cdot \hat{n}\right) dA = 0$$

For the control volume shown in Fig. 4.7, $\vec{v}_r \cdot \hat{n} = 0$ along the walls of the channel, because u = v = 0 at the wall. The flow is two-directional, so

$$\vec{v}_r = u\hat{i} + v\hat{j}$$

At the outlet plane, the unit outward normal vector is + î. At the inlet plane, the unit outward normal vector is - î.

$$\oint_{A_{cv}} \left(\vec{v}_r \cdot \hat{n}\right) dA$$
$$= \int_{A_{out}} \left(u\hat{i} + v\hat{j}\right)\cdot\left(\hat{i}\right) dA + \int_{A_{in}} \left(u\hat{i} + v\hat{j}\right)\cdot\left(-\hat{i}\right) dA$$
$$= \int_{A_{out}} u\, dA - \int_{A_{in}} u\, dA$$

Substituting for u at the exit, we have

$$\int_{A_{out}} u\, dA = Wu_0 \int_{-Y_l}^{+Y_l} 2\left[1 - \frac{y}{Y_l}\right] dy$$

where Y_1 is the magnitude of the channel half-height at x = l and W is the width of the channel (perpendicular to the paper). Integrating, we have

$$\int_{A_{out}} u\, dA = \frac{8Wu_0 Y_l}{3}$$

As Y_1 = 0.5 m and u_0 = 1.0 m/s,

$$\int_{A_{out}} u\, dA = \frac{4}{3}W$$

Similarly,

$$\int_{A_{in}} u\, dA = Wu_0 \int_{-Y_0}^{+Y_0} 2\left[1 - \left(\frac{y}{Y_0}\right)\right] dy$$

where Y_0 is the magnitude of the channel half-height at x = 0. Integrating, we obtain

$$\int_{A_{in}} u\, dA = \frac{4Wu_0 Y_0}{3}$$

as Y_0 = 1.0 m and u_0 = 1.0 m/s

$$\int_{A_{in}} u\, dA = \frac{4}{3}W$$

Then

$$\oint_{A_{cv}} \left(\vec{v}_r \cdot \hat{n} \right) dA = \frac{4}{3}W - \frac{4}{3}W = 0$$

4.5   Derivation of the general energy equation

We obtain the general energy equation by combining the transport theorem with the law of conservation of energy. Because energy is conserved, we can write

$$\left[\begin{array}{c} \text{Rate of change of the} \\ \text{energy of a system} \end{array} \right] = \left[\begin{array}{c} \text{Net rate of transfer of} \\ \text{energy to the system} \end{array} \right]$$

Energy is transferred to a system by two different processes heat (Q) and work (W). Intrinsic energy is energy stored in a system (that is, energy contained in the system's mass). There are five forms of intrinsic energy:
1. kinetic energy,
2. potential energy,
3. internal energy,
4 chemical energy, and
5. nuclear energy.

In many problems in fluid mechanics, chemical and nuclear reactions are absent; accordingly, we neglect chemical and nuclear energies in subsequent discussions. We often deal with specific energy, which is energy per unit mass. Specific kinetic energy is $v^2/2$. Specific potential energy is gz. Specific internal energy $\tilde{u}$ is a property that depends only on other specific properties, primarily temperature. For later discussion, we classify various energies as either thermal or mechanical. Using these concepts, the energy balance can be written.

$$\left[\begin{array}{c} \text{Rate of} \\ \text{heat transfer} \\ \text{to system} \end{array} \right] + \left[\begin{array}{c} \text{Rate of work} \\ \text{done on} \\ \text{system} \end{array} \right] = \left[\begin{array}{c} \text{Rate of increase of intrinsic} \\ \text{(kinetic + potential + internal)} \\ \text{energy of system} \end{array} \right]$$

If we neglect electrical and other equivalent forms of work, three types of work might be done on or by the fluid inside the control volume, as shown in Fig. 4.8.
- Shaft work (W_{shaft}) is transmitted by a rotating shaft, such as a pump drive shaft.
- Shear work (W_{shear}) is done by shear stresses in the fluid acting on the boundaries of the control volume.
- Pressure work ($W_{pressure}$) is done by fluid pressure acting on the boundaries of the control volume.

Fig. 4.8:

Various forms of work exchange with moving fluid.
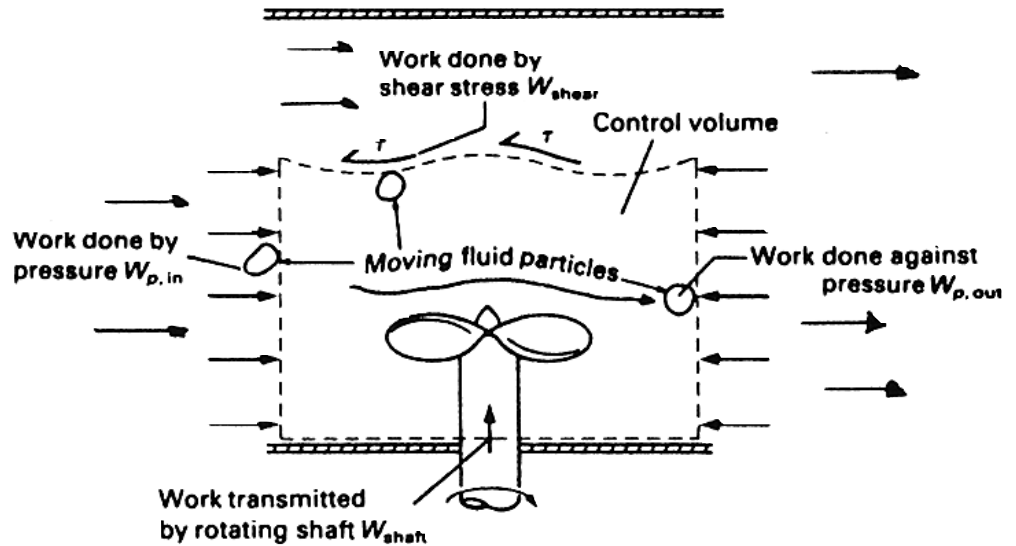
We usually find it convenient to combine $\dot{W}_{Shaft}$ and $\dot{W}_{Shear}$ into a single work $\dot{W}_S$ which is the work done on the fluid inside the control volume by forces other than those resulting from pressure.

We classify work done by pressure acting at the control volume boundary as either flow work or work of (control volume) deformation. We must always include flow work in the energy equation for moving fluids. Work of deformation occurs only if we select a deforming control volume.

We develop an expression for flow work by examining outflow and inflow for a control volume (Fig. 4.9). The total rate of flow work is

$$\dot{W}_{flow} = \oint_{A_{cv}} p \left(\vec{v}_r \cdot \hat{n} \right) dA$$

$\vec{v}_r$ is the velocity relative to the control surface.

Fig. 4.9:

Detail of flow outward from control volume for calculation of pressure work.
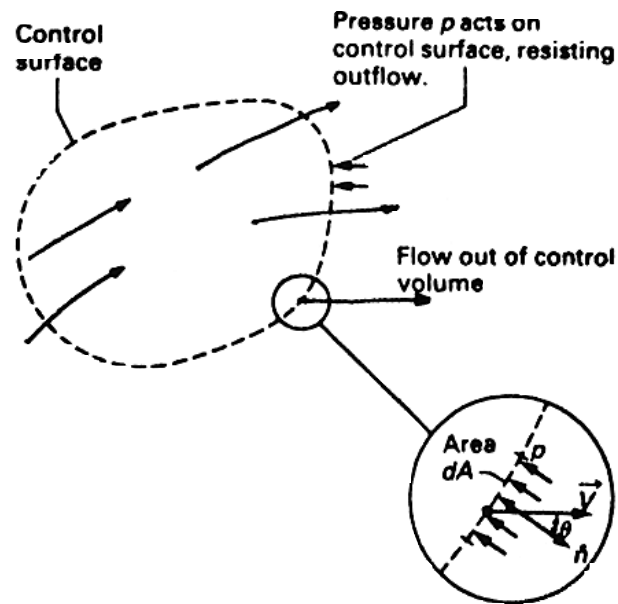
Work of deformation (W_D) occurs if the control volume is deforming. This work is the product of the pressure acting on the control surface and the displacement of the control surface. The rate of work is the product of pressure and the velocity of the control surface $\vec{v}_c$

$$\dot{W}_D = \oint_{A_{cv}} p\left(\vec{v}_c \cdot \hat{n}\right) dA$$

The general energy equation can be written

$$\dot{Q} - \dot{W}_s - \oint_{A_{cv}} p\left(\vec{v}_c \cdot \hat{n}\right) dA = \frac{d}{dt} \int_{V_{cv}} \rho\left(\tilde{u} + \frac{v^2}{2} + gz\right) dV$$

$$+ \oint_{A_{cv}} \rho\left(\tilde{u} + \frac{p}{\rho} + \frac{v^2}{2} + gz\right)\left(\vec{v}_r \cdot \hat{n}\right) dA$$

4.5.1 Some simplified forms of the general energy equation

Steady flow, fixed, rigid control volume. A great many applications involve steady flow through a fixed, rigid control volume. The general equation reduces to:

$$\dot{Q} - \dot{W}_s = \oint_{A_{cv}} \rho\left(\tilde{u} + \frac{p}{\rho} + \frac{v^2}{2} + gz\right)\left(\vec{v}_r \cdot \hat{n}\right) dA$$

A common simplification is the assumption that the control volume has uniform inflow and outflow at a finite number of inlets and outlets (see Fig. 4.10).

Fig. 4.10:

Apparatus with several inlets and outlets.
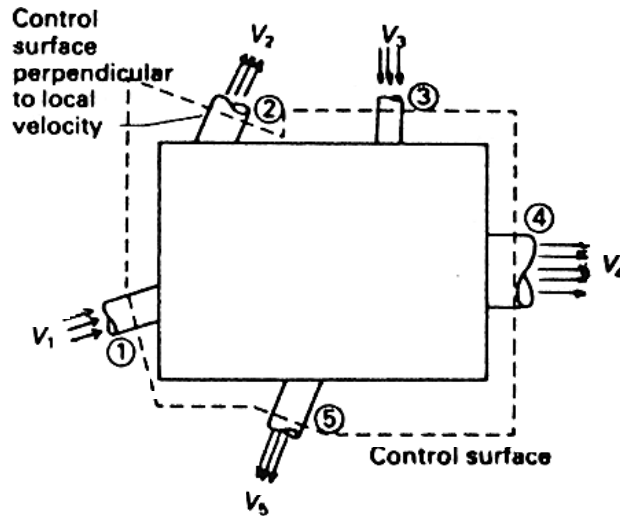
If we assume that the control volume is fixed and rigid, the general energy equation is:

$$\dot{Q} - \dot{W}_s = \frac{\partial}{\partial t} \int_{V_{cv}} \rho \left(\tilde{u} \frac{v^2}{2} + gz \right) dV$$

$$+ \sum_{out} \left(\rho A v_n \right) \left(\tilde{u} + \frac{p}{\rho} + \frac{v^2}{2} + gz \right)$$

$$- \sum_{in} \left(\rho A v_n \right) \left(\tilde{u} + \frac{p}{\rho} + \frac{v^2}{2} + gz \right)$$

Energy equation for a streamline. Figure 4.11(a) shows a single streamline in a steady flow, and Fig. 4.11(b) shows a small streamtube that surrounds the streamline.

Fig. 4.11:

Flow along streamlines.
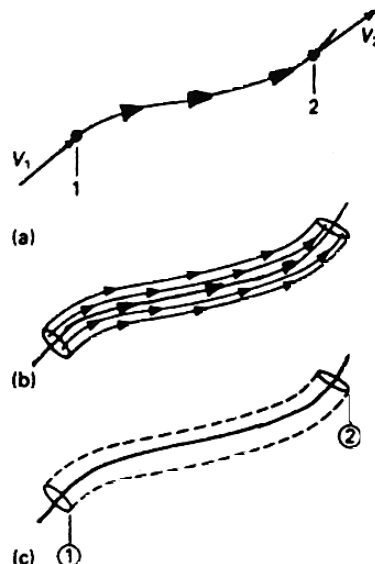
There is no velocity component perpendicular to the walls of a streamtube, so fluid enters or leaves only at the ends. We select a control volume that is coincident with the streamtube and perpendicular to the central streamline at the ends. The flow is one-dimensional and one-directional. Thus, the steady-flow general energy equation along a streamline is

$$q - w_s = (\tilde{u}_2 - \tilde{u}_1) + \left(\frac{p_2}{\rho_2} - \frac{p_1}{\rho_1}\right) + \left(\frac{v_2^2}{2} - \frac{v_1^2}{2}\right) + (gz_2 - gz_1)$$

4.5.2   The mechanical energy equation

The general energy equation is not as widely used in fluid mechanics as you might expect. Instead, the mechanical energy equation, which is a special form of the energy equation, is often used, especially for incompressible fluid flows. Let's consider steady flow along a streamline. The fluid may be compressible or incompressible, and we consider both mechanical and thermal forms of energy. After rearranging the energy equation for a streamline and taking the integral along the streamline (this evaluation requires the knowledge of the process experienced by a fluid particle as it travels from point 1 to point 2), the energy equation for steady flow along a streamline is

$$-w_s - \int_1^2 \frac{dp}{\rho} - gh_L = \left(\frac{v_2^2}{2} + gz_2\right) + \left(\frac{v_1^2}{2} + gz_1\right)$$

with,

$$gh_L \equiv \left[\tilde{u}_2 - \tilde{u}_1 - q + \int_1^2 pdv\right]$$

This single term has the following characteristics:
-    gh_L is always positive or zero (a process with gh_L negative would violate the second law of thermodynamics),
-    gh_L represents the loss of potential to perform useful work, and
-    gh_L is zero only in an ideal process.

4.5.3   Bernoulli's equation

We consider a single streamline in a steady, incompressible flow. The flow may be internal or external, as shown in Fig. 4.12.

Fig. 4.12:
Two points 1 and 2 on the same streamline.

(a)   **(b)**
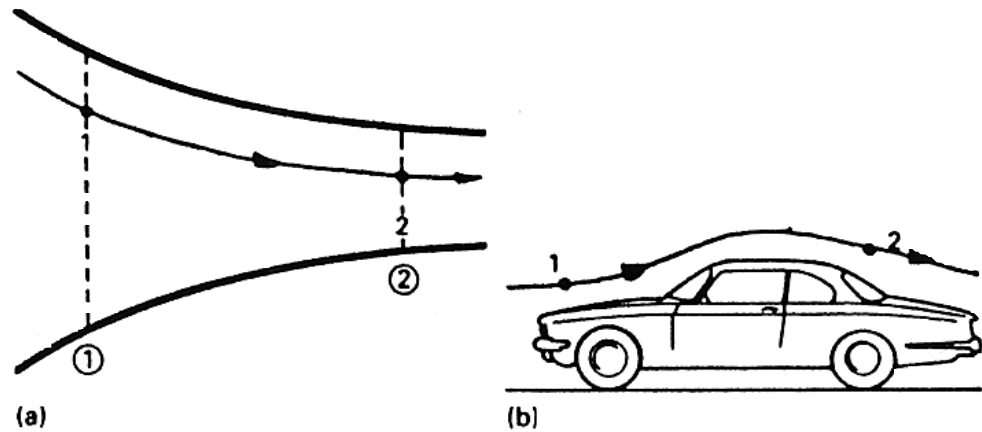
We apply the mechanical energy equation between two points on the streamline and we assume that the flow is frictionless (inviscid) and that there is no shaft or shear work. Then

$$\frac{p_1}{\rho} + \frac{v_1^2}{2} + gz_1 = \frac{p_2}{\rho} + \frac{v_2^2}{2} + gz_2$$

As points 1 and 2 are arbitrary, the sum of the three terms is the same for any point on the streamline. Thus an alternate form of the equation is

$$\frac{p}{\rho} + \frac{v^2}{2} + gz = \text{Constant}$$

Bernoulli's equation is probably the simplest form of the energy equation. It tells us that the fluid's mechanical energy, measured by gravitational potential energy, kinetic energy, and pressure, is constant if there is no external work or shear stress. If the flow is incompressible, heat transfer has no effect on Bernoulli's equation.

4.6   The momentum equation

Together with the continuity and energy equations, the momentum equation is one of the cornerstones of the control volume approach. The following are the main differences between the momentum equation and the continuity and energy equations:
- The momentum equation deals with vector quantities (force and momentum), whereas the continuity and energy equations deal with scalar quantities.
- The continuity and energy equations deal with quantities that are conserved (mass and energy), whereas the momentum equation deals with a balance between entities that are not conserved (force and momentum).

We obtain the momentum equation by combining the transport theorem with Newton's second law of motion for a system. Figure 4.13 shows a flow field that includes a solid object in contact with a moving fluid and a control volume of arbitrary shape superimposed on the flow field.

Fig. 4.13:
Flow field with solid object and superimposed control volume.
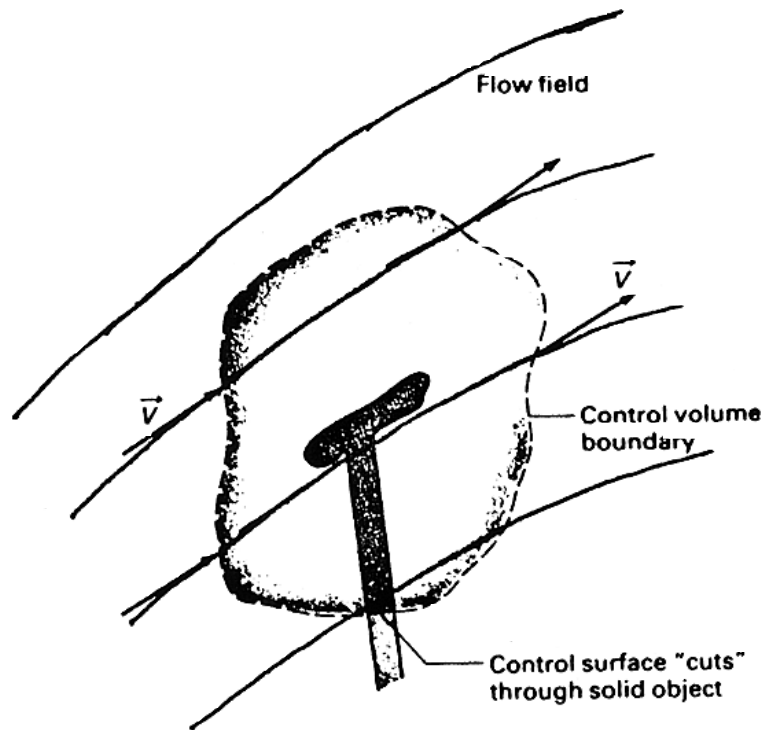
Newton's second law for this system is

$$\frac{d\vec{M}_{sys}}{dt} = \Sigma \vec{F}_{sys}$$

where $\vec{M}_{sys}$ is the system momentum,

$$\vec{M}_{sys} = \int_{V_{sys}} \rho \vec{v} \, dV$$

and $\Sigma \vec{F}_{sys}$ is the sum of the forces acting on the system. To use the transport theorem, we first note that the property B is the momentum, and that the per-unit mass property is the velocity.

$$\frac{d}{dt}\int_{V_{cv}} \rho \, \vec{v} \, dV + \oint_{A_{cv}} \rho \, \vec{v} \left(\vec{v}_r \cdot \hat{n} \right) dA = \Sigma \vec{F}$$

$$\frac{d}{dt}\int_{V_{cv}} \rho \, \vec{v} \, dV + \int_{A_{out}} \rho \, \vec{v} \left(v_n \right) dA - \int_{A_{in}} \rho \, \vec{v} \left(v_n \right) dA = \Sigma \vec{F}$$

Either of these equations may be called the momentum equation. The following verbal expression is the linear momentum theorem:

$$\begin{bmatrix} \text{Rate of} \\ \text{Accumulation} \\ \text{of momentum} \\ \text{inside the} \\ \text{control volume} \end{bmatrix} + \begin{bmatrix} \text{Rate of} \\ \text{momentum} \\ \text{flow leaving} \\ \text{the control} \\ \text{volume} \end{bmatrix} - \begin{bmatrix} \text{Rate of} \\ \text{momentum} \\ \text{flow entering} \\ \text{the control} \\ \text{volume} \end{bmatrix} = \begin{bmatrix} \text{Sum of} \\ \text{forces on the} \\ \text{mass inside} \\ \text{the control} \\ \text{volume} \end{bmatrix}$$

The momentum equation has three important characteristics.

- The velocity $\vec{v}$ represents the momentum and must be measured relative to an inertial reference. The velocity $\vec{v}_r$ or v_n represents the flow rate passing through the control surface and must be measured relative to the control surface.

- $\Sigma\vec{F}$ is the vector sum of all forces acting on the mass within the control volume. Forces from all sources (gravitational, pressure, magnetic, etc.) are included.

- The momentum equation is a vector equation. As such, it represents three separate component (x, y, z or r, θ, x etc.) equations.

Example:
Calculation of the force terms for the momentum equation
Lubricating oil at 20 °C flows upward through a vertical pipe with an inside diameter of 2.0 cm and a length of 1.0 m. The axial velocity profile is

$$u = u_{max}\left[1-\left(\frac{r}{R}\right)^2\right]$$

where R is the pipe radius and u_{max} = 1.0 m/s and is identical at each cross section. For the control volume shown in Fig. 4.14, find the net force acting on the fluid.

Fig. 4.14:
Flow of oil upward through a vertical pipe.
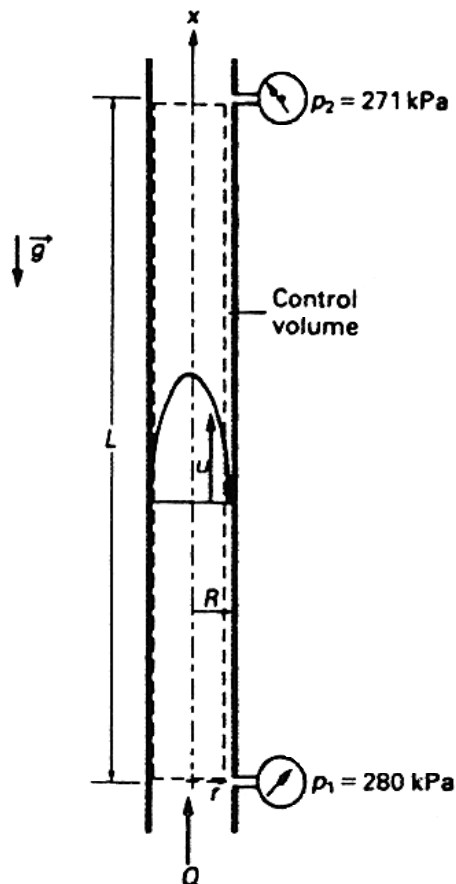
In this problem, we are concerned with the force in the axial direction, ΣF_x. This force consists of
- pressure force $(F_x)_p$,
- shear force $(F_x)_s$ and
- gravity force $(F_x)_g$.

The pressure force is

$$(F_x)_p = \int_{A_{in}} p\,dA - \int_{A_{out}} p\,dA$$

We assume that the pressure is uniform over each horizontal plane, as the pressure force is

$$(F_x)_p = \frac{(p_1 - p_2)\pi D^2}{4} = 2.83\ N$$

The shear force is

$$(F_x)_s = \int_{A_w} \tau_w\,dA$$

because the oil is a Newtonian fluid

$$\tau_w = \mu \left(\frac{du}{dr}\right)_{r=R}$$

Substituting for u and for τ_w
$$(F_x)_s = -4\pi\,u_{max}\,L = -\,0.16N$$

with $\mu = 1.31 \times 10^{-2}\ N\bullet s/m^2$

The gravity force is

$$(F_x)_g = -\int_{V_{ev}} \gamma\,dV = -\gamma\,V_{cv}$$

where γ is the specific weight and $V_{cv} = \pi R^2 L$. Thus
$$(F_x)_g = -\gamma\,\pi\,R^2\,L = -2.68N$$

with $\gamma = \rho g = 8542\ N/m^3$

The net axial force ΣF_x is
$$\Sigma F_x = (F_x)_s + (F_x)_p + (F_x)_g = 2.83 - 0.16 - 2.68 = -0.01N$$

The velocity profile does not change between the inlet and the outlet of the control volume. Thus there is no momentum change, and the net axial force should be zero, by the momentum theorem. The small value that we calculated is the result of round-off error.

Fluid Mechanics - Single Phase Flow: Part 2

Training Objectives

The participant will be introduced to:
1   hydraulic resistance of networks.
2   friction coefficients and roughness.
3   form losses of components.
4   pumps.

Fluid Mechanics - Single Phase Flow: Part 2

Table of Contents

1   Introduction

This lesson deals with flow in closed conduits. If a conduit has a circular cross section of constant area, it is called a pipe. Constant-area conduits with other cross sections (the most common being rectangular and annular) are called ducts. Fluid transport systems composed of pipes or ducts have many practical applications. Power plants contain many pipes and ducts for transporting fluids involved in the energy-conversion process.

We will consider fully developed flow. The flow in a constant-area pipe or duct is said to be fully developed if the velocity profile is the same at all cross sections. Fully developed flow is relatively simple to analyse because it is one dimensional. Many pipe flows are fully developed.

2   Hydraulic Resistance of Networks

In each flow system, as well as in its separate segments, the portion of the total pressure which is spent in overcoming the forces of hydraulic resistance is irreversibly lost. The molecular and turbulent viscosity of the moving medium irreversibly converts the mechanical work of the resistance forces into heat. Therefore, the total energy (thermal energy inclusive) of the flow over the given segment of the pipe remains constant in the absence of heat conduction through the walls. However, the state of the flow undergoes a change because of the pressure drop. The temperature, on the other hand, does not change at constant velocity. This can be attributed to the fact that the work of expansion due to a pressure drop is entirely converted into the work of overcoming the resistance forces and the heat generated by this mechanical work compensates for the expansion-induced cooling.

At the same time, the energy acquired by the flow resulting from the work of a compressor, fan, etc., in the form of kinetic or thermal energy, is lost for the given system during the fluid's discharge into the atmosphere or into another reservoir.

Two types of the total pressure (hydraulic resistance) losses in the pipeline are considered:
- Pressure losses resulting from friction (frictional drag), Δp_{fr}
- Local pressure losses (local resistance), Δp_{loc}, see Figure 2.1.

Fig. 2.1:
Static head gradient and head loss for a local resistance.
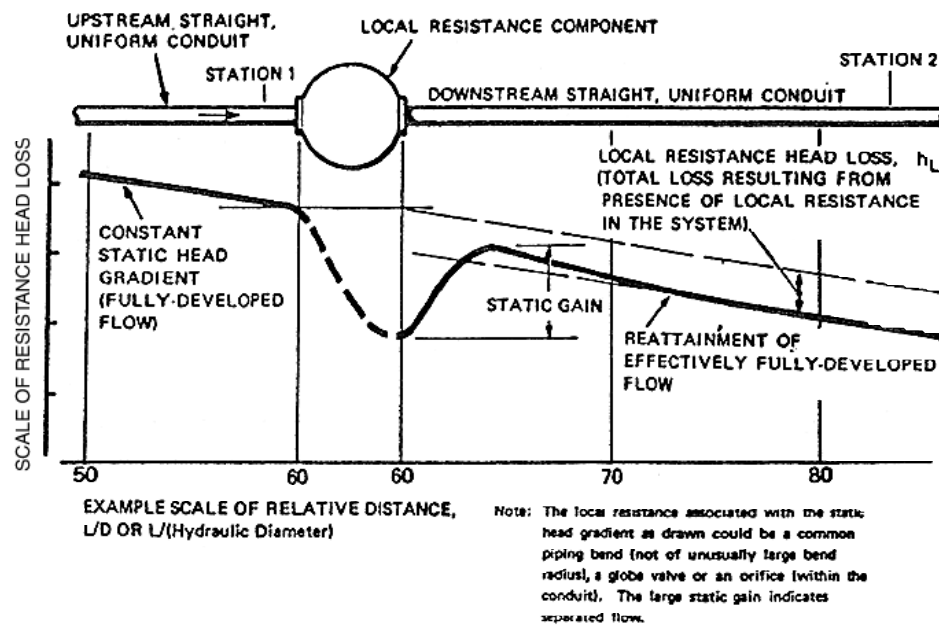
The fluid friction loss is due to the viscosity (both molecular and turbulent) of real liquids and gases in motion, and results from momentum transfer between the molecules (in laminar flow) and between the individual particles (in turbulent flow) of adjacent fluid layers moving at different velocities.

The local losses of total pressure are caused by the following: local disturbances of the flow; separation of flow from the walls; and formation of vortices and strong turbulent agitation of the flow at places where the configuration of the pipeline changes or fluid streams meet or flow past obstructions (entrance of a fluid into the pipeline, expansion, contraction, bending and branching of the flow, flow through orifices, grids, or valves, filtration through porous bodies, flow past different protuberances, etc.). All of these phenomena contribute to the exchange of momentum between the moving fluid particles (i.e., friction), thus enhancing energy dissipation.

The local pressure losses also include the dynamic pressures losses occurring during liquid (gas) discharge from the system or network into the atmosphere.

The phenomena of flow separation and eddy formation is associated with the difference of velocities over the cross section of the flow and with a positive pressure gradient along the flow. The latter develops when the flow velocity is retarded (for example, in an expanding channel, downstream of a sharp bend, when passing a body) in accordance with the Bernouilli equation. The difference in velocities over the cross section of a negative pressure gradient (e.g., accelerated motion in a contracted channel) does not lead to flow separation.

The flow in smoothly contracting segments is even more stable than over segments of constant cross section.

Physically speaking, the total pressure losses in any complex element of the pipeline are inseparable. However, for ease of calculation they are arbitrarily subdivided, in each element of the pipeline, into local losses (Δp_{loc}) and frictional losses (Δp_{fr}). It is also assumed that the local losses (local resistance) are concentrated in one section, although they can occur virtually throughout the entire length, except, of course, for the case of flow leaving the system, when its dynamic pressure becomes immediately lost.

The two kinds of losses are summed according to the principle of superposition of losses and consists of the arithmetic sum of the frictional and local losses:

$$\Delta p_{ov} = \Delta p_{fr} + \Delta p_{loc}$$

In fact, the value of Δp_{fr} should be taken into account only for relatively long fittings or only for elements (branch pipes, diffusers with small divergence angles, etc.), or when this value is commensurable with Δp_{loc}.

Present-day hydraulic calculations use the dimensionless coefficient of fluid resistance, which conveniently has the same value in dynamically similar flows, that is, flows over geometrically similar regions and with equal Reynolds numbers or other pertinent similarity criteria, irrespective of the kind of fluid or of the flow velocity and dimensions of the segments being calculated.

The fluid resistance coefficient is defined as the ratio of the total energy (power) lost over the given segment to the kinetic energy (per unit time) at section F, or, at constant rate of flow per unit width at the wall. It is the ratio of the total pressure loss Δp_{tot} to the dynamic pressure at section F:

$$k = \frac{\Delta p_{tot}}{\rho v^2 / 2}$$

The value of ξ depends on the velocity, and consequently on the flow cross section. In a general case (ρ is variable along the flow) the resistance coefficient based on the flow velocity in the given section (F_1) is calculated for another section (A_o) using the formula:

$$k_o = k_1 \left(\frac{v_1}{v_2}\right)^2 = k_1 \frac{\rho_1 A_1}{\rho_o A_o} \left(\frac{v_1}{v_o}\right)^3$$

$$= k_1 \left(\frac{\rho_o}{\rho_1}\right)^2 \left(\frac{A_o}{A_1}\right)^2 \, since \, \frac{v_1}{v_o} = \frac{\rho_o}{\rho_1} \frac{v_o}{v_1}$$

for $\rho_o = \rho_1$, *this becomes*

$$k_o = k_1 \left(\frac{A_o}{A_1}\right)^2$$

The overall fluid resistance of any network element is

$$\Delta p_{ov} = \Delta p_{loc} + \Delta p_{fr} = \left(k_{loc} + k_{fr}\right) \frac{\rho v^2}{2} = k_{ov} \frac{\rho v^2}{2}$$

In accordance with the arbitrarily accepted principle of superposition of losses we have

$$k_{ov} = k_{loc} + k_{fr}$$

where

$$k_{fr} = \frac{\Delta p_{fr}}{\left(\rho_{op} \frac{v_{op}^2}{2}\right)}$$

= *friction loss coefficient in the given element of pipe*

$$k_{loc} = \frac{\Delta p_{loc}}{\left(\rho_{op} \frac{v_{op}^2}{2}\right)}$$

= *coefficient of local resistance of the given element of pipe*

v_{op} = mean flow velocity at section A under the operating conditions
ρ_{op} = density of a liquid or a working gas
A = cross-sectional area of the pipe element being calculated

The local resistance coefficient κ_{loc} is mainly a function of the geometric parameters of the pipe (channel) element considered and also of some general factors of motion, which include:
- The velocity distribution at the entrance of the pipe element considered; this velocity profile, in turn, depends on the flow regime, the shape of the inlet, the shape of various fittings and obstacles, and their distance upstream from the element considered, as well as the length of the preceding straight pipe;
- The Reynolds number; and
- The Mach number, $M = w/a$.

The principle of superposition of losses is used not only for calculation of a separate element of the pipe (channel), but also in the hydraulic calculation of the entire network. This means that an arithmetic summation of the losses in separate elements of the pipe (channel) yields the total resistance of the system, Δp_{tot}.

By summing the resistance coefficients of separate elements of the system, which were first normalized to the velocity W_o at a chosen section F_o, and then expressing the total resistance of the system through its total coefficient of resistance.

$$k_{o.tot} = \sum_{i=1}^{n} k_{oi} = \sum_{i=1}^{n} k_i \left(\frac{\rho_o}{\rho_i}\right)\left(\frac{A_o}{A_i}\right)^2$$

where ξ_{oi} is the overall resistance coefficient of the given (*i*th) element of the system reduced to the velocity w_o at a chosen factor F_o and ξ_i is the overall resistance coefficient of the given (*i*th) element of the system reduced to the velocity w_i at section F_i of the same element. The coefficient ξ_i involves also, as a rule, the correction for the interaction of adjacent elements of the system. Hence, for the entire system

$$\Delta p_{tot} = k_{o.tot} \frac{\rho_o v_o^2}{2}$$
$$= \sum_{i=1}^{n} k_{oi} \frac{\rho_o v_o^2}{2}$$
$$= \sum_{i=1}^{n} k_i \left(\frac{\rho_o}{\rho_i}\right)\left(\frac{A_o}{A_i}\right)^2 \frac{\rho_o v_o^2}{2}$$

3 Friction Coefficients and Roughness

3.1 Hydraulic radius

For conduits having noncircular cross sections, some value other than the diameter must be used for the linear dimension in the Reynolds number. Such a characteristic is the *hydraulic radius*, defined as

$$R_h = \frac{A}{P}$$

where A is the cross-sectional area of the flowing fluid, P is the *wetted perimeter*, that portion of the perimeter of the cross section where there is contact between fluid and solid boundary. For a circular pipe flowing full, $R_h = \pi r^2/2\pi r = r/2$, or D/4. Thus R_h is not the radius of the pipe, and hence the term "radius" is misleading.

The hydraulic radius is a convenient means for expressing the shape as well as the size of a conduit, since for the same cross-sectional area the value of R_h will vary with the shape.

3.2 General equation for friction

The general equation for friction which applies to either laminar or turbulent flow and to any shape of cross section is

$$h_L = C_f \frac{L}{R_h} \frac{V^2}{2g} = f \frac{L}{D_h} \frac{V^2}{2g}$$

where $\quad f = 4 \, C_f$
$$D_h = 4 \, R_h$$

This equation is known as the pipe-friction equation, and is also commonly referred to as the Darcy-Weisbach equation.

Note: The Fanning equation is in a slightly different form where D is replaced by the hydraulic radius R_h

$$h_L = \frac{f}{4} \frac{L}{R_h} \frac{V^2}{2g}$$

Like the coefficient Cf, the friction factor f is dimensionless and is also some function of Reynolds number.

Reynolds number is the ratio of the inertial forces to the viscous force.
$$Re_L = \rho \, VL/\mu$$
where various reference conditions may be used to evaluate ρ, V, and μ. Reynolds numbers based on the concentration, momentum, energy and displacement thicknesses are obtained by setting
$$L = A, \, F, \text{ and } \delta \text{ respectively}$$

The use of the hydraulic diameter D_h as the characteristic length in the pipe-friction equation is permissible only in cases when the thickness δ_o of the boundary layer (within which the velocity changes from zero to nearly a maximum value) is very small over the entire or almost the entire perimeter of the cross section compared with the dimensions of the channel cross section ($\delta_o \ll D_h$).

Due to the overriding effects of the viscosity forces in laminar flow, even flow past surface asperities appear to be smooth. Therefore the roughness of the walls, unless it is very significant, does not affect the flow resistance. Under these conditions of flow the friction coefficient is always a function of the Reynolds number alone.

As the Reynolds number increases, the inertia forces, which are proportional to the velocity squared, begin to dominate. Turbulent motion is then initiated, which is characterized by the development of transverse velocity components giving rise to agitation of the fluid throughout the entire stream and to momentum exchange between randomly moving masses of fluid. All this causes a significant increase in the resistance to motion in turbulent flow as compared with the case for laminar flow.

When the surface of the walls is rough, separation occurs in the flow past roughness asperities and the resistance coefficient becomes a function not only of the Reynolds number but also of the relative roughness, ε/D_h.

Pipes and channels can be either smooth or rough, with the roughness being

either uniform or nonuniform. These two types of roughness differ according to the shape of such protuberances, their dimensions, the spaces between them, etc. The majority of commercial pipes and tubes have nonuniform roughness.

The averaged height ε_o of asperities, in terms of the absolute length units, is called the absolute geometric roughness. The ratio of the average height of asperities to the tube diameter, ε/D_h, is called the relative roughness.

In view of the fact that the geometric characteristics of the roughness cannot adequately determine the flow resistance of the tube, the concept of a derived hydraulic or equivalent roughness ε is introduced, which is determined by measuring the resistance.

The dependence of the frictional resistance coefficient f on Re and ε for a stabilized flow in tubes with nonuniform roughness (commercial tubes) suggests the existence of three principal regimes of flow (see Figure 3.1 -Moody chart).

Fig. 3.1:
Friction factor for pipes.
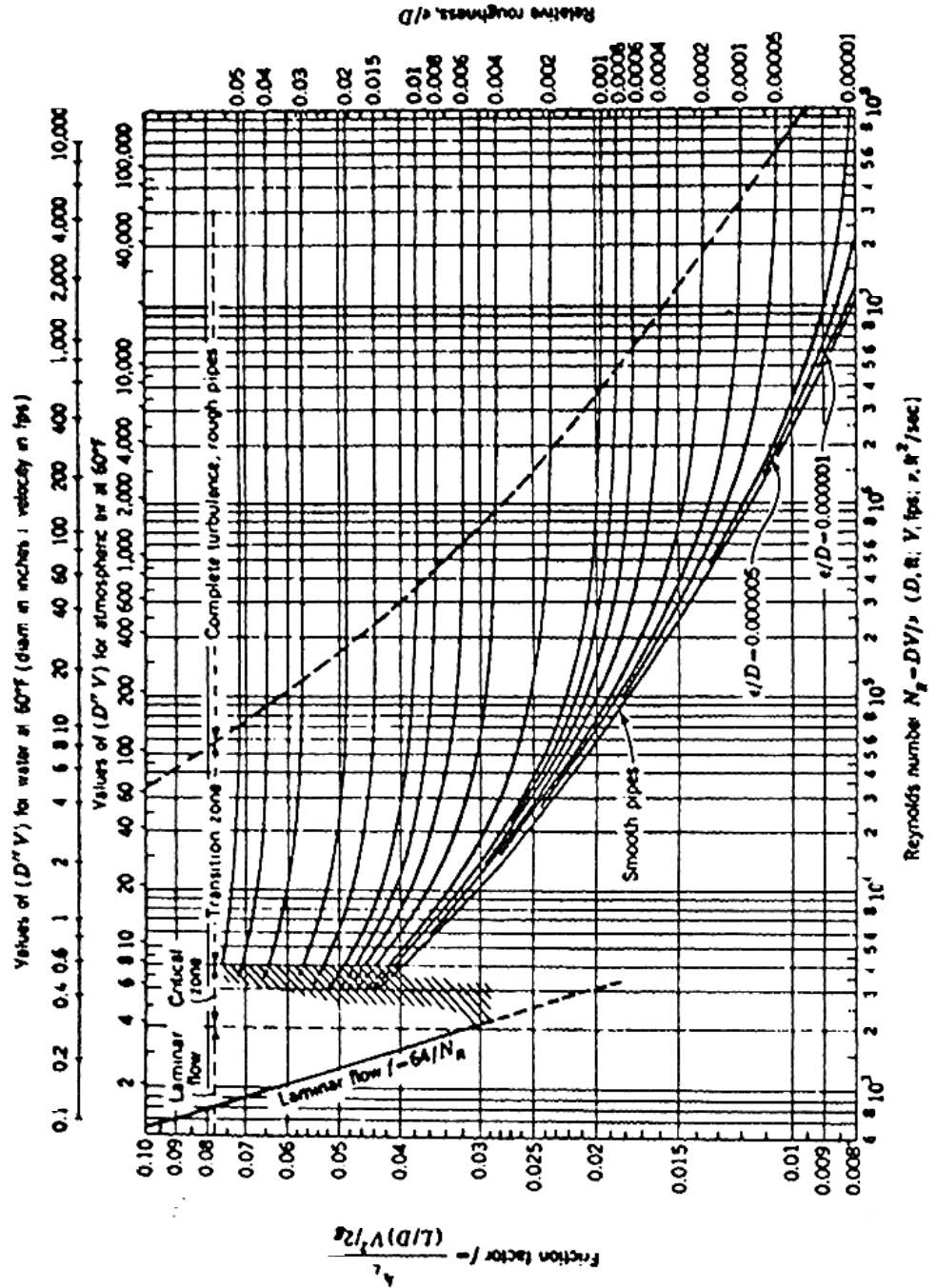
3.2.1 Laminar Regime

The first regime, called the laminar regime, involves small values of the Reynolds number (up to Re ≈ 2000) and is characterized by f being independent of roughness. From the Hagen-Poiseuille law

$$f = \frac{64}{Re}$$

3.2.2 Transition Regime

The second regime, called the transition regime, consists of two segments of the resistance curve for nonuniform roughness.
- For different degrees of roughness the resistance coefficient is not the same over the section related to the transition region between the laminar and turbulent flows (critical zone or zone of change of regime) and depends on the relative roughness ε and the Reynolds number; pressure losses in this zone are proportional to the velocity raised to a power greater than two.
- The transition segment of a purely turbulent regime is free of a deflection typical of the curves for uniform grain roughness. In this case, there is a progressive and smooth decrease in the resistance curves with increase in Re, with the lowest position being attained in the quadratic regime.

3.2.3 Quadratic Regime

The third regime is called the quadratic or square-law region, the regime of rough walls, and sometimes the regime of turbulent self-similarity. It is characterized by the resistance coefficients for each value of the relative roughness becoming constant, independent of Re.

3.3 Friction factor expressions

The single-phase friction factor can be evaluated from the following expressions
- Laminar flow (smooth or rough pipes)

$$f = \frac{64}{Re}\left(Re < 2000\right)$$

- Nikuradse correlation
Smooth – pipe flow $\delta_1 > 5\varepsilon$

$$\frac{1}{\sqrt{f}} = 2\log\ Re\sqrt{f}\ - 0.8\ \left(Re > 4000\right)$$

- Blasius correlation
Smooth pipe flow

$$f = \frac{0.316}{Re^{0.25}}\left(3000 < Re < 100000\right)$$

- Colburn correlation
Smooth pipe flow

$$f = \frac{0.184}{Re^{0.2}}\left(Re > 100000\right)$$

- Colebrook correlation
transitional flow
$$\left(5\varepsilon > \delta_1 > 0.3\varepsilon\right)$$

$$\frac{1}{\sqrt{f}} = 2\log\left[\frac{\varepsilon/D}{3.70} + \frac{2.51}{Re\ \sqrt{f}}\right]$$

- Von Karmen correlation
Fully – turbulent flow

where
ε = absolute roughness

$$\delta_l \quad = \quad \text{nominal thickness of viscous sublayer}$$
$$Re \quad = \quad \text{Reynolds Number} = DV\rho/\mu$$
$$D \quad = \quad \text{pipe diameter}$$
$$V \quad = \quad \text{fluid velocity}$$
$$\rho \quad = \quad \text{fluid density}$$
$$\mu \quad = \quad \text{absolute viscosity of fluid}$$

The Moody charts (Figure 3.1) for the determination of friction factors in either smooth or rough pipes were prepared from the equations described above.

4   Form Losses of Components

The pressure drop losses through more complicated piping components, i.e., bends, elbows, reducers, diffusers, orifices, venture meters, end fittings, fuel bundles, etc. are assessed using an appropriate non-recoverable form loss coefficient ξ_{loc}.

The ξ_{loc}. factors may be obtained from available handbooks and manuals (References 1, 2, 3 and 4) or from in-house experimental data.
-    In many cases, engineering judgement is used to subdivide a complicated component into two or more simpler sub-components for which the form loss coefficient is obtained from handbooks.

4.1   NUCIRC Slave Channel
Each of the components (i.e., inlet/outlet feeder pipes, inlet/outlet end fittings and fuel channels) of a slave channel are nodalized to a high degree as illustrated by the orificed channel B9 in Figure 4.1. A typical feeder configuration is shown in Figure 4.2 for channel T20.

Fig. 4.1:

NUCIRC nodalization model.
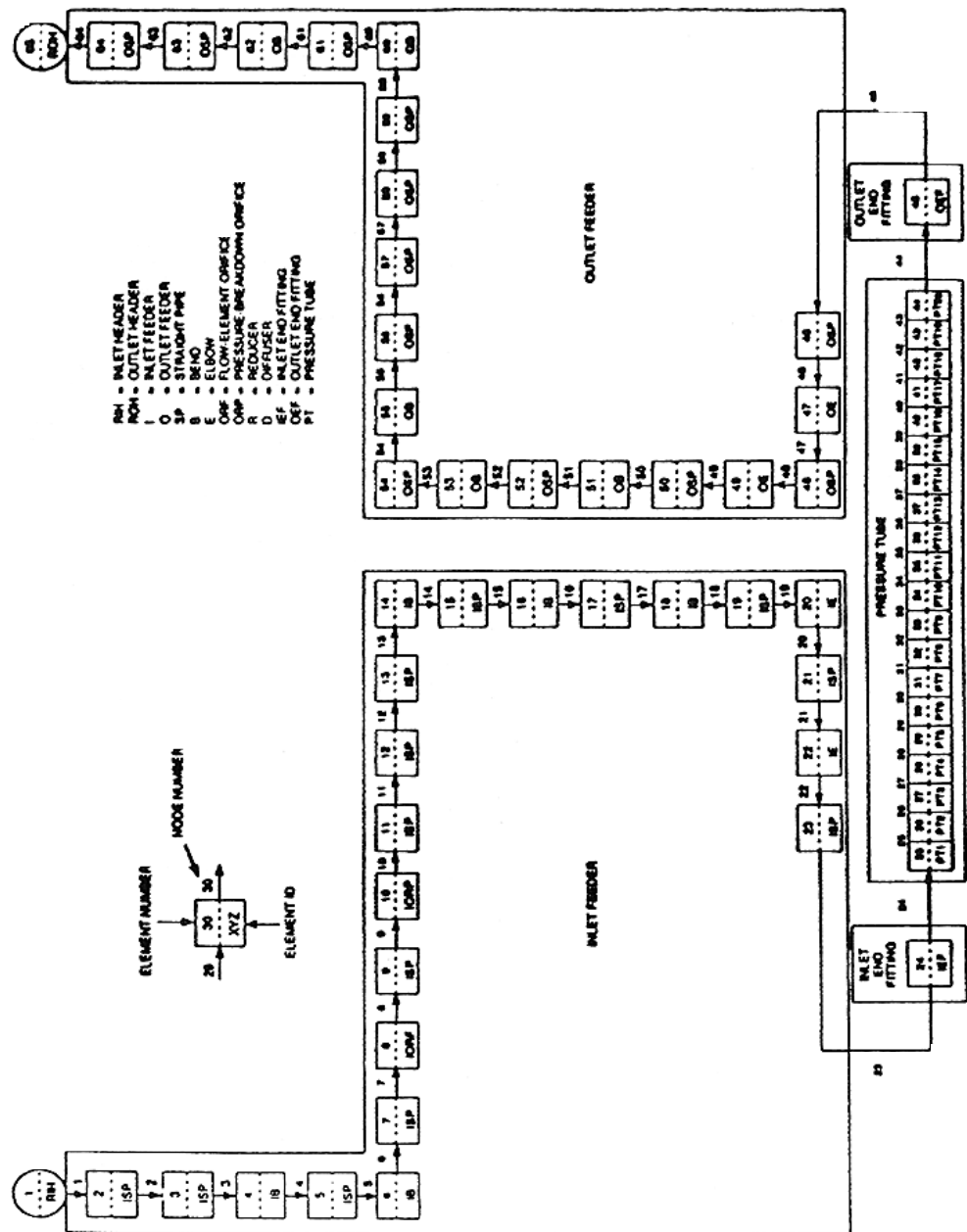
Fig. 4.2:
Heat transport system - Typical feeder configuration.
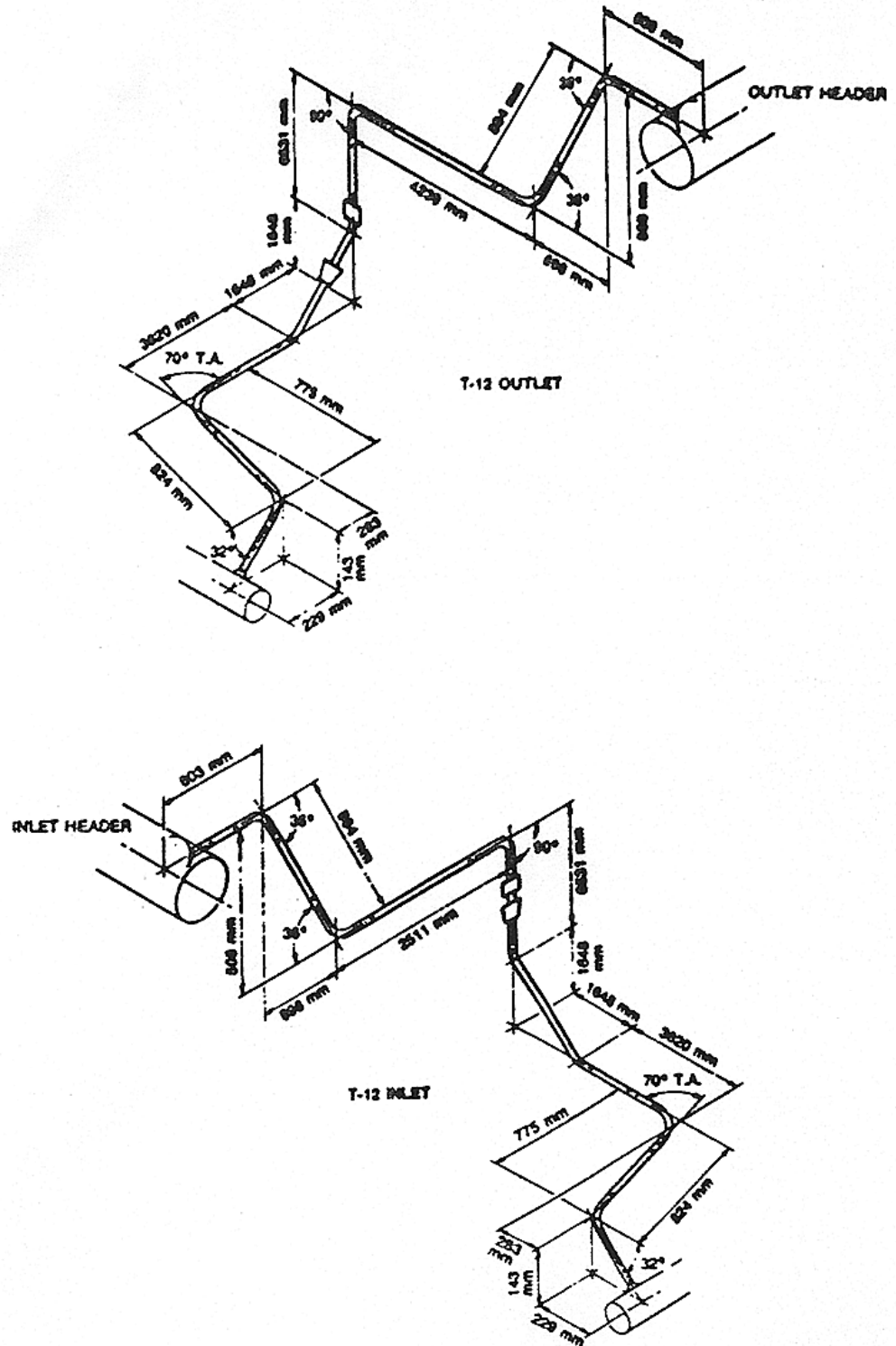
4.1.1 Inlet/Outlet Feeder Pipe

The function of the inlet/outlet feeder pipes is to carry D_2O coolant to and from the inlet/outlet headers via the reactor core.

The centreline geometry of the inlet/outlet feeder pipe is defined in terms of differential x, y and z global coordinates from the end fitting sideport (i.e., grayloc) up to the axial centreline of the header.

The transition segment between the feeder entrance/exit nozzle and the inlet/outlet header centreline is modelled solely for its elevation head contribution.

4.1.1.1 Elbow (Bend)

In the majority of cases, for the convenience of engineering calculations, the total resistance coefficient of elbows and bends is determined as the sum of the coefficient of local resistance of the bend and the friction coefficient (see Fig. 4.3):

Fig. 4.3:
Elbow.
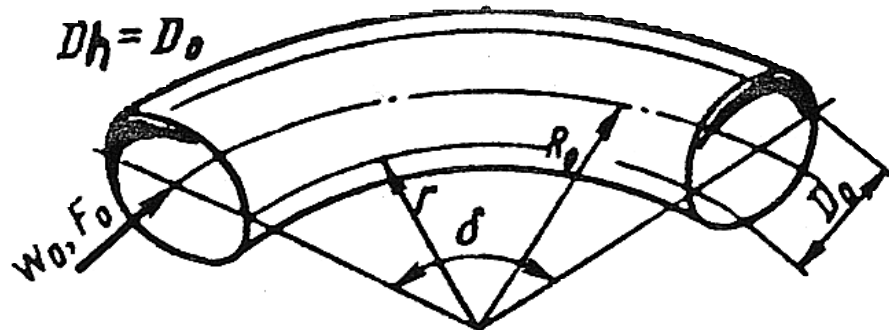
$$k = k_{loc} + k_{fr}$$

where

$$k_{loc} = A_1 + B_1 + C_1 \quad (\textit{reference } 2)$$

$$A_1 = 0.9 \, x \sin (\delta°) \quad (\textit{for } \delta° \leq 70°)$$

$$= 1.0 \qquad\qquad (\textit{for } \delta° = 90°)$$

$$= 0.7 + 0.35 \frac{\delta°}{90} \quad (\textit{for } \delta° \geq 100°)$$

$$= 0.8457 + \left((0.007715) \times \delta° - 70° \right) (\textit{for } 90° > \delta° > 70°)$$

$$= 1.0 + \left((0.008889) \times (\delta° - 90°) \right) \quad (\textit{for } 100° > \delta° > 90°)$$

$$B_1 = 0.21 \ / \ \sqrt{R_c / D_h} \qquad\qquad \textit{for } R_c / D_h \geq 1.0$$

$$= 0.21 \left(\frac{R_c}{D_h} \right)^{-0.25} \qquad\qquad \textit{for } \frac{R_c}{D_h} \ 1.0$$

$$C_1 = 1.0$$

$$k_{fr} = 0.0175 \times f \times \frac{R_c}{D_h} \times \delta°$$

with

δ = angle of turning (of a branch, elbow)

R_c = radii of cross sections of a curved pipe length

D_h = hydraulic diameter

4.1.1.2   Diffuser

It is sometimes convenient in engineering calculations to resort to a conventional method of dividing the total losses in a diffuser Δp into two parts: Δp_{fr}, the friction losses along the length of the diffuser, and Δp_{exp}, the local losses associated with expansion of the cross section. The total resistance coefficient of the diffuser ξ_d is accordingly composed of the friction resistance coefficient ξ_{fr} and the expansion resistance coefficient ξ_{exp} (see Fig. 4.4):

Fig. 4.4:
Diffuser.
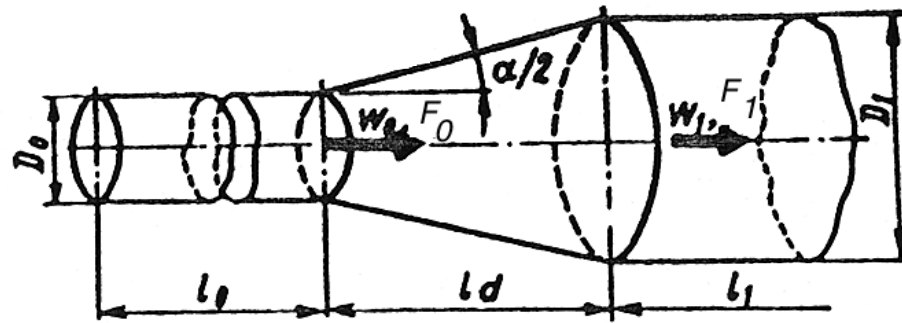
$$k_d = k_{fr} + k_{exp}$$

$$k_{exp} = 3.2 \times \left(\tan \frac{\alpha}{2} \right)^{1.25} \times \left(1 - \frac{1}{n_1} \right)^2 \quad (reference\, 2)$$

$$k_{fr} = \frac{f}{8 \times \sin \frac{\alpha}{2}} \times \left(1 - \frac{1}{n_1} \right)^2$$

where

α = central angle of divergence

n_1 = F_1/F_0 area ratio (degree of enlargement of cross section)

f = friction coefficient

4.1.1.3 Orifice

Five correlations are available for calculating the non-recoverable loss coefficient for the orifice. The available choices are as follows:

4.1.1.3.1 Spink's Correlation

$$k = 1.002591 \times \frac{C_c}{\left(F_a \times F_c \times S\right)^2} \quad (\textit{References } 3 \textit{ and } 4)$$

where
C_c = 1.0 - $(0.884 \times \beta^{1.693})$
F_a = $0.998287 + 1.966694 \times 10^{-5} \times T$
F_c = 1.05 - $0.1 \times \beta$
S = $0.595 \times \beta^2 + 0.01\,\beta^3 + 0.00001947 \times \beta^2 \times (10 \times \beta)^{4.425}$
β = D_0/D_1

4.1.1.3.2 Idel'chik Correlation (see Fig. 4.5) (reference 2)

Fig. 4.5:
Orifice.
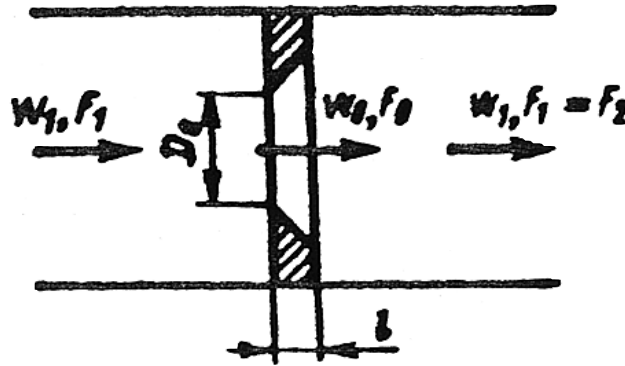
$$k = \left[1.0 + 0.707 \times \sqrt{1-\beta^2} - \beta^2\right]^2 \left(\frac{1}{\beta}\right)^4$$

4.1.1.3.3 COG Correlation (reference 7)
1-1/2″ CANDU Pressure - Breakdown Orifice

$$k = \left[1.0 + 0.707 \times \sqrt{1-\beta^2} - \beta^2\right]^2 \left(\frac{1}{\beta^4}\right)$$
$$+ \sqrt{1-\beta^2} \times \left[-0.22792 + 0.53091 \times \sqrt{1-\beta^2} - 0.82243 \times \beta^2\right] \times \left(\frac{1}{\beta^4}\right)$$
$$+ 0.06413 \times Log\left(R_e\right)$$

4.1.1.3.4 2″ CANDU Pressure - Breakdown Orifice (reference 7)

$$k = \left[1.0 + 0.707 \times \sqrt{1-\beta^2} - \beta^2\right]^2 \left(\frac{1}{\beta^4}\right)$$
$$+ \sqrt{1-\beta^2} \times \left[-11.91722 + 11.92846 \times \sqrt{1-\beta^2} - 6.18243 \times \beta^2\right] \times \left(\frac{1}{\beta^4}\right)$$
$$+ 0.16575 \times Log\left(R_e\right)$$

4.1.1.3.5   2″ ASME Pressure - Breakdown Orifice - ß = 0.75 (reference 7)

$$k = 0.7178 + 0.2763 \times Log(R_e)$$

4.1.1.4   Header-To-Feeder Nozzles

The recoverable and non-recoverable loss coefficients of the inlet feeder entrance (at the RIH) and the outlet feeder exit (at the ROH) have been calculated for each channel, based on the ultrasonic flow measurements obtained during commissioning. The entrance and exit loss coefficients are provided in a feeder nozzle data file.

4.1.2   Inlet/Outlet End Fittings

The primary function of the inlet/outlet end fitting is to provide a suitable high pressure closure that can be operated by the fuelling machine to allow insertion and removal of fuel. In addition, the end fitting provides a transition between the pressure tubes and the primary circuit piping, as well as providing support for the pressure tubes and their contents.

The hydraulic resistance model is given by:

$$\Delta P = \phi^2 \left(f \frac{L}{D_h} + k_{EF} \right) \frac{1}{2\rho} \left(\frac{\dot{M}}{A} \right)^2$$

where
k_{EF} = form loss coefficient
L = flow length from Grayloc to liner holes
D_h = hydraulic diameter of flow area through annulus
A = flow area through annulus
$\dot{M}$ = channel flow
ρ = liquid density
ϕ^2 = two-phase friction multiplier
f = friction factor = $\dfrac{0.184}{\text{Re}^{0.2}}$ (Colburn equation for smooth pipe flow)

4.1.3   Fuel String Resistance

The pressure drop across the fuel string is calculated with the k-fuel model (Reference 8):

$$k_T = c\, f \frac{L}{D} + k_{SUB}$$

others
k_T = total hydraulic resistance of fuel string
c = skin correction factor
f = friction factor calculated via explicit formulation of Colebrook and White formula (Reference 8)
L = length of fuel string
D = hydraulic diameter
k_{SUB} = form loss coefficient consisting of fuel string entrance and exit losses, bundle spacer losses and bundle junction losses

For 13 bundle fuel string:

$$k_{sub} = k_I + 12k_j + 12k_{sp} + k_0$$

k_I = fuel string entrance loss coefficient

k_o = fuel string exit loss coefficient

k_J = junction loss coefficient

k_{sp} = spacer loss coefficient

These k's are measured for real fuel in real channel.

5   Pumps

5.1   Classification of Pumps

The types of pumps used in a CANDU plant are not vastly different from those used in other industries.

Figure 5.1 presents a classification of pumps. Figure 5.2 presents a classification of centrifugal pumps. Tables 5.1 and 5.2 present a cross section of the various CANDU 6 pumps.

Fig. 5.1:
Classification of pumps.

Pumps
- Positive displacement
  - Reciprocating
    - Piston / Plunger
      - Double acting → Simplex / Duplex → Steam
      - Single acting / Double acting → Simplex / Duplex / Triplex / Multiplex → Power
    - Diaphragm → Simplex / Multiplex → Fluid operated / Mech. operated
  - Slow case
  - Rotary
    - Single rotor → Vane / Piston / Flexible member / Screw
    - Multiple rotor → Gear / Lobe / Circumferential piston / Screw
- Kinetic
  - Centrifugal
    - Radial flow / Mixed flow → Single suction / Double suction → Self-priming / Non self-priming; Single stage / Multistage → Open impeller / Semi-open impeller / Closed impeller
    - Axial flow → Single suction → Single stage / Multistage → Open impeller / Closed impeller
  - Peripheral → Single stage / Multistage → Self-priming / Non self-priming
  - Special → Jet (ejector boosted) / Gas lift / Hydraulic ram / Electromagnetic

Fig. 5.2:
Classification of centrifugal pumps.

Centrifugal
- Radial flow / Mixed flow → Single suction / Double suction → Self-priming / Non self-priming; Single stage / Multistage → Open impeller / Semi-open impeller / Closed impeller
- Axial flow → Single suction → Single stage / Multistage → Open impeller / Closed impeller

Table 5.1:

Design data for various CANDU 6 pumps.

No.	Pump	BSI and Pump Orientation	Pump Design Parameters			Rated Pump Motor Horsepower & Speed (N.M.)	Number of Pumps per Unit	ASME & CSA Code Classification
			Rated Head	Rated Flow	Rated Temperature/ Suct. Pressure			
1.	Primary Heat Transport Pump	33122 (Vertical)	705 feet (213 metres)	29,400 IGPM (2205 l/sec)	511°F (266°C) 1381 psia (9.52 MPA)	9000 HP 1800 RPM	4 x 75%	Section III Class 1 CSA Z299.1
2.	Shutdown Cooling Pump	33412 (Vertical)	242 feet (73.8 metres)	2400 IGPM (180 l/sec)	100°F to 350°F (38°C to 177°C) 3 to 1434 psig	225 HP 1800 RPM	2 x 100%	Section III Class 1 CSA Z299.1
3.	D_2O Feed Pump	33312 (Horizontal Multi-stage)	4200 feet 3700 feet 1100 feet	20 IGPM 90 IGPM 220 IGPM 470 IGPM	104.4°C (220°F) 2200 psig (15.17 MPa)	306 HP 3600 RPM	2 x 100%	Section III Class 3 CSA Z299.2
4.	D_2O Recovery Pump	33383 (Vertical)	200 feet (61 metres)	240 IGPM (18 l/sec)	214°F (101°C)	18 HP 3600 RPM	2 x 100%	Section III Class 3 CSA Z199.3
5.	Emergency Core Cooling Pump	34322 (Vertical)	200 feet (61 metres) NPSH=20 feet	8000 IGPM (600 l/sec)	220°F (104°C) 225 psig (1.55 MPag)	600 HP 1800 RPM	2 x 100%	Section III Class 2 CSA Z299.2
6.	Liquid Zone Control Pump	34812 (Horizontal)	351 feet (107 metres)	226 IGPM (17 l/sec)	183°F (84°C)	30 HP 3600 RPM	3 x 100%	Section III Class 3 CSA Z299.2
7.	Main Moderator Pump	32112 (Vertical)	180 feet (55 metres)	12433 IGPM (940 l/sec)	176°F (80°C)	1000 HP Pony: (20 HP) 1200 RPM Pony: 300 RPM	2 x 100	Section III Class 3 CSA Z299.2

Table 5.2:
Cernavoda canned motor pumps.

System	BSI	No. of Pumps per Unit	Head (metres)(C6)	Flow (litres/sec)	Efficiency of Motor %	Pump Type (RUTSCHI)
1. Heavy Water Management System						
1.1 D$_2$O Supply Pumps (2x100)	38112	2 (cl.3)	55	6.3	68	SMR65-200
1.2 D$_2$O Clean-up Pumps	38412	6 (cl.3)	20	1.1	60	SMR40-125
1.3 D$_2$O Vapour Recovery Pumps	38312	3 (cl.3)	15	0.4	60	SMR40-125
2. Moderator System						
2.1 Resin Transfer Pumps	3222221	(cl.3)	65	1.0	70	SMR3-160-2
2.2 D$_2$O Collection Pumps	32512	1 (cl.3)	30	1.1	66	SMR-40-160
2.3 Mod. Liquid Poison Pumps	32712	2 (cN/N)	6.2	0.19	60	SMR-40-125
2.4 Mod. Cover Gas Booster Pumps	32312	2 (cl.3)	16.75	0.76	60	SMR-40-125
3. Heat Transport System						
3.1 Resin Transfer Pumps	33362	1 (cl.3)	65	3.8		SMR5-160-2
3.2 Duet/De-deuterium Sys. Pumps	33362	1 (cl.3)	9.1	0.4	60	SMR5-160-2
3.3 D$_2$O Collection Pumps	33812	2 (cl.3)	61	3.8	67	SMR5-160-2
3.4 Duet/De-deuterium Pumps	33362	1 (cl.3)	65	3.8	67	SMR40-125
4. Sampling System						
4.1 LISS Sampling Pumps	34712	1 (cl.1)	19.8	0.076	60	SMR40-125
4.2 D$_2$O Upgrading Pumps	35232	2 (cl.2)	92 & 79	.76 & 3.3	68	SMR40-250
5.1 Reflux Pumps	38422	4 (cl.3)	45	0.50	70	SMR3-160-2
5.2 D$_2$O Upgrading Pumps	38422	8 (cl.3)	20	0.30	76	SMR40-125

About 90% of all the pumps used for a CANDU plant are centrifugal pumps. Only a few pumps in the plant are positive displacement (p.d.) type. Screw, reciprocating, diaphragm and liquid ring seal types of p.d. pumps and compressors are used in the plant.

The reasons for using a centrifugal pump are:

Its operation is smooth, whereas the operation of a positive displacement pump is often pulsating.

Its shutoff head is limited, whereas the shutoff head of a p.d. pump is theoretically infinite. This makes a safety relief valve, on the discharge side of a p.d. machine mandatory.

Its capacity can be varied by throttling, if necessary, whereas, the capacity of a p.d. pump is practically constant, throttled or unthrottled. However, not many centrifugal pumps in a CANDU plant are operated by a flow control valve, or by any kind of throttling. All valves in most of the process lines remain fully open. That means, flow remains fairly constant for most systems.

Centrifugal pumps are cheaper and more readily available.

Process conditions like head, flow rate, and viscosity of fluid in the vast majority of process systems in a CANDU plant are more suitable for centrifugal pumps.

A p.d. pump is considered for a system only when the capacity is too low in respect of its head, and a suitable centrifugal pump is not available. Also, when the liquid handled is too viscous, a p.d. pump is the only choice.

Vertical or horizontal orientation of any pump is selected according to the configuration of piping system and space available. Horizontal pumps are always given the first preference if adequate space is available, as they are cheaper than the vertical pumps and easier to maintain. Horizontal pumps have fewer rotor dynamics problems in comparison with the vertical ones.

The largest, and probably the most important pump in a CANDU plant, namely the Heat Transport pump, is vertical. The choice was entirely dependent on the availability of space, suitable location in the piping arrangement, and the ease of shielding the pump inside containment while keeping the motor outside for some stations.

5.2 Features of CANDU Pumps

There are, however, some special features that make most of the pumps in a CANDU plant slightly different.

December 1995

First of all, most of the CANDU pumps are of nuclear type: the pumps are constructed to nuclear codes and standards. The manufacturing process and the quality assurance process thus are quite stringent. Every step in manufacturing is rigorously inspected and recorded. This makes the pumps highly reliable and, of course, costly.

Secondly, most of the CANDU pumps handle heavy water which is costly. Therefore, the pumps are designed to be leak-proof.

There is another important reason for the pumps to be leak proof. D_2O gets irradiated in the nuclear process, causing the formation of radioactive tritiated water, the concentration of which is to be kept limited in the containment for the safety of the operating personnel.

Mechanical seals are used on most pumps rather than shaft packing. Mechanical seals are not absolutely leak proof, even when they look dry from outside. Liquid leaks into the atmosphere through seal faces in the form of vapour or droplets. A seamless variety of pump, called canned motor pump, is a zero leakage pump. This is extensively used in a CANDU plant for application where the pump is small. Large capacity canned motor pumps are not available. The bearings of canned motor pumps are made of carbon, and are flushed by the operating liquid. The liquid must be absolutely clean and grit-free. Excessive wear and tear of these bearings have been reported in several cases. The designer is aware of the susceptibility of the design to these types of problems and takes appropriate measures.

Mechanical seals, where used, are of excellent quality, so that the loss of D_2O and the leakage of tritium thereby, are reduced to a minimum.

The Heat Transport pumps operate at high temperature and pressure, where sealing of the pump shaft is a real challenge. The seals of these pumps are of special design. They have been developed by AECL in collaboration with the manufacturer of the pumps.

Materials of construction for equipment in a nuclear plant are selected carefully. Some materials, e.g. teflon, loose their mechanical properties when they are irradiated for a long time. These materials are avoided if possible. Some other materials, e.g. Cobalt-60, convert themselves into a further source of radiation when they are irradiated. These materials are also avoided if possible. CANDU plants are built for a life of 30 years. Selection of suitable materials of construction and providing adequate factor of safety is therefore important.

Certain pumps in some CANDU stations have a dual capacity. This is accomplished by operating the same pump at two different speeds. For instance, the Main Moderator system needs D_2O circulation during the shutdown period or after a Loss of Coolant Accident (LOCA) to remove the decay heat. In 600 MW stations, the moderator pump is operated at one-fourth of its normal

speed during the shutdown or after a LOCA by a separate motor, called pony motor, mounted on the same shaft than the main motor. The moderator pump thus can operate at one-fourth of its original flow during shutdown.

The benefit of operating the Heat Transport pumps at a reduced speed of one-third of normal speed, after a LOCA, has recently been assessed. Bruce B heat transport pumps are being modified for operating also at one-third of normal speed. The reduced speed will be achieved, in this case, by the solid state control of a silicon control rectifier. The reduced speed operation is under consideration for the HT pumps in other CANDU stations.

Another special feature of some CANDU pumps is a minimum rotational requirement. Normally, a pump comes to a dead stop within a few seconds of a power cutoff. That means, flow is practically zero within a few seconds of a power cutoff. If there is a power failure, the heat transport pumps require continuous operation for some time to continue adequate fuel cooling. A flywheel of high inertia is attached to the motor shaft which helps sustain D_2O flow for a certain length of time. The minimum rotational inertia, where required, is a function of the safety criteria to be met. The physical means of provision of the inertia in the rotating assembly is decided by the supplier in conjunction with the equipment designer.

There are quite a few large pumps in a CANDU plant, as illustrated in Table 5.1. All other pumps are less than 100 HP. In fact, most of them are 5 HP or less.

5.3 Pump Performance Parameters

5.3.1 Pump Characteristic Curve
The mode of operation of a pump depends on the system on which it is operating. The pump characteristic curve shows the relation between the head developed by the pump and its rate of discharge when the pump is operating at a given rotative speed.

The system characteristic curve shows the relation between the required pumping head and the flow rate in the pipeline.
The actual pump-operating head and flow rate are determined by the intersection of the two curves. The usual mode of operation of a pump is at constant speed. The efficiency of the pump drops off as the rotative speed is moved away from the optimum speed. It is possible to vary the pump characteristics with different impeller and casing designs. Thus a flat characteristic permits a considerable variation in the rate of discharge with but little change in head, while a steep characteristic gives only a small variation in the flow for a relatively large change in head.

Figures 5.3, 5.4 and 5.5 illustrate the performance curves for Gentilly-2 and Wolsong 2 HT pumps and a D2O pump, respectively.

Fig. 5.3:

Gentilly-2 heat transport pump characteristics.
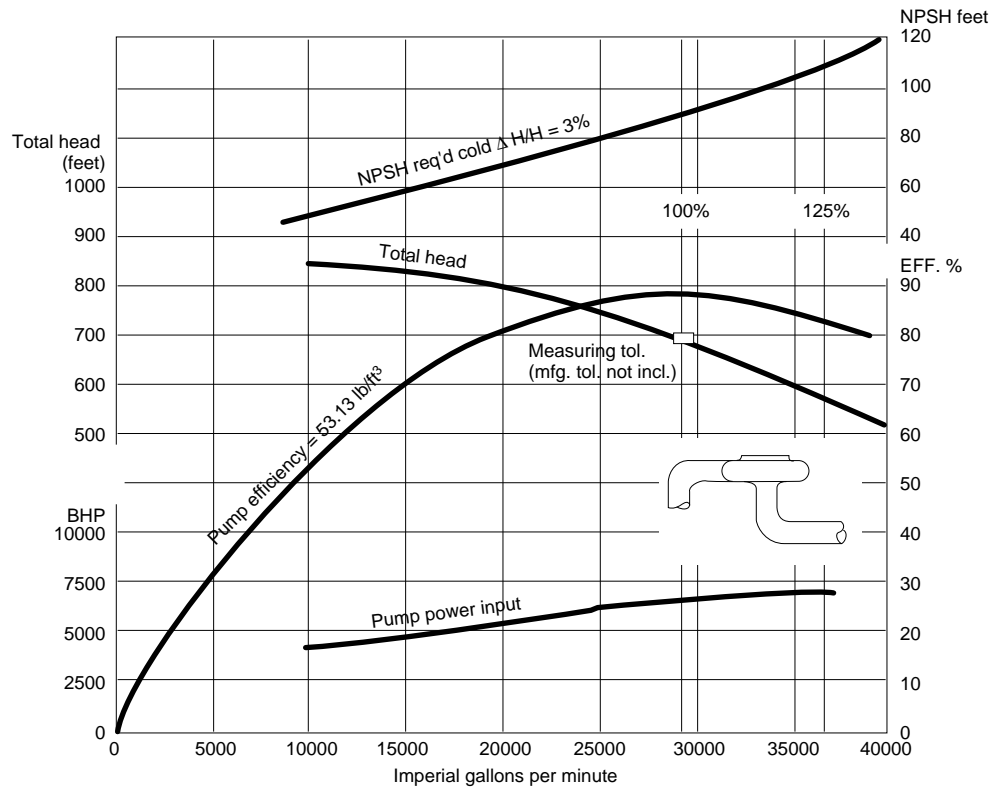
Fig. 5.4:

Wolsong 2 heat transport pump characteristics.
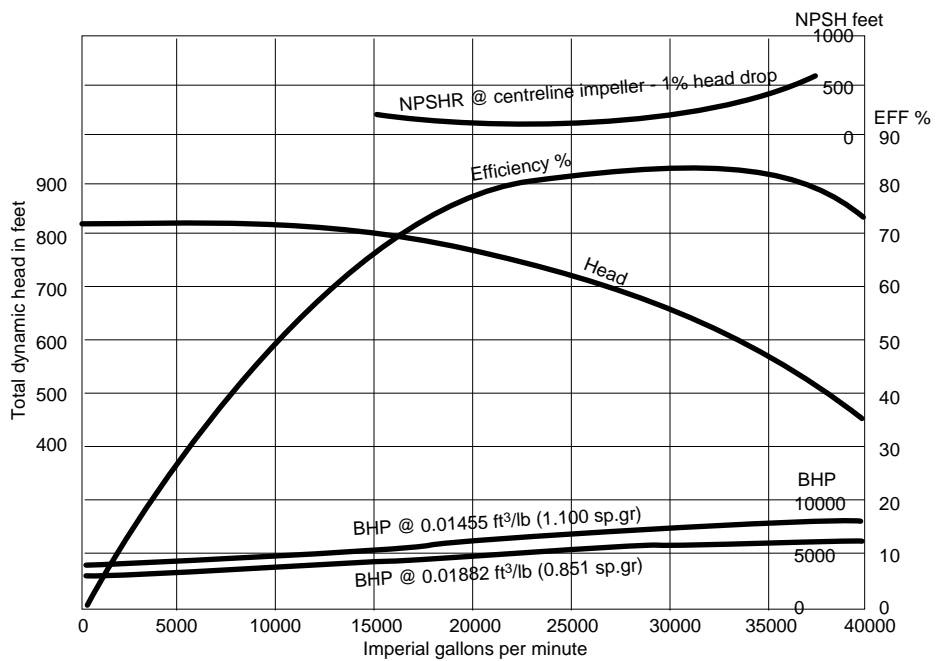
Fig. 5.5:
D_2O feed pump characteristics.
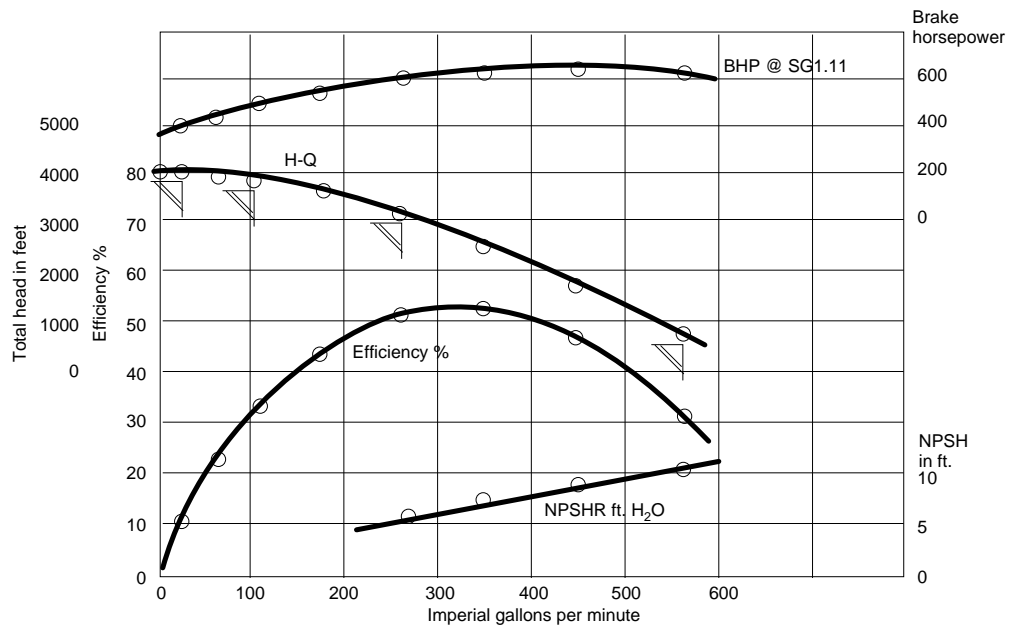
HT Pumps
- HT pumps use a 9000 HP motor.
- High efficiency at the rated point essential.
- Guaranteed efficiency of 89% required at the rated point.

D_2O Feed Pumps - 14-Stage Horizontal Pump
- Pump curve is required to pass through four points. This is an extremely difficult requirement to meet.
- Additional requirement: minimum pump efficiency at the intermediate flow shall not be less than 30%.
- Both these requirements were met and confirmed by performance testing.

5.3.2   Specific Speed
The most common definition of specific speed N_s is given by:

$$N_S = \frac{n_e \sqrt{Q}}{h^{3/4}}$$

where
n_e = rotative speed for maximum efficiency in rpm
Q = flow rate in gpm
h = pump head in ft

The only value of specific speed that has any real significance in that corresponding to the values of head, discharge and speed at the point of maximum efficiency.

Figure 5.6
illustrates the useful operating ranges for pumps used in large nuclear and fossil power generating stations.

Fig. 5.6:
Anticipated useful operating ranges for pumps used in large nuclear and fossil power generating units.
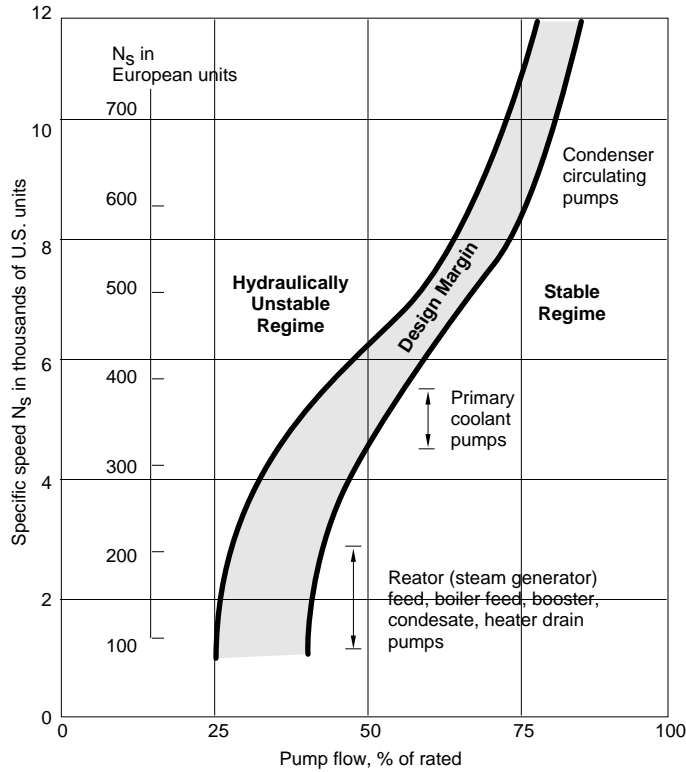
5.3.3   Shutoff Head
When a pump filled with the fluid to be pumped is operated at normal speed with the discharge valve closed, the head developed is called the **shutoff head**.

The actual shutoff head is affected by the value of the impeller-vane angle at exit, by the design of the case, and even by the nature of the intake, since the latter has some influence on the prerotation.

5.3.4   Pump Efficiency
Volumetric efficiency

$$e_v = \frac{Q}{Q + Q_L}$$

where
Q   = actual flow delivered
Q_L = leakage from the high-pressure side to the low-pressure side of the pump

Hydraulic efficiency

$$e_h = \frac{h}{h'}$$

where

h = net head delivered to the fluid by the pump
h' = head transferred from the rotor to the fluid

Mechanical efficiency

$$e_m = \frac{bp - fp}{bp}$$

where

bp = power at the pump shaft ($=T\omega$)
fp = power lost to mechanical friction in the bearings and stuffing
   boxes as well as in the disk friction.

Overall efficiency

$$e = \frac{\gamma\, Qh}{T\,\omega} = e_v\, e_h\, e_m$$

5.3.5   Cavitation

An important factor in satisfactory operation of a pump is the avoidance of cavitation, both for good efficiency and for the prevention of impeller damage. For pumps a cavitation parameter has been defined as:

$$\sigma = \frac{\left(P_s\right)\,/\,\gamma + V_s^2\,/\,2g - P_v\,/\,\gamma}{h}$$

where subscript s refers to values at the suction side of the pump, h is the head developed by the pump, and P_v is the vapour pressure. As the latter is normally given in absolute units, it follows that P_s must also be absolute pressure.

The critical value σ_c is that at which there is an observed change in efficiency or head or some other property indicative of the onset of cavitation. The value will depend not only upon the criterion used, but also upon the conditions of operation.

For safe operation it is desirable to operate at values above the critical value for the capacity involved. The critical value σ_c for any specified operating condition depends upon the design of the particular pump, and in any important installation it should be determined experimentally from a model.

Since cavitation is determined by conditions at entrance to the impeller and not by those at discharge, an expression has been devised known as suction specific speed, which is analogous to the usual specific speed except that the net head is replaced by the total suction head above the vapour pressure head. This is the

numerator in the previous equation and is designated as NPSH, which stands for net positive suction head. The suction specific speed is then

$$S = \frac{n\sqrt{Q}}{NPSH^{3/4}}$$

For a double-suction pump the total capacity should be divided by two for the determination of S.

Inasmuch as the critical value σ_c has been found to depend upon both the usual specific speed and the suction specific speed, the relation

$$\sigma_c = \frac{NPSH}{h} = \left(\frac{N_s}{S}\right)^{4/3}$$

is obtained by eliminating $n\sqrt{Q}$ between the expressions for N_s and S. In order to obtain σ_c, it is necessary to use the critical value of NPSH in evaluating S.

The primary heat transport system pumps are operated during system warmup. During this period it is essential to assure sufficient net positive suction head (NPSH) to prevent pump cavitation.

Several events can lead to reduced HTS pressure (and hence low NPSH) during operation: these include loss of D_2O feed pumps and spurious opening of the liquid relief valves. Possible conditions for restarting the primary pumps are outlined below in order of preference.

5.3.5.1 Heat Transport System of Full Pressure, Pressurizer Connected
This configuration provides the greatest margin against system depressurization and pump cavitation since the high pressure inventory of the pressurizer is available to maintain HTS pressure.

5.3.5.2 Heat Transport System at Reduced Pressure, Pressurizer Connected
The primary heat transport system pumps may be operated with the pressurizer connected when the system pressure is below normal operating pressure. The required pressure is given as a function of system temperature.

The risk of pump cavitation in the event of a failure leading to system depressurization is greatest at low operating pressures, and reduces with increasing pressure.

5.3.5.3 Heat Transport System at Full Pressure, Pressurizer Isolated
The pumps can be operated with "solid mode" pressure control if necessary. Since the pressurizer inventory is not available to maintain HTS pressure, events leading to reduced HTS pressure are more severe; the risks of low NPSH and pump cavitation are greatest in this mode of operation.

6 References

[1] Miller, D.S., "Internal Flow Systems", BHRA Engineering, 1978.

[2] Idelchik, I.E., "Handbook of Hydraulic Resistance, Hemisphere Publishing Corporation, 2nd Edition, 1978.

[3] Bean, H.S., "Fluid Meters: Their Theory and Application", the American Society of Mechanical Engineers, 6th Edition, 1971.

[4] Spink, L.K., "Principles and Practice of Flow Meter Engineering", the Foxboro Company, 9th Edition, 1967.

[5] Ozisik, M.N., "Basic Heat Transfer", McGraw-Hill Book Company, 1977.

[6] Idelchik, I.E., "Handbook of Hydraulic Resistance: Coefficients of Local Resistance and of Friction", Israel Program for Scientific Translation Ltd., AEC-tr-6630, 1966.

[7] Soulard, M.R., "Generic Non-Recoverable Loss Coefficient Correlations for CANDU Pressure-Breakdown Orifices", COG-89-95, January 1992.

[8] Soulard, M.R. and Hau, K.F., "Recent Model Developments in NUCIRC and Applications to CANDU 6 Heat Transport System Performance Evaluation", Paper presented at the 16th Annual Nuclear Simulation Symposium held in Saint John, New Brunswick, 1991 August 25-28.

Two Phase Flows

Training Objectives

The participant will be able to understand:

1   the definition related to two phase flow;
2   the difference between void and quality;
3   the principle of the slip factor;
4   the flow regimes;
5   the flow regime maps;
6   the importance of the void correlations;
7   the two phase flow multiplier;
8   the two phase flow heat transfer.

Two Phase Flows

Table of Contents

1.   Introduction

Two-phase flow phenomena are of utmost importance in liquid cooled reactors. When a flowing coolant undergoes a partial change in phase, two-phase flow occurs, giving rise to complicated heat-transfer and fluid-flow problems. The phenomena occur regularly in boiling-water reactors, and in pressurized-water reactors at high power densities. In general, two-phase flow implies the concurrent flow of two phases, such as liquid and its vapor (one component), liquid and gas (two components), gas and solid, etc. This chapter deals mainly with the first type, liquid and vapor flow. Flow in reactor channels, past restrictions, and critical flow will be discussed.

The accurate prediction of two-phase pressure drop in the coolant conduits of CANDU reactors is important because the channel pressure drop is intimately related to the coolant flow and enthalpy distribution. The total pressure drop, during the flow of a two-phase mixture consisting of a liquid and vapor, is the sum of the hydrostatic head, acceleration pressure drop (momentum flux contribution) and the frictional pressure losses. Evaluation of two-phase pressure drop requires adoption of a void fraction correlation to calculate the hydrostatic and acceleration components of two-phase pressure drop and a two-phase friction multiplier correlation to calculate frictional pressure drop. Over the past forty years, a great deal of effort has been expended in an attempt to understand the mechanisms contributing to the frictional pressure losses in two-phase flow. Although a number of correlations, both theoretical and empirical have been proposed, none are general enough to provide an accurate calculation of two-phase frictional pressure drop over a wide range of pressures, flow rates, geometries and fluids.

2.   Two-Phase Flow Theory and Definitions

A full notation is given at the end of the lesson. This section introduces the primary variables used throughout this lesson and derives some simple relationships between them for one-dimensional flow.

To distinguish between gas and liquid, the subscripts "g" for gas and "f" for liquid (fluid) will be used. Consider a channel in which two phases are flowing cocurrently. The flow is one-dimensional: there are no changes in system properties in directions normal to the direction of flow. The flow area of the channel is denoted by A and the flow areas of the gas and liquid phases by A_g and A_f respectively. The mass rate of flow will be represented by the symbol W and will be the sum of the individual phase flow rates W_f and W_g. The velocity of the individual phases is denoted by the symbols U_g and U_f. The volumetric rate of flow is represented by the symbol Q and will be the sum of the individual volumetric flow rates Q_f and Q_g.

Two-phase flow takes several forms, shown in Figures 1 to 5.

Bubble flow is the case in which individual dispersed bubbles move independently up the channel (Figure 1).

Figure 1
Bubble flow

Liquid   Vapour
          bubbles
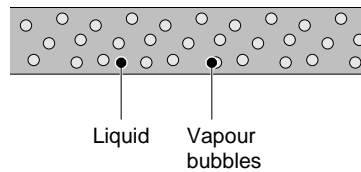
Plug, or slug flow is the case where patches of coalesced vapor fill most of the channel cross section as they move from inlet to outlet (Figure 2). Slug flow has been reported as being both a stable and an unstable transition flow between bubble flow and the next type, annular flow.

Figure 2
Slug flow

Liquid   Vapour
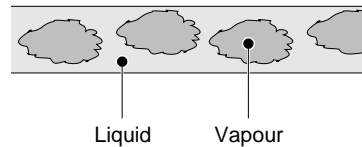
In annular flow the vapor forms a continuous phase, carrying only dispersed liquid droplets, and travels up the channel core, leaving an annulus of superheated liquid adjacent to the walls as shown in Figure 3.

Figure 3
Annular flow

Vapour   Liquid   Liquid
                          film   drops
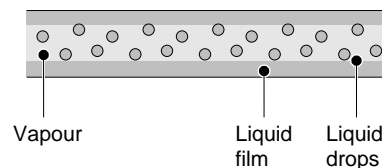
The fourth type shown in Figure 4 is called fog, dispersed, or homogeneous flow. This is the opposite of the first type, bubble flow, in that in the latter case the vapor fills the entire channel and the liquid is dispersed throughout the vapor in the form of individual droplets.

Figure 4
Fog flow

Vapour   Liquid
          drops
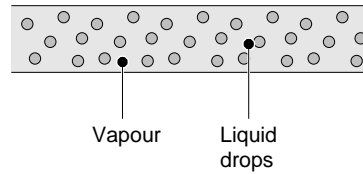
The fifth type, stratified flow, occurs at low flows in horizontal pipes when the steam and the water can separate due to gravity and buoyancy forces. That type of flow is of particular importance in Candu reactors because of their horizontal fuel channels and the potential for flow stratification when the primary system in not in nominal conditions.

Figure 5
Stratified flow

Vapour   Liquid
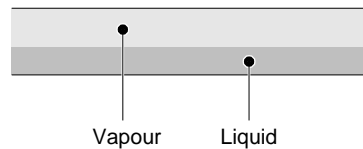
The paragraphs below introduce terms and definitions that characterize two phase flow such as quality, void, slip,...

2.1   Mass quality, x

The quality x of a vapor liquid mixture in a nonflow system, or where no relative motion between the vapor and liquid phases exists, is defined as:

$$x = \frac{\text{mass of vapour in mixture}}{\text{total mass of mixture}}$$

It is often convenient to use the fraction of the total mass flow which is composed of vapor or liquid.

$$x = \frac{W_g}{W_g + W_f}$$

2.2   Void fraction, a

The void fraction a is defined as:

$$\alpha = \frac{volume\ of\ vapour\ in\ mixture}{total\ volume\ of\ mixture}$$

The term void here is somewhat misleading, since there is actually no void but vapor.

The ratio of the cross-sectional area occupied by the gas phase to the total cross-sectional area is defined as the void fraction:

$$\alpha = \frac{A_g}{A}$$

and the non voided fraction as:

$$1 - \alpha = \frac{A_f}{A}$$

2.3 Relationship between quality and void

The relationship between x and α in a nonflow system can be obtained by assuming a certain volume containing 1 kg of mixture in thermal equilibrium as shown in Figure 6. That volume will be equal to $\upsilon = (1-x)\upsilon_f + x\upsilon_g$ where υ is the specific volume of the mixture.

Figure 6
Two phase mixture

Vapour   Liquid
bubbles
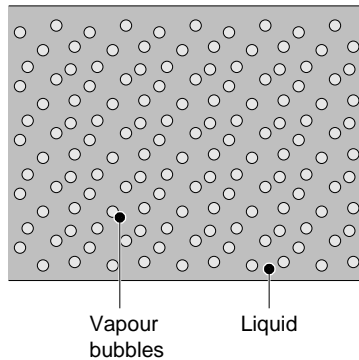
In an equilibrium mixture, the two phases are saturated liquid and saturated vapor and the volume of vapor present is equal to its mass, x, times its specific volume υ_g and α is thus given by:

$$\alpha = \frac{x\, v_g}{(1-x)\, v_f + x\, v_g}$$

This equation can also be written in the form

$$\alpha = \frac{1}{1 + \left(\dfrac{1-x}{x}\right)\left(\dfrac{v_f}{v_g}\right)}$$

where the specific volumes are all taken at the system pressure from appropriate thermodynamic property tables. Figure 7 shows calculated values for α versus x for light water at various pressures.

Figure 7
Void versus quality for different pressures
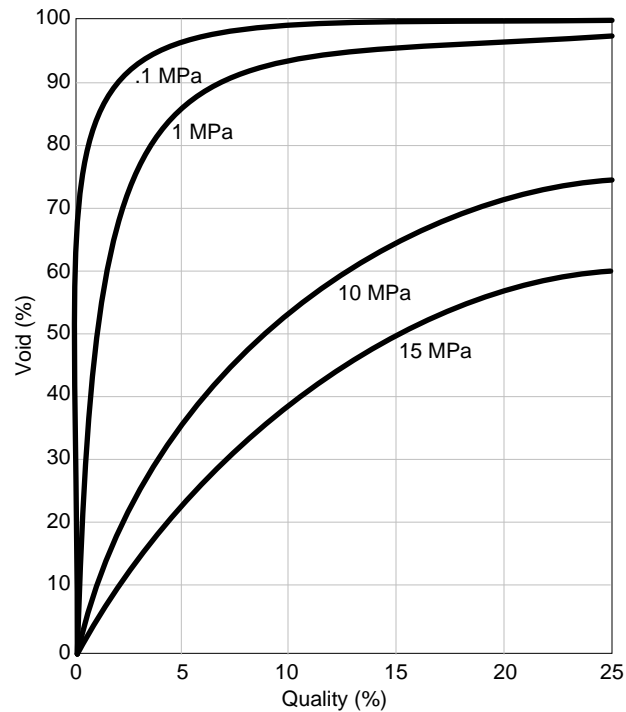
Examination of the curves reveals the following:
1. For constant x, α decreases with pressure.
2. For any pressure, dα/dx decreases with x.
3. At low values of x, dα/dx increases as the pressure decreases and becomes very large at low pressure.

At atmospheric pressure, it can be noted that a small quality (about 2 %) generates almost 100 % void.

2.4   Mass Flux, G
The rate of mass flow divided by the flow area is given the name mass flux or mass velocity.

$$G = \frac{W}{A}$$
$$W_g = G\,A\,x$$
and
$$W_f = G\,A\,(1 - x)$$

The gas velocity can be written as:

$$U_g = \frac{W_g}{\rho_g A_g} = \frac{Q_g}{A_g} = \frac{G \, x}{\alpha \, \rho_g}$$

and the liquid velocity as:

$$U_f = \frac{W_f}{\rho_f A_f} = \frac{Q_f}{A_f} = \frac{G(1-x)}{\rho_f(1-\alpha)}$$

where ρ_g and ρ_f are the densities of the vapor and the liquid phases.

2.5 Volumetric quality, ß

Sometimes, it is necessary to use the fraction of the total volumetric flow which is composed of vapor or liquid.

$$\beta = \frac{Q_g}{Q_g + Q_f} \quad \text{and} \quad (1-\beta) = \frac{Q_f}{Q_g + Q_f}$$

2.6 Volumetric flux, j

The volumetric flux or superficial velocity j is defined as the rate of volumetric flow divided by the flow area.

$$j = \frac{Q}{A}$$

The liquid and gas volumetric fluxes are then defined as:

$$j_g = \frac{Q_g}{A} = U_g \, \alpha \ = j \, \beta \ = \frac{G \, x}{\rho_g}$$

and

$$j_f = \frac{Q_f}{A} = U_f(1-\alpha) = j(1-\beta) = \frac{G(1-x)}{\rho_f}$$

2.7 Slip ratio, S

In the above calculations it was assumed that no relative motion existed between the two phases. However, if a two-phase mixture is moving, the vapor, because of its buoyancy and its different resistance characteristics, has a tendency to slip past the liquid and move at a higher velocity than that of the liquid. This is particularly true in vertical sections. The homogeneous solution in which each phase is assumed to move at the same speed, however, has been found satisfactory in most cases. In the homogeneous system, a slip ratio S, equal to 1 in nonflow or homogeneous flow and greater than 1 in nonhomogeneous two-phase systems is used. It is defined as the ratio of the average velocity of the vapor U_g to that of the liquid U_f. Thus the definition of the slip ratio:

$$S = \frac{U_g}{U_f}$$

The slip ratio modifies the relationship between void fraction and quality developed in the previous section. This will now be shown with the help of Figure 8 which shows a two-phase mixture flowing horizontally in a channel. A

certain section, between the dotted lines, small enough so that x and α remain unchanged, is considered.

Figure 8
Two phase mixture

Fuel   Liquid / Vapour
elements   Mix
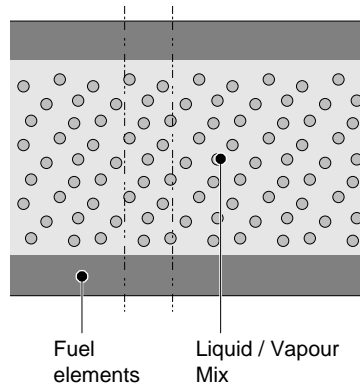
In a flow system, the quality at any one cross section is defined by

$$x = \frac{\textit{Mass flow rate of vapour}}{\textit{Mass flow rate of mixture}}$$

Thus if the total mass flow of the mixture is W, the vapor-flow rate is xW and the liquid-flow rate is (1-x)W, where x is the quality at the particular section. Applying the continuity equation, the velocities of vapor and liquid are given by:

$$U_g = \frac{v_g W}{A_g} x$$

and

$$U_f = \frac{v_f (1-x) W}{A_f}$$

where A_g and A_f are the cross-sectional areas of the two phases, perpendicular to flow direction, if the two phases are imagined to be completely separated from each other such as in Figure 9.

Figure 9
Separated two phase mixture

Fuel   Vapour   Liquid
elements
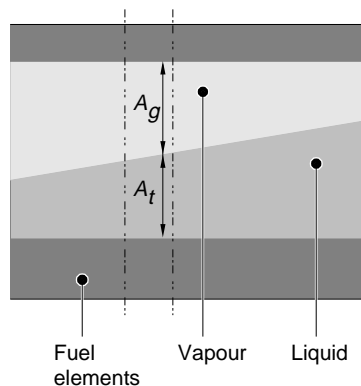
Combining the above equations gives

$$S = \frac{U_g}{U_f} = \frac{x}{1-x} \frac{A_f}{A_g} \frac{v_g}{v_f}$$

The void fraction in the section considered is the ratio of the vapor-phase volume to the total volume within the section. In the small section of channel considered, this is the same as the ratio of cross-sectional area of vapor A_g to the total cross-sectional area of the channel. Thus

$$\alpha = \frac{A_g}{A_g + A_f}$$

or

$$\frac{A_f}{A_g} = \frac{1-\alpha}{\alpha}$$

The slip factor S can then be written as :

$$S = \frac{x}{1-x} \frac{1-\alpha}{\alpha} \frac{v_g}{v_f}$$

This equation can be rearranged to give a relationship between α and x, including the effect of slip, as:

$$\alpha = \frac{1}{1 + \left(\frac{1-x}{x}\right)\left(\frac{v_f}{v_g}S\right)} = \frac{1}{1 + \left(\frac{1-x}{x}\right)\psi}$$

and

$$x = \frac{1}{1 + \left(\frac{1-\alpha}{\alpha}\right)\frac{1}{\psi}}$$

By re-arranging the above expression, the following relationship for void fraction can be produced.

$$\frac{1}{\alpha} = 1 + \frac{S(1-x)\rho_g}{x\,\rho_f} = 1 + \frac{S(1-\beta)}{\beta}$$

By re-arranging the above expression, the following relationship for volumetric quality can be produced.

$$\beta = \left[1 + \frac{(1-x)}{x}\frac{\rho_g}{\rho_f}\right]^{-1}$$

Note that the relationship between α and x for no slip (S = 1) is a special case of the general relationship.

The effect of slip is to decrease the value of α corresponding to a certain value of x below that which exists for no slip. This can be seen in the slip equation.

At constant pressure and quality, the factor$(1 - \alpha)/\alpha$ is directly proportional to S. Thus, α decreases with S. A high S is thus an advantage from both the heat-transfer and moderating-effect standpoints. Figure 10 shows α versus x for light water at 100 bars and several slip ratios.

Figure 10
Void versus quality for different slip ratios
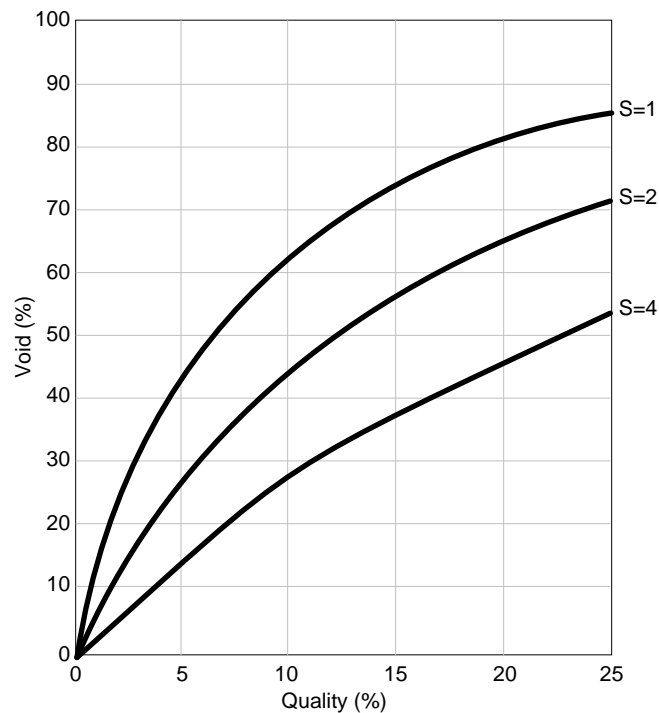
S has been experimentally found to decrease with both the system pressure and the volumetric flow rate and to increase with power density. It has also been found to increase with the quality at high pressures but to decrease with it at very low pressures.

As a function of the channel length, S has been found to increase rapidly at the beginning and then more slowly as the channel exit is approached. At the exit itself, turbulence seems to cause a sudden jump in the value of S.

Experimental data or theoretical correlations for S covering all possible operating and design variables do not exist. In boiling-reactor studies, values for S may be estimated from data that closely approach those of interest. In this a certain amount of individual judgment is necessary. Otherwise, experimental values of S under similar conditions of a particular design must be obtained. This procedure is usually expensive and time-consuming but may be necessary in some cases. The importance of obtaining accurate values of S may best be emphasized by the following: One step in the procedure of core channel design

is to set a maximum value of α at the channel exit.

This is usually determined from nuclear (moderation) considerations. A corresponding value of x, at the selected S, is then found from the above equations. The latter determines the heat generated in the channel.

In design, the usual procedure is to assume a constant value of S along the length of the channel. This, of course, is a simplification, which may introduce further error into the results. However, S is seen to be fairly constant over most of the channel length, indicating this assumption to be a good one.

2.8 Two-Phase density, ρ_{tp}

The magnitude of the two-phase density, ρ_{tp}, depends on the specific void fraction relationship used for the calculation.

$$\rho_{tp} = \alpha\,\rho_g + \left(1 - \alpha\right)\rho_f$$

3. Flow Regimes

The analysis of single-phase flow is made easier if it can be established that the flow is either laminar or turbulent and whether any separation or secondary flow effect occurs. Although this information is equally useful in the study of gas-liquid flow, the topology or geometry of the flow is perhaps of greater importance. When a liquid is vaporized in a heated channel, the liquid and vapor generated take up a variety of configurations known as flow patterns. The particular flow pattern depends on pressure, flow, heat flux, entrance conditions (i.e., local phase distribution at inlet) and channel geometry. Because the name given to a flow pattern is to a large extent subjective, there exists in the literature a multitude of terms purporting to describe the various possible phase distributions.

The sequence of flow patterns encountered generally in vertical upwards co-current flow for increasing levels of quality is shown below:

$$\rightarrow \begin{array}{c} single-phase \\ liqiud \\ (x = 0) \end{array} \rightarrow \begin{array}{c} bubbly \\ flow \end{array} \rightarrow \begin{array}{c} slug \\ flow \end{array} \rightarrow \begin{array}{c} churn \\ flow \end{array} \rightarrow \begin{array}{c} wispy-annular \\ flow \end{array} \rightarrow \begin{array}{c} steam \\ only \\ (x = 1) \end{array}$$

The flow patterns observed in co-current two-phase in **horizontal** and **inclined** tubular channels are complicated by asymmetry of the phases resulting from the influence of gravity. The generally-accepted flow patterns are:

$$\rightarrow \begin{array}{c} single\text{--}phase \\ liqiud \\ (x=0) \end{array} \rightarrow \begin{array}{c} bubbly \\ flow \end{array} \rightarrow \begin{array}{c} slug \\ flow \end{array} \rightarrow \begin{array}{c} churn \\ flow \end{array} \rightarrow \begin{array}{c} wispy\text{--}annular \\ flow \end{array} \rightarrow \begin{array}{c} steam \\ only \\ (x=1) \end{array}$$

Flow-regime determination is important in thermalhydraulic analysis as both the Critical Heat Flux (CHF) and the pressure drop are strongly affected by the occurrence of flow stratification.

One flow pattern map, that of Baker has become generally accepted and widely used for horizontal channels (1) and is shown in Figure 11.

Figure 11
Baker flow pattern

Groeneveld and Leung (16) have recently recommended the Taitel and Dukler flow-regime map for use with CANDU heat transport system components, especially the fuel string, in horizontal flow. Taitel and Dukler (17) have developed a sound mechanistic model for predicting the transition between flow regimes inside both diabatic and adiabatic horizontal tubes. Their analysis considers the conditions for transition between five basic horizontal flow regimes:
a)   stratified-smooth flow
b)   stratified-wavy flow
c)   intermittent (slug or plug flow) flow
d)   annular flow
e)   dispersed-bubbly flow.

The Taitel-Dukler flow-regime map shown in Figure 12 is valid for very wide ranges of pressure, quality, mass flux and tube diameter.

Figure 12
Taitel-Dukler flow pattern
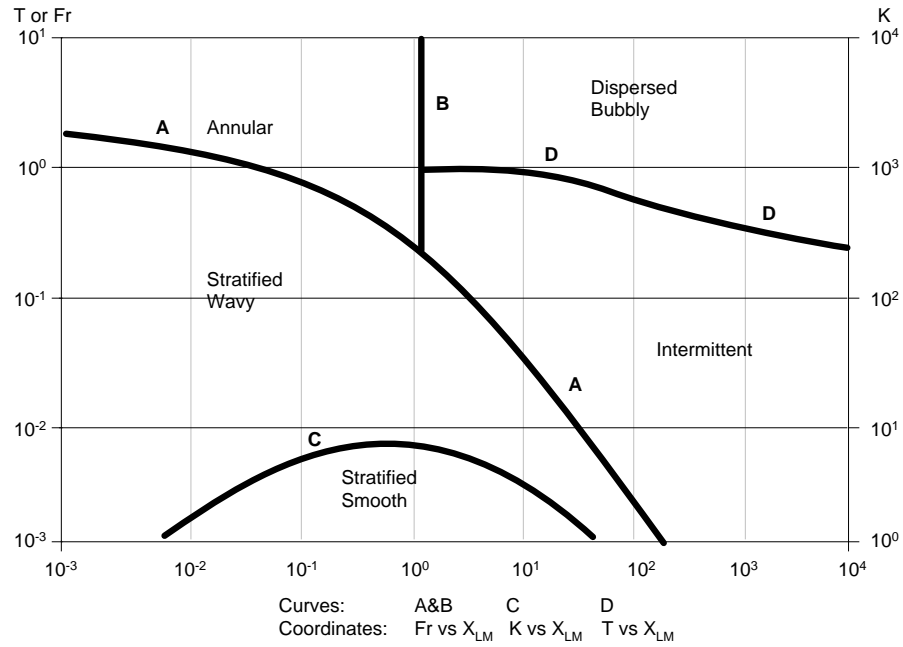
Many flow-regime maps for vertical flow have been developed over the past two decades, but only a few of them are relatively useful. Hewitt and Roberts (1) have developed a flow-regime map shown in Figure 13 from observations on low-pressure air-water and high-pressure steam-water flows in vertical tubes with small diameter. The axes represent the superficial momentum fluxes of the liquid $(\rho_f j_f^2)$ phases, respectively.

Figure 13
Hewitt and Roberts flow pattern
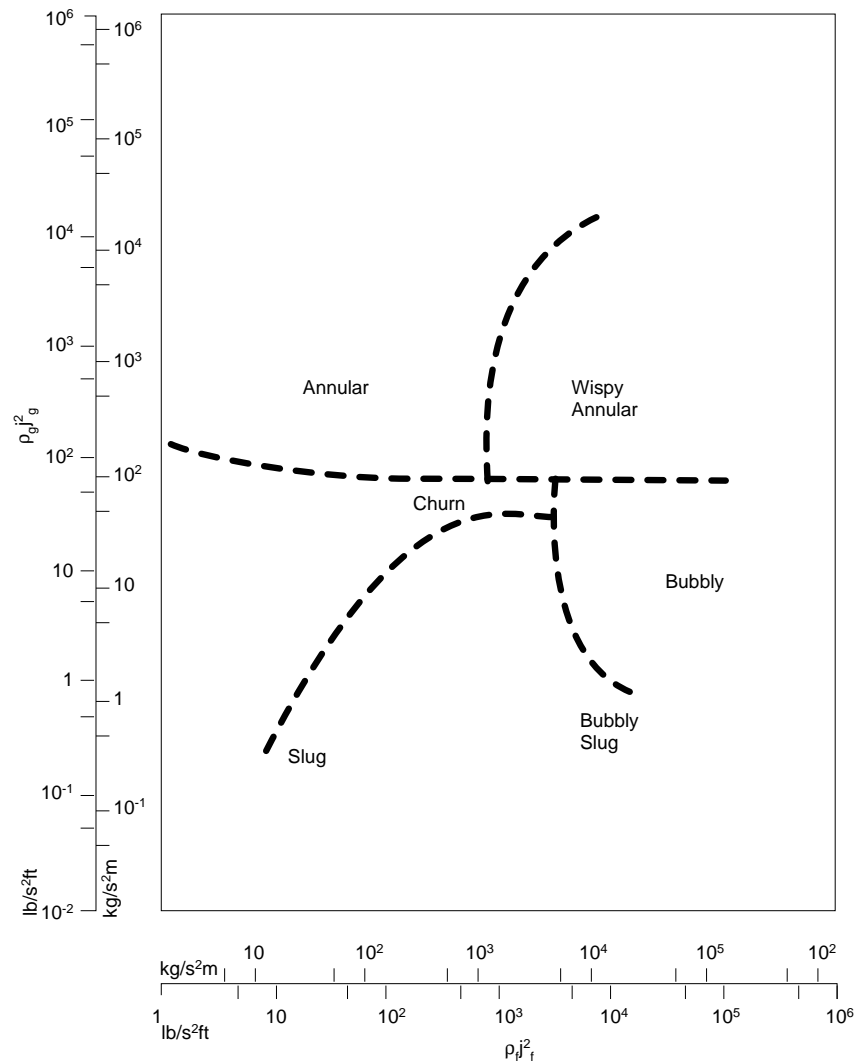
However, this may be regarded as no more than a rough guide, because the momentum fluxes alone are not adequate to represent the influence of fluid properties on the channel diameter.

Groeneveld and Leung (16) have tentatively recommended the Taitel and Dukler flow-regime map for use with CANDU heat transport system components in vertical flow. Taitel and Dukler (21) analyzed the transitions between different flow regimes based on their physical model and created a flow-regime map shown in Figure 14 with simple co-ordinates (j_f and j_g).

Figure 14
Taitel and Dukler simplified flow regime map
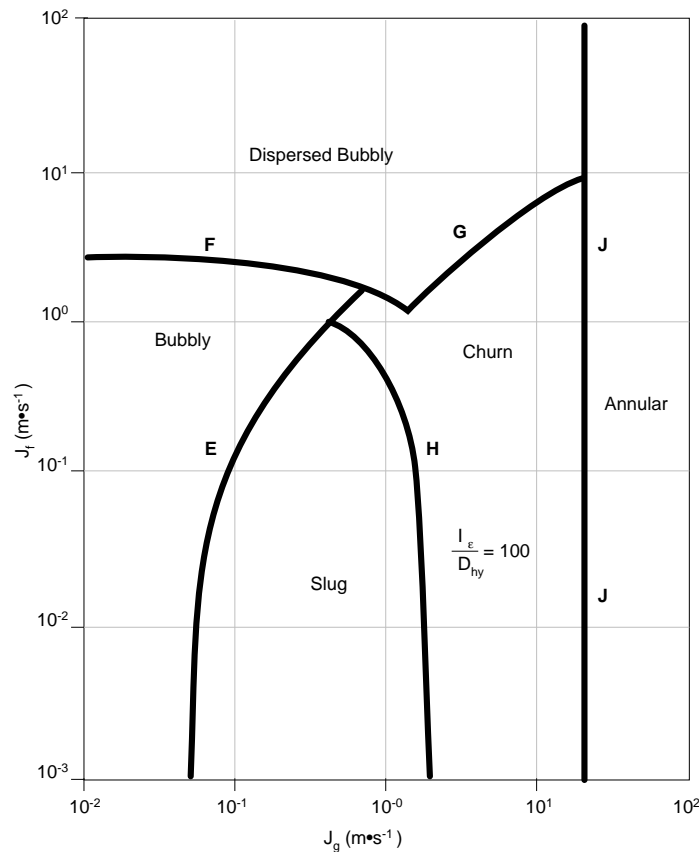
At different pressures and tube diameters, the flow-regime map may vary to a certain degree.

4.   Basic Models

There are three main types of flow models in the analysis of two-phase flow pressure drops:
a)   the `homogeneous' flow model,
b)   the `separated' flow model,
c)   the `flow pattern' or `drift flux' models. In this more sophisticated approach, the two phases are considered to be arranged in one of three or four definite prescribed geometries. These geometries are based on the various configurations or flow patterns found when a gas and a liquid flow together in a channel. The basic equations are solved within the framework of each of these idealized representations. In order to apply these models, it is necessary to know when each should be used and to be able to predict the transition from one pattern to another.

The homogeneous model and the separated flow model are the two most widely used and tested treatments of two-phase flow presently available.

4.1   The homogeneous flow model

The homogeneous model considers the two-phase flow as a homogenized mixture (pseudo-fluid) possessing mean fluid properties. It neglects any effect flow patterns may have on the two-phase flow and ignores interaction between the phases.

The basic assumptions of the homogeneous model are:
a) Equal vapor and liquid linear velocities
$$U_g = U_f = U \quad \text{(slip ratio } S = 1\text{)}$$

b) Thermal equilibrium exists between the two phases
$$T_g = T_f = T_{sat}(p)$$
where $T_{sat}(p)$ is the saturation temperature at the pressure p.

c) Frictional pressure drop can be calculated by substituting suitable weighted average values for properties such as velocity, density, and viscosity in the single-phase equations.

For the homogeneous flow model, the mixture density is given by
$$v = (1 - x) v_f + x\, v_g = \frac{1}{\rho_h}$$
where ρ_h is the mean density of the homogeneous fluid, and the void fraction is given by:
$$\frac{1 - \alpha}{\alpha} = \frac{1 - x}{x} \frac{v_f}{v_g} \quad \text{where slip ratio } S = 1$$

or

$$\alpha = \beta$$

The ratio of the two-phase and single-phase pressure gradients is defined as the two-phase friction multiplier which, for the homogeneous flow model, can be expressed as:

$$\phi_{LO}^2 = \frac{f_{tp}}{f} \left[1 + x \left(\frac{v_g}{v_f} - 1 \right) \right]$$

where ϕ^2_{LO} = two-phase friction multiplier for total flow assumed liquid.
f = single-phase friction factor
f_{tp} = two-phase friction factor

In the homogeneous model, the underlying idea is to replace the two-phase fluid by an equivalent compressible single-phase fluid. The homogeneous model is applicable only if there is no rapid variation of flow parameters and its thermal non-equilibria have no great influence. Although the homogeneous model predicts the dependence of two-phase friction multiplier on pressure and quality reasonably well, it has two unsatisfactory features:
a. the friction multiplier is a function of pressure and quality only and is independent of mass flux, and
b. it generally underpredicts low quality data.

The effect of mass velocity on the two-phase friction multiplier has been widely reported. Experimental data from various sources show that there is a mass velocity effect with steam-water flow at high pressure. The higher the pressures and velocities, the more realistic the homogeneous model. The homogeneous model generally gives good agreement for mass fluxes greater than 2000 kg/m^2.s. Considering the various possible flow patterns which occur in two-phase flow, it is apparent that the theoretical concept of a homogeneous flow can be approached only in mist or finely dispersed bubbly flow.

4.2   The separated flow model

The separated flow model considers the two phases to be artificially segregated into two streams: one of liquid and one of vapor. Conservation equations are written separately for each phase and interaction between phases if taken into account by constitutive relationships. The basic equations for the separated flow model are not dependent on the particular flow configuration adopted. The basic assumptions of the separated flow model in the analysis of the two-phase pressure drop are:

a) The velocities of each phase are constant, but not necessarily equal, in any given cross-section, within the zone occupied by the phase.
b) Thermodynamic equilibrium exists between the two phases.
c) The use of empirical correlations to relate the two-phase friction multiplier ϕ^2 and the void fraction α to the dependent variables of the flow.

From a consideration of the various flow patterns it would be expected that this model would be most valid for the annular flow pattern.

The frictional pressure gradient can be expressed in terms of single-phase pressure gradient for the total flow considered as liquid.

Now, using the Blasius equation

$$\frac{f_f}{f_{fo}} = \left[\frac{1}{(1-x)}\right]^{0.25}$$

one obtains:

$$\phi_{fo}^2 = \phi_f^2 \left(1-x\right)^2 \frac{f_f}{f_c} = \phi_f^2 \left(1-x\right)^{1.75}$$

The mean density of the two-phase fluid is:

$$\frac{1}{\rho_m} = \frac{(1-x)^2}{\rho_f(1-\alpha)} + \frac{x^2}{\rho_g\,\alpha}$$

Assuming that the gas phase and liquid phase pressure drops are equal, irrespective of the flow pattern, and the acceleration and elevation pressure drops are negligible then the two-phase multiplier for the separated flow model is given by:

$$\phi_{fo}^2 = \frac{\rho_f}{\rho_m} = \left[\frac{(1-x)^2}{(1-\alpha)} + \frac{\rho_f\,x^2}{\rho_g\,\alpha}\right]$$

In order to evaluate the frictional pressure gradient and the acceleration and elevation pressure drops it is necessary to develop expressions for the two-phase multiplier ϕ^2_{fo} and the void fraction α in terms of the independent flow variables.

4.2.1 Martinelli-Nelson correlation

Martinelli-Nelson developed one of the earliest models for the two-phase pressure drop based on the basic assumptions of the separated flow model. The correlation was originally developed by Martinelli for round pipes with no heat addition. Martinelli-Nelson obtained values for the two-phase friction multiplier and void friction as functions of pressure and mass quality based on the diabatic data of Davidson (20). A major shortcoming of the Martinelli-Nelson two-phase friction multiplier correlation is that it assumes the multiplier to be dependent on steam quality and pressure only and does not include the effect of mass velocity which has been observed experimentally. Figure 15 shows the two phase friction multiplier for various pressure and qualities.

Figure 15
Martinelli-Nelson two phase flow multiplier
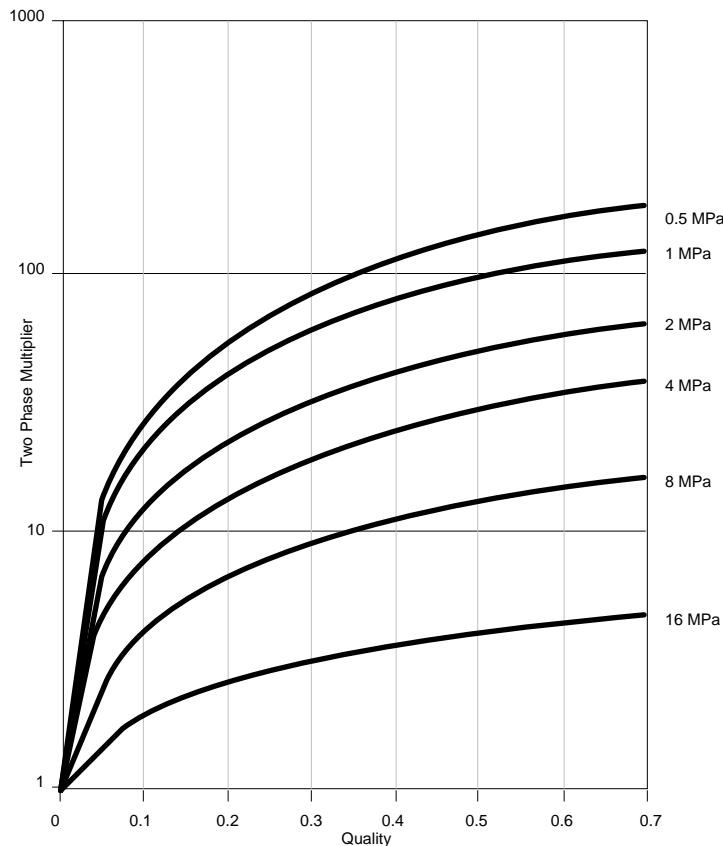
4.2.2   Thom correlation

Based on high pressure steam, water pressure drop data obtained in horizontal and vertical tubes in diabatic as well as adiabatic conditions, Thom obtained a consistent set of values for the two-phase friction multiplier and void fraction in terms of pressure and quality.

This correlation predicts high pressure experimental data better than the Martinelli-Nelson. However, it has the same shortcoming as that of Martinelli-Nelson in that it does not include the effect of mass flow on the two-phase friction multiplier correctly.

$$\phi_L = 1 + \frac{C}{X_{LM}} + \frac{1}{X_{LM}^2}$$

with,

$$C = 1.1 \left[\left(\frac{v_g}{v_f} \right)^{1/2} + \left(\frac{v_f}{v_g} \right)^{1/2} \right] - 0.2$$

And

$$X_{LM}^2 = \left(\frac{1-x}{x} \right)^{1.8} \left(\frac{v_f}{v_g} \right) \left(\frac{\mu_f}{\mu_g} \right)^{0.2}$$

4.3   The drift flux model

This model has been developed principally by Zuber (23) and Wallis (24) together with their co-workers.

The essential relationships of the drift flux model are presented below.

Relative velocity between the phases, $U_{gf,}$ can be expressed as:

$$U_{gf} = \left(U_g - U_f \right) = \frac{j_g}{\alpha} - \frac{j_f}{\left(1 - \alpha \right)}$$

A drift flux, $j_{gf,}$ is defined as:

$$j_{gf} = U_{gf} \, \alpha \left(1 - \alpha \right) = j_g - \alpha j$$

The drift flux $j_{gf,}$ physically represents the volumetric rate at which vapor is passing forwards (in up-flow) or backwards (in down-flow) through unit area of a plane normal to the channel axis already travelling with the flow at a velocity j. To preserve continuity an equal and opposite drift flux of liquid (j_{fg}) must also pass across this same plane.

Rearranging,

$$j_g = \alpha j + j_{gf}$$

The above relationship is true for one-dimensional flow or at any local point in the flow. It is often desirable to relax the restriction of one-dimensional flow.

Denoting the average properties of the flow by a bar, thus, $\overline{u}$, then,

$$j_g = \left(\overline{\alpha j}\right) + \left(j_{gf}\right)$$

Define a parameter, C_o, such that,

$$C_O = \frac{\left(\overline{\alpha j}\right)}{\left(\overline{\alpha}\right)\left(\overline{j}\right)}$$

It is also found convenient to define a weighted mean drift velocity,

$$\overline{u}_{gj} = \frac{\overline{j_{gf}}}{\overline{\alpha}}$$

then

$$\overline{u}_g = \frac{\overline{j_g}}{\overline{\alpha}} = C_O\left(\overline{j}\right) + \overline{u}_{gj}$$

or

$$\overline{\alpha} = \frac{\dfrac{\overline{\beta}}{C_O + \left(\overline{u}_g\right)}}{\left(\overline{j}\right)}$$

It will be seen that if there is no local relative motion between the phases

$$\left(\overline{u}_g = 0\right) \text{ then } \overline{\alpha} = \frac{\overline{\beta}}{C_O}$$

for one-dimensional homogeneous flow, $\alpha = \beta$. In other words the parameter C_o represents an empirical factor correcting the one-dimensional homogeneous theory to account for the fact that the concentration and velocity profiles across the channel can vary independently of one another.

The drift flux model can be used with or without reference to any particular flow regime.

Experimental data plotted as $\left(\overline{j_g}\right) / \left(\overline{\alpha}\right)$ *vs* $\left(j\right)$

are used to yield expressions for C_O *and* $\left(j_{gf}\right)$ *(or alternatively* $\overline{u}_{gj}$*)*

The particular values these parameters take up will vary depending upon whether or not the chosen is restricted to a particular flow pattern.

The drift flux approach, therefore, satisfactorily accounts for the influence of mass velocity on the void fraction as seen in the separated flow model and equation and an empirical expression for C_o may be used to provide the required relationship between void fraction and the independent flow pattern.

The drift flux model is valuable only when the drift velocity is significant compared with the total volumetric flux say ($\bar{u}_{gi} > 0.05$ j).

5. Pressure Gradients and Pressure Drops

5.1 Acceleration

When a coolant expands or contracts because of heat exchange, it has to accelerate as it travels through a channel. There will therefore be a force F equal to the change in momentum of the fluid. This force equals an acceleration pressure drop times the cross-sectional area of the channel. This pressure drop is usually small in single-phase flow, but can be quite large in two-phase flow. In reactor work where single-phase fluid enters the channel and two-phase fluid, with a high exit void fraction, leaves it, the change in momentum is particularly important. In such a case the pressure gradient due to the acceleration of the flow is determined from the momentum balance:

$$\frac{dP}{dz}\Big|_{mom} = G^2 \left[\frac{x^2 v_g}{\alpha} + \frac{(1-x)^2}{(1-\alpha)} v_f\right]\Bigg|_1^2 \theta\, 1\, \Delta\ set\ point$$

5.2 Gravity

The pressure gradient due to gravity is determined from:

$$\frac{dP}{dz}\Big|_{gravity} = g \sin \theta \left[\alpha\, \rho_g + (1-\alpha)\, \rho_f\right]$$

The evaluation of the gravity pressure gradient is extremely important in the case of thermosyphoning in single or two phase flow, since it is the only driving force for the flow in the system.

5.3 Pressure drop at restrictions

Two-phase mixtures encounter sudden area changes, such as when they enter and leave fuel channels, fuel bundles, pass by spacers, and others. The pressure changes associated with these are usually small. Their magnitude could, however, as in natural-circulation systems, be large relative to the driving pressures, and therefore must be evaluated as accurately as possible since they can influence coolant flow rates and consequently maximum power.

As with friction, these pressure changes are higher in two-phase than in single-

phase flow because of the increased speed of the coolant caused by the presence of steam. It also follows that the larger the void fraction, the larger the pressure change.

In the analysis one must evaluate integrated momentum and kinetic energy before and after the area change. These, however, cannot be evaluated with complete accuracy because detailed velocity distributions between the phases and the extent of equilibrium between the phases are not well known. Experimental data and empirical or semiempirical approaches are often used.

The following analysis assumes a one-dimensional flow, adiabatic flow across the area change, so that x is constant, and pressure changes that are small compared to the total pressure so that ρ_f and ρ_g do not change significantly.

The following continuity equations, derived with reference to Figure 6 will aid in the analysis. The total flow entering the channel can be expressed as:

$$W = \rho \, V \, A$$

The liquid flow as:

$$W_f = (1 - x) \, W = (1 - \alpha) \, \rho_f V_f A$$

and the steam flow as:

$$W_g = x \, W = \alpha \, \rho_g \, V_g \, A$$

Consequently the velocities of the phases can be expressed as:
for the liquid inlet velocity,

$$V_{f_i} = \frac{(1-x)}{1-\alpha_i} \frac{W}{\rho_f A_i}$$

for the liquid outlet velocity,

$$V_{f_o} = \frac{(1-x)}{1-\alpha_o} \frac{W}{\rho_f A_o}$$

for the steam inlet velocity,

$$V_{g_i} = \frac{x}{\alpha_i} \frac{W}{\rho_g A_i}$$

and for the steam outlet velocity,

$$V_{g_o} = \frac{x}{\alpha_o} \frac{W}{\rho_g A_o}$$

where the subscripts i and o refer to before and after the area change respectively.

5.4 Pressure rise at expansion

In two phase flow the calculation of the total pressure change across a sudden expansion can be calculated as follows. A momentum balance is written assuming, that P_i still acts on A_o immediately after expansion, as follows

$$P_i A_o + W_{fi} V_{fi} + W_{gi} V_{gi} = P_0 A_0 + W_{fo} V_{fo} + W_{go} V_{go}$$

Using the relationships developed for the velocities and a relationship between α_2 and α_1 the pressure rise across the expansion can be written as:

$$p_o - p_i = \frac{w^2}{Ai^2}\left(1 - \frac{Ai}{Ao}\right)^2 \left(\frac{(1-x)^2}{\rho_f (1-\alpha)} + \frac{x^2}{\rho_g \alpha}\right)$$

As in single-phase, there is a net pressure rise across an expansion. It can be seen that for the same mass-flow rate and areas, since x is smaller than α, the pressure rise in two-phase flow is greater than in single-phase flow. The two-phase equation can be reduced to the single phase equation with $x = \alpha = 0$.

6. Void Fraction Correlations

In order to calculate the change of static pressure along a two-phase flow system, it is essential to obtain the void fraction of the mixture at every point in the flow. The number of void fraction correlations that have been developed is extensive. At present, there are over thirty different methods of correlating void fraction with other flow parameters. Most of these relationships are based on one and two component adiabatic flow data. Systematic comparisons have been made between accepted correlations and data banks containing void fraction or density measurements. Ten parameters may be considered to affect the void fraction of the mixture for two-phase flow in a round, straight pipe under adiabatic correlations:

a) the liquid and gas (or vapor) mass flow rates (W_f, W_g),
b) the liquid and gas (or vapor) densities (ρ_f, ρ_g),
c) the liquid and gas (or vapor) viscosities (μ_f, μ_g),
d) the surface tension (σ),
e) the pipe inside diameter (D),
f) the pipe roughness (ε),
g) the orientation of the pipe (θ).

The effects of heat flux and possible mass transfer between the phases (evaporation or condensation), together with the effects of complex geometries, bends and sudden flow changes should be considered for more general conditions.

6.1   Homogeneous model

The void fraction is given by:

$$\alpha = \frac{x\, v_g}{\left(1-x\right) v_f + x\, v_g}$$

The homogeneous void fraction correlation applies best for flows where the two phases are almost similar in density, single component flows near critical pressure. This correlation predicts, on average, higher values of void than are found experimentally. As expected, the correlation holds near the conditions of 100% void for all flows.

The prediction of mean density using the homogeneous theory always gives an underestimated value. This error increases with increase in the ratio of the density of the phases. Under all conditions the error on predicted mean density decreases with increase in mass velocity.

6.2   Von Glahn correlation

The Von Glahn correlation has the form:

$$\alpha = \left[\frac{1}{1 + \dfrac{\left(1-x\right)}{x}\, y^{0.67}}\right]^{y^{0.1}}$$

where

$$y = \frac{\rho_g}{\rho_f}$$

The exponents were derived empirically to obtain the best fit to available steam-water data for flow in unheated pipes.

The predicting ability of the Von Glahn correlation gets worse as the phase density ratio decreases and with increased velocity.

6.3   Rooney correlation

The Rooney correlation has the form

$$\alpha = k \, \beta$$

with

$$k = f\left(\frac{U_R}{j}\right) = a\left(\frac{U_R}{j}\right)^b + 1$$

and

$$U_R = \left[\frac{\sigma \, g \, \Delta \, \rho}{\rho_f^2}\right]^{0.25}$$

$$j = \frac{Q}{A}$$

$$\Delta \, \rho = \frac{\rho_f}{\rho_g}$$

The Rooney correlation does not necessarily fulfil the end condition that $\alpha \to 1$ as $\beta \to 1$. Unless very low mass velocity flows are considered, the correlation will give correct values at 100% void. Mass velocity has little effect on the prediction of this correlation except for large phase density ratios when an increase in mass velocity improves the predicted value.

6.4   Armand and Massena correlation

This modified homogeneous void fraction correlation has the following form:

$$\alpha_{A-M} = k \, \alpha_h$$

where

$$k = 0.833 + 0.167 \times$$

and

$$\alpha_h = \frac{x \upsilon_q}{(1-x)\upsilon_f \upsilon_q}$$

The Armand and Massena correlation is a modification of Armand's correlation to allow void fraction $\alpha \to 1$ as $x \to 1$, based on steam-water flow data. The Armand and Massena correlation only predicts correctly for high voids for high pressure steam flows.

6.5 Smith Correlation

The Smith correlation is based on an annular flow model with liquid and mist phases, each having the same momentum flux. The entrainment of the liquid into the gas phase was found empirically. The entrainment coefficient is defined as:

$$e = \frac{\text{liquid entrained}}{\text{total liquid flow rate}}$$

The slip ratio takes the form

$$S = e + \left(1 - e\right) \left[\frac{\frac{v_g}{v_f} + e\left(\frac{1-x}{x}\right)}{1 + e\left(\frac{1-x}{x}\right)} \right]^{1/2}$$

The Smith correlation predictions are more accurate in horizontal flow than in vertical flow. The predicted void is generally underestimated for high pressure steam flows. In all conditions the predictions improve at high mass velocity.

6.6　　　Chisholm correlation

The Chisholm correlation has the following form for the slip ratio:

$$S = \left[1 + x\left(\frac{v_g}{v_f} - 1\right) \right]^{1/2} \quad \text{for } \beta < 0.9$$

Figures 16 shows the calculated voids versus quality for a series of void correlations. It can be noted that the homogeneous model predicts the highest void for any given quality.

Figure 16
Void versus quality for different correlations
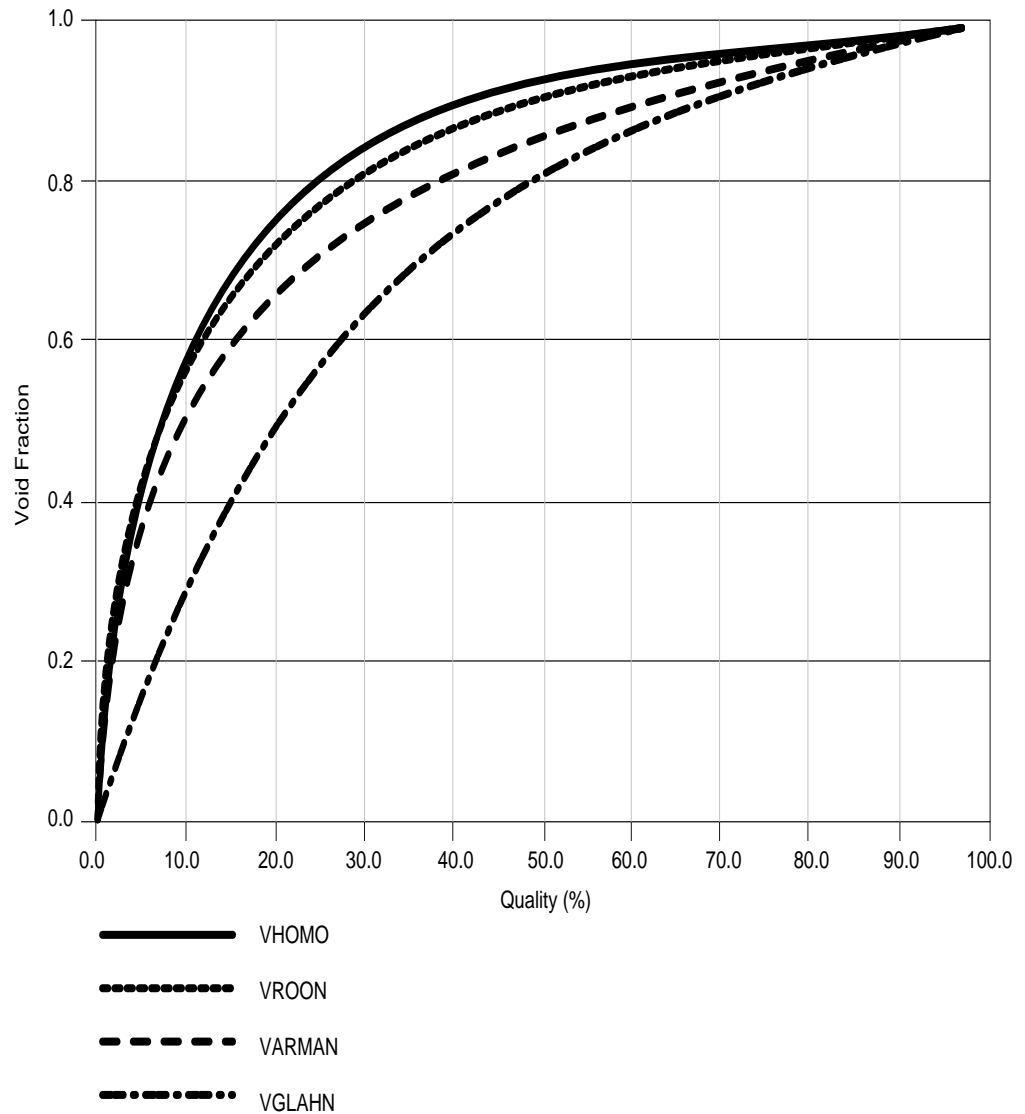
Two phase flow is an area of continuous research and development. The introduction of new calculation tools does not prevent the necessary knowledge of experimental results on which the numerous correlations are based on. The careful selection of the solution scheme along with the use of appropriate correlations is of utmost importance when solving two phase phenomena.

7. Notation

Symbol	Description	SI Units
A	Flow area	m^2
A_g	Flow area occupied by gaseous phase	m^2
A_f	Flow area occupied by liquid phase	m^2
D	Pipe diameter	m
D_h	Hydraulic diameter	m
e	Entrainment coefficient	
f	Single-phase friction factor	
f_{tp}	Two-phase friction factor	
g	Acceleration due to gravity	m/s^2
G	Mass flux	$kg/s.m^2$
h_{fg}	Latent heat of vaporization	J/kg
j	Volumetric flux (superficial velocity)	m/s
j_f	Superficial velocity of liquid phase	m/s
j_g	Superficial velocity of vapor phase	m/s
k	Coefficient in modified homogeneous model $(\alpha = k\beta)$	
P	Fluid pressure	Pa
q	Heat flux	W/m^2
Q	Volumetric rate of flow	m^3/s
Q_f	Volumetric rate of flow of liquid phase	m^3/s
Q_g	Volumetric rate of flow of vapor phase	m^3/s
R_c	Radius of curvature of bend	m
S	Slip ratio	
T	Temperature	°C
T_F, T_L	Bulk liquid temperature	°C
T_g	Vapor temperature	°C
T_{sat}	Saturation temperature	°C
u	Velocity	m/s
U_f	Actual velocity of liquid phase	m/s
U_g	Actual velocity of vapor phase	m/s
V	Velocity of fluid	m/s
v_f	Specific volume of liquid	m^3/kg
v_g	Specific volume of vapor	m^3/kg
w	Angular velocity	kg/s
W	Mass rate of flow	kg/s
W_f	Mass rate of flow of liquid phase	kg/s
W_g	Mass rate of flow of vapor phase	kg/s
x, x_{IN}	Thermodynamic quality	
X_{LM}	Lockhart-Martinelli parameter	
z	Length in direction of flow	m

Greek

α_f	Homogeneous liquid volume fraction	
α	Void fraction	
β	Volumetric quality	
ε	Pipe roughness	m
δ_1	Nominal thickness of viscous sublayer	m
ρ	Density	kg/m^3
ρ_f	Liquid density	kg/m^3
ρ_g	Vapor density	kg/m^3
ρ_H	Mean density of homogeneous fluid	kg/m^3
ρ_m	Mean density of two-phase fluid	kg/m^3
σ_{tp}	Two-phase density	kg/m^3
ϕ	heat flux	W/m^2
ϕ^2	Two-phase friction multiplier	
ϕ^2_{LO}	Two-phase frictional multiplier based on pressure gradient for total flow assumed liquid	
ϕ^2_{MN}	Martinelli-Nelson multiplier	
μ	Absolute viscosity	N.s/m^2
μ_f	Liquid viscosity	N.s/m^2
μ_g	Vapor viscosity	N.s/m^2
μ_{TP}	Two-phase viscosity	N.s/m^2
σ	Surface tension for planar interface	N/m
θ	Orientation of pipe: angle to horizontal	deg.

Dimensionless Numbers

Fr   Froude Number
Re   Reynolds Number

Subscripts

f   liquid phase
g   vapor phase
lo   liquid only
sc   subcooled
tp   two-phase

8.   References

Collier, J.G., "Convective Boiling and Condensation", McGraw-Hill Book Company, 1972.

Delhaye, J.M., et al, "Thermalhydraulics of Two-Phase Systems for Industrial Design and Nuclear Engineering", Hemisphere Publishing Corporation, 1981.

Beigles, A.E., Collier, J.G., Delhaye, J.M., et al, "Two-Phase Flow and Heat Transfer in the Power and Process Industries", Hemisphere Publishing Corporation, 1981.

Collier, J.G., Chisholm, D., et al, "Two-Phase Pressure Drop and Void Fractions in Tubes", HTFS-DF15/AERE-R6454, 1972 August.

Dougherty, R.L., and Franzini, J.B., "Fluid Mechanics with Engineering Applications", McGraw Hill Book Company, 7th Edition, 1977.

Reddy, D.G., Sreepada, S.R., and Nahavandi, A.N., "Two-Phase Friction Multiplier Correlation for High Pressure Steam-Water Flow", NP-2522/813, 1982, Columbia University, New York.

Idsiinga, W., Todreas, N., and Bowring, R., "An Assessment of Two-Phase Pressure Drop Correlations for Steam-Water Systems", Int. J. Multiphase Flow, 3 (1977), 401-413.

Snoek, C.W., "A Comparison of Prediction Methods for Pressure Drop in Multi-Element CANDU Fuel Channels", CRNL-4017, 1986 July.

Snoek, C.W., and Leung, L.K.H.;, "An Accurate Model for Pressure Drop Prediction in Multi-Element CANDU Fuel Channels", AECL-9236, Paper presented at the 4th International Symposium on Multi-Phase Transport and Particulate Phenomena, Miami Beach, Florida, 1986.

Snoek, C.W. and Ahmad, S.Y., "Development of a Two-Phase Multiplier Correlation Based on Pressure Drop Measurements in a Fully Segmented 37-Element Fuel String", CRNL-2286, 1983.

Friedel, L., "Improved Friction Pressure Drop Correlations for Horizontal and Vertical Two-phase Pipe Flow", 3-International, Volume 18, No. 7, pp. 485-492, 1979.

Chenoweth, J.M., and Martin, M.W., "Turbulent Two-Phase Flow", Petroleum Refiner, 34, No. 10, pp. 151-155, 1955 October.

Fitzsimmons, D.E., "Two-Phase Pressure Drop in Piping Components", HW80970 Revision 1, 1964 March.

Carver, M.B., Carlucci, L.N. and Inch, W.W.R., "Thermal-Hydraulics in Recirculating Steam Generators - THIRST Code User's Manual", AECL-7254, April 1981.

Banerjee, S. Hetsroni, G., Hewitt, G.F. and Yadigaroglw, G., "Multiphase Flow and Heat Transfer: Bases and Applications", Short Course held at the University of California (Santa Barbara), January 9-13, 1989.

Groeneveld, D.C. and Leung, L.K.H., "Compendium of Thermalhydraulic Correlations and Fluid Properties (Version 1991, Rev. 0)", COG-90-86 (ARD-TD-243), 1990 December.

Taitel, Y. and Dukler, A.E., "A Model For Predicting Flow Regime Transitions in Horizontal and Non Horizontal Gas-Liquid Flow", ASME 75-WA/HT-29, 1975.

Carlucci, L.N., "Review of Fluid Flow Correlations For Steam Generator Thermal-Hydraulic Analysis", CRNL-1999, 1980 January.

Freidel, L., "Mean Void Fraction and Friction Pressure Drop: A Comparison of Some Correlations With Experimental Data", Paper A7, European Two Phase Flow Group Meeting, Grenoble, 1977.

Davidson, W.F. et al, "Studies of Heat Transmission Through Boiler Tubing at Pressure From 500 to 3000 Pounds", Transactions of ASME, Vol. 65, 1993, pp 553-591.

Taitel, Y., and Duckler, A.E., "Flow Pattern Transitions in Gas-Liquid Systems: Measurement and Modelling", Multi-phase Science and Technology, Vol. II, pp. 1-94, 1986.

Jones, A.B., and Dight, D.G., "Hydrodynamic Stability of a Boiling Channel", Part 2, KAPL-2208, 1962.

Zuber, N., and Findlay, J., "Average Volumetric Concentration in Two-Phase Flow Systems", Trans. ASME J. Heat Transfer, 87, 453 (1965).

Wallis, G.B., "One Dimensional Two-Phase Flow", McGraw-Hill Book Company, 1969.

Operation Under Two Phase Flows

Training Objectives

The participant will be able to understand:
1   the areas of concern in two phase flow
2   the thermosyphoning implications
3   the present situation in the understanding of two-phase phenomena

Operation Under Two Phase Flows

Table of Contents

1.   Introduction

In this lesson we will briefly describe the situations in which two-phase flow occurs and assess the consequences on the overall reactor behaviour. Three areas have been identified: critical flow, pumps and natural circulation.

Critical flows occur when the velocity of the two phase mixture is controlled by its upper limit, i.e. the sonic velocity of the mixture. That velocity is a very strong function of quality, since it can vary from 300 m/s to 1400 m/s from single phase steam to single phase liquid for water.

The pumps are normally operated under single-phase conditions. Under degraded conditions two-phase mixture at the inlet of the pump can create severe vibrations that could either deteriorate the pump hydraulics or break a pipe.

Thermosyphoning is a mode of cooling that is relied upon, under no forced flow conditions. In many scenarios the pressure and inventory control of the HT cannot preclude the formation of void and the HT is operating under two-phase flow conditions.

2.   Critical Flows

2.1   Two-phase flow in orifices

The main object of orifices is to measure flow rates, which are functions of the square roots of pressure drops across them. Orifices, however, approximate many flow restrictions, such as spacers in reactor cores and other obstacles. It is the intent here to evaluate the pressure drop across orifices. The relation will be used for break discharge flows determination

2.1.1   Single-phase flow

The mass-flow rates for liquid and vapor are obtained from the continuity and energy equations, and given by the well-known equations

$$\dot{m}_f = A_0' \sqrt{2\, g_c\, \rho_f \left(\Delta\, p_{SP}\right)_f}$$

and

$$\dot{m}_g = A_0' \sqrt{2\, g_c\, \rho_g \left(\Delta\, p_{SP}\right)_g}$$

where

$$A_0' = C_d\, \frac{A_0}{\sqrt{1 - \left(\dfrac{A_0}{A_C}\right)^2}}$$

(Δp_{SP}) is the single-phase pressure drop, A_0 and A_c are the cross-sectional areas of the orifice and channel (figure 2.1) and C_d is a coefficient of discharge, obtained from experiments and is a function of the type of orifice, pressure-tap locations, etc.

Figure 2.1:
Channel with thin plate orifice.

Orfice area, A_O

Channel area, A_C
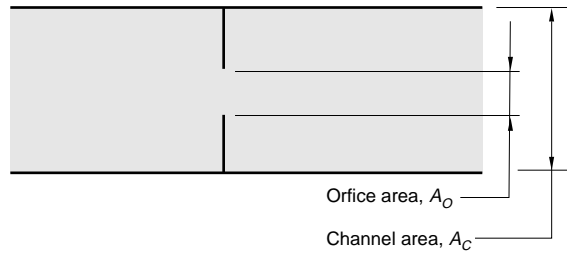
2.1.2   Two-phase flow

In two-phase flow, two similar expressions can be written for coexistent liquid and vapor phases of the above mass-flow rates as:

$$\dot{m}_f = A'_{0f} \sqrt{2\, g_c\, \rho_f \left(\Delta p_{TP}\right)_f}$$

and

$$\dot{m}_g = A'_{0g} \sqrt{2\, g_c\, \rho_g \left(\Delta p_{TP}\right)_g}$$

$(\Delta p_{TP})_f$ and $(\Delta p_{TP})_g$ are the two-phase pressure drops due to liquid and vapor respectively. A'_{0f} and A'_{0g} are given by

$$A'_{0f} = C_d \frac{A_{0f}}{\sqrt{1 - \left(\dfrac{A_0}{A_C}\right)^2}}$$

and

$$A'_{0g} = C_d \frac{A_{0g}}{\sqrt{1 - \left(\dfrac{A_0}{A_C}\right)^2}}$$

where A_{0f} and A_{0g} are the flow areas within the orifice occupied by liquid and vapor respectively. Thus

$$A'_{0f} + A'_{0g} = C_d \frac{\left(A_{0f} + A_{0g}\right)}{\sqrt{1 - \left(\dfrac{A_0}{A_C}\right)^2}}$$

and since $A_{0f} + A_{0g} = A_0$, $A_{0f}' + A_0g' = A_0'$

Assuming C_d does not change materially, the above equations can be combined to give

$$\sqrt{\frac{\left(\Delta p_{SP}\right)_f}{\left(\Delta p_{TP}\right)_f}} + \sqrt{\frac{\left(\Delta p_{SP}\right)_g}{\left(\Delta p_{TP}\right)_g}} = 1$$

Noting that $(\Delta p_{TP})_f$ and $(\Delta p_{TP})_g$ must both be equal to a two-phase pressure drop

Δp_{TP}, the above equation reduces to:

$$\sqrt{\Delta\ p_{TP}} = \sqrt{\left(\Delta\ p_{SP}\right)_f} + \sqrt{\left(\Delta\ p_{SP}\right)_g}$$

Δp_{TP} is therefore simply obtained from calculated pressure drops of the liquid and vapor phases as if they were flowing alone through the orifice. Their respective flow rates are obtained from the total flow rate and quality.

Experimental work from Murdoch on a wide range of operating conditions, showed that the above equation should be modified to

$$\sqrt{\Delta\ p_{TP}} = 1.26\ \sqrt{\left(\Delta\ p_{SP}\right)_f} + \sqrt{\left(\Delta\ p_{SP}\right)_g}$$

2.2   Critical flow

When the back pressure p_b is reduced below a constant upstream pressure p_0 in a flow system (line 1 in figure 2.2), flow begins and a gradient is established in the connecting channel between p_0 and a pressure p_e at the exit of the channel. The flow increases as p_b is reduced further (line 2). p_e remains equal to p_b to a point. This point, represented by line 3, is reached when p_b is reduced sufficiently to cause the flow velocity at the exit of the channel to equal that of the speed of sound at the temperature and pressure at the exit of the channel, V^*. At that point, the mass flow attains a maximum value.

Further reduction in p_b results in no further increase in mass flow rate or decrease in p_e (lines 4 and 5). The flow remains at the above maximum value and is said to be critical. The channel, and flow, are also said to be restricted or chocked. As p_b is reduced and p_e remains constant, free expansion of the fluid between p_e and p_b occurs outside the channel and the flow takes on a paraboloid shape there.

Figure 2.2:
Critical flow model.
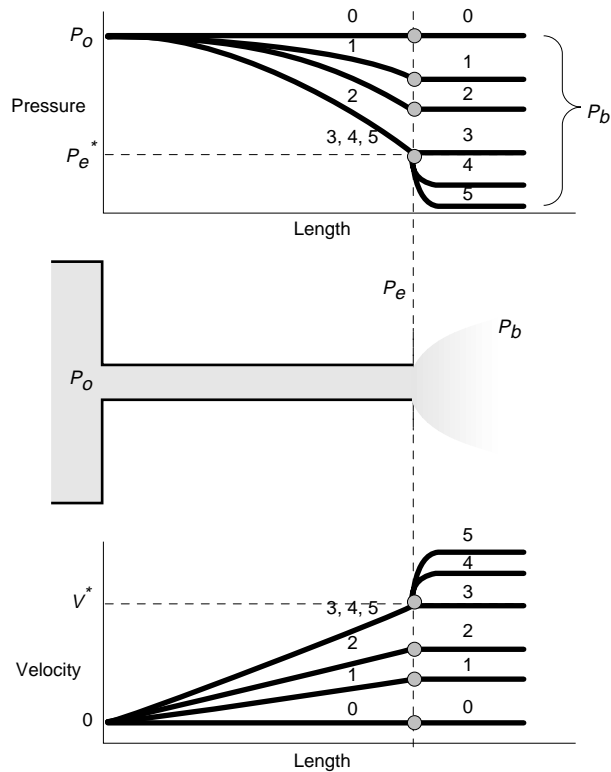
This phenomenon occurs in both single- and two- phase flow. It occurs and is utilized, in many flow and measuring systems. In two-phase flow, serious theoretical and experimental studies of the phenomenon have been made only in recent years, although the phenomenon has long been observed in boiler and turbine systems, flow of refrigerants and rocket propellants, and many others.

In nuclear reactors, the phenomenon is of utmost importance in safety considerations of both boiling and pressurized systems. A break in a primary coolant pipe causes two-phase critical flow in either system since even in a pressurized reactor, the reduction of pressure of the hot coolant from about 10 MPa to near atmospheric causes flashing and two-phase flow. This kind of break results in a rapid loss of coolant and is considered to be the maximum credible accident in power reactors built to date.

An evaluation of the rate of flow in critical two-phase systems is therefore of importance for the design of emergency cooling and for the determination of the extent and causes of damage in accidents.

2.3 Single-phase critical flow

Compressible, one dimensional horizontal flow with no work or heat transfer will be assumed. The continuity and momentum equations are:

$$\dot{m} = \rho \, A \, V$$

and

$$d\left(pA\right) + \frac{\dot{m}}{g_c} dV = dF$$

where F is a frictional force, A is the cross-sectional area and p is the pressure. Ignoring friction and combining the above two equations yields for constant A:

$$\frac{dV}{dp} + \frac{g_c}{\rho V} = 0$$

The continuity equation is now differentiated with respect to p (with $dA/dp = 0$) to give

$$\frac{1}{\dot{m}} \frac{d\dot{m}}{dp} = \frac{1}{\rho} \frac{d\rho}{dp} + \frac{1}{V} \frac{dV}{dp}$$

When critical flow is reached the mass flow rate becomes a maximum, $\dot{m}_{max}$, and $dm/dp = 0$ in isentropic flow. Thus

$$\frac{1}{V} \frac{dV}{dp} = -\frac{1}{\rho} \frac{d\rho}{dp}$$

or

$$\frac{dV}{dp} = -\frac{\dot{m}_{max}}{\rho^2 A} \frac{d\rho}{dp}$$

Combining the equations, and rearranging give

$$\left(\frac{\dot{m}_{max}}{A}\right)^2 = g_c \, \rho^2 \frac{dp}{d\rho}$$

The above equation is written in the more usual form

$$G^2_{max} = -g_c \frac{dp}{dv}$$

where G is the mass velocity $\dot{m}/A$ and v the specific volume ($v = \rho^{-1}$, $d\rho/dv = -\rho^{-2}$). This equation is identical to the equation for the speed of sound in isentropic flow, indicating that sonic velocity is reached in critical flow.

The energy equation (no heat transfer or work)

$$dh + \frac{V \, dV}{g_c} = 0$$

which integrates to

$$h_0 = h + \frac{V^2}{2 \, g_c}$$

where h and h_0 are the specific enthalpy and stagnation enthalpy of the fluid.

Thus

$$V = \sqrt{2\,g_c\left(h_0 - h\right)}$$

The above equation applies whether the process is reversible or not. For an ideal gas $dh = C_p dT$, so that it becomes

$$V = \sqrt{2\,g_c\,C_p\left(T_0 - T\right)}$$

$$= \sqrt{2\,g_c\,C_p\,T_0\left(1 - \frac{T}{T_0}\right)}$$

where T_0 is the stagnation temperature. Recalling that for an ideal gas $T/T_0 = (p/p_0)^{(\gamma-1)/\gamma}$ (reversible) and $\rho = p/RT = (p_0/RT_0)(p/p_0)^{1/\gamma}$, where γ is the ratio of specific heats, and applying the continuity equation, the above equation becomes

$$\dot{m} = \frac{A\,p_0}{R\,T_0}\sqrt{2\,g_c\,C_p\,T_0\left[\left(p/p_o\right)^{2/\gamma} - \left(p/p_o\right)^{\gamma+1/\gamma}\right]}$$

where p_0 is the stagnation pressure and R the gas constant. This equation plots as *abd* in figure 2.3 if the pressure ratio p/p_0 were assumed to vary between 1.0 and 0. However, only the back-pressure ratio p_b/p_0 can vary between 1.0 and 0. The channel exit pressure p_e follows p_b as it is lowered until it reaches the critical value p_e^* indicated by the critical pressure ratio $r_p^* = p_e^*/p_0$ (figure 2.3) and remains fixed for all values of p_b below as indicated earlier.

Figure 2.3:
Effect of pressure ratio on mass-flow rate
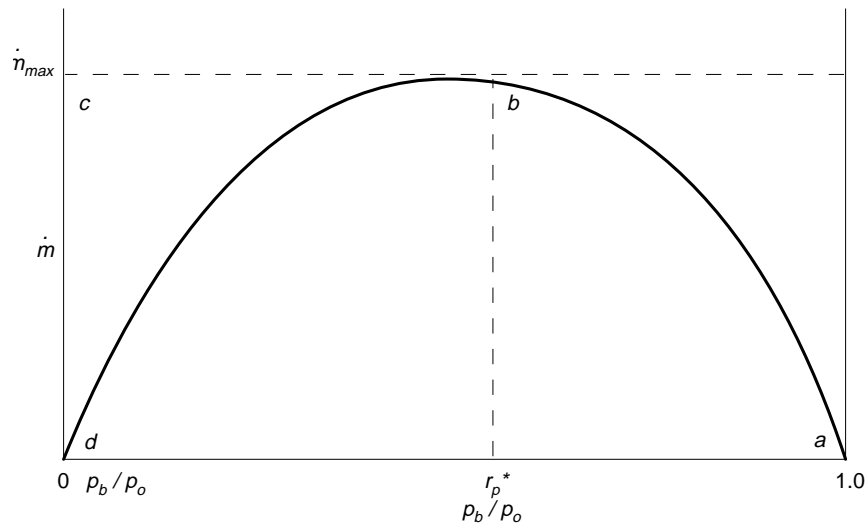
Also, the mass-flow rate increases as p_b/p_0 is lowered, reaches its maximum value m_{max} at r_p^* and remains fixed for all values of p_b/p_0 below r_p^*. The actual flow curve, therefore is *abc* in figure 2.3. The flow between *b* and *c*, again, is critical, restricted, or chocked. The value of r_p^* can be obtained by differentiating m in the above equation with respect to p and equating to zero. This results in

$$r_p^* = \left(\frac{2}{\gamma+1}\right)^{\frac{\gamma}{\gamma-1}}$$

A representative value of r_p^* is 0.53 for air at low temperatures ($\gamma = 1.4$). While steam is not a perfect gas, r_p^* for single-phase steam flow is approximated from the perfect gas relationship by replacing γ with 1.3 for superheated and supersaturated or metastable (a case where actual condensation lags behind theoretical condensation in rapid expansion) steam, resulting in an r_p^* value of 0.545.

2.4 Two-phase critical flow

For frictionless liquid and vapor flow, the momentum equations, for the same pressure drop, are

$$d\left(pA_f\right) + \frac{1}{g_c}\, d\left(\dot{m}_f V_f\right) = 0$$

or

$$d\left(pA_f\right) + \frac{1}{g_c}\, d\left(\rho_f A_f V_f^2\right) = 0$$

and

$$d\left(pA_g\right) + \frac{1}{g_c}\, d\left(\rho_g A_g V_g^2\right) = 0$$

where now the flow areas, densities and mass-flow rates of liquid and vapor are variable. The above equations are added to give

$$dp = -\frac{1}{g_c A}\, d\left[\left(\rho_f A_f V_f^2\right) + \left(\rho_g A_g V_g^2\right)\right]$$

where $A_f + A_g = A$, the channel total area. Using the continuity equation for the two phases and the relationship $A_g/A = \alpha$, and $A_f/A = (1 - \alpha)$, this equation becomes

$$dp = -\frac{G^2}{g_c}\, d\left[\frac{(1-x)^2}{\rho_f(1-\alpha)} + \frac{x^2}{\rho_g\,\alpha}\right]$$

where G is the total mass velocity $\dot{m}_t/A$, and x and α are the quality and void fraction respectively. Using the lumped model, it can be shown that the specific volume of the mixture is related to v_f and v_g by

$$v = v_f\frac{1-x}{1-\alpha} = \frac{1-x}{\rho_f(1-\alpha)}$$

and

$$v = v_g\frac{x}{\alpha} = \frac{x}{\rho_g\,\alpha}$$

so that the quantity between the brackets in the previous equation is simply equal to v and

$$G^2 = -g_c\frac{dp}{dv}$$

which is identical in form to the equation for single-phase flow.

2.5   Two-phase critical flow in long channels

It is assumed, as in single-phase flow, that critical flow occurs when the pressure gradient at channel exit has reached a maximum value. In long channels, residence time is sufficiently long and thermodynamic equilibrium between the phases is attained. The liquid partially flashes into vapor as the pressure drops along the channel, and the specific volume of the mixture v attains a maximum value at the exit. Since v is a function of both x and α, it must be a function of the slip ratio S.

Different values of S therefore result in different values of G. Maximum pressure gradient (and maximum G) are therefore obtained at a slip ratio when $\delta v/\delta S = 0$. This model, called the slip equilibrium model, is suggested by Fauske. It assumes thermodynamic equilibrium between the two phases, and therefore applies to long channels.

The slip ratio is now combined with v, to eliminate α, giving

$$v = \frac{1}{S}\left(v_f\left(1 - x\right)S + v_g x\right)\left(1 + x\left(S - 1\right)\right)$$

 thus

$$\frac{\partial v}{\partial S} = \left(x - x^2\right)\left(v_f - \frac{v_g}{S^2}\right)$$

Equating the above to zero, the value of S giving maximum flow, S^*, is

$$S^* = \sqrt{\frac{v_g}{v_f}}$$

G_{max} can now be obtained by combining the equations as:

$$G_{max}^2 = \frac{-g_c}{-\frac{d}{dp}\left(v_f\left[\left(1 - x\right)S + v_g x\left(S - 1\right)\right]\right)}$$
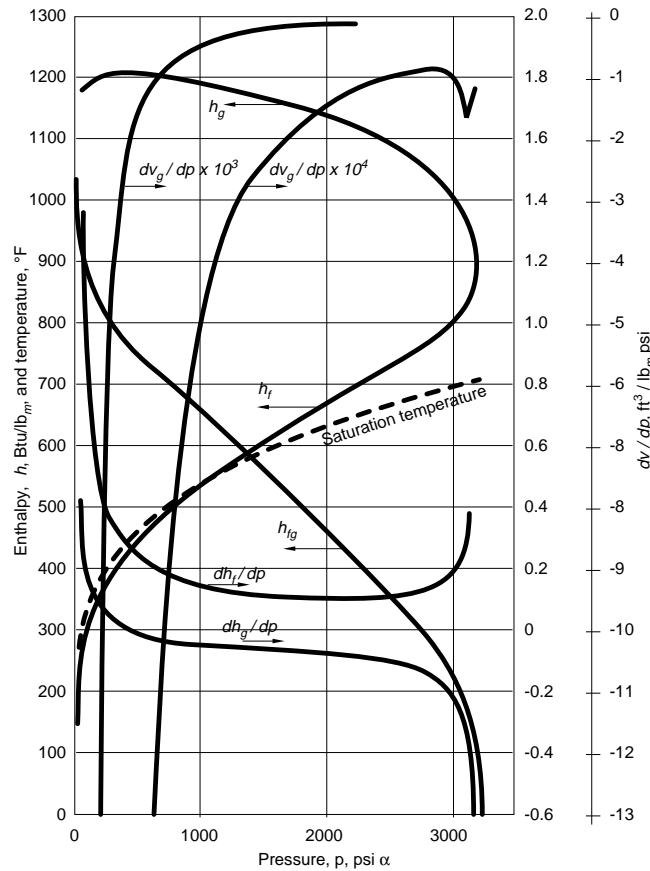
giving finally

$$G_{max}^2 = \frac{-g_c S^*}{F_S}$$

The enthalpy of the water-steam mixture will not change with pressure, so that $dh/dp = 0$.

The derivatives dh_f/dp and dh_g/dp in equation above are sole functions of the pressure. They are given in figure 2.4 for the ordinary-water-steam system.

Figure 2.4:
*Some thermodynamic properties of saturated water and steam*

The value of x is obtained from the equation written for the two phases and can be rewritten in terms of mass velocity G and slip ratio S as

$$h_0 = \left(1-x\right)h_f + xh_g + \frac{G^2}{2g_c}\left[\left(1-x\right)Sv_f + xv_g\right]^2\left(x + \frac{1-x}{S^2}\right)$$

where v_f, h_f, v_g and h_g are evaluated at the critical pressure. The latter can be determined from experimental data by Fauske. This data was run on 0.25 in. ID channels with sharp-edged entrances having length-to-diameter, L/D, ratios between 0 (an orifice) and 40, and is believed to be independent of diameter alone. The critical pressure ratio was found to be approximately 0.55 for long channels in which the L/D ratio exceeds 12, region III in figure 2.5. This is the region in which the Fauske slip-equilibrium model has been found applicable.

Figure 2.5:

Experimental critical pressure ratio data as a function of length / diameter ratio

Data   Initial Pressure, psig
 ○ Low (100-500)
 ▢ Intermediate (700-1200)
 △ High (1200-1800)
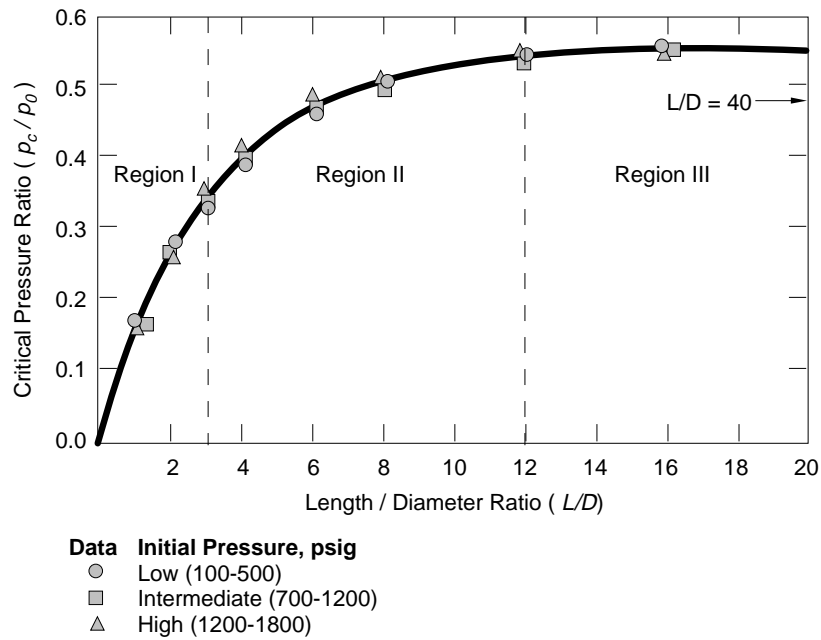
The critical pressure ratio has been found to vary with *L/D*, for shorter channels, but appears to be independent of the initial pressure in all cases.

Solutions for the set of equations defining the Fauske slip-equilibrium model have been prepared by Fauske and are presented in figure 2.6.

Figure 2.6:

Predictions of critical steam-water flow rates with slip equilibrium model
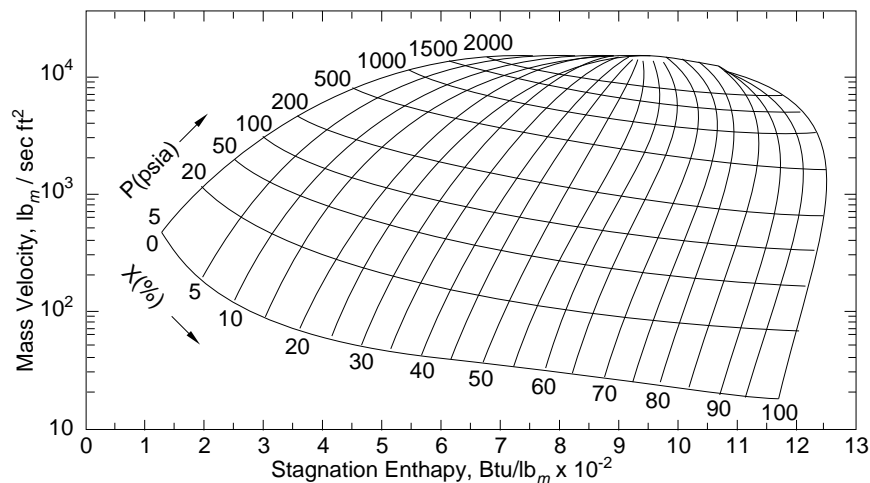
The critical flow is described by the local conditions at the channel exit. The flow

is seen to increase with increasing pressure and with decreasing quality at the exit.

The Fauske model assumes thermodynamic equilibrium (no metastability, below) a case which due to the duration of flow, applies to long flow channels. Experimental data by many investigators showed the applicability of the Fauske model to L/D ratios above 12.
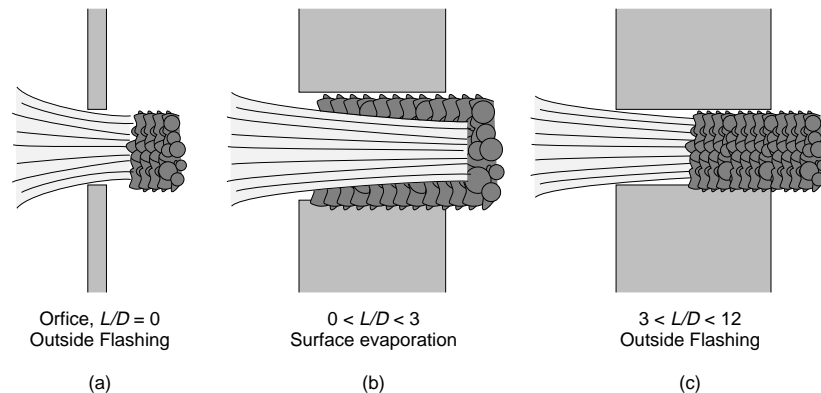
2.6   Two-phase critical flow in short channels

Flashing of liquid into vapor, if thermal equilibrium is maintained, occurs as soon as the liquid moves into a region at a pressure lower than its saturation pressure. Flashing, however, could be delayed because of the lack of nuclei about which vapor bubbles may form, surface tension which retards their formation, due to heat-transfer problems, and other reasons. When this happens, a case of metastability is said to occur. Metastability occurs in rapid expansions, particularly in short flow channels, nozzles, and orifices.

The case of short channels has not been completely investigated analytically. The experimental data obtained covered both long and short tubes, $0 < L/D < 40$. For L/D between 0 and 12 the critical pressure ratios depend upon L/D , unlike long channels (figure 2.5). For orifices ($L/D = 0$) the experimental data showed that because residence time is short,

Figure 2.7:
Two-phase critical flow in orifices and short channels

Orfice, $L/D = 0$	$0 < L/D < 3$	$3 < L/D < 12$
Outside Flashing	Surface evaporation	Outside Flashing
(a)	(b)	(c)

flashing occurred outside the orifice (figure 2.7a) and no critical pressure existed. The flow is accurately determined from the incompressible flow orifice equation

$$G = 0.61 \sqrt{2 \, g_c \, \rho \left(p_0 - p_b \right)}$$

For region I, figure 2.5, $0 < L/D < 3$, the liquid immediately speeds up and becomes a metastable liquid core jet where evaporation occurs from its surface (figure 2.7b). The flow is determined from
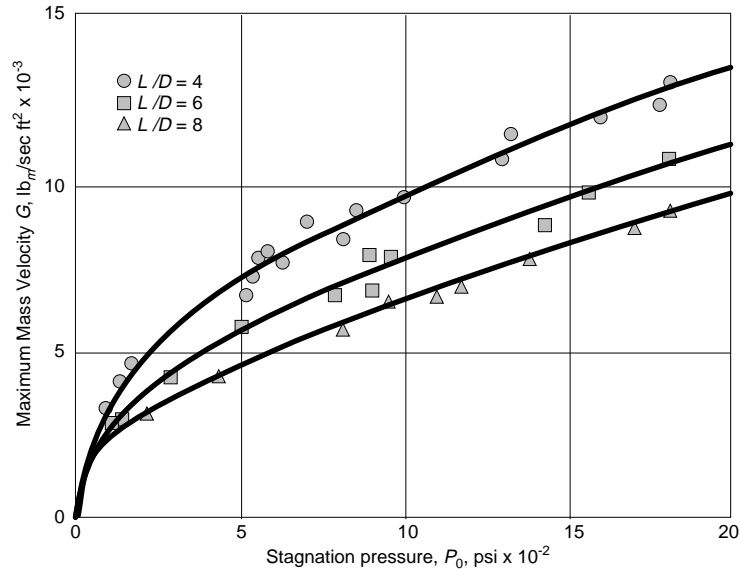
$$G = 0.61 \sqrt{2 \, g_c \, \rho \left(p_0 - p_c \right)}$$

where p_c is obtained from figure 2.5.

In region II, $3 < L/D < 12$, the metastable liquid core breaks up (figure 2.7c), resulting in high-pressure fluctuations. The flow is less than would be predicted. Figure 2.8 shows experimental critical flows for region II.

Figure 2.8:
Experimental two-phase critical flow rates for region II of figure 2.5

All the above data were obtained on sharp entrance channels. In rounded-entrance channels, the metastable liquid remains more in contact with the walls and flow restriction requires less vapor. For $0 < L/D < 3$ channels, such as nozzles, the rounded entrances result in higher critical pressure ratios than indicated by figure 2.5 as well as greater flows. The effect of rounded entrances is negligible for long channels ($L/D > 12$) so that the slip equilibrium model can be used there. The effect of L/D ratio on flow diminishes between 3 and 12.

The condition of the wall surface is not believed to affect critical flow in sharp-entrance channels, since the liquid core is not in touch with the walls and evaporation occurs at the core surface or by core break up. It will have some effect on rounded-entrance channels. The existence of gases or vapor bubbles will affect the flow also, since they will act as nucleation centres.

3.   Pumps Operation

3.1   Introduction

This chapter deals with potential vibrations and their associated fatigue damage on the piping in a CANDU primary heat transport system. The vibration can be induced by the HT pumps when a LOCA or secondary side event causes suction pressure to fall below saturation. The LOCA event may produce conditions in the HTS which may invoke cavitation of the HT pumps. The LOCA event is assumed not to change the piping geometry: either by virtue of being small or by occurring outside the piping actually analyzed.

The existing HT piping is robust as a consequence of the seismic design and is thus expected to withstand well over 15 minutes of vibration. This conclusion remains valid even if the event should take place at the end of the plant life when thermal cycles have exacted their anticipated toll of fatigue.

3.2   Full scale HT pump tests

A full scale test facility for HT pumps has been in operation at Ontario Hydro's Kipling Avenue Laboratories since 1977. Several HT pumps for different Ontario Hydro Nuclear Generating Stations have been tested under rough two-phase flow conditions.

3.3   Darlington two-phase pump test conditions

The Darlington two-phase pump tests were part of a complete HT pump test program performed at Ontario Hydro's Nuclear Process Components Test Facility. The following describes the main characteristics of these tests.

The Darlington HT pump test loop is shown in Figure 3.1. Beside the normal Nuclear Process Components Test Facility, process instrumentation (loop temperature, flowrates, static pressures etc...), the loop was equipped with vibration instrumentation. In order to monitor pressure pulses during two-phase flow conditions, pressure transducers were installed at the single suction pipe, the two discharge pipes and the common discharge header.

Figure 3.1:
Bruce and Darlington test section
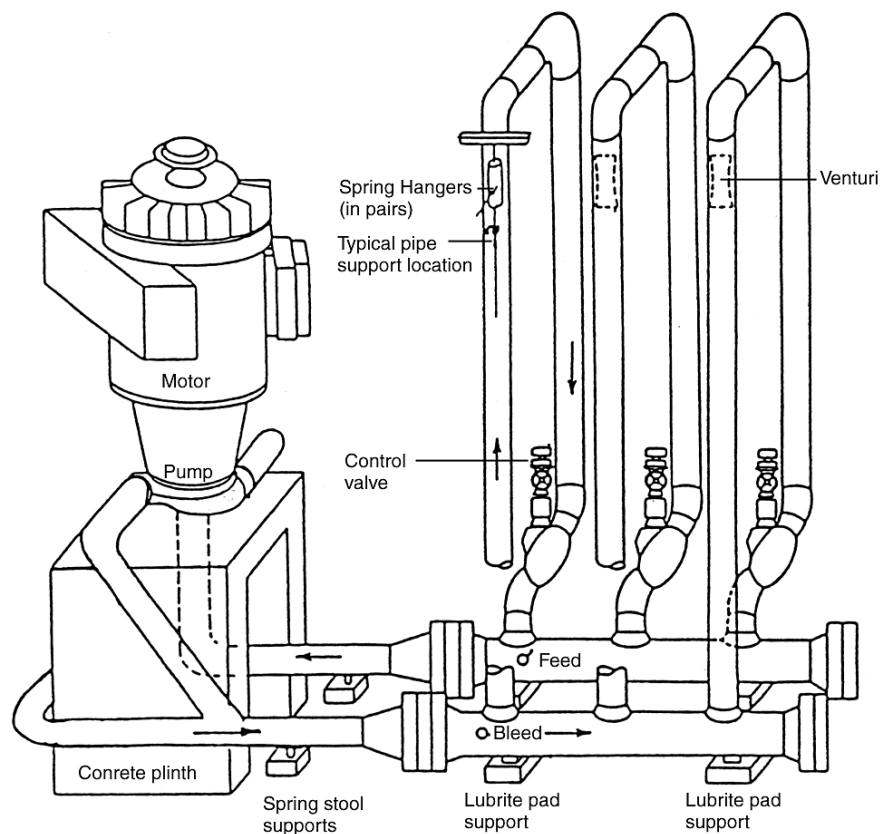
3.4   Results of two-phase pump tests

The Darlington two-phase pump tests have demonstrated the ability of the pumpsets to withstand operation under rough two-phase flow conditions without damage or loss of function. The toughness of the other HT pumpsets had also been proven in the previous Bruce two-phase pump tests as well as the Pickering two-phase pump tests.

However, severe vibration of the test loop piping specially at low frequencies was encountered during two-phase pump tests. This led to analyses of actual plant piping integrity under two-phase flow conditions in the HT pumps following certain postulated LOCA scenarios. Darlington two-phase pump test results provides relevant information, namely the forcing function which depends on the pressure pulse magnitude, the velocity of pressure pulse and the location of the excitation points.

3.4.1 Pressure pulse magnitude versus frequencies

Darlington two-phase pump tests indicate that large amplitude pressure pulses occur mainly at low frequencies. As the pressure pulse frequencies increase, their amplitudes decrease. The largest amplitude pressure pulse occurs during the initial head degradation.

3.4.2 Pressure pulse wave velocity

The Darlington two-phase pump test was not set up to measure two-phase wave velocity. Indeed the pressure measurement points available were too far apart. One measurement point was at the pump discharge and the other after the Y junction, which is located 10 m from the pump discharge pressure measurement.

3.5 Discussions

The force driving a section of pipe limited by two excitation points under pressure pulsation conditions can be represented by

$$F = P(f)\, A\, X \sin\left(2\pi \frac{f\,L}{V}\right)$$

where,

P(f): pressure pulse amplitude depending upon the frequency f
A: pipe cross-section
L: pipe length between 2 excitation points
V: wave velocity
X: attenuation factor

The mechanisms which cause pressure pulses is complex. There are complicated interactions between fluid dynamics and piping response. Further testing is required to understand the fundamental mechanisms involved in the generation and transmission of unsteady pressures.
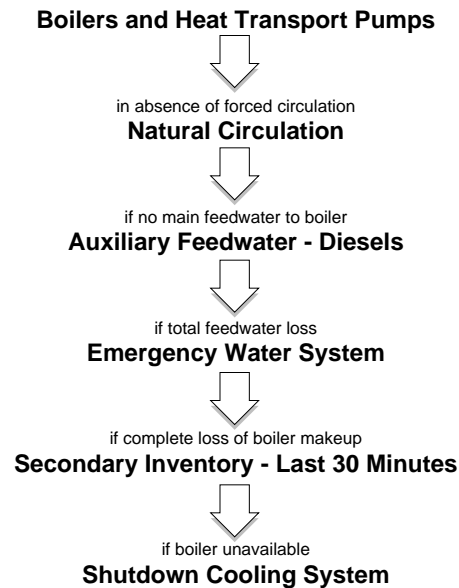
4. Natural Circulation

4.1 Introduction

The CANDU reactor has several modes of decay heat removal. The boilers provide the normal heat sink with forced circulation provided by the heat transport pumps. The boilers are the only heat sink capable of accommodating the full reactor power. The shutdown cooling system, with its independent heat exchangers and pumps, removes decay heat at pressures up to nominal primary circuit pressures. In the absence of any forced circulation of the primary circuit coolant, heat transport to the boilers can be provided by natural circulation. Natural circulation refers to the individual channel flow or total circuit flow of the primary coolant induced by the difference in the coolant densities in the vertical sections of the reactor inlet and outlet piping. Secondary side coolant to the boilers is provided by the normal feedwater system, the auxiliary feedwater pumps or by an emergency water supply system following depressurization of

the secondary circuit. The decay heat removal in CANDU reactors is shown schematically in Figure 4.1. In this section, only the natural circulation modes are discussed in detail.

Figure 4.1:

Decay heat removal modes in the CANDU reactor

Boilers and Heat Transport Pumps

in absence of forced circulation
Natural Circulation

if no main feedwater to boiler
Auxiliary Feedwater - Diesels

if total feedwater loss
Emergency Water System

if complete loss of boiler makeup
Secondary Inventory - Last 30 Minutes

if boiler unavailable
Shutdown Cooling System

Many modes of natural circulation of the primary coolant in CANDU at decay power level are possible. These modes are as follows:

a. Thermosyphoning.
b. Reflux condensation.
c. Intermittent flow.
d. Standing start.
e. Oscillatory flow.
f. Steady stratified flow.

Thermosyphoning is associated with the total circuit flow. The modes (b) to (e) are associated with the coolant flows in the individual channels. For a given condition, one or more of these modes may be active simultaneously in the primary circuit.

Thermosyphoning is defined as natural circulation of the primary circuit coolant over the top of the boiler U-tubes. It is the predicted mode of heat transport in many postulated scenarios in reactor safety analysis. Loss of forced circulation of the primary coolant with the reactor at decay power prior to the end of pump rundown is a common feature of these scenarios. The flow can be single- or two-phase. Single-phase thermosyphoning is predicted under full primary coolant inventory conditions. Two-phase thermosyphoning is predicted to occur under reduced primary coolant inventory conditions. This may be caused either by a net primary coolant leakage from the system or by uncompensated primary

coolant shrinkage due to cooldown. Thermosyphoning is induced by the difference in densities between the reactor inlet and outlet piping. This density difference is induced by the reactor and by the boilers.

4.2 Thermosyphoning

4.2.1 Single-Phase Thermosyphoning

Scenarios for which single-phase thermosyphoning could occur in a full primary circuit loop or loops of a CANDU reactor can be classified in two general categories. The first includes events which do not depressurize the circuit below the setpoint for loop isolation. In such cases, as in a loss of electrical power for example, the heat transport system remains connected to the pressurizer and feed/bleed connections.

These systems maintain a heavy-water-filled circuit as the system cools down. The effectiveness of single-phase thermosyphoning in this type of situation has been demonstrated at all power plants and by commissioning tests at the Gentilly-2 and Point Lepreau generating stations (References 1 and 2) and by an inadvertent loss of electrical power (References 3 and 4). Recorded data from the tests and this event have been interpreted to provide an understanding of the characteristics of single-phase thermosyphoning for such a scenario. This understanding has been further augmented by simulations of the commissioning tests with network thermalhydraulics codes.

The second category of events which could lead to single-phase thermosyphoning includes loss-of-coolant events in either the primary or secondary circuits and with a subsequent loss of the heat transport pumps. For these events, the two loops are isolated and emergency core cooling injection is initiated, thereby keeping the circuits filled. Without the pumps running, single-phase thermosyphoning is not expected to occur in the intact loop following a primary circuit loss of coolant, as well as following a large steamline break inside containment. There is an additional difference between thermosyphoning following a loss of electrical power and thermosyphoning following a loss-of-coolant accident. A potential flow bypass around the boilers is created once the D20 isolation (injection) valves open. Because there is a negligible pressure difference between the injection points, there is little flow through this bypass. Therefore, single-phase thermosyphoning characteristics following a loss-of-coolant accident would be similar to those for loss of Class IV power scenarios, except for the effects of different circuit conditions (i.e., pressure, temperature, power).

4.2.2 Characteristics of Single-Phase Thermosyphoning

Single-phase thermosyphoning of the type associated with a simple loss of forced circulation that does not involve loop isolation or emergency core coolant injection was studied using information recorded from the tests at the Gentilly-2 and Point Lepreau generating stations (References 1 and 2), the inadvertent loss

of electrical power event at Point Lepreau on 1986 January 13 (Reference 3) and station loss of Class IV power at Gentilly-2 on 1988 April 18 caused by a province-wide blackout (Reference 4).

Measurements of temperature increase across a core pass (inlet to outlet header) and across individual channels (inlet header to outlet feeders) were recorded at several reactor power levels. From a heat balance using recorded reactor and individual channel powers, single-phase coolant flow was inferred. Figure 4.2 shows normalized loop coolant flow, calculated from the commissioning tests and the loss of electrical power event, against normalized reactor power.

Figure 4.2:

Single-phase thermosyphoning flows
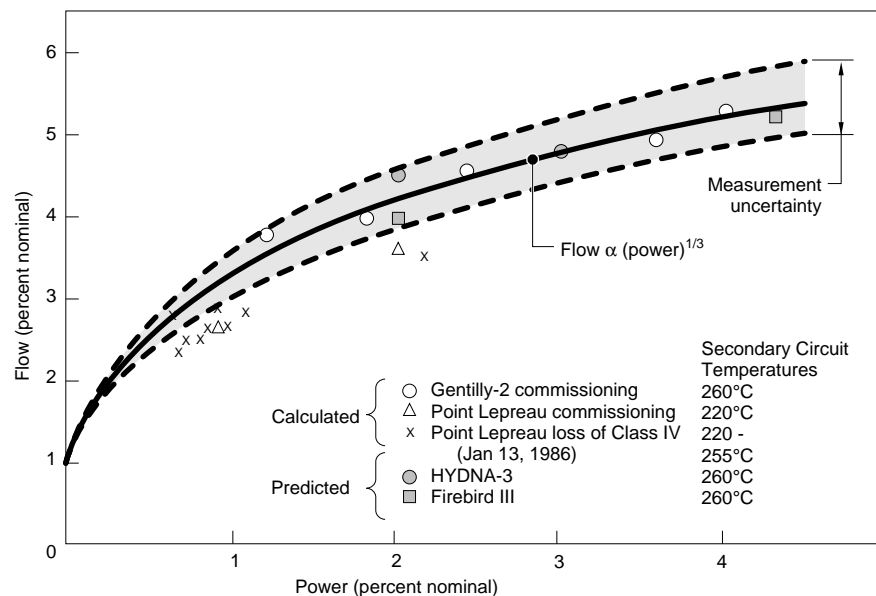
Measurements for both Gentilly-2 and Point Lepreau suggest a continuous relationship between single-phase thermosyphoning flow and reactor power, notwithstanding the effects of varying boiler temperature. An analytical formulation relating flow with power results in the following idealized relationship.

$$\omega = \frac{g\, H\, \rho \left| \left(\frac{\delta\rho}{\delta T} \right)_{P,T_B} \right| \dot{Q}^{1/3}}{R.C_p}$$

where
g   is the gravitational acceleration,
H   is the elevation difference between the mid-elevation
      channel and the top of the boiler tubes,
R   is an overall loop frictional resistance,
ρ is an average loop coolant density (single-phase),
C_p is the average coolant heat capacity,

$\left(\dfrac{\delta\rho}{\delta T}\right)_{P,T_B}$ is the average rate of change of density with coolant temperature at circuit pressure P and boiler temperature T_B, and

$\dot{Q}$ is the reactor heat generation.

The calculated flows in Figure 4.2 for the various measurements from commissioning tests and the loss-of-electrical-power event correspond to a range of secondary side temperatures between 220 and 260°C. Over this range, the quantity in the preceding relationship which depends on temperature,

$\dfrac{\rho}{C_P}\left(\dfrac{\delta\rho}{\delta T}\right)_{P,T_B}$ varies only slightly, by less than 3 %.

Reactor inlet header temperatures in this situation can be cooler than boiler saturation temperature because of heavy water feed inflow via the purification circuit on one side of the core and via the gland seals of all four pumps. This was seen as an asymmetry in the recorded header temperatures following the loss of electrical power event, where the two reactor inlet header temperatures in each loop consistently differed by about 6°C. The difference is attributed to heavy water feed.

A curve drawn through the points in Figure 4.2 for either station is consistent with the relationship of flow with heat generation to the one-third power.

Also shown in Figure 4.2 are the predictions of single-phase thermosyphoning flows at various reactor powers for the Gentilly-2 circuit with the network thermalhydraulics codes, FIREBIRD-III and HYDNA-3. All predictions agree well within uncertainties with calculated flows from the Gentilly-2 commissioning tests.

4.2.3   Two-Phase Thermosyphoning Characteristics
Two-phase thermosyphoning can be expected for design basis earthquake events, overcooling events, and, in the intact loop, for a loss of coolant plus loss of Class IV power prior to refill.
The following statements on the important thermosyphoning characteristics draw on the information derived from experiments and from the analyses of the specific scenarios.

a. Primary Circuit Coolant Distribution
At low boiler temperature, primary circuit pressure is low and the liquid saturation enthalpy is a strong function of pressure. Hot water from the core flashes to steam as its pressure reduces en route to the boilers. There is no steady boiling in the core at system void fractions of interest.

At the nominal boiler temperature of 260°C, the primary circuit pressure is high, the liquid saturation enthalpy is nearly constant for small changes in pressure, and boiling in the core exists even at low system void fraction.

b. Header-To-Header Pressure Drop

The header-to-header (inlet to outlet) pressure difference is positive at low boiler temperatures because of the void concentration above the reactor outlet header. It can be slightly negative at high boiler pressure with forward flow because the buoyancy forces below the header are larger than the frictional forces.

c. Effect of Primary Circuit Void on Flow

The system flow increases with increasing system void up to a maximum at 20 percent. Thereafter, void penetrates past the top of the boiler tubes reducing the buoyancy head whereas frictional forces continue to increase with void.

d. Effect of Boiler Secondary Side Temperature on Flow

Single-phase flows increase with increasing temperature because density decreases faster with temperature at the higher temperatures. Two-phase flows increase with decreasing boiler temperature, because the primary circuit pressure is lower causing flashing of water to steam in the vertical components rather than boiling in the horizontal fuel channels. This enhances the buoyancy force and increases frictional pressure drop.

e. Flow Oscillations

For the conditions of interest, two types of flow oscillation (channel and system) are possible depending on coolant inventory and boiler temperature.

f. Effect of Outlet Header Interconnect

Tests in RD-14 and analyses have shown that the outlet header interconnect has no significant effect on steady or oscillatory thermosyphoning flow.

g. Thermosyphoning Flow Reversal

Two tests in RD-14 exhibited reversal in the circuit flow at high (about 25 percent) loop void. In one of the tests, this reversal occurred when the void extended over the top of the boiler U-tubes and reached the test section inlet. In the second test, thermosyphoning flow stopped for about 350 seconds during draining at 85 percent loop inventory. This caused coolant phase separation in the test sections and heater heatup. Subsequently, superheated steam from the channel flowed up the inlet piping through the boiler cold legs. This steam flow eventually induced a reversed single-phase thermosyphoning at about 81 percent loop inventory.

h. Effect of Emergency Coolant Injection

Four RD-14 natural circulation tests were conducted with emergency coolant injection to only the inlet or all headers at about 30 percent and 50 percent loop void. Injection to all headers collapsed nearly all of the loop void and caused the loop pressure to rise rapidly to the injection pressure (about 5.5 MPa) and then less rapidly to about 6 MPa. It also resulted in forward thermosyphoning flow. Injection to only the inlet headers caused no significant loop pressurization and

resulted in forward thermosyphoning flow.

i. Two-Phase Thermosyphoning Breakdown

Experiments in facilities with single and two channels per pass and code predictions using a single-channel-per-pass model have shown that at low loop inventory (less than 50 percent), void penetrates the boiler cold leg over the top of the U-tubes reducing the thermosyphoning driving head. At low enough inventory, the reactor inlet headers begin to receive a two-phase fluid. As a consequence, the channel flow decreases sufficiently to stratify, resulting in channel heatup.

Similar behaviour is expected for a multiple-channel-per-pass facility or model. In fact, experiments in the large-scale header facility have shown that the phases in the header separate with the presence of the smallest amount of void. Thus, some feeders may receive pure steam while others may receive only water. For the inlet feeders which are receiving pure liquid, the gravity head is sufficient to provide a net positive flow through the channel. However, the flowrate in these feeders is sufficiently low to cause the channel coolant to stratify and expose the upper fuel elements to steam and radiative cooling.

4.3   Standing start

Standing start is a mode of natural circulation associated with the individual fuel channels. Standing start refers to a subcooled stagnant initial condition in a fuel channel. This condition may occur after pump rundown and as a consequence of balance between the header-to-header pressure difference, difference between the hydrostatic heads in the inlet and outlet feeders, and suction force of an inlet header break, if any. Standing start may occur for a small or large break in an inlet header or for reduced loop inventory (as, for example, in the shutdown cooling mode with full or drained-to-header circuit, or in the intact loop following a break and loop isolation, or in both loops following an overcooling event). For standing start to occur, the channel coolant must be subcooled as is the case following emergency core coolant injection.

4.4   Intermittent flow

Intermittent channel flow behaviour is a repetitive standing start cycle of boiling, phase separation, end fitting heatup, steam venting and channel refilling. The duration of channel heatup in an intermittent channel flow cycle is generally shorter than in the preceding cycle as the system heats up. Intermittent flow occurs, for example, following the steam venting in the first standing-start cycle for medium initial coolant subcooling. For intermittent flow pattern, the fuel heats up intermittently and, hence, the extent of fuel heatup is limited.

4.5   Oscillatory flow

Oscillatory channel flow is an unstable boiling channel flow, that is, the channel coolant conditions including channel characteristics is such that the non-zero

flow is unstable to any disturbance. For these conditions, boiling occurs in the channel and a two-phase mixture exists in the channel and outlet feeder. The oscillations, once excited, grow in amplitude to a limit cycle. If the limit cycle amplitude is small, a net positive flow is maintained. Otherwise, temporary reverse channel flow and void collapse in the channel, end fitting and part of the outlet feeder occur. Generally, there is no significant fuel heatup for oscillatory channel flow because the oscillation period is not too long. Oscillatory channel flow may be expected for some conditions following steam venting in the standing-start phenomenon.

4.6   Steady stratified flow

Steady stratified channel flow is a mode of natural circulation where the coolant boils in the channel and the resulting phases separate, with steam at the top and water at the bottom parts of the channel, and this channel flow pattern remains unchanged for a significant length of time. Generally, the coolant in the corresponding "inlet" feeder (i.e., the feeder from which the coolant enters the channel) is single-phase liquid-filled and the "outlet" feeder contains a two-phase fluid. The driving force for stratified flow is the hydrostatic head difference between the inlet and outlet feeder and header-to-header pressure difference. The phase separation in the channel causes the upper fuel elements which are exposed to steam to heat up. The extent of this heatup depends on the duration of the channel flow stratification and the extent of steam cooling.

4.7   Boiler tubes behaviour and reflux condensation

Reflux condensation is a mode of natural circulation in a vertical condensing tube where water and steam phases flow counter-currently to one another under the action of gravity. The steam rises up inside the tube, condenses as it rises, and the condensate flows down the tube wall in a thin film. In CANDU boiler tubes the reflux condensation mode of heat removal may occur at very low total primary circuit flow and, in particular, following thermosyphoning breakdown. It is estimated that the reflux condensation mode can remove as much as four percent full power from the reactor core at primary circuit pressures exceeding 1 MPa.

Reflux condensation may have occurred in a series of natural circulation tests in RD-14M. It has been studied extensively experimentally and analytically. The following four flow patterns were observed in the tests with a single inverted condenser U-tube as the steam flow was increased:

a. At low steam flow, counter-current steam-water flow mode occurred. In this mode, the steam rose up inside the tube and the condensate ran down the tube walls in a thin film.

b. At steam flows exceeding the flooding limit for counter-current flow at the tube inlet, a water column began to form above an annular two-phase region. This flow pattern is referred to as the complete reflux condensation mode.

c. Unstable or oscillatory water column in the complete reflux condensation mode occurred for some range of steam flow.

d. Above a certain steam flow, the water column length increased until some of the water was dumped into the cold leg of the tube. Subsequently, the cycle

of water column growth and dumping was repeated. This mode is referred to as the fill-and-dump mode.

The above flow patterns can be characterized by a plot of steam flow versus pressure drop between the ends of the U-tube, as shown in Figure 4.3.

Figure 4.3:
Steam flow versus pressure drop
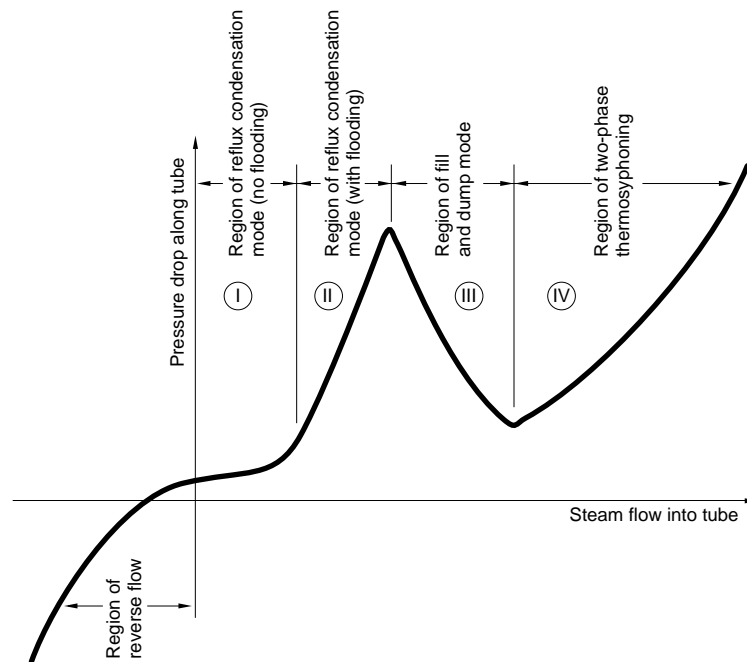
The above four flow patterns were also observed in tests with multiple-tube condensers. However, deviations from the single-tube flow behaviour was observed due to different characteristics of the different U-tubes. As the steam flow was reduced, the longest tube developed a steady water column in the region of the pressure drop-flow characteristics curve where the tube by itself would have exhibited fill and dump mode. The steady water column was supported by the pressure drop imposed by the unblocked (i.e., with no water column) tubes. With further reduction in the steam flow, more tubes became blocked (i.e., developed steady water columns). When the last tube became blocked, the water column in one of the tubes extended over the top of the U-tube and some of the water was dumped into the cold leg. This process then occurred in other tubes in a cyclic manner. In the integral-effects tests conducted in scaled-down pressurized water reactor type test facilities, the following additional phenomena were observed:

a. Under either single- or two-phase flow conditions, the flow in some of the boiler tubes either stagnated or reversed. This resulted in reduction of the total circuit flow as well as of heat removal.

b. Under single-phase conditions, significant temperature stratification was observed in the boiler plena as well as flow bypassing the boiler outlet pipe and flowing back through the outlet plenum and some of the boiler tubes to the inlet plenum.

The above tests seem to indicate that, for an accurate description of reflux condensation flow behaviour in multiple-tube boilers, it may be necessary to determine the flow/pressure drop characteristics of at least three (longest, intermediate and shortest) tubes and to use a multiple-tube (at least three) boiler model.

5.   REFERENCES

1   R. Lafleur, "Thermosyphon", Preliminary Test Report, Hydro-Quebec, 1982 December 03.
2   W. Pilkington, "Primary Heat Transport and Auxiliary Systems Thermosyphoning Test", NB Power Report, 1982 December 21.
3   J.N. Barkman, "Assessment of Thermosyphoning Flows Following Loss of Class IV Power" (January 13, 1986), NB Power Information Report IR-03500, Rev. 0, 1986 March.
4   M. Garceau, "Analysis des Donnees Relatives au Thermosiphon Lors de la Perte de Categorie IV du 18 Avril 1988", Centrale Nucéaire Gentilly 2 Rapport technique G2-RT-88-12, USI 33100, 1988 Novembre.
5   66 SR, Gentilly-2 Safety Report, Part 2, Accident Analyses, Vol. 4, 1991 May.
6   87 SR, Point Lepreau Safety Report, Part 2, Accident Analysis, Vol. 4, 1991 May.
7   R. Ko. " Piping Vibration from Pumped Two-phase Flow Part II: Analysis Methods and Preliminary Results", Third International Topical Meeting on Nuclear Power Plant Thermal Hydraulics and Operations, Seoul, Korea, November 1988.

Heat Exchangers

Training Objectives

The participant will be introduced to:
1   heat exchanger types.
2   the overall heat transfer coefficient.
3   heat exchanger analysis: use of the log mean temperature difference.
4   heat exchanger analysis: the effectiveness-NTU method.
5   compact heat exchangers.

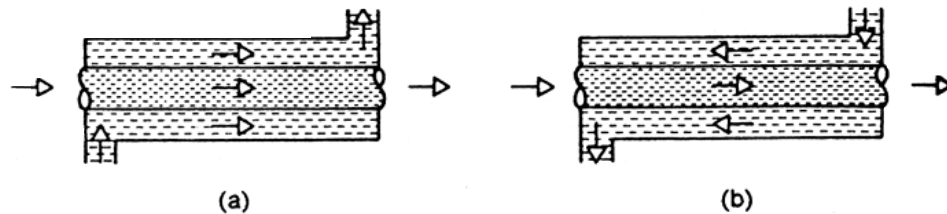# Heat Exchangers

Table of Contents

1   Introduction

The process of heat exchange between two fluids that are at different temperatures and separated by a solid wall occurs in many engineering applications. The device used to implement this exchange is termed a *heat exchanger,* and specific applications may be found in space heating and air-conditioning, power production, waste heat recovery, and chemical processing. In this lesson we consider the principles of heat transfer needed to design and/or to evaluate the performance of a heat exchanger.
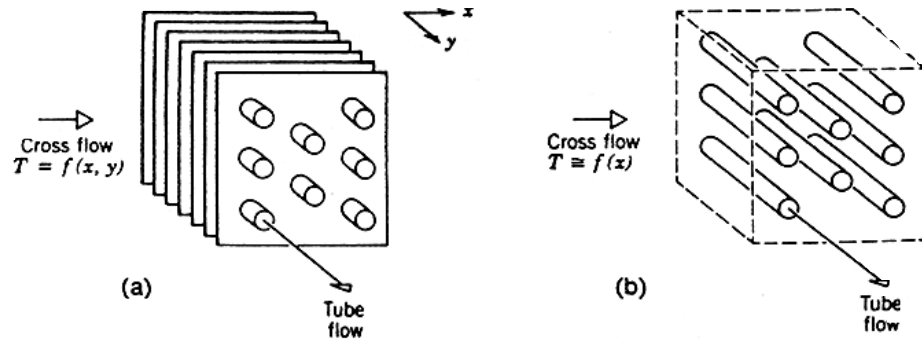
2   Heat Exchanger Types

Heat exchangers are typically classified according to *flow arrangement* and *type of construction.* The simplest heat exchanger is one for which the hot and cold fluids move in the same or opposite directions in a *concentric tube (or double-pipe)* construction. In the *parallel-flow* arrangement of Figure 2.1a, the hot and cold fluids enter at the same end, flow in the same direction, and leave at the same end. In the *counterflow* arrangement of Figure 2.1b, the fluids enter at opposite ends, flow in opposite directions, and leave at opposite ends.

Fig. 2.1:
Concentric Tube Heat Exchangers.
(a) Parallel flow. (b) Counterflow.

Alternatively, the fluids may move in *cross flow* (perpendicular to each other), as shown by the *finned* and *unfinned* tubular heat exchangers of Figure 2.2. The two configurations differ according to whether the fluid moving over the tubes is *unmixed* or *mixed.* In Figure 2.2a, the fluid is said to be unmixed because the fins prevent motion in a direction (y) that is transverse to the main-flow direction (x). In this case the fluid temperature varies with x and y. In contrast, for the unfinned tube bundle of Figure 2.2b, fluid motion, hence mixing, in the transverse direction is possible, and temperature variations are primarily in the main-flow direction. Since the tube flow is unmixed, both fluids are unmixed in the finned exchanger, while one fluid is mixed and the other unmixed in the unfinned exchanger. The nature of the mixing condition can significantly influence heat exchanger performance.

Fig. 2.2:

Cross-Flow Heat Exchangers. (a) Finned with both Fluids Unmixed.
(b) Unfinned with one Fluid Mixed and the other Unmixed.

Another common configuration is the *shell-and-tube* heat exchanger [1]. Specific forms differ according to the number of shell and tube passes, and the simplest form, which involves single tube and shell *passes,* is shown in Figure 2.3. Baffles are usually installed to increase the convection coefficient of the shell-side fluid by inducing turbulence and a cross-flow velocity component. Baffled heat exchangers with one shell pass and two tube passes and with two shell passes and four tube passes are shown in Figures 2.4a and 2.4b, respectively.

Fig. 2.3:

Shell-and-Tube Heat Exchanger with one Shell Pass
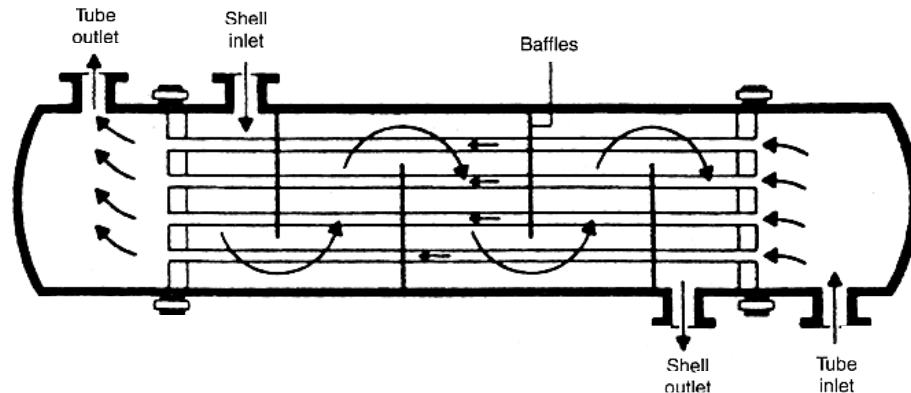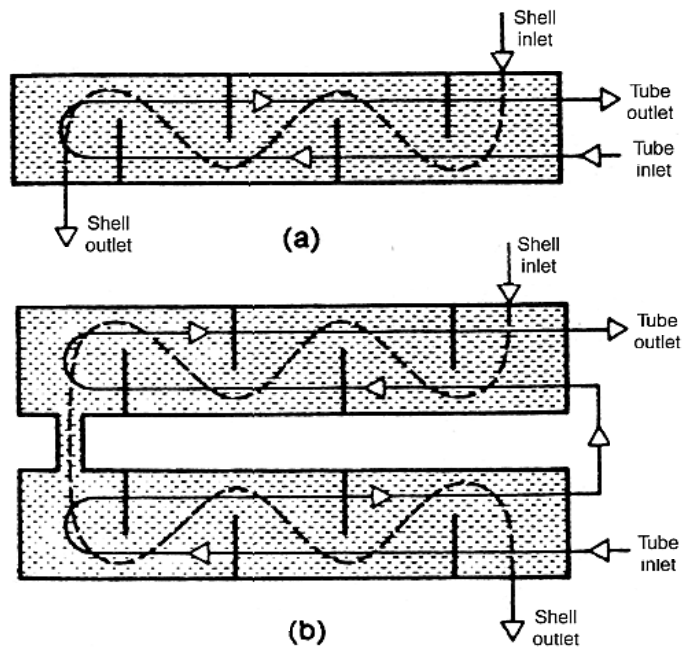*and one Tube Pass (Cross-Counterflow Mode of Operation).*

Fig. 2.4:

Shell-and-Tube Heat Exchanger. (a) One Shell Pass
and Two Tube Passes. (b) Two Shell Passes and Four Tube Passes.

A special and important class of heat exchangers is used to achieve a very large (≥ 700 m^2/m^3) heat transfer surface area per unit volume. Termed *compact heat exchangers*, these devices have dense arrays of finned tubes of plates and are typically used when at least one of the fluids is a gas, and is hence characterized by a small convection coefficient. The tubes may be *flat* or *circular,* as in Figure 2.5a and 2.5b, c, respectively, and the fins may be *plate* or *circular,* as in Figures 2.5a, b and 2.5c, respectively. Parallel plate heat exchangers may be finned or corrugated and may be used in single-pass (Figure 2.5d) or multipass (Figure 2.5e) modes of operation. Flow passages associated with compact heat exchangers are typically small ($D_h \leq 5$ mm), and the flow is usually laminar.

Fig. 2.5:

Compact Heat Exchanger Cores. (a) Fin-Tube (flat tubes, continuous
plate fins). (b) Fin-Tube (circular tubes, continuous plate fins). (c) Fin-Tube
(circular tubes, circular fins). (d) Plate-Fin (single pass).
(e) Plate-Fin (multipass)
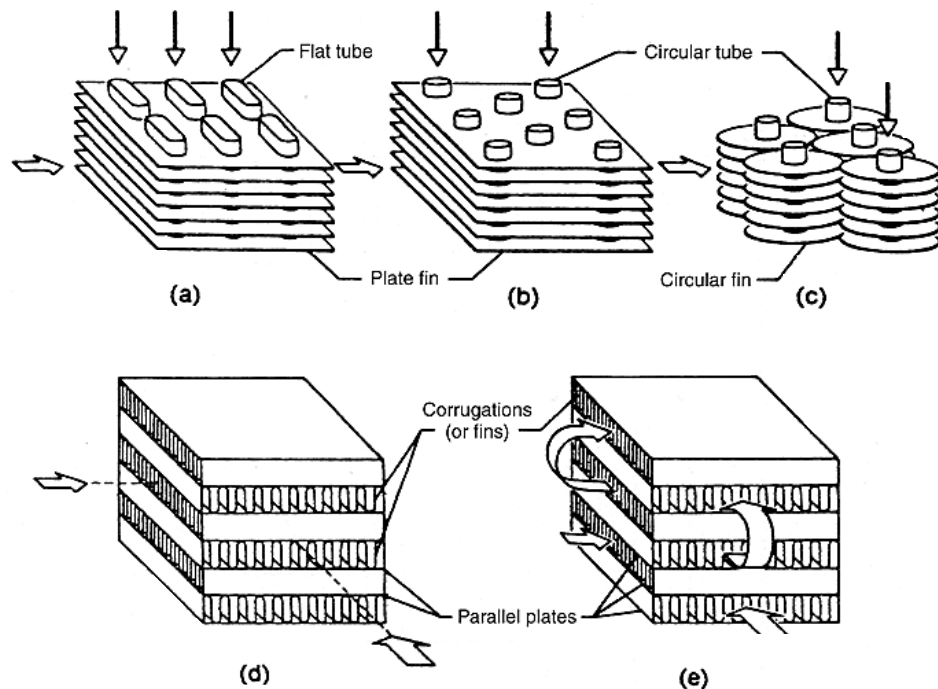
2.1 Principal Types of Heat Exchangers Used in CANDU 6 Stations

Three general categories of heat exchangers (HX) are used in CANDU reactor systems: shell-and-tube heat exchangers, plate type (or plate-fin) heat exchangers and other miscellaneous types.

Heat exchange equipment, for a CANDU station, is located primarily in the Reactor, Turbine and Service buildings.

The heat transfer in these heat exchanger equipment could be from liquid to liquid, liquid to gas or gas to gas.

A wide variety of tubing material is used in CANDU heat exchangers. Copper, nickel, 304 stainless steel, titanium, monel, Sandvik 3RE60, Inconel 600 and Incoloy 800 are some of the tubing materials used.

CANDU heat exchangers use small diameter tubes - typically 16 mm or 13 mm in outside diameter. This is because smaller tubes generally result in more compact (hence less D_2O inventory) and cheaper heat exchangers.

CANDU reactor systems use both horizontally and vertically oriented heat

exchangers and the selection is dependent upon the piping system configuration and space availability.

Table 2.1 provides a list of the majority of the heat exchangers used in a CANDU 6 station with particular reference to Point Lepreau.

Table 2.1:
Heat Exchangers Used at Point Lepreau.

Heat Exchanger	SI	Type	Tube Side Data						Shell Side Data					
			Fluid	Temperature °C Inlet	Outlet	Pressure (MPa)	ΔP (kPa)	Flow (L/s)	Fluid	Temperature °C Inlet	Outlet	Pressure (MPa(g))	ΔP (kPa)	Flow (L/s)
Moderator System HXs	32111	vert.u-tube	D₂O	71	42	0.62	152.0	473	H₂O	22	43	0.345	0.170	720
Moderator Purification System HXs	32211	horiz.c-tube	D₂O	71	43	0.62	NA	16.57 kg/s	H₂O	22	41	0.690	NA	22.75 kg/s
Steam Generators	33110	vert.u-tube	D₂O	318	266	11.0	210.0	1990 kg/s	H₂O	260	steam	5.07	NA	240.0 kg/s
PHTS Pumps Main Cooler	33121	straight tube	H₂O	17.7	27.7	0.69	-	360.0	air	-	-	-	-	-
PHTS Pumps Upper and Lower Oil Coolers	33121	helical coil design	H₂O	17.7	27.7	0.69	-	150/16	lubric-ating oil	-	-	-	-	-
Degasser Cooler	33321	horiz.u-tube	D₂O	168-204	66	0.65-1.62	103.0	22.7	H₂O	22	48.4	0.55-0.69	207.0	121.2
Degasser Vent Condenser	33325	vert.u-tube	H₂O	22	29.5	1.03	69	3.8 kg/s	D₂O vapour	170	92	0.59	69	0.051 kg/s
Gland Seal Heat Exchanger	33341	vert.u-tube	D₂O	279.4	37.8	11.4	83	1.44 kg/s	H₂O	22	38.2	0.69	-	15.15 kg/s
PHTS Purification Circuit Heat Interchangers	33351	tube in shell (HX1/HX3)	D₂O	265/194	194/103	10.95	100	70.7 kg/s	D₂O	159/65	240/159	9.63	70	65/68.5
PHTS Purification Cooler	33351	tube in shell	D₂O	103	65	11	100	70.7 kg/s	H₂O	22	56	0.7	210	225 kg/s
Shutdown Cooling System HXs	33411	horiz.u-tube	D₂O	54	42	0-11.3	-	227	H₂O	22	37	0.55-0.7	207	189
PHTS Sample Coolers	33711	coiled tube in shell	D₂O	279-317	-	-	-	20 kg/s	H₂O	22	-	-	-	8
D₂O Collection System Cooler	33811	horiz.u-tube	H₂O	22.2	42.5	0.552-0.69	-	1.5	D₂O	101	38	-	-	-
D₂O Collection System Vent Condenser	33811	inverted vert.u-tube	H₂O	22	49	0.7	-	7.5	D₂O vapour	101	101	-	-	0.41
D₂O Vapour Recovery System Heat Exchangers	38311	coiled tube in shell	H₂O vapour	-	-	-	-	-	D₂O vapour	-	-	-	-	-
Shield Cooling Circuit HXs	34111	tube in shell	H₂O	61	49	0.52	-	69.4	H₂O	22.2	37.8	0.28	-	51.5
Dousing System Coolers	34310	-	H₂O	22	23.5	0.713	-	6.3	tubes are immersed in dousing tank water					

Heat Exchanger	SI	Type	Fluid	Tube Side Data					Shell Side Data					
				Temperature °C		Pressure (MPa)	ΔP (kPa)	Flow (L/s)	Fluid	Temperature °C		Pressure (MPa(g))	ΔP (kPa)	Flow (L/s)
				Inlet	Outlet					Inlet	Outlet			
ECC System Heat Exchanger	34321	plate-type HX	H₂O	22.2	36	1.0	24.0	767	D₂O & H₂O	66	49	0.5	60	606
Spent Fuel Reception Bay HX	34411	tube in shell	H₂O	61	49	-	-	69.4	H₂O	22	38.5	-	-	51.5
Main Storage Bay HX	34411	tube in shell	H₂O	61	49	-	-	69.4	H₂O	22	38.5	-	-	51.5
L2C Supply Circuit HX	34811	horiz tube in shell	H₂O	22.2	37.7	1.0	100	54 kg/s	H₂O	93.3	37.7	1.4	55	13.12 kg/s
L2C Control System Helium Gas Cooler	34811	finned tube in shell	H₂O	22	23	0.69	-	5400 kg/hr	He gas	66	38	1.0	-	27.8 kg/hr
Annulus Gas System HX	34981	finned tube	CO₂ gas	232	65.6	-	-	7	air cooled by natural circulation					
F/M D₂O Supply Heaters	35230	spiral tube bundle in shell	D₂O	26.2	191	14.5	28	-	H₂O steam	263	263	4.82	-	-
F/M Oil Cooler HX	35240	tube in shell	Oil	66 (max)	-	-	-	2280	H₂O	13.22	-	-	-	2760
F/M Auxiliary HX	35260	coiled tube in shell	D₂O	48.9	37.7	0.414	-	-	H₂O	26.7	51.7	0.69	-	-
Boiler Water Sample Coolers	36611	coiled tube in shell	H₂O	250	40	4.59	-	-	H₂O	15.6	37.8	-	-	-
Reheaters	41131	tube in shell	H₂O	-	-	-	-	-	-	-	-	-	-	-
Gland Steam Condenser	41151	tube in shell	-	-	-	-	-	-	-	-	-	-	-	-
Hydrogen Cooler	41231	finned tube in shell	H₂O	-	-	-	-	-	H₂ gas	60	35.40	-	-	-
Stator Cooler	41241	plate type HX	H₂O	62.2	40	0.62	-	49	H₂O	22.2	32.3	-	-	108.7
Seal Oil Cooler	41341	tube in shell	H₂O	-	-	-	-	-	seal oil	-	-	-	-	-
Lubricating Oil Cooler	41351	tube in shell	H₂O	-	-	-	-	-	lubric-ating oil	-	-	-	-	-
Main Condenser	42101	3-shell single pass unit	sea water	6.1	20.5	-	-	1314	wet steam	-	-	-	-	3.12x 10⁶
Low Pressure Feedwater Heaters	43120	horiz-a-tube	H₂O	40.3	68.9	1.0	-	1308 Mg/hr	steam	742	-	0.033	-	67.6 Mg/hr

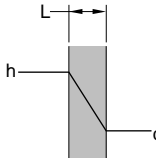| Heat Exchanger | S1 | Type | Tube Side Data | | | | | | Shell Side Data | | | | | |
			Fluid	Temperature °C Inlet	Outlet	Pressure (MPa)	ΔP (kPa)	Flow (L/s)	Fluid	Temperature °C Inlet	Outlet	Pressure (MPa(g))	ΔP (kPa)	Flow (L/s)
Low Pressure Feedwater Heaters	43120	horiz.u-tube	H₂O	92.5	113.8	0.74	-	1308 Mg/hr	steam	127.2	-	0.173	-	50.4 Mg/hr
Low Pressure Feedwater Heaters	43120	horiz.u-tube	H₂O	68.9	92.5	0.88	-	1308 Mg/hr	steam	94.8	-	0.084	-	53.8 Mg/hr
Drain Coolers	43120	horiz.u-tube	H₂O	36.3	40.3	1.14	-	363 kg/s	H₂O	4	-	0.032	-	174 Mg/hr
High Pressure Feedwater Heaters	43120	horiz.u-tube	H₂O	136.6	154.9	0.63	-	1724 Mg/hr	steam	157.1	-	0.566	-	51.9 Mg/hr
High Pressure Feedwater Heaters	43120	horiz.u-tube	H₂O	154.9	186.7	6.13	-	1724 Mg/hr	steam	189.9	-	1.23	-	122 Mg/hr
Steam Sample Coolers	45111	tube in shell	H₂O vapour	260	40	-	-	-	H₂O	16	28	-	-	-
Deaerator	43122	..	-	-	-	-	-	-	-	-	-	-	-	-
Failed Fuel Location System Coolers	63105	vert.coil in concentric tube	D₂O/H₂O	277/5-50	-	-	-	-	-	-	-	-	-	-
Recirculated Cooling Water System HXs	71341	horiz.n-tube	sea water	13-22	-	-	-	-	H₂O	37.8	27.8	0.69	-	-
Glycol Coolers	73010	tube in shell	50% Glycol & 5% H₂O	71.1	85	0.69	-	36.3	H₂O steam	-	-	0.10	-	0.9 kg/s

3 The Overall Heat Transfer Coefficient

An essential, and often the most uncertain, part of any heat exchanger analysis is the determination of the *overall heat transfer coefficient*. This coefficient is defined in terms of the total thermal resistance to heat transfer between two fluids. The coefficient is determined by accounting for conduction and convection resistances between fluids separated by composite plane and cylindrical walls, respectively. It is important to acknowledge, however, that such results apply only to *clean, unfinned* surfaces.

During normal heat exchanger operation, surfaces are often subject to fouling by fluid impurities, rust formation, or other reactions between the fluid and the wall material. The subsequent deposition of a film or scale on the surface can greatly increase the resistance to heat transfer between the fluids. This effect can be treated by introducing an additional thermal resistance, termed the *fouling factor, R_f*. Its value depends on the operating temperature, fluid velocity, and length of service of the heat exchanger.

In addition, we know that fins are often added to surfaces exposed to either one or both fluids and that, by increasing the surface area (A), they reduce the resistance to convection heat transfer. Accordingly, with inclusion of surface fouling and fin (extended surface) effects, the overall heat transfer coefficient, U, may be expressed as

$$\frac{1}{UA} = \frac{1}{U_c A_c} = \frac{1}{U_h A_h}$$

$$= \frac{1}{(\eta_0 hA)_c} + \frac{R''_{f,c}}{(\eta_0 A)_c} + R_w + \frac{R''_{f,h}}{(\eta_0 A)_h} + \frac{1}{(\eta_0 hA)_h}$$

where *c* and *h* refer to the cold and hot fluids, respectively. Note that calculation of the *UA* product does not require designation of the hot or cold side $(U_c A_c = U_h A_h)$. However, calculation of an overall coefficient depends on whether it is based on the cold or hot side surface area, since $U_c \neq U_h$ if $A_c \neq A_h$. Although representative fouling factors are listed in Table 3.1, the factor is a variable during heat exchanger operation (increasing from zero for a clean surface, as deposits accumulate on the surface). Comprehensive discussions of fouling are provided in References 2 through 4.

Table 3.1:

Representative Fouling Factors.

| Fluid	R_f (m²·K/W)
Seawater and treated boiler feedwater (below 50°C)	0.0001
Seawater and treated boiler feedwater (above 50°C)	0.0002
River water (below 50°C)	0.0002-0.001
Fuel oil	0.0009
Refrigerated liquids	0.0002
Steam	0.0001

The quantity η_o in Equation 3.1 is termed the *overall surface efficiency* or *temperature effectiveness* of a finned surface. It is defined such that, for the hot or cold surface, the heat transfer rate is

$$q = \eta_0 hA (T_b - T_\infty)$$

where T_b is the base surface temperature and A is the total (fin plus exposed

base) surface area and

$$\eta_0 = 1 - \frac{A_f}{A}\left(1 - \eta_f\right)$$
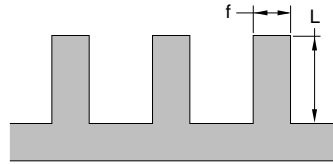
where A_f is the entire fin surface area and η_f is the efficiency of a single fin. If a straight or pin fin of length L is used and an adiabatic tip is assumed,

$$\eta_f = \frac{\tan h\left(mL\right)}{mL}$$

where m = $(2h/kt)^{1/2}$ and t is the fin thickness.

The wall conduction term in Equation 3.1 may often be neglected, since a thin wall of large thermal conductivity is generally used. Also, one of the convection coefficients if often much smaller than the other, and hence dominates determination of the overall coefficient. For example, if one of the fluids is a gas and the other is a liquid or a liquid-vapour mixture experiencing boiling or condensation, the gas-side convection coefficient is much smaller. It is in such situations that fins are used to enhance gas-side convection. Representative values of the overall coefficient are summarized in Table 3.2.

Table 3.2:
Representative Values of the Overall
Heat Transfer Coefficient.

Fluid Combination	*U* **(W/m²K)**
Water to water	850-1700
Water to oil	110-350
Steam condenser (water in tubes)	1000-6000
Ammonia condenser (water in tubes)	800-1400
Alcohol condenser (water in tubes)	250-700
Finned-tube heat exchanger (water in tubes, air in cross flow)	25-50

For the unfinned, tubular heat exchangers of Figure 3.1 to 3.4, Equation 3.1 reduces to

$$\frac{1}{UA} = \frac{1}{U_i A_i} = \frac{1}{U_o A_o}$$

$$= \frac{1}{h_i A_i} + \frac{R''_{f,i}}{A_i} + \frac{R_w}{A_o} + \frac{R''_{f,o}}{A_o} + \frac{1}{h_o A_o} \; where \; R_w = \frac{D_o l_n \frac{D_o}{D_o}}{2K}$$

where subscripts i and o refer to inner and outer tube surfaces ($A_i = \pi D_i L$, $A_o = \pi D_o L$), which may be exposed to either the hot or the cold fluid. K is the conductivity of the metal tube wall.

The overall heat transfer coefficient may be determined from knowledge of the hot and cold fluid convection coefficients and fouling factors and form appropriate geometric parameters. For unfinned surfaces, the convection coefficients may be estimated from correlations. For standard fin configurations, the coefficients may be obtained from results compiled by Kays and London [5].

4　　　Heat Exchanger Analysis: Use of the Log Mean Temperature Difference

To design or to predict the performance of a heat exchanger, it is essential to relate the total heat transfer rate to quantities such as the inlet and outlet fluid temperatures, the overall heat transfer coefficient, and the total surface area for heat transfer. Two such relations may readily be obtained by applying overall energy balances to the hot and cold fluids, as shown in Figure 4.1.

Fig. 4.1:

Overall Energy Balances for the Hot and Cold

Fluids of a Two-Fluids Heat Exchanger.
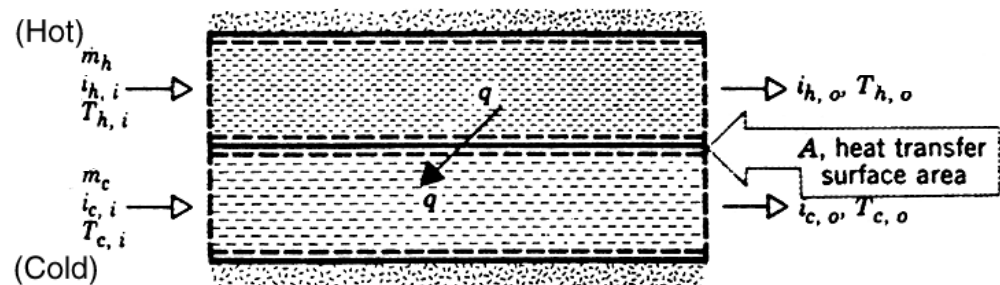
In particular, if q is the total rate of heat transfer between the hot and cold fluids and if there is negligible potential and kinetic energy changes, application of energy balance gives,

$$q = \dot{m}_h \left(i_{h,i} - i_{h,o} \right)$$

and

$$q = \dot{m}_c \left(i_{c,o} - i_{c,i} \right)$$

where i is the fluid enthalpy. The subscripts h and c refer to the hot and cold fluids, whereas i and o designate the fluid inlet and outlet conditions. If the fluids are not undergoing a phase change and constant specific heats are assumed, these expressions reduce to

$$q = \dot{m}_h c_{p,h} \left(T_{h,i} - T_{h,o} \right)$$

and

$$q = \dot{m}_c c_{p,c} \left(T_{c,o} - T_{c,i} \right)$$

where the temperatures appearing in the expressions refer to the *mean* fluid temperatures at the designated locations. Note that Equations 4.1 and 4.2 are independent of the flow arrangement and heat exchanger type.

Another useful expression may be obtained by relating the total heat transfer rate q to the temperature difference ΔT between the hot and cold fluids, where

$$\Delta T \equiv T_h - T_c$$

Such an expression would be an extension of Newton's law of cooling, with the overall heat transfer coefficient U used in place of the single convection coefficient h. However, since ΔT varies with position in the heat exchanger, it is necessary to work with a rate equation of the form

$$q = UA \, \Delta T_m$$

where ΔT_m is an appropriate *mean* temperature difference. Equation 4.4 may be used with Equation 4.1 and 4.2 to perform a heat exchanger analysis. Before this can be done, the specific form of ΔT_m must be established. Consider first the parallel-flow heat exchanger.

4.1 The Parallel-Flow heat Exchanger

The hot and cold fluid temperature distributions associated with a parallel-flow heat exchanger are shown in Figure 4.2. The temperature difference ΔT is initially large but decays rapidly with increasing x, approaching zero asymptotically. It is important to note that, for such an exchanger, the outlet temperature of the cold fluid never exceeds that of the hot fluid. In Figure 4.1 the subscripts 1 and 2 designate opposite ends of the heat exchanger. This convention is used for all types of heat exchangers considered. For parallel flow, it follows the $T_{h,i} = T_{h,1}$, $T_{h,o} = T_{h,2}$, $T_{c,i} = T_{c,1}$ and $T_{c,o} = T_{c,2}$.

The form of ΔT_m may be determined by applying an energy balance to differential elements in the hot and cold fluids. Each element is of length dx and heat transfer surface is dA, as shown in Figure 4.2.

Fig. 4.2:
Temperature Distribution for a Parallel-Flow Heat Exchanger.
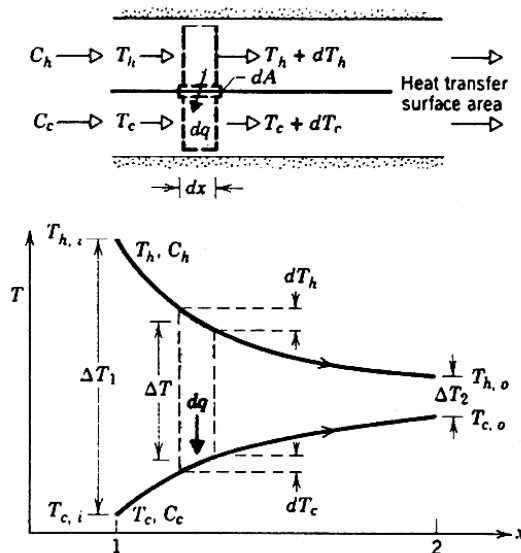
The energy balances and the subsequent analysis are performed subject to the following assumptions.
1. The heat exchanger is insulated from its surroundings, in which case the only heat exchange is between the hot and cold fluids.
2. Axial conduction along the tubes is negligible.
3. Potential and kinetic energy changes are negligible.
4. The fluid specific heats are constant.
5. The overall heat transfer coefficient is constant.

The specific heats may of course change as a result of temperature variations, and the overall heat transfer coefficient may change because of variations in fluid properties and flow conditions. However, in many applications such variations are not significant, and it is reasonable to work with average values of $C_{p,c}$, $C_{p,h}$, and U for the heat exchanger.

Applying an energy balance to each of the differential elements of Figure 4.2, it follows that

$$dq = - \dot{m}_h \, c_{p,h} dT_h \equiv - C_h dT_h$$

and

$$dq = \dot{m}_c \, c_{p,c} dT_c \equiv C_c dT_c$$

where C_h and C_c are the hot and cold fluid *heat capacity rates*, respectively. These expressions may be integrated across the heat exchanger to obtain the overall energy balances given by Equations 4.1b and 4.2b. The heat transfer across the surface area dA may also be expressed as

$$dq = U \, \Delta T \, dA$$

where $\Delta T = T_h - T_c$ is the local temperature difference between the hot and cold fluids.

To determine the integrated form of Equation 4.7, we begin by substituting Equations 4.5 and 4.6 into the differential form of Equation 4.3

$$d(\Delta T) = dT_h - dT_c$$

to obtain

$$d(\Delta T) = - dq \left(\frac{1}{C_h} + \frac{1}{C_c} \right)$$

Substituting for *dq* from Equation 4.7 and integrating across the heat exchanger, we obtain

$$\int_1^2 \frac{d(\Delta T)}{\Delta T} = - U \left(\frac{1}{C_h} + \frac{1}{C_c} \right) \int_1^2 dA$$

or

$$\ln \left(\frac{\Delta T_2}{\Delta T_1} \right) = - UA \left(\frac{1}{C_h} + \frac{1}{C_c} \right)$$

Substituting for C_h and C_c from equation 4.1b and 4.2b, respectively, it follows that

$$\ln\left(\frac{\Delta T_2}{\Delta T_1}\right) = -UA\left(\frac{T_{h,i}-T_{h,o}}{q} + \frac{T_{c,i}-T_{c,o}}{q}\right)$$

$$= -\frac{UA}{q}\left[\left(T_{h,i}-T_{c,i}\right)-\left(T_{h,o}-T_{c,o}\right)\right]$$

Recognizing that, for the parallel-flow heat exchanger of Figure 4.2, $\Delta T_1 = (T_{h,i} - T_{c,i})$ and $\Delta T_2 = (T_{h,o} - T_{c,o})$, we then obtain

$$q = UA\,\frac{\Delta T_2 - \Delta T_1}{\ln\left(\Delta T_2 / \Delta T_1\right)}$$

Comparing the above expression with Equation 4.4, we conclude that the appropriate average temperature difference is a *log mean temperature difference, (LMTD)* ΔT_{lm}. Accordingly, we may write

$$q = UA\,\Delta T_{lm}$$

where

$$LMTD = \frac{\Delta T_2 - \Delta T_1}{ln\left(\Delta T_2 / \Delta T_1\right)} = \frac{\Delta T_1 - \Delta T_2}{ln\left(\Delta T_1 / \Delta T_2\right)}$$

remember that, for a parallel – flow exchanger

$$\begin{bmatrix}\Delta T_1 \equiv T_{h,1} - T_{c,1} = T_{h,i} - T_{c,i} \\ \Delta T_2 \equiv T_{h,2} - T_{c,2} = T_{h,o} - T_{c,o}\end{bmatrix}$$

4.2 The Counterflow Heat Exchanger

The hot and cold fluid temperature distributions associated with a counterflow heat exchanger are shown in Figure 4.3. In contrast to the parallel-flow exchanger, this configuration provides for heat transfer between the hotter portions of the two fluids at one end, as well as between the colder portions at the other end. For this reason, the change in the temperature difference, $\Delta T = T_h - T_c$, with respect to x is nowhere as large as it is for the inlet region of the parallel-flow exchanger. Note that the outlet temperature of the cold fluid may now exceed the outlet temperature of the hot fluid.

Fig. 4.3:

Temperature Distributions for a Counterflow Heat Exchanger.
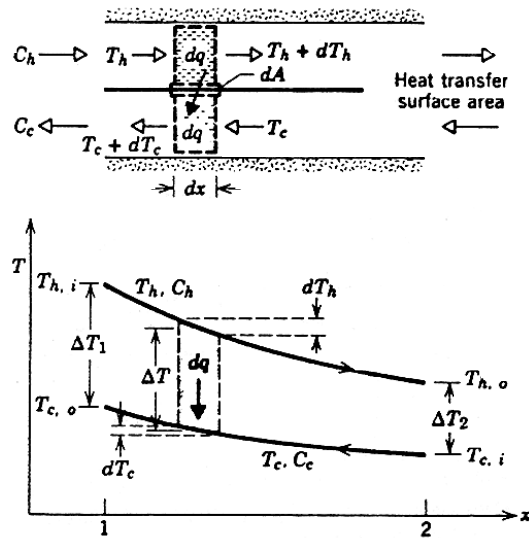
Equations 4.1b and 4.2b apply to any heat exchanger, and hence may be used for the counterflow arrangement. Moreover, from an analysis like that performed in Section 4.1, it may be shown that Equations 4.9 and 4.10 also apply. However, for the *counterflow exchanger* the endpoint temperature differences must now be defined as

$$\left[\begin{array}{l} \Delta T_1 \equiv T_{h,1} - T_{c,1} = T_{h,i} - T_{c,o} \\ \Delta T_2 \equiv T_{h,2} - T_{c,2} = T_{h,o} - T_{c,i} \end{array}\right]$$

Note that, for the same inlet and outlet temperatures, the log mean temperature difference for counterflow exceeds that for parallel flow, $\Delta T_{lm, CF} > \Delta T_{lm, PF}$. Hence the surface area required to effect a prescribed heat transfer rate q is smaller for the counterflow than for the parallel-flow arrangement, assuming the same value of U. Also not that $T_{c,o}$ can exceed $T_{h,o}$ for counterflow but not for parallel flow.

4.3   Special Operating Conditions

It is useful to note certain special conditions under which heat exchangers may be operated. Figure 4.4a shows temperature distributions for a heat exchanger in which the hot fluid has a heat capacity rate, $C_h \equiv \dot{m}_h c_{p,h}$, which is much larger than that of the cold fluid, $C_h \equiv \dot{m}_h c_{p,c}$. For this case the temperature of the hot fluid remains approximately constant throughout the heat exchanger, while the temperature of the cold fluid increases. The same condition is achieved if the hot fluid is a condensing vapour. Condensation occurs at constant temperature, and, for all practical purpose, $C_h \rightarrow \infty$. Conversely, in an evaporator or a boiler (Figure 4.4b), it is the cold fluid that experiences a change in phase and remains at a nearly uniform temperature ($C_c \rightarrow \infty$). The same effect is achieved without phase

change if $C_h \ll C_c$. Note that with condensation or evaporation, the heat rate is given by Equation 4.1a or 4.2a. The third special case (Figure 4.4c) involves a counterflow heat exchanger for which the heat capacity rates are equal $(C_h = C_c)$. The temperature difference $\Delta T_1 = \Delta T_2 = \Delta T_{lm}$.

Fig. 4.4:

Special Heat Exchanger Conditions (a) $C_h \gg C_c$

or a Condensing Vapour. (b) An Evaporating Liquid or

$C_h \ll C_c$. (c) A Counterflow Heat Exchanger with

Equivalent fluid heat capacities ($C_h = C_c$)
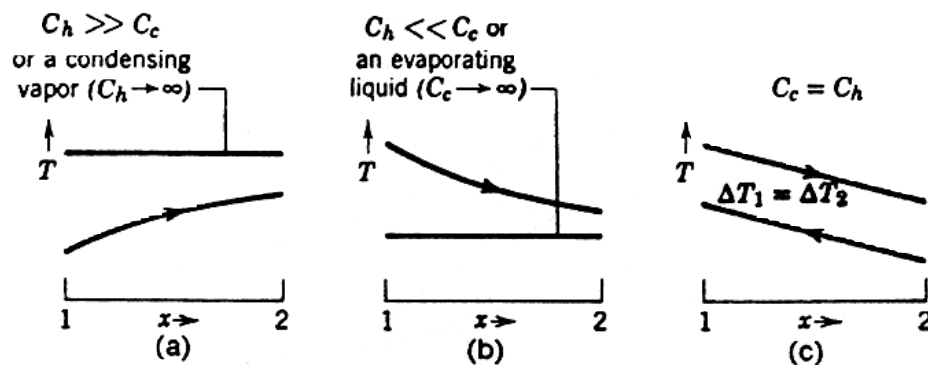
4.4 Multipass and Cross-flow Heat Exchangers

Although flow conditions are more complicated in multipass and cross-flow heat exchangers, Equations 4.1, 4.2, 4.9 and 4.10 may still be used if the following modification is made to the log mean temperature difference [6].

$$\Delta T_{lm} = F \, \Delta T_{lm,CF}$$

That is, the appropriate form of ΔT_{lm} is obtained by applying a correction factor to the value of ΔT_{lm} that would be computed under the assumption of counterflow conditions.
Hence from Equation 4.12, $\Delta T_1 = T_{h,i} - T_{c,o}$ and $\Delta T_2 = T_{h,o} - T_{c,i}$.

Algebraic expressions for the correction factor F have been developed for various shell-and-tube and cross-flow heat exchanger configurations [1, 6, 7], and the results may be represented graphically. Selected results are shown in Figures 4.5 to 4.8 for common heat exchanger configurations. The notation *(T, t)* is used to specify the fluid temperatures, with the variable *t* always assigned to the tube-side fluid. With this convention it does not matter whether the hot fluid or the cold fluid flows through the shell or the tubes. An important implication of Figures 4.5 to 4.8 is that, *if the temperature change of one fluid is negligible*, either *P* of *R* is zero and *F* is 1. *Hence heat exchanger behaviour is independent of the specific configuration.* Such would be the case if one of the fluids underwent a phase change.

Fig. 4.5:
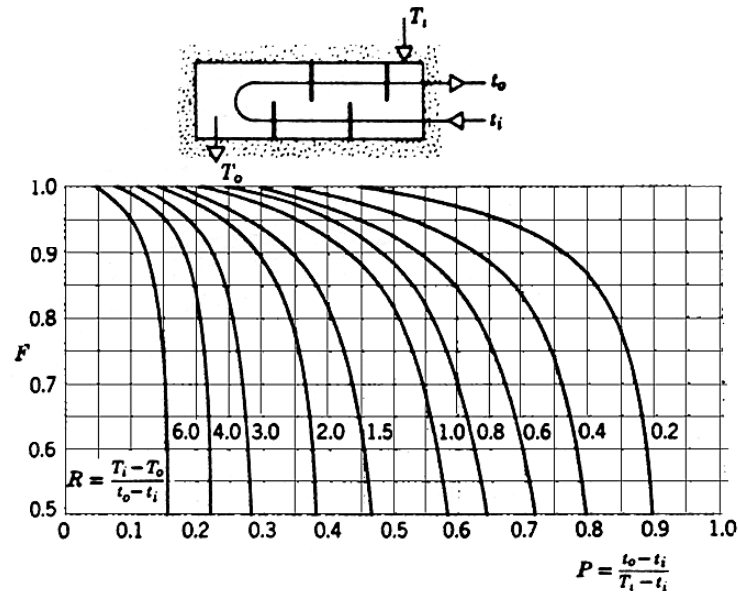Correction Factor for a Shell-and-Tube Heat Exchanger with One Shell and any Multiple of Two Tube Passes.

Fig. 4.6:
Correction Factor for a Shell-and-Tube Heat Exchanger with Two Shell Passes and any Multiple of Four Tube Passes.
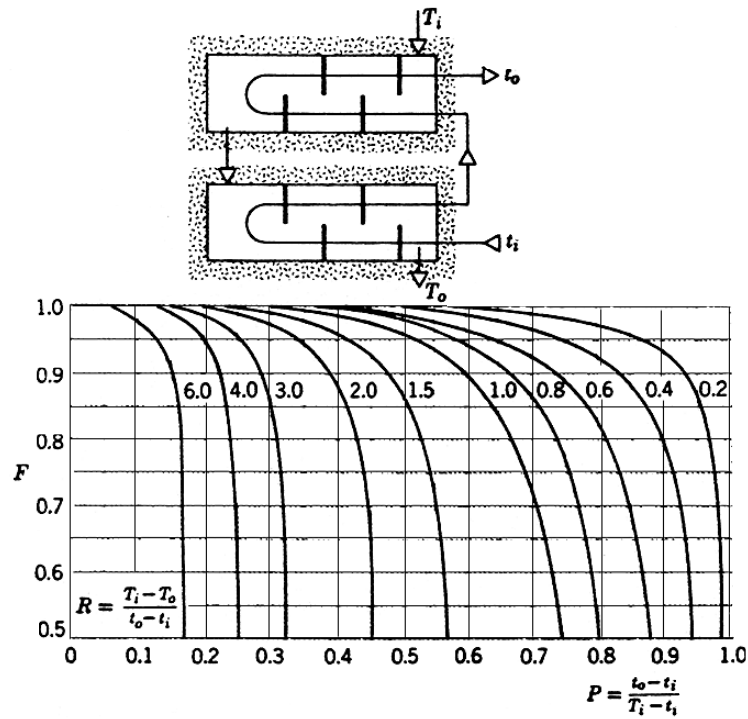
Fig. 4.7:

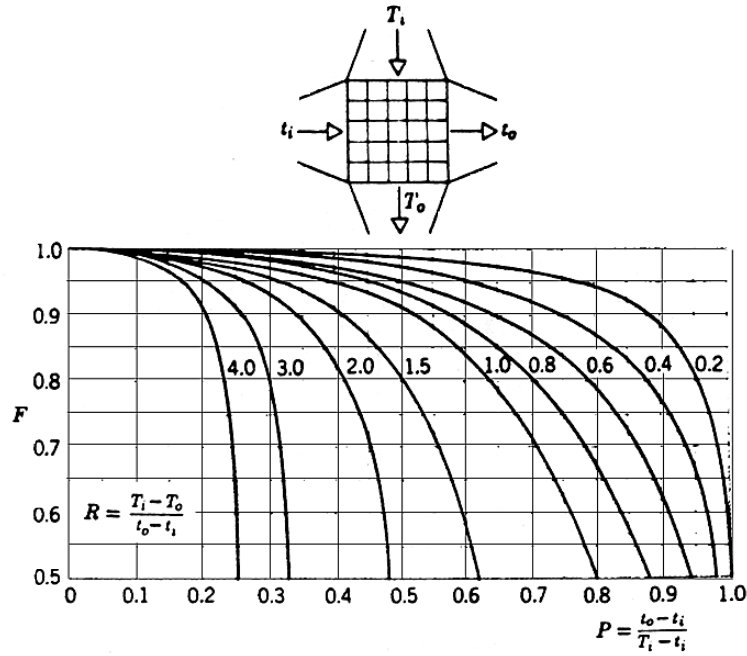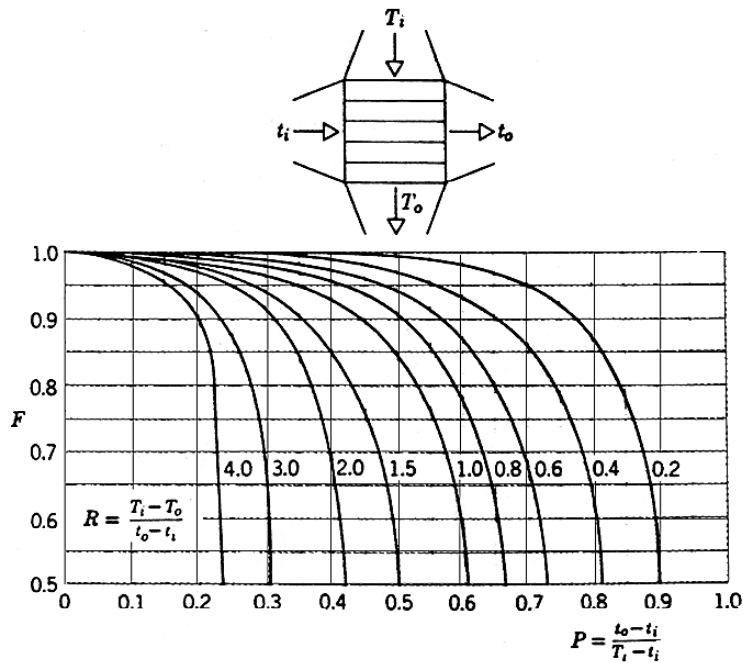*Correction Factor for a Single-Pass, Cross-Flow Heat Exchanger with Both Fluids Unmixed.*

Fig. 4.8:

Correction Factor for a Single Pass, Cross-Flow Heat Exchanger with One Fluid Mixed and the Other One Unmixed.

5   Heat Exchanger Analysis: The Effectiveness-NTU Method

It is a simple matter to use the log mean temperature difference (LMTD) method of heat exchanger analysis when the fluid inlet temperatures are known and the outlet temperatures are specified or readily determined form the energy balance expressions, Equations 4.1b and 4.2b. The value of ΔT_{lm} for the exchanger may then be determined. However, if only the inlet temperatures are known, use of the LMTD method requires an iterative procedure. In such cases it is preferable to use an alternative approach, termed the *effectiveness-NTU* method.

5.1   Definitions

To define the *effectiveness of a heat exchanger*, we must first determine the *maximum possible heat transfer rate, q_{max},* for the exchanger. This heat transfer rate could, in principle, be achieved in a counterflow heat exchanger (Figure 4.3) of infinite length. In such an exchanger, one of the fluids would experience the maximum possible temperature difference, $T_{h,i} - T_{c,i}$. To illustrate this point, consider a situation for which $C_c < C_h$, in which case, from Equations 4.5 and 4.6, $|dT_c| > |dT_h|$. The cold fluid would then experience the larger temperature change, and since $L \rightarrow \infty$, it would be heated to the inlet temperature of the hot fluid $(T_{c,o} = T_{h,i})$. Accordingly, from Equation 4.2b.

$$C_c < C_h: \quad q_{max} = C_c \left(T_{h,i} - T_{c,i} \right)$$

Similarly, if $C_h < C_c$, the hot fluid would experience the larger temperature change and would be cooled to the inlet temperature of the cold fluid $(T_{h,o} = T_{c,i})$. From Equation 4.1b we then obtain

$$C_h < C_c: \quad q_{max} = C_h \left(T_{h,i} - T_{c,i} \right)$$

From the foregoing results we are then prompted to write the general expression

$$q_{max} = C_{min} \left(T_{h,i} - T_{c,i} \right)$$

(C is heat capacity rate Q pertime per °C)

where C_{min} is equal to C_c or C_h, whichever is smaller. For prescribed hot and cold fluid inlet temperatures, Equation 5.1 provides the maximum heat transfer rate that could possibly be delivered by the exchanger. A quick mental exercise should convince the reader that the maximum possible heat transfer rate is *not* equal to $C_{max} (T_{h,i} - T_{c,i})$. If the fluid having the larger heat capacity rate were to experience the maximum possible temperature change, conservation of energy in the form $C_c(T_{c,o} - T_{c,i}) = C_h(T_{h,i} - T_{h,o})$ would require that the other fluid experience yet a larger temperature change. For example if $C_{max} = C_c$ and one argues that it is possible for $T_{c,o}$ to be equal to $T_{h,i}$, it follows that $(T_{h,i} - T_{h,o}) = (C_c /C_h)(T_{h,i} - T_{c,i})$, in which case $(T_{h,i} - T_{h,o}) > (T_{h,i} - T_{c,i})$. Such a condition is clearly impossible.

It is now logical to define the *effectiveness*, ε as the ratio of the actual heat transfer rate for a heat exchanger to the maximum possible heat transfer rate.

$$\varepsilon \equiv \frac{q}{q_{max}}$$

From Equation 4.1b, 4.2b, and 5.1, it follows that

$$\varepsilon = \frac{C_h \left(T_{h,i} - T_{h,o}\right)}{C_{min} \left(T_{h,i} - T_{c,i}\right)}$$

or

$$\varepsilon = \frac{C_c \left(T_{c,o} - T_{c,i}\right)}{C_{min} \left(T_{h,i} - T_{c,i}\right)}$$

By definition the effectiveness, which is dimensionless, must be in the range $0 \leq \varepsilon \leq 1$. It is useful because, if ε, $T_{h,i}$, and $T_{c,i}$ are known, the actual heat transfer rate may readily be determined from the expression.

$$q = \varepsilon\, C_{min}\left(T_{h,i} - T_{c,i}\right)$$

For any heat exchanger it can be shown that [5]

$$\varepsilon = f\left(NTU, \frac{C_{min}}{C_{max}}\right)$$

where C_{min}/C_{max} is equal to C_c/C_h or C_h/C_c, depending on the relative magnitudes of the hot and cold fluid heat capacity rates. The number of transfer units (NTU) is a dimensionless parameter that is widely used for heat exchanger analysis and is defined as

$$NTU = \frac{UA}{C_{min}} \ or \ NTU = \frac{\Delta T_{max}}{LMDT}$$

5.2   Effectiveness-NTU Relations

To determine a specific form of the effectiveness-NTU relation, Equation 5.6, consider a parallel flow heat exchanger for which $C_{min} = C_h$. From Equation 5.3 we then obtain

$$\varepsilon = \frac{T_{h,i} - T_{h,o}}{T_{h,i} - T_{c,i}}$$

and from Equations 4.1b and 4.2b it follows that

$$\frac{C_{min}}{C_{max}} = \frac{\dot{m}_h\, c_{p,h}}{\dot{m}_c\, c_{p,c}} = \frac{T_{c,o} - T_{c,i}}{T_{h,i} - T_{h,o}}$$

Now consider Equation 4.8, which may be expressed as

$$\ln\left(\frac{T_{h,o} - T_{c,o}}{T_{h,i} - T_{c,i}}\right) = -\frac{UA}{C_{min}}\left(1 + \frac{C_{min}}{C_{max}}\right)$$

or from Equation 5.7

$$\frac{T_{h,o} - T_{c,o}}{T_{h,i} - T_{c,i}} = \exp\left[-NTU\left(1 + \frac{C_{min}}{C_{max}}\right)\right]$$

Rearranging the left-hand side of this expression as

$$\frac{T_{h,o} - T_{c,o}}{T_{h,i} - T_{c,i}} = \frac{T_{h,o} - T_{h,i} + T_{h,i} - T_{c,o}}{T_{h,i} - T_{c,i}}$$

and substituting for $T_{c,}o$ from Equation 5.9, it follows that

$$\frac{T_{h,o} - T_{c,o}}{T_{h,i} - T_{c,i}} = \frac{\left(T_{h,o} - T_{h,i}\right) + \left(T_{h,i} - T_{c,i}\right) - \left(C_{min} / C_{max}\right)\left(T_{h,i} - T_{h,o}\right)}{T_{h,i} - T_{c,i}}$$

or from Equation 5.8

$$\frac{T_{h,o} - T_{c,o}}{T_{h,i} - T_{c,i}} = -\varepsilon + 1 - \left(\frac{C_{min}}{C_{max}}\right)\varepsilon = 1 - \varepsilon\left(1 + \frac{C_{min}}{C_{max}}\right)$$

Substituting the above expression into Equation 5.10 and solving for ε, we obtain for the *parallel-flow heat exchanger*

$$\varepsilon = \frac{1 - \exp\left\{-NTU\left[1 + \left(C_{min} / C_{max}\right)\right]\right\}}{1 + \left(C_{min} / C_{max}\right)}$$

Since precisely the same result may be obtained for $C_{min} = C_{c}$, Equation 5.11a applies for any parallel-flow heat exchanger, irrespective of whether the minimum heat capacity rate is associated with the hot or cold fluid.

In heat exchanger design calculations, it is more convenient to work with E-NTU relations of the form

$$NTU = f\left(\varepsilon, \frac{C_{min}}{C_{max}}\right)$$

The foregoing expressions are represented graphically in Figures 5.1 to 5.6. For Figure 5.6 the solid curves correspond to C_{min} mixed and C_{max} unmixed, while the dashed curves correspond to C_{min} unmixed and C_{max} mixed. Moreover, if NTU ≤ 0.25, all heat exchangers have the same effectiveness regardless of the value of C_r. More generally, for $C_r > 0$ and NTU ≥ 0.25, the counterflow exchanger is the most effective. For any exchanger, maximum and minimum values of the effectiveness are associated with $C_r = 0$ and $C_r = 1$, respectively.

Fig. 5.1:
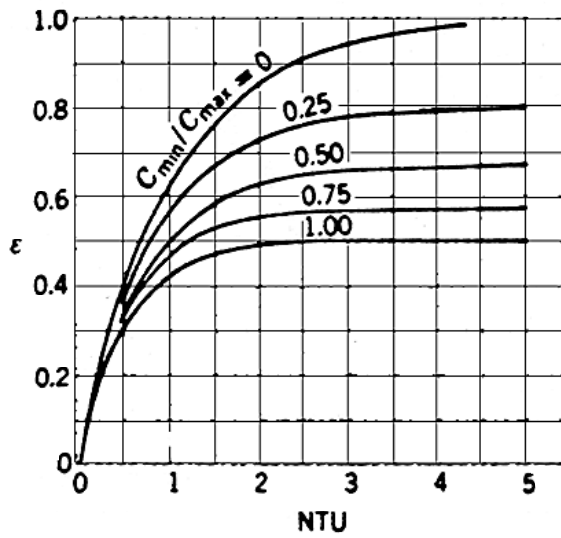*Effectiveness of a Parallelflow Heat Exchanger*

Fig. 5.2:
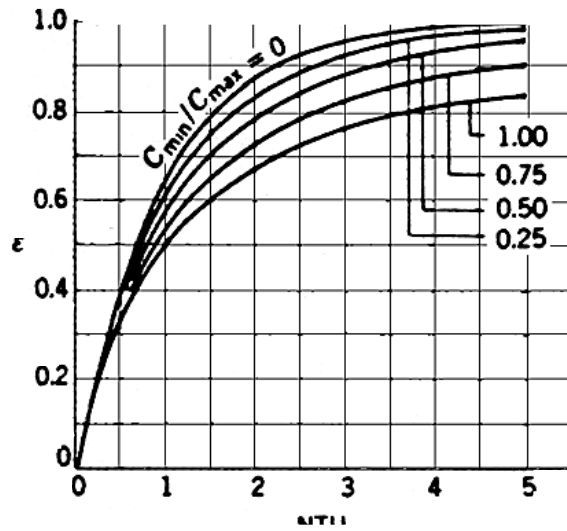*Effectiveness of a Counterflow Heat Exchanger*

Fig. 5.3:
Effectiveness of a Shell-and-Tube Heat Exchanger
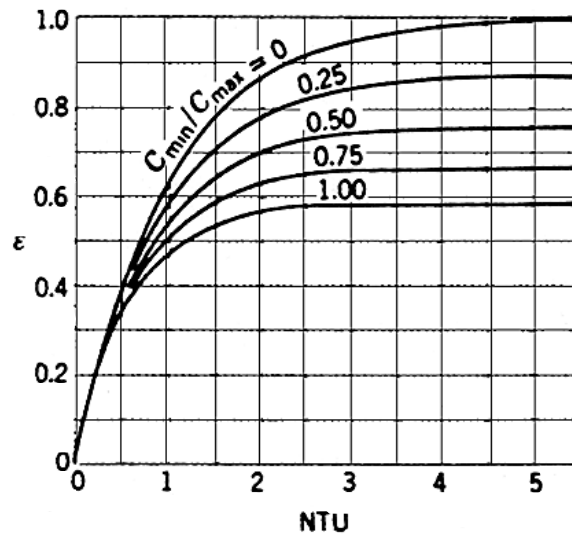*with One Shell and any Multiple of Two Tubes Passes*

Fig. 5.4:
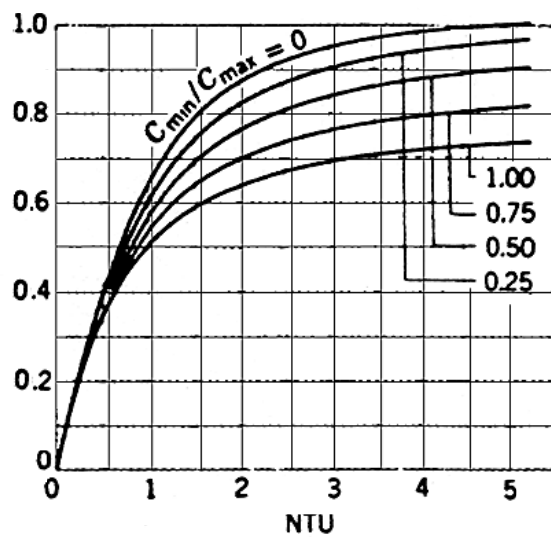*Effectiveness of a Shell-and-Tube Heat Exchanger with Two Shell passes and any Multiple of Four Tubes*
Passes

Fig. 5.5:

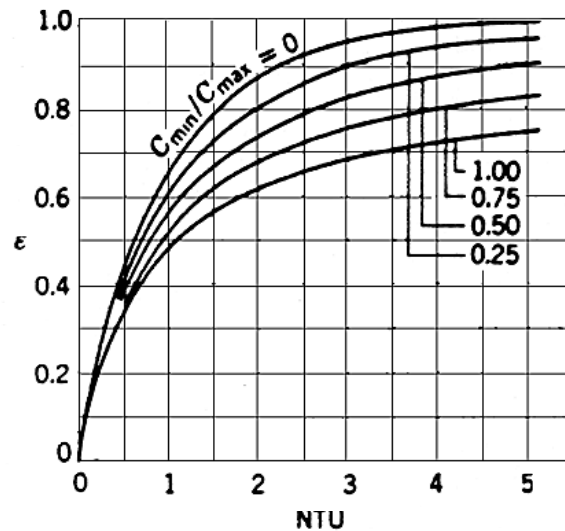*Effectiveness of a Single-Pass, Cross-Flow Heat Exchanger with Both Fluids Unmixed*
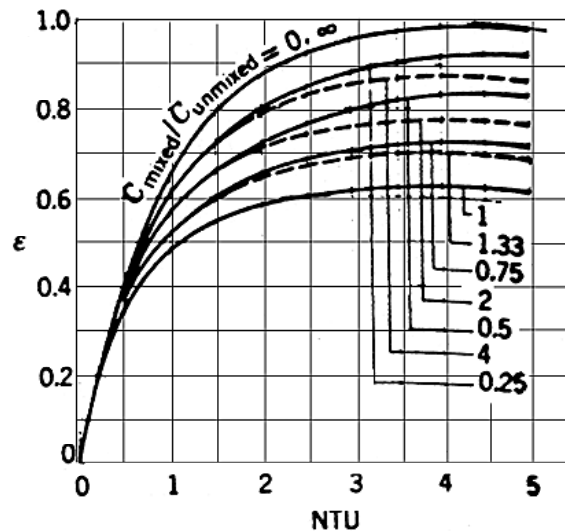

Fig. 5.6:

Effectiveness of a Single-Pass, Cross-Flow Heat Exchanger with One Fluid Mixed and the Other Unmixed

6   Methodology of a Heat Exchanger Calculation

We have developed two procedures for performing a heat exchanger analysis, the LMTD method and the NTU approach. For any problem both methods may be used to obtain equivalent results. However, depending on the nature of the problem, the NTU approach may be easier to implement.

Clearly, use of the LMTD method, Equations 4.9 and 4.10, is facilitated by knowledge of the hot and cold fluid inlet and outlet temperatures, since ΔT_{lm} may then be readily computed. Problems for which these temperatures are

known may be classified as *heat exchanger design problems*. Typically, the fluid inlet temperatures and flow rates, as well as a desired hot or cold fluid outlet temperature, are prescribed. The design problems is then one of selecting an appropriate heat exchanger type and determining the size, that is, the heat transfer surface area A, required to achieve the desired outlet temperature. For example, consider an application for which $\dot{m}_c$, $\dot{m}_h$, $T_{c,i}$ and $T_{h,i}$ are known, and the objective is to specify a heat exchanger that will provide a desired value of $T_{c,o}$. The corresponding values of q and $T_{c,i}$, and $T_{h,o}$ may be computed from the energy balances, Equations 4.2b and 4.1b, respectively, and the value of ΔT_{lm} may be found from its definition, Equation 4.10. Using the rate equation (4.9), it is then a simple matter to determine the required value of A. Of course, the NTU value, which in turn may be used to determine A. Of course the NTU method may also be used to obtain A by first calculating ε and (C_{min}/C_{max}). The appropriate chart (or equation) may then be used to obtain the NTU value, which in turn may be used to determine A.

Alternatively, the heat exchanger type and size may be known and the objective is to determine the heat transfer rate and the fluid outlet temperatures for prescribed fluid flow rates and inlet temperatures given design conditions change. Although the LMTD method may be used for such a heat exchanger *performance calculation*, the computations would be tedious, requiring iteration. For example, a guess could be made for the value of $T_{c,o}$, and Equations 4.2b and 4.1b could be used to determine q and $T_{h,o}$, respectively. Knowing all fluid temperatures, ΔT_{lm} could be determined and Equation 4.9 could then be used to again compute the value of q. The original guess for $T_{c,o}$ would be correct, if the values of q obtained from Equations 4.2b and 4.9 were in agreement. Such agreement would be fortuitous, however, and it is likely that some iteration on the value of $T_{c,o}$ would be needed.

The iterative nature of the above solution could be eliminated by using the NTU method. From knowledge of the heat exchanger type and size and the fluid flow rates, the NTU and (C_{min}/C_{max}) values may be computed and ε may then be determined from the appropriate chart (or equation). Since q_{max} may also be computed from Equation 5.1, it is a simple matter to determine the actual heat transfer rate from the requirement that $q = \varepsilon q_{max}$. Both fluid outlet temperatures may then be determined from Equations 4.1b and 4.2b.

7   Compact Heat Exchangers

As discussed in Section 2, *compact heat exchangers* are typically used when a large heat transfer surface area per unit volume is desired and at least one of the fluids is a gas. Many different tubular and plate configurations have been considered, where differences are due primarily to fin design and arrangement. Heat transfer and flow characteristics have been determined for specific configuration and are typically presented in the format of Figures 7.1 and 7.2. Heat transfer results are

correlated in terms of the Colburn j factor $j_H = St\ Pr^{2/3}$ and the Reynolds number, where both the Stanton $(St = h\ /Gc_p\ )$ and Reynolds $(Re = GD_h\ /\mu)$ numbers are based on the maximum mass velocity.

$$G \equiv \rho\ V_{max} = \frac{\rho\ V\ A_{fr}}{A_{ff}} = \frac{\dot{m}}{A_{ff}} = \frac{\dot{m}}{\sigma A_{fr}}$$

The quantity σ is the ratio of the minimum free-flow area of the finned passages (cross-sectional area perpendicular or flow direction), A_{ff}, to the frontal area A_{fr} of the exchanger. Values of σ, D_h (the hydraulic diameter of the flow passage), α (the heat transfer surface area per total heat exchanger volume), $A_f\ /A$ (the ratio of fin to total heat transfer surface area), and other geometrical parameters are listed for each configuration. The ratio $A_f\ /A$ is used in Equation 3.3 to evaluate the temperature effectiveness η_o. In a design calculation, α would be used to determine the required heat exchanger volume, after the total heat transfer surface area has been found; in a performance calculation it would be used to determine the surface area from knowledge of the heat exchanger volume.

In a compact heat exchanger calculation, empirical information, such as that provided in Figures 7.1 and 7.2, would first be used to the determine the average convection coefficient of the finned surfaces. The overall heat transfer coefficient would then be determined, and using the LMTD or ε-NTU method, the heat exchanger design or performance calculations would be performed.

where :

$$N_u = \frac{LD}{K}$$

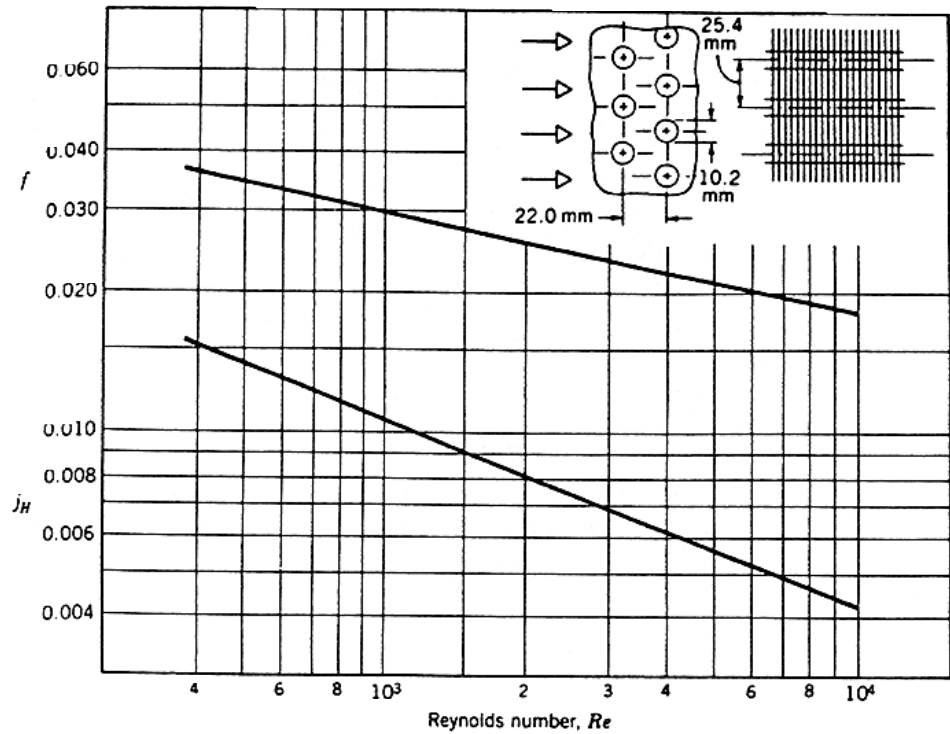$$P_r = \frac{C_p \mu}{K}$$

$$R_e = \frac{GD}{\mu}$$

(Stanton) $ST = \dfrac{h}{C_p G}$

$$j = ST\ P_r^{2/3} = (Nu\ P_r^{1/3}\ /\ R_e$$

Friction + H.T. :

$$j = ST\ P_r^{2/3}\ and\ \frac{hD}{K} = 0.023\ R_e^{.8}\ P_r^{.3}$$

Fig. 7.1:

Heat Transfer and Friction Factor for a Circular Tube-Circular Fin Heat Exchanger, Surface CF-7.0-5/8J from Kays and London [5].

Tube outside diameter, D_o = 10.2 mm
Fin pitch = 315 per meter
Flow passage hydraulic diameter, D_h = 3.63 mm
Fin thickness = 0.330 mm
Free-flow area/frontal area, σ = 0.534
Heat transfer area/total volume, α = 587 m²/m³
Fin area/total area = 0.913
Note: Minimum free-flow area is in spaces transverse to flow.

Fig. 7.2:

Heat Transfer and Friction Factor for a Circular Tube-Continuous Fin Heat Exchanger, Surface 8.0-3/8T from Kays and London [5].
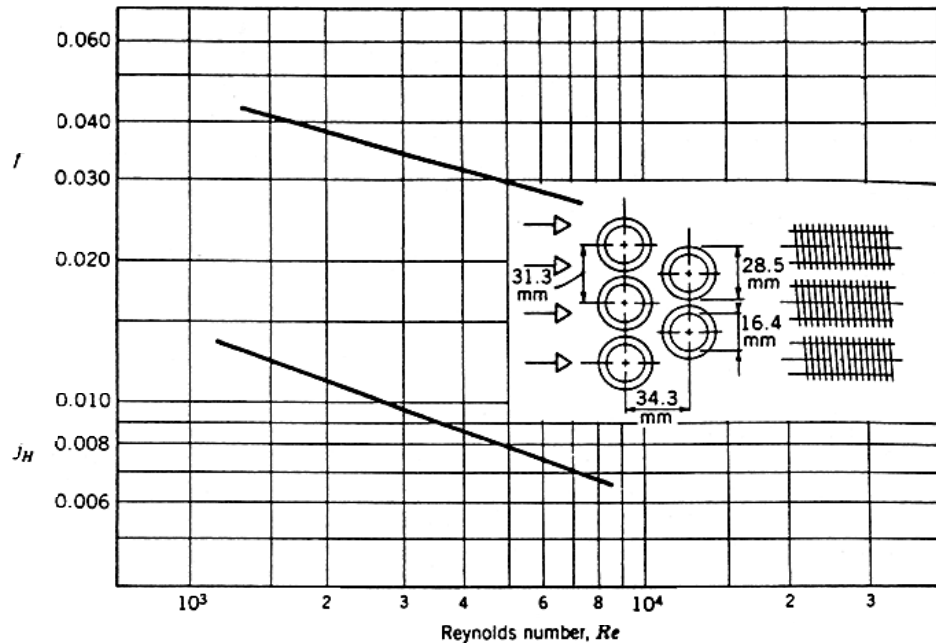
Tube outside diameter, D_o = 16.4 mm
Fin pitch = 275 per meter
Flow passage hydraulic diameter, D_h = 6.68 mm
Fin thickness, t = 0.254 mm
Free-flow area/frontal area, σ = 0.449
Heat transfer area/total volume, α = 269 m²/m³
Fin area/total area, A_f/A = 0.830
Note: Minimum free-flow area is in spaces transverse to flow.

The pressure drop associated with flow across finned-tube banks, such as those of Figures 7.1 and 7.2, may be computed from the expression
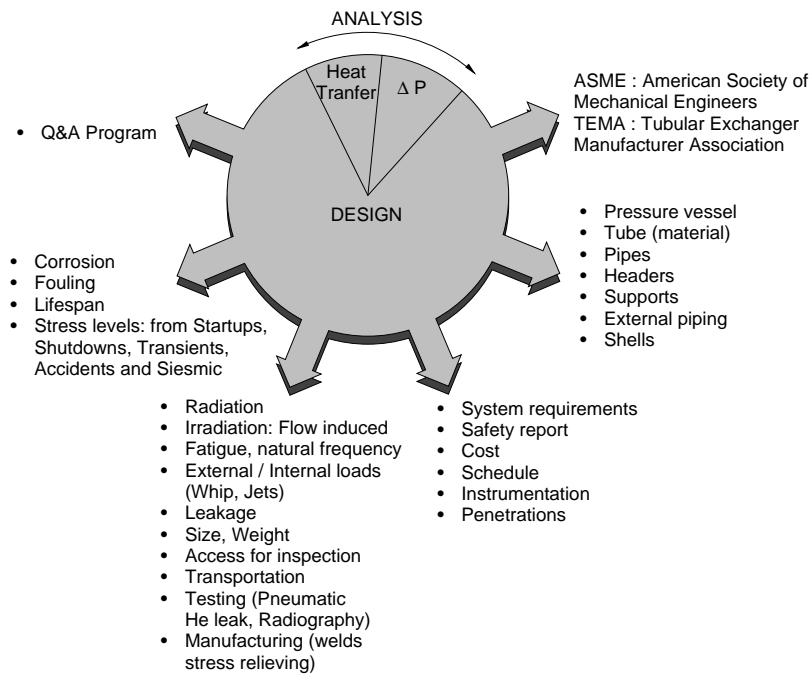
$$\Delta P = \frac{G^2 v_i}{2} \left[(1 + \sigma^2) \left(\frac{v_o}{v_i} - 1 \right) + f \frac{A}{A_{ff}} \frac{v_m}{v_i} \right]$$

where v_i and v_o are the fluid inlet and outlet specific volumes and $v_m = (v_i + v_o)/2$. The first term on the right-hand side of Equation 7.2 accounts for the effects of acceleration or deceleration as the fluid passes through the heat exchanger, while the second term accounts for losses due to fluid friction. For a prescribed core configuration, the friction factor is known as a function of Reynolds number, as, for example, from Figures 7.1 and 7.2; and for a prescribed heat exchanger size, the area ratio may be evaluated from the relation $(A/A_{ff}) = (\alpha V/\sigma A_{fr})$, where V is the total heat exchanger volume.

The classic work of Kays and London [5] provides Colburn j and friction factor data for many different compact heat exchanger cores, which include flat tube (Figure 2.5a) and plate-fin (Figure 2.5d, e) configurations, as well as other circular tube configurations (Figure 2.5b, c). Other excellent sources of information are provided by References 3, 4, 8 and 9.

8   Summary

Although we have restricted ourselves to heat exchangers involving separation of hot and cold fluids by a stationary wall, there are other important options. For example, *evaporative* heat exchangers enable *direct contact* between a liquid and a gas (there is no separating wall), and because of latent energy effects, large heat transfer rates per unit volume are possible. Also, for gas-to-gas heat exchanger, use is often made of *regenerators* in which the same space is alternately occupied by the hot and cold gases. In a fixed regenerator such as a packed bed, the hot and cold gases alternately enter a stationary, porous solid. In a rotary regenerator, the porous solid is a rotating well, which alternately exposes its surfaces to the continuously flowing hot and cold gases. Detailed descriptions of such heat exchangers are available in the literature [3, 4, 8, 11-15].

ANALYSIS

Heat Tranfer   Δ P

DESIGN

- Q&A Program

ASME : American Society of Mechanical Engineers
TEMA : Tubular Exchanger Manufacturer Association

- Pressure vessel
- Tube (material)
- Pipes
- Headers
- Supports
- External piping
- Shells

- Corrosion
- Fouling
- Lifespan
- Stress levels: from Startups, Shutdowns, Transients, Accidents and Siesmic

- Radiation
- Irradiation: Flow induced
- Fatigue, natural frequency
- External / Internal loads (Whip, Jets)
- Leakage
- Size, Weight
- Access for inspection
- Transportation
- Testing (Pneumatic He leak, Radiography)
- Manufacturing (welds stress relieving)

- System requirements
- Safety report
- Cost
- Schedule
- Instrumentation
- Penetrations

References

[1]   S*tandards of the Tubular Exchange Manufacturers Association*, 6th ed., Tubular Exchanger Manufacturers Association, New York, 1978.

[2]   Chenoweth, J.M., and M. Impagliazzo, Eds., *Fouling in Heat Exchange Equipment*, American Society of Mechanical Engineers Symposium Volume HTD-17, ASME, New York, 1981.

[3]   Kakac, S., A. E. Bergles, and F. Mayinger, Eds., *Heat Exchangers*, Emisphere Publishing Corp., New York, 1981.

[4]   Kakac, S., R.K. Shah, and A.E. Bergles, Eds., *Low Reynolds Number Flow Heat Exchangers*, Hemisphere Publishing Corp., New York, 1983.

[5]   Kays, W.M., and A.L. London, *Compact Heat Exchangers*, 3rd ed.,

McGraw-Hill, New York, 1984.

[6]   Bowman, R.A., A.C. Mueller, and W.M. Nagle, *"Mean Temperature Difference in Design"*, Trans. ASME, 62, 283, 1940.

[7]   Jakob, M., *Heat Transfer,* Vol. 2, Wiley, New York, 1957.

[8]   Shah, R.K., C.F. McDonald, and C.P. Howard, Eds., *Compact Heat Exchangers*, American Society of Mechanical Engineers Symposium Volume HTD-10, ASME, New York, 1980.

[9]   Webb, R.L., "Compact Heat Exchangers", in E.U. Schlünder, Ed., *Heat Exchanger Design Handbook*, Section 3.9, Hemisphere Publishing Corp., New York, 1983.

[10]   Marner, W.J., A.E. Bergles, and J.M. Chenoweth, "On the Presentation of Performance Data for Enhanced Tubes Used in Shell-and-Tube Heat Exchangers", *Trans. ASME, J. Heat Transfer*, 105, 358, 1983.

[11]   Schlünder, E.U., Ed.-in-Chief, *Heat Exchanger Design Handbook*, Vols. 1-5, Hemisphere Publishing Corp., New York, 1983.

[12]   Coppage, J.E., and A.L. London, "The Periodic Flow Regenerator: A Summary of Design Theory", *Trans. ASME*, 75, 779, 1953.

[13]   Treybal, R.E., *Mass Transfer Operations*, 2nd ed., McGraw-Hill, New York, 1968.

[14]   Sherwood, T.K., R.L. Pigford, and C.R. Wilkie, *Mass Transfer*, McGraw-Hill, New York, 1975.

[15]   Schmidt, F.W., and A.J. Willmott, *Thermal Energy Storage and Regeneration*, Hemisphere Publishing Corp., New York, 1981.

Boiling Heat Transfer

Training Objectives

The participant will be introduced to:
1 boiling curve.
2 pre CHF heat transfer.

Boiling Heat Transfer

Table of Contents

1 Introduction

This lesson describes the process of boiling, particularly for the case where the fluid or coolant is evaporated in a heated channel or duct.

Boiling is strictly a thermodynamic process in which a change from liquid to vapour phase takes place.

The choice of correlation for a particular application depends frequently on the heat-transfer mode and flow regime, as well as the geometry, the orientation of the surface, the direction of the flow-velocity vector, and the local phase distribution. Common heat-transfer configurations encountered in in-reactor and out-reactor components are shown in Figure 1.1, while Figure 1.2 shows a map of the forced-convective heat-transfer modes. Figure 1.3 illustrates the occurrence of these heat transfer modes and is valid for the case of a gradually increasing enthalpy or vapour quality.

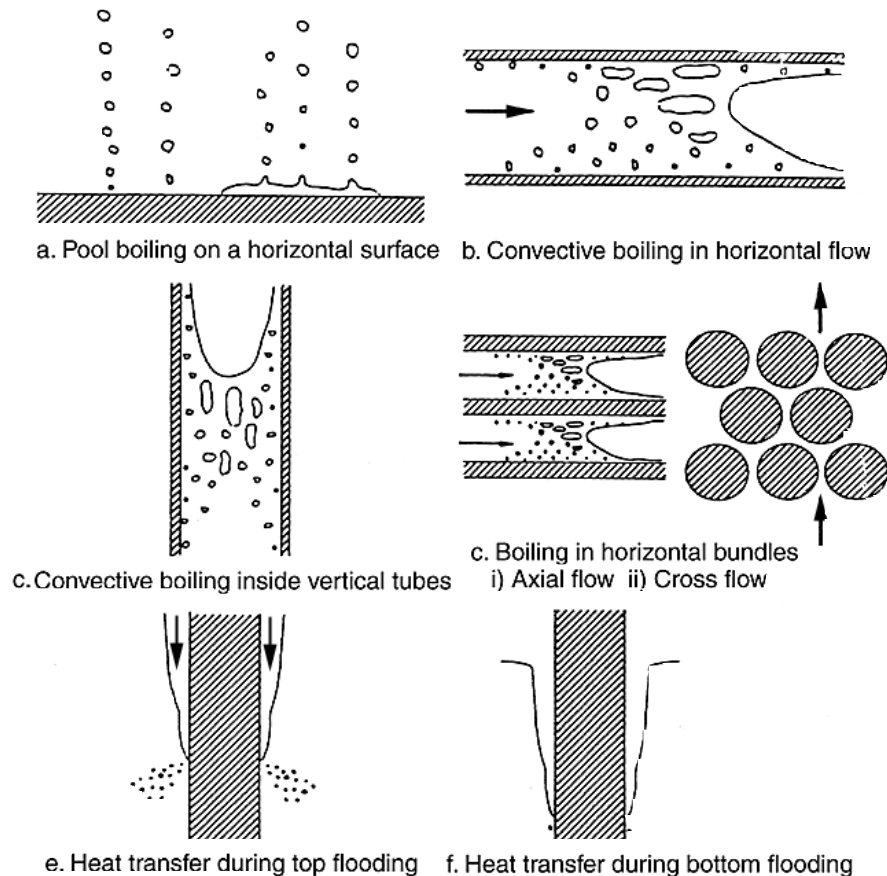*Fig. 1.1:*
Heat-Transfer Configurations

a. Pool boiling on a horizontal surface   b. Convective boiling in horizontal flow

c. Convective boiling inside vertical tubes

c. Boiling in horizontal bundles
  i) Axial flow ii) Cross flow

e. Heat transfer during top flooding   f. Heat transfer during bottom flooding

Fig. 1.2:

Map of Forced-Convective Heat-Transfer Modes

Subcooled
film boiling

Heat Flux

Subcooled
nucleate
boiling

Film
boiling

Saturated
nucleate
boiling

Forced
convection
to liquid
phase

Forced
convection
evaporation

Single phase
forced
convection
to vapour

0   **Thermodynamic Quality**   **1.0**

Fig. 1.3:

Convective Heat-Transfer Modes

Convective
heat transfer
to vapour

Liquid
deficient
region

Forced
convective
heat transfer
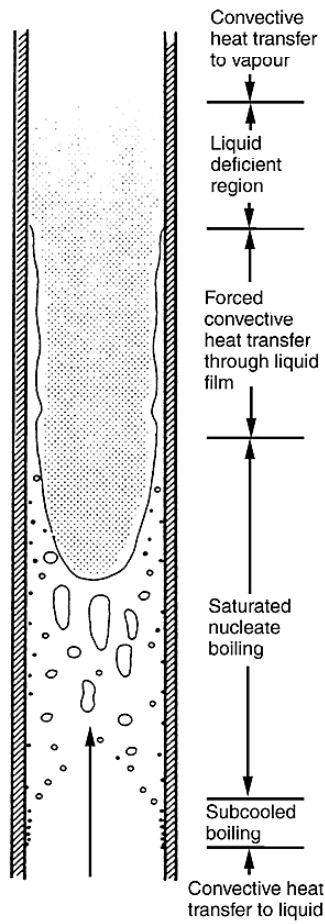through liquid
film

Saturated
nucleate
boiling

Subcooled
boiling

Convective heat
transfer to liquid

Although the shape of the boiling curve (see Figure 2.1) changes somewhat with a change in pressure, mass flux, enthalpy and geometry, the basic relationship between the individual heat-transfer modes remains unaltered. Various heat-transfer modes are separated from each other by transition points. Among them, the transition between nucleate boiling and transition boiling (Critical Heat Flux (CHF) point: T_{CHF}, q_{CHF}) as well as the transition between transition boiling and film boiling (minimum film-boiling point: T_{min}, q_{min}), are the most important (see Figure 2.2). The remaining transition point located between forced convection to liquid and nucleate boiling (onset of nucleate-boiling point) is less critical, since the transition is gradual.

An empirical approach is often necessary to evaluate the heat-transfer rate. This approach may employ separate heat-transfer correlations for every heat-transfer mode and flow regime, resulting in a proliferation of correlations. A simplification, frequently used, is to combine these separate heat-transfer correlations (for one heat-transfer mode) using some suitably defined local parameters (e.g. quality, hydraulic-equivalent diameter, or void fraction) to characterize the heat-transfer process.

Most heat-transfer and fluid-flow correlations are based on tube data, as a heated tube is the simplest test geometry. Extrapolation of tube correlations to other geometries (e.g. bundle, annuli) is common practice in reactor safety analysis, as is extrapolation outside the range of test conditions of the tube database. Improvements in the prediction methods can often be made using suitable derived extrapolation factors.

2 Boiling Curve

The `boiling curve' is a convenient way to characterize the boiling process (see Figure 2.1).

The two most important boiling types are pool boiling and convective boiling.

2.1 Pool boiling

The simplest form of boiling is pool boiling in which a heated surface at a temperature above the saturation temperature of a liquid and immersed below the free surface of a liquid causes boiling. At this point it should be determined whether the main body of the liquid in the immediate vicinity of the heated surface is at (or slightly above) the saturation temperature or below the saturation temperature. The latter is called subcooled (or local) boiling because the vapour bubbles that are formed at the hot metal surface either collapse without leaving the surface or collapse immediately upon leaving the surface.

The former is called saturated (or bulk) boiling because liquid is maintained at saturation temperature. Figure 2.1 illustrates the variation of the heat-transfer coefficient as a function of the temperature difference between the wall-surface T_w and the liquid-saturation T_s temperatures in the pool boiling of a liquid at saturation temperature.

Fig. 2.1:

Principal Boiling Regimes in Pool Boiling of Water at Atmospheric Pressure and Saturation Temperature T_s, from an electrically heated platinum wire
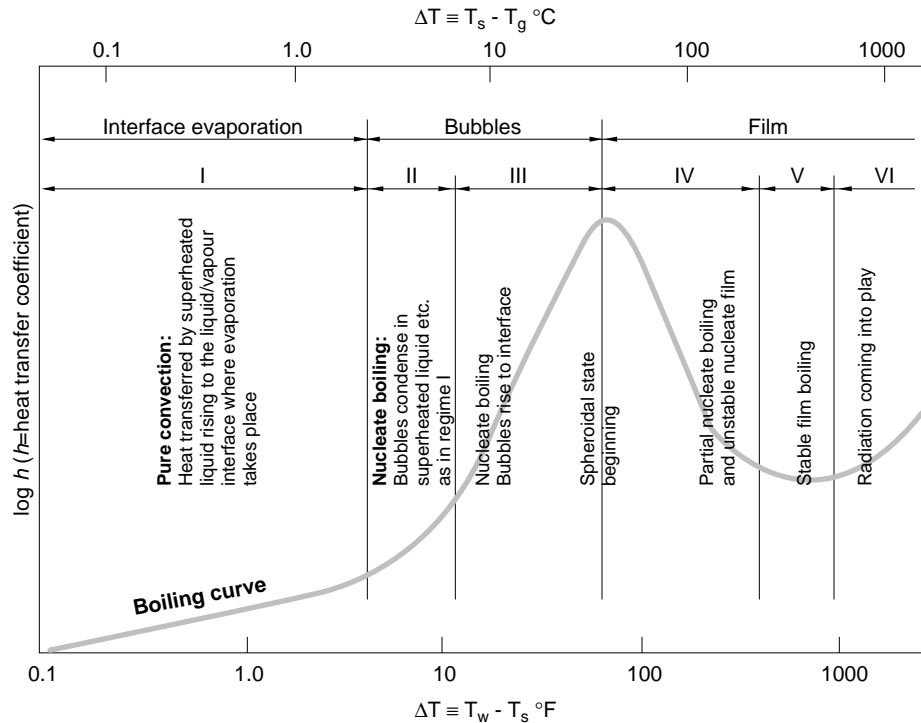
The following regions can be identified:

Region I - Natural Convection Region

In region I, no vapour bubbles are formed because the energy transfer from the heated surface to the saturated liquid is by free-convection currents which produce sufficient circulation so that the heat is removed by evaporation from the free surface.

Regions II and III - Nucleate Boiling Region

In region II, bubbles begin to form at the hot surface, but as soon as they are detached from the surface they are dissipated in the liquid. In region III, bubbles detached from the surface rise to the surface of the liquid where they are dissipated.

CHF - Interface Between Regions III and IV

Critical Heat Flux (CHF) is the upper limit of the nucleate boiling where a restriction occurs for the liquid to contact the heated surface. The maximum heat-flux point, e.g. CHF, in the nucleate boiling region is also called the burnout point.

Region IV - Transition Boiling Region
In region IV, the bubble formation is so rapid that bubbles begin to coalesce before they are detached; as a result a large fraction of the heating surface is blanketed by an unstable film of vapour which causes an abrupt loss in the heat flux and in the boiling heat-transfer coefficient.

Region V and VI - Stable Film Boiling
In region V, the heat flux drops to a minimum and the surface is blanketed with a stable film of vapour; it is called the stable film-boiling region. In region VI, both the heat flux and the heat-transfer coefficient increase with T_w - T_s because the surface temperature in this region is sufficiently high for thermal radiation effects to augment heat transfer through the vapour film. In this region the boiling also takes place as stable film boiling but radiation effects are dominant.

2.2 Forced - convection boiling

If boiling takes place on the inside surface of a heated tube through which the liquid flows with some velocity, boiling is called forced-convection boiling. Since the velocity inside the tube affects the bubble growth and separation, the mechanism and hydrodynamics of boiling in forced convection are much more complex than in the pool boiling of a quiescent liquid. The heat-transfer mode is determined based on the knowledge of the boiling curve shown schematically in Figure 2.2.

Fig. 2.2:
Boiling Curve
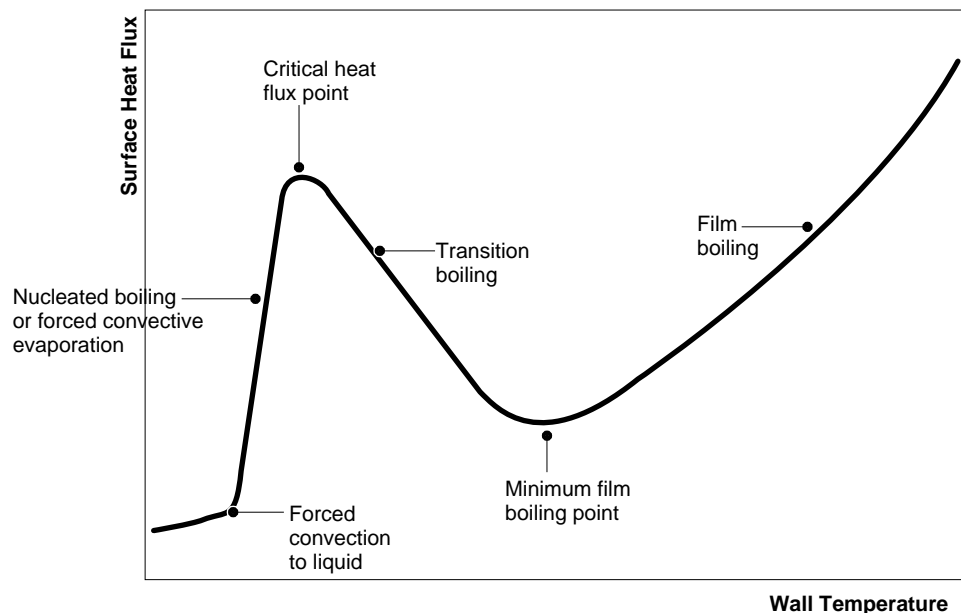
The following heat-transfer regimes, as illustrated in Figure 2.3, will be encountered sequentially in a heated channel having a subcooling liquid inlet and superheated steam outlet:

Fig. 2.3:
Regions of Heat Transfer in Convective Boiling
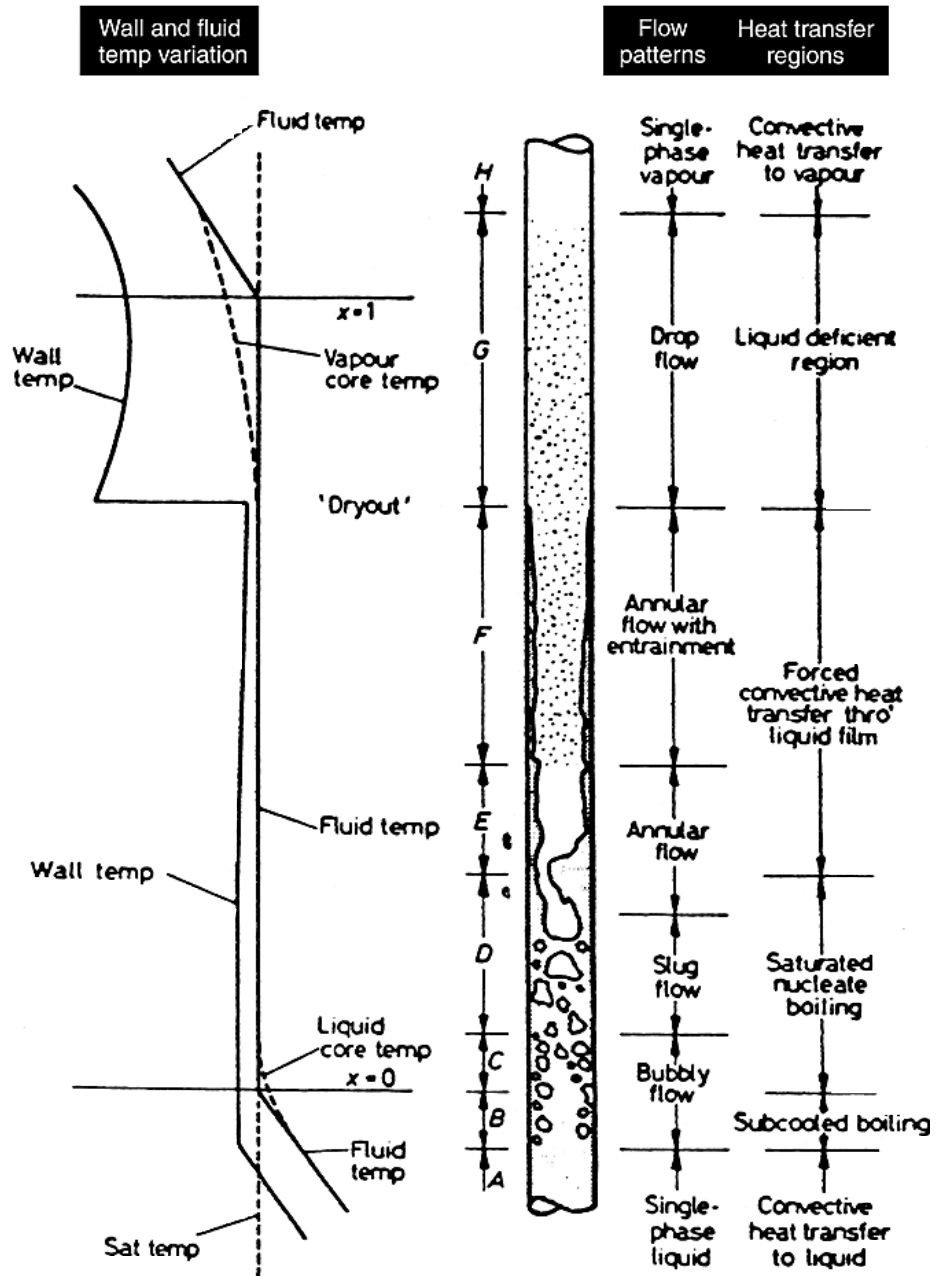
Region A - Forced Convection to a Liquid
Liquid is heated but wall temperature is below nucleation temperature and the heat transfer process is single phase convective heat transfer to the liquid phase. The difference between the saturation and local bulk fluid temperatures is called the "degree of subcooling" (T_{sub}).

Region B - Subcooled Nucleate Boiling
Wall temperature is enough for vapour formation from nucleation sites but fluid temperature is still below saturation.

Regions C and D - Saturated Nucleate Boiling
This region starts when the liquid reaches the saturation temperature or quality x = 0, i.e., found by simple heat balance calculations. The amount by which the wall temperature exceeds the saturation temperature is called the "degree of superheat" (T_{sat}). The "saturated nucleate boiling" process starts at x = 0.

Regions E and F - Forced Convective Heat Transfer Through Liquid Film
As the quality increases through the saturation nucleate boiling region, a point is reached where the process of boiling is replaced by the process of evaporation, A change in flow pattern takes place: from bubbly or slug flow to annular flow. The liquid film thickness is such that the heat is carried away from the wall by forced convection in the film to the liquid-vapour core interface where evaporation occurs. Nucleation is completely suppressed and the heat transfer process can not any more be called "boiling". These regions are referred as the "two-phase forced convective region" of heat transfer.
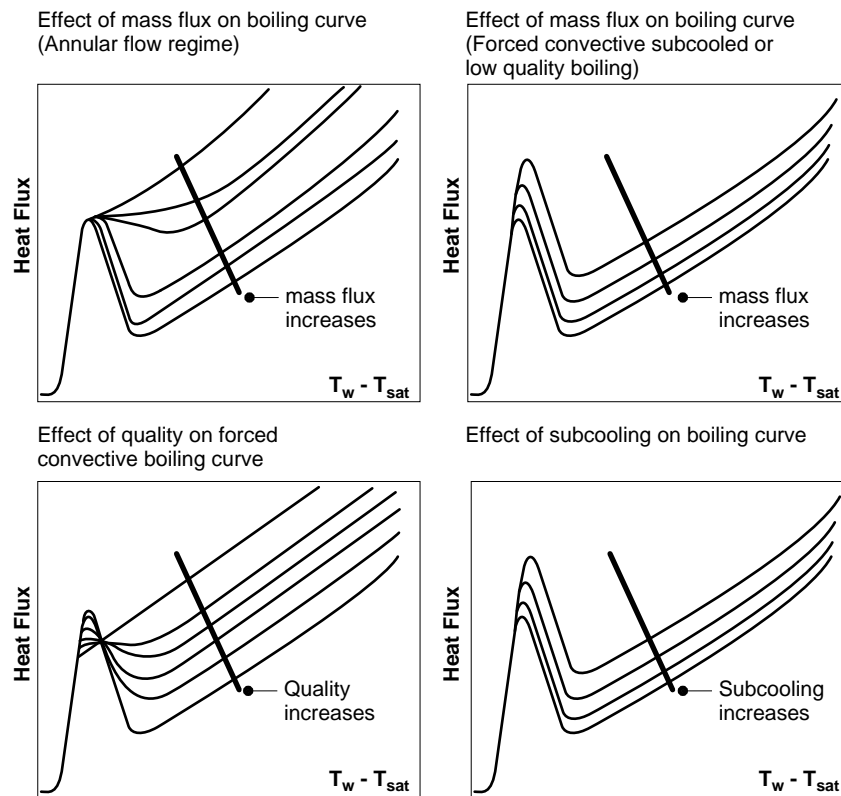
Region G - Liquid Deficient Region: Transition Boiling and Film Boiling
At some critical quality the breaking of the liquid film occurs. This transition is called "dryout" and is accompanied by a rise in the wall temperature. This region is called the "liquid deficient region", i.e., no liquid film.

The transition-boiling regime may not be encountered in a heat-flux controlled system, as can be seen from the boiling curve.

Figure 2.4 shows the effect of a change in mass flux and quality on the boiling curve.

Fig. 2.4:

Effect of a Change in Mass Flux and Quality on the Boiling Curve

Effect of mass flux on boiling curve
(Annular flow regime)

Effect of mass flux on boiling curve
(Forced convective subcooled or
low quality boiling)

Effect of quality on forced
convective boiling curve

Effect of subcooling on boiling curve

Region H - Forced Convection to Vapour

3 Pre CHF Heat Transfer

The regions that are going to be considered here are (see Figure 2.2):
- Single-phase forced-convective heat transfer.
- Onset of subcooled nucleate boiling.
- Partial-subcooled nucleate boiling.
- Fully developed subcooled nucleate boiling.
- Saturated-nucleate boiling and forced-convective evaporation.
- Fully developed nucleate boiling and forced-convective evaporation.

Since the heat transfer mechanisms are different in each of these regions, there
are as many different heat transfer coefficient correlations.

3.1 Single-Phase Forced-Convective Heat Transfer

3.1.1 General

Single-phase heat transfer is the most commonly encountered mode of energy exchange in heat-transfer equipment. For a fully developed laminar flow inside tubes (Re < 2 300), heat transfer by conduction is the dominant mode. The heat transfer coefficient is calculated with

$$h_b = 3.657 \, \frac{k_b}{D} \quad \text{for uniform wall temperature, and}$$

$$h_b = 4.3636 \, \frac{k_b}{D} \quad \text{for uniform heat flux}^{\cdot}$$

For a fully developed turbulent flow inside tubes (Re > 10^4), the heat-transfer rate is often predicted with a Dittus-Boelter type [1930] correlation

$$h_l = A \, \frac{k_1}{D} \text{Re}_l^{\,m} \text{Pr}_l^{\,n}$$

where

$$\text{Re}_l = \frac{GD}{\mu_l}$$
$$\text{Pr}_l = \frac{\mu_l Cp_l}{k_l}$$

The constants, A, m and n, in the original Dittus-Boelter equation for heating are 0.024, 0.8 and 0.4, respectively. They were re-optimized later to 0.023, 0.8 and 0.333 by Colburn [1964] with wider range of data.

Recently, Petukhov [1970] developed an analytical equation for predicting heat transfer in a circular tube with uniform heat flux. To account for the variation in fluid properties during heating, cooling and with uniform wall temperature, an empirical ratio of viscosities has been introduced. The Petukhov equation predicts closely the most reliable experimental data (±5%) for the ranges of Prandtl number between 0.5 and 10^6 and Reynolds number between 4 000 and 5×10^6. Gnielinski [1976] later modified the Petukhov equation to extend the range of application to Re > 2 300. The Gnielinski equation is expressed as

$$h_b = \frac{\left(\frac{f}{8}\right)\left(\text{Re}_b - 1000\right)\text{Pr}_b}{1 + 12.7\left(\text{Pr}_b^{\,2/3} - 1\right)\left(\frac{f}{8}\right)^{0.8}} \left(\frac{\mu_b}{\mu_w}\right)^n \frac{k_b}{D}$$

where

n	=	0.11	heating with uniform T_w ($T_w > T_b$) for liquid
n	=	0.25	heating with uniform T_w ($T_w < T_b$) for liquid
n	=	0	uniform-wall heat flux or for gases

$$f = \frac{1}{\left(1.82\ \log Re_b - 1.64\right)^2}$$

where f is the friction factor for a smooth surface.

For water flow inside a centrally heated annulus, Nixon (1968) derived an empirical correlation for heat-transfer coefficient

$$h_l = 0.02\ \frac{k_l}{D_{hy}} Re_l^{0.8} Pr_l^{0.333} \left(\frac{D_{out}}{D_{in}}\right)^{0.5}$$

For low flow conditions where heat-transfer mode is dominant by either conduction, free convection or forced convection, the heat-transfer coefficient is evaluated with

$$h_l = \max (h_{conduction},\ h_{free\ convection},\ h_{forced\ convection})$$

3.1.2 Nomenclature

C_p	Specific heat at constant pressure	$J \cdot kg^{-1} \cdot K^{-1}$
D	Tube diameter	m
D_{inn}	Inner diameter of annulus	m
D_{hy}	Hydraulic-equivalent diameter (= 4 flow area / wetted perimeter)	m
D_{out}	Outer diameter of annulus	m
f	Friction factor-	
G	Mass flux	$kg \cdot m^{-2} \cdot s^{-1}$
h	Heat-transfer coefficient	$W \cdot m^{-2} \cdot K^{-1}$
k	Thermal conductivity	$W \cdot m^{-1} \cdot K^{-1}$
L_{he}	Heated length	m
Pr	Prandtl number	-
Re	Reynolds number	-
T	Temperature	°C
μ	Dynamic viscosity	$kg \cdot m^{-1} \cdot s^{-1}$

Subscripts

b   properties evaluated at bulk fluid temperature

w   properties evaluated at wall temperature

l properties evaluated at film temperature ($= 1/2 \, (T_b + T_w)$)

3.1.3 Range of validity

The laminar flow equations are valid for Reynolds number (Re) less than 2 300, except for low Re, where free-convective heat transfer becomes dominant. The Gnielinski equation has been verified against data within the ranges of

Reynolds number	:	2 300	-	5 000 000
Prandtl number	:	0.5	-	2 000
Viscosity ratio (μ_w/μ_b)	:	0.08	-	40

The Hadaller and Banerjee equation was derived from data of

Fluid	:	superheated stream			
Pressure	:	2 000	-	21 500	kPa
Reynolds number	:	60 000	-	600 000	
Diameter	:	0.0025	-	0.0375	m
Length-to-diameter ratio	:	3	-	385	

The Nixon equation was derived from data of

Fluid	:	water			
Prandtl	:	2.0	-	8.5	
Reynolds number	:	60 000	-	600 000	
Hydraulic-equivalent diameter	:	0.0053	-	0.0453	m
Outer-to-inner diameter ratio	:	1.33	-	2.45	

3.1.4 Applicability to CANDU-bundle geometries

In a tightly packed bundle, the temperature is not constant around the circumference of the fuel rods due to the poor heat transfer in the gap between two rods. Two approaches may be used:

i)   The temperature of that portion of a rod facing a subchannel may be predicted by a combination of a subchannel code (to predict the mass flow and coolant temperature in the subchannel) and the Petukhov equation (to predict the heat-transfer coefficient based on the hydraulic-equivalent diameter and flow conditions of the subchannel).

ii) The procedure developed by Groeneveld [1973] should be used for predicting the rod-surface temperature in the gap between two rods. It is based on a large number of single-phase heat-transfer studies which measured the circumferential temperature distributions of the rods inside a bundle.

3.2 Onset of Subcooled Nucleate Boiling

The onset of subcooled nucleate boiling corresponds to the boundary between single-phase heat transfer and nucleate boiling (Figure 3.1). It is characterized by the bubble formation on the heated surface and an increase in both heat-transfer coefficient and pressure gradient above the single-phase values.

Fig. 3.1:

Transition of Heat-Transfer Mode in the Subcooled and Bulk Boiling Regions
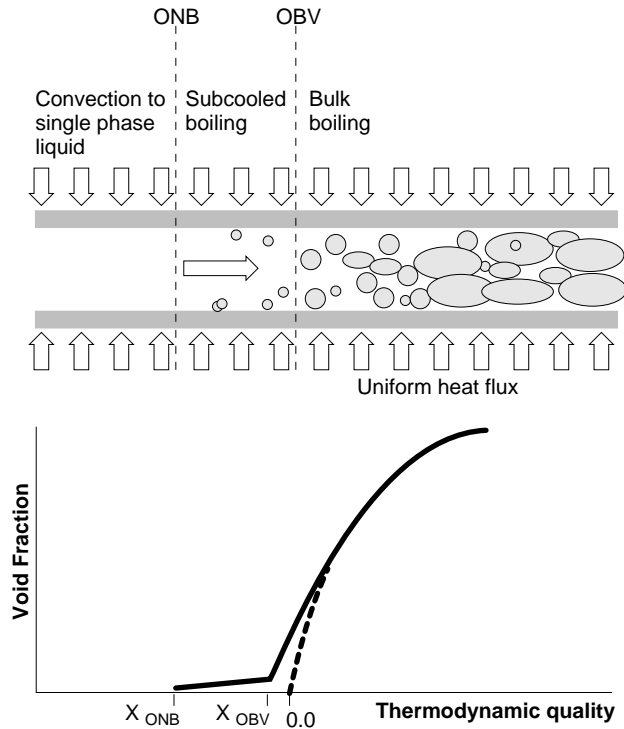
3.2.1 Method

The Davis & Anderson [1966] equation for predicting the onset of subcooled nucleate boiling is recommended:

$$q_{ONB} = \frac{k_f H_{fg} \rho_g}{8 \, \sigma \, T_{sat}} \left(T_w - T_{sat} \right)^2$$

Nucleate boiling will be initiated if, for the same wall superheat, $q_{ONB} < q_{sp}$ where

$$q_{sp} = h_{sp}\left(T_w - T_b\right)$$

Note that q_{ONB} is independent of the liquid velocity, but is a function of the heater surface properties. It is based on the assumption that a continuous range of cavity sizes is available. (The effect of not having a distribution of all cavity sizes is to shift the onset of nucleate boiling to higher temperature difference).

3.2.2 Nomenclature

h_{sp}	Single-phase heat-transfer coefficient	$W \cdot m^{-2} \cdot K^{-1}$
H_{fg}	Latent heat of vaporization	$J \cdot kg^{-1}$
k_f	Thermal conductivity of saturated fluid	$W \cdot m^{-1} \cdot K^{-1}$
k_l	Thermal conductivity of liquid film	$W \cdot m^{-1} \cdot K^{-1}$
P_{rl}	Prandtl number of liquid film	-
q_{ONB}	Heat flux at onset of nucleate boiling	$W \cdot m^{-2}$
q_{sp}	Heat flux at single-phase forced convection	$W \cdot m^{-2}$
Re_l	Reynolds number of liquid film	-
T_b	Bulk-fluid temperature	K
T_l	Liquid-film temperature	K
T_{sat}	Saturation temperature	K
T_w	Wall temperature at onset of nucleate boiling	K
μ_l	Viscosity of liquid film	$kg \cdot m^{-1} \cdot s^{-1}$
ρ_g	Density of saturated vapour	$kg \cdot m^{-3}$
σ	Surface tension	$N \cdot m^{-1}$

3.2.3 Range of validity

The data base for this correlation covers a range of flow velocity from 0.305 to 15.24 $m.s^{-1}$ and pressure from 103 to 14 000 kPa.

3.3 Partial-Subcooled Nucleate Boiling

In forced-convective boiling, nucleation will occur when the heat flux or the wall superheat exceeds the corresponding value at the onset of the subcooled nucleate boiling (ONB) point (see Figure 3.1). Before reaching fully developed boiling, however, a small transition region called partial-subcooled boiling is encountered (see Figure 3.2). The difference between these heat-transfer modes (i.e., forced-convective boiling, partial-subcooled boiling and fully developed subcooled boiling) depends on the number of active bubble-nucleation sites. At the ONB point, in general, the first nucleation site becomes active. The heat-transfer mode is the same as or very close to single-phase forced convection. In partial-subcooled boiling region, the number of nucleation sites increases with heat flux. Heat transfer in this region is a combination of the single-phase forced convection and the nucleate-boiling modes, as illustrated in Figure 3.3. In fully developed subcooled boiling, the whole surface is covered by nucleation sites.
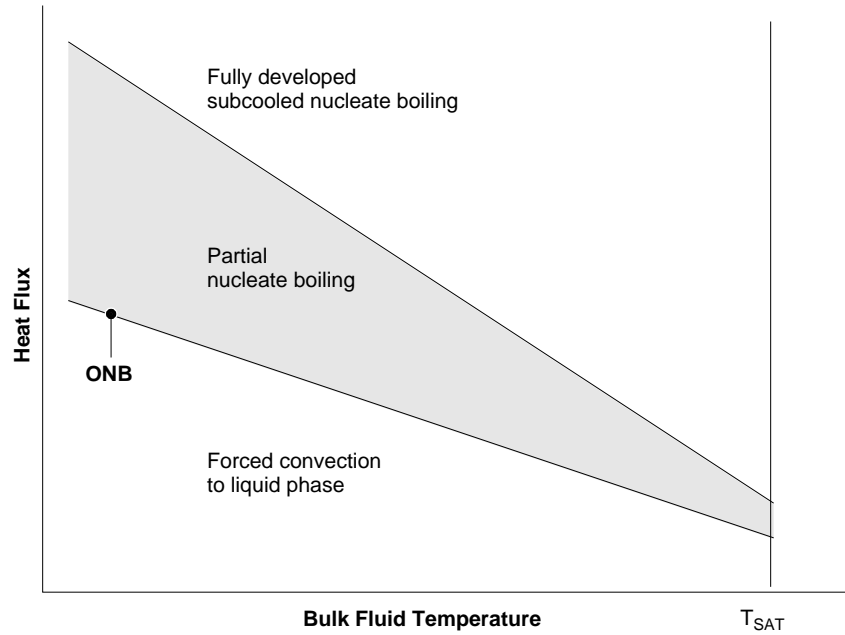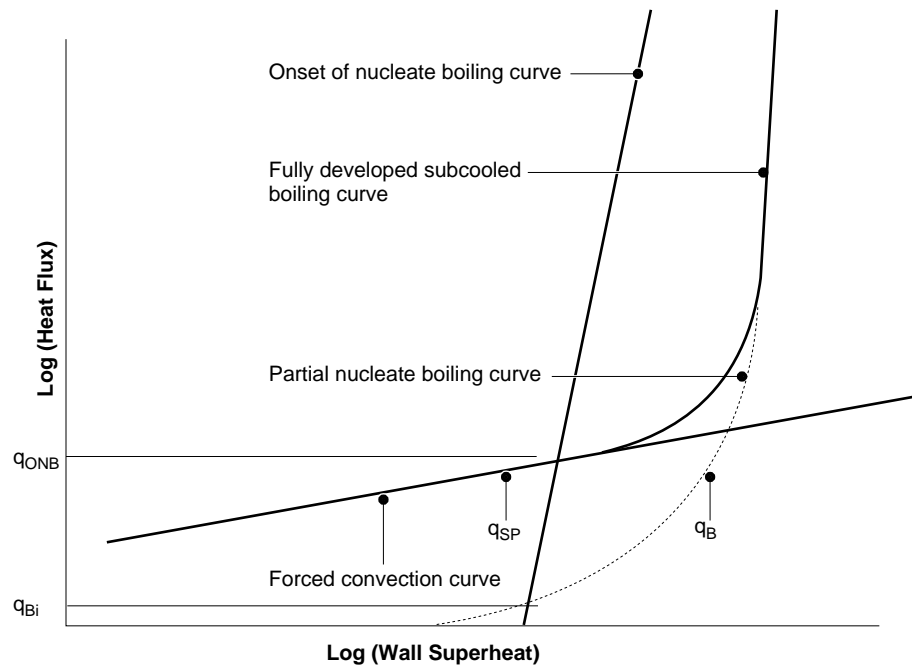
Fig.3.2:

Partial Boiling Heat-Transfer Mode

Fig. 3.3:

Partial Nucleate-Boiling Region in the Boiling Curve

3.3.1   Method

The prediction of either the heat flux or the wall superheat in partial-subcooled boiling requires the estimation of the respective values in single-phase forced convection, at the onset of nucleate boiling, and in fully developed subcooled boiling.

$$q_{pb} = q_{sp} + q_b - q_{Bi}$$

The heat fluxes and the construction of the partial-boiling curves are presented in Figure 3.3. The procedure for the construction is described as follows [Bergles and Rohsenow, 1963]:

(i)   Calculate the surface heat flux assuming single-phase heat transfer prevails, q_{SP}.

(ii)   Calculate the surface heat flux with the ONB correlation. If the value obtained in (i) is larger than that in (ii), the heat-transfer mode will be single-phase forced convection and there is no nucleation. If the value obtained in (i) is smaller than that in (ii), boiling is taking place.

(iii)   Calculate the surface heat flux for fully developed subcooled boiling, q_B.

(iv)   Iterate (i) and (ii) until the ONB point is reached.

(v)   Find the surface heat flux at the ONB point with the fully developed subcooled-boiling correlation, q_{Bi}.

(vi)   The surface heat flux during partial boiling is expressed as

$$q_{PB} = q_{sp}\left(1 + \left[\frac{q_b}{q_{sp}}\left(1 - \frac{q_{Bi}}{q_B}\right)\right]^2\right)^{0.5}$$

Note that a similar iterative technique is used for evaluating the wall superheat at ONB if the heat flux is known.

3.3.2   Nomenclature

q_B	Heat flux at fully developed subcooled boiling	$W \cdot m^{-2}$
q_{Bi}	Heat flux at onset of nucleate boiling	$W \cdot m^{-2}$
q_{PB}	Heat flux at partial-subcooled boiling	$W \cdot m^{-2}$
q_{sp}	Heat flux at single-phase forced-convective boiling	$W \cdot m^{-2}$

3.3.3   Range of validity

Since the prediction method requires various correlations in different regions, its range of validity depends on the correlations on which it is based.

3.3.4   Applicability to CANDU-bundle geometries

The prediction method should be applicable to CANDU-type bundles.

3.3.5   Comments

As a simplification, the entire partial-boiling curve is often ignored. The calculation follows the forced-convection curve until intersecting with the fully developed subcooled-boiling curve. In practice, this means that either (i) one compares the wall-superheat values predicted with correlations for the single-phase forced convection and the fully developed subcooled boiling, and selects the lowest value, or (ii) one compares the surface heat flux values and selects the highest value.

3.4 Fully Developed Subcooled Nucleate Boiling

In forced-convective boiling, nucleation (boiling) commences at the onset of nucleate boiling (ONB) (see Figure 3.1). As the heat flux (or the wall superheat) is increased, the number of bubble nucleation sites increases until the whole surface is covered by bubbles. At that stage, the flow is considered to have reached fully developed nucleate boiling. For subcooled conditions, the liquid temperature is lower than the saturation temperature. The vapour bubbles are then condensed when they depart from the heated surface and migrate to the free stream. As a result, no net vapour is produced. At high subcooling, the bubbles collapse while still being attached to the surface, in partial, not fully developed subcooled boiling.

3.4.1 Method

Most of the recommended correlations are of the following form:

$$T_w - T_{sat} = \Psi \left(\frac{1}{1\,000\,000} \right)^n$$

with Ψ and n are obtained empirically from experimental data [Collier, 1981].

Thom's form of the above correlation [Thom, 1965] is recommended for water:

$$T_w - T_{sat} = 22.65 \exp \left(- \frac{P}{8\,700} \right) \left(\frac{q}{1\,000\,000} \right)^{0.5}$$

3.4.2 Nomenclature

P	Pressure	kPa
q	Heat flux	$W \cdot m^{-2}$
T_{sat}	Saturation temperature	˚C
T_w	Wall temperature	˚C

3.4.3 Range of validity

The prediction agrees well with water data at high pressure and high mass flux [Thom et al., 1965]. Rohsenow [1972] compared Thom's and other correlations and stated that Thom's correlation is also applicable at low pressure. The pressure range for which Thom's correlation has been tested is 207 to 13 800 kPa.

3.4.4 Applicability to CANDU-bundle geometries

Nucleate boiling is a local phenomena and is not much dependent on the heater geometry. Hence, the correlation is also applicable to CANDU fuel bundles provided that the local conditions are known.

3.5 Saturated-Nucleate Boiling and Forced-Convective Evaporation

Saturated-nucleate boiling and forced-convective evaporation refer to the convective-boiling mode, where the bulk-liquid temperature has reached saturation, and the heat flux is less than the critical heat flux (CHF). Collier [1981] has concluded that Chen's correlation [1963] (Chapter 3.6) is probably the most accurate one. The disadvantage of Chen's correlation is that it is awkward

to use. Shah [1982] has recommended a graphical prediction method which was found to closely follow Chen's predictions, but is more user-friendly, especially for hand calculations. Algebraic expressions for the various curves have also been presented by Shah [1982]. For computer application, the Chen method (Chapter 3.6) is still recommended.

3.5.1   Method

Figure 3.4 shows the relationship between h_{TP}, Co, Fr, Bo and h_f^*, where

Fig. 3.4:

Shah's Graphical Prediction Method for Convective Boiling
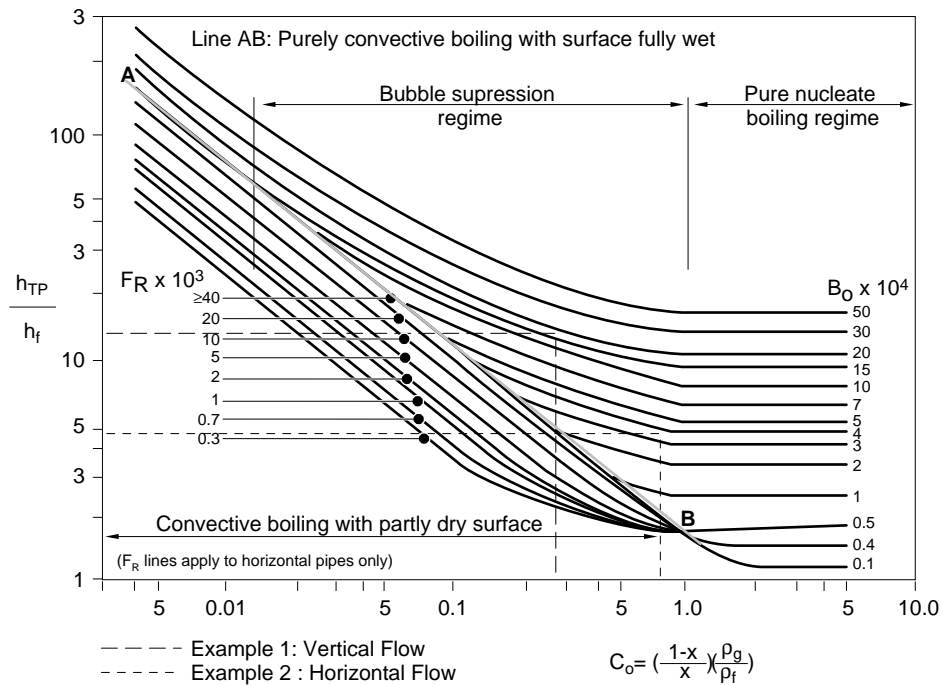
$$h_f^* = 0.023 \frac{k_f}{D_{hy}} \left(\frac{G(1-x)D_{hy}}{\mu_f} \right)^{0.8} \left(\frac{\mu_f\, Cp_f}{k_f} \right)^{0.4}$$

$$Co = \left(\frac{1-x}{x} \right)^{0.8} \left(\frac{\rho_g}{\rho_f} \right)^{0.5}$$

$$Fr = \frac{G^2}{\rho_f^2\, g\, D_{hy}}$$

$$Bo = \frac{q}{G\, h_{fg}}$$

Figure 3.4 illustrates the use of the chart. Values of Co, Bo, h_f^* and Fr (horizontal flow only) are calculated for the conditions of interest. For vertical flow, a vertical line is drawn form the X-axis until it intersects the appropriate Bo curve (curve AB represents the lower bound to all Bo curves). From this point, a

horizontal line is drawn to the Y-axis to find $h_{TP}/h_f{}^*$. For horizontal flow, a vertical line is drawn form the X-axis until it intersects the appropriate Fr curve, followed by a horizontal line to the right to intersect with AB. From this intersection, another vertical line is drawn upwards to the appropriate Bo curve. Finally, a horizontal line is drawn from this point to the left to find the $h_{TP}/h_f{}^*$ value.

3.5.2   Nomenclature

Cp_f	Specific heat of saturated liquid	$J{\cdot}kg^{-1}{\cdot}K^{-1}$
D_{hy}	Hydraulic-equivalent diameter	m
g	Acceleration due to gravity	$m{\cdot}s^{-2}$
G	Mass flux	$kg{\cdot}m^{-2}{\cdot}s^{-1}$
$h_f{}^*$	Superficial liquid heat-transfer coefficient	$W{\cdot}m^{-2}{\cdot}K^{-1}$
h_{TP}	Two-phase heat-transfer coefficient $[q/(T_w - T_{sat})]$	$W{\cdot}m^{-2}{\cdot}K^{-1}$
h_{fg}	Latent heat of vaporization	$J{\cdot}kg^{-1}$
q	Surface heat flux	$W{\cdot}m^{-2}$
T_{sat}	Saturation temperature	°C
T_w	Heated surface temperature	°C
X	Vapour quality	-
ρ_f	Saturated liquid density	$kg{\cdot}m^{-3}$
ρ_g	Saturated vapour density	$kg{\cdot}m^{-3}$
μ_f	Saturated liquid viscosity	$kg{\cdot}m^{-1}{\cdot}s^{-1}$

3.5.3   Range of validity

Shah has tested his graphical approach in tubes and annuli for a wide range of fluids and turbulent-flow conditions covering those of interest in CANDU reactors.

3.6   Fully Developed Nucleate Boiling and Forced-Convective Evaporation

Shah's method is convenient for hand calculations, but it does not lend itself to computer applications. Chen's method [1973], described in this section, has an accuracy similar to that of Shah's; it is more cumbersome to use in hand calculations, but it can be used for computer applications.

3.6.1   Method

The Chen correlation is recommended for both the subcooled and saturated nucleate boiling as well as forced-convective evaporation regions. The correlation is expressed as:

$$h_{NB} = Fh_{conv} + Sh_{pool}$$

where

$$h_c = 0.023 \left(\frac{G(1-x)D}{\mu_f} \right)^{0.8} \left(\frac{\mu c_p}{k} \right)_f^{0.4} \left(\frac{k_f}{D} \right)$$

$$h_{pool} = 0.00122 \left[\frac{k_f^{0.79} C_{pf}^{0.45} \rho_f^{0.49}}{\sigma^{0.5} \mu_f^{0.29} H_{fg}^{0.24} \rho_g^{0.24}} \right] \Delta T_{sat}^{0.24} \Delta P_{sat}^{0.75}$$

$$\Delta T_{sat} = T_w - T_{sat}$$

$$\Delta P_{sat} = P_w - P_{sat}$$

The Reynolds number, factor F, and the suppression factor S, were presented graphically in Chen's original paper. Butterworth [Bjornard & Griffith, 1977] derived the following expressions for the Reynolds number factor

F = 1 for $X_{tt}^{-1} \leq 0.1$, and

$$F = 2.35 \left(\frac{1}{X_{tt}} + 0.213 \right)^{0.736} \quad \text{for } X_{tt}^{-1} > 0.1,$$

where $X_{tt} = \left(\frac{1}{X} - 1 \right)^{0.9} \left(\frac{\rho_g}{\rho_f} \right)^{0.5} \left(\frac{\mu_f}{\mu_g} \right)^{0.1}$

The suppression factor is expressed as

$$S = \frac{1}{1 + 0.12 \, Re_{TP}^{1.14}} \quad \text{for } Re_{TP} < 32.5,$$

$$S = \frac{1}{1 + 0.42 \, Re_{TP}^{0.78}} \quad \text{for } 32.5 \leq Re_{TP} \leq 70.0, \text{ and}$$

S = 0.1 for $Re_{TP} > 70.0$,

where $Re_{TP} = 0.0001 \, F^{1.25} \frac{G(1-x)D}{\mu_f}$

For subcooled conditions, F is set to unity and Re_{TP} becomes

$$Re_{TP} = 0.0001 \, \frac{GD}{\mu_f}$$

The calculations of X_{tt} is based on the actual quality, which is the same as the equilibrium quality in an equilibrium system. Under non-equilibrium conditions such as subcooled boiling, the actual and the equilibrium qualities can be significantly different since the actual quality can be greater than zero (entrained bubbles) while the equilibrium quality is still negative ($T_{b,eq} < T_{sat}$).

With a known surface temperature, the heat flux is calculated with

$$q_{NB} = h_{NB} (T_w - T_{sat})$$

for saturated nucleate boiling, and

$$q_{NB} = Fh_{conv} (T_w - T_b) + Sh_{pool} (T_w - T_{sat})$$

for subcooled boiling.

3.6.2   Nomenclature

Cp	Specific-heat capacity at constant pressure	$J \cdot kg^{-1} \cdot K^{-1}$
D	Diameter	m
G	Mass flux	$kg \cdot m^{-2} \cdot s^{-1}$
h	Heat-transfer coefficient	$W \cdot m^{-2} \cdot K^{-1}$
H_{fg}	Latent heat of vaporization	$J \cdot kg^{-1}$
k	Thermal conductivity	$W \cdot m^{-1} \cdot K^{-1}$
P	Pressure	kPa
Pr	Prandtl number	-
q	Heat flux	$W \cdot m^{-2}$
Re	Reynolds number	-
T	Temperature	°C or K
X	Quality	-
X_{tt}	Martinelli parameter	-
Δ	Difference	-
μ	Viscosity	$kg \cdot m^{-1} \cdot s^{-1}$
ρ	Density	$kg \cdot m^{-3}$
σ	Surface tension	$N \cdot m^{-1}$

Subscripts

b	bulk fluid condition
conv	convective-boiling component
f	bases on saturated liquid
g	based on saturated vapour
NB	at nucleate boiling
pool	pool-boiling component
sat	saturation condition
TP	two-phase
tt	turbulent-liquid/turbulent-vapour flow
w	wall

3.6.3 Range of validity

The Chen correlation [1963] was tested against data obtained over the ranges of

Pressure	:	55.1	-	3 480	kPa
Liquid velocity	:	0.061	-	4.48	$m.s^{-1}$
Quality	:	0.01	-	0.71	-
Heat flux	:	40.9-	-	2 397.5	$kW.m^{-2}$

for many fluids (e.g., water, methanol, pentane, heptane, benzene, cyclo-hexane). The overall average error is 11.6%. Gungor and Winterton [1986] assessed this correlation with an even larger data base and indicated that the Chen correlation is generally acceptable in the saturated-boiling region, but that it underestimated the subcooled-boiling data.

3.6.4 Applicability to CANDU-bundle geometries

The above prediction method is also applicable to bundle geometries, since nucleate boiling is primarily a local phenomenon and therefore not significantly affected by channel cross-sectional geometry. For subcooled nucleate boiling of water, Thom's correlation (Chapter 3.4) is recommended.

3.7 References

Bergles, A.E. and Rohsenow, W.M., (1963), "The Determination of Forced Convection Surface Boiling Heat Transfer", ASME paper 63-HT-22.

Bjornard, T.A. and Griffith, P., (1977), "PWR Blowdown Heat Transfer", Symp. on the Thermal and Hydraulic Aspects of Nuclear Reactor Safety, Atlanta, Georgia, Nov. 27 - Dec. 2, Vol. 1, Light Water Reactors, pp. 17-41.

Chen, J.C., (1963), "A Correlation for Boiling Heat Transfer to Saturated Fluids in Convective Flow", ASME 63-HT-34.

Colburn, A.P., (1964), "A Method of Correlating Forced Convection Heat Transfer Data and a Comparison with Fluid Friction", Int. J. Heat Mass Transfer, Vol. 7, pp. 1359-1384.

Collier, J.G., (1981), "Convective Boiling and Condensation", 2nd Edition, McGraw-Hill.

Davis, E.J. and Anderson, G.H., (1966), "The Incipience of Nucleate Boiling in Forced Convection Flow", AIChE J., Vol. 12, No. 4, pp. 774-480.

Dittus, F.W. and Boelter, L.M.K., (1930), "Heat Transfer in Automobile Predictions of the Tubular Type", University of California Publications, Vol. 2, pp. 443-461.

Frost, W. and Dzakowic, G.S., (1967), "An Extension of the Method of Predicting Incipient Boiling on Commercially Finished Surfaces", Paper 67-HT-61 presented at ASME-AIChE Heat Transfer Conference, Seattle, Aug..

Gnielinski, V., (1976), "New Equations for Heat and Mass Transfer in Turbulent Pipe Channel Flow", Int. Chem. Eng., Vol. 16, pp. 359-368.

Groeneveld, D.C., (1973), "Forced Convection Heat Transfer to Superheated Steam in Rod Bundles", AECL-4450.

Groeneveld, D.C. and Snoek, C.W., (1986), "A Comprehensive Examination of Heat Transfer Correlations Suitable for Reactor Safety Analysis", Multiphase Science and Technology, Vol. 2, pp. 181-274.

Gungor, K.E. and Winterton, R.H.S., (1986), "A General Correlation for Flow Boiling in Tubes and Annuli", Int. J. Heat Mass Transfer, Vol. 29, pp. 351-358.

Hadaller, G. and Banerjee, S., (1969), "Heat Transfer to Superheated Steam in Round Tubes", WDI-147.

Nixon, M.L., (1968), "Heat Transfer to Water Flowing Turbulently in Tubes and Annuli", CRNL-165.

Petukhov, B.S., (1970), "Heat Transfer and Friction in Turbulent Pipe Flow with Variable Physical Properties", Advances in Heat Transfer, Academic, New York, pp. 504-564.

Rohsenow, W.M., (1972), "Status of and Problems in Boiling and Condensation Heat Transfer", Progress in Heat and Mass Transfer, Vol. 6, pp. 1-44.

Rohsenow, W.M. and Clark, J.A., (1951), "Heat Transfer and Pressure Drop Data for High Heat Flux Densities to Water at High Sub-Critical Pressure", Heat Transfer and Fluid Mechanic Institute, Stanford University Press, Stanford, Calif.

Shah, M.M., (1982), "Chart Correlation for a Saturated Boiling Heat Transfer: Equation and Further Study", ASHRAE Trans., Vol. 88, Part 1, pp. 185-196.

Thom, J.R.S., Walker, W.M., Fallon, T.A. and Reising, G.F.S., (1965), "Boiling in Subcooled Water During Flow Up Heated Tubes or Annuli", Proc. Inst. Mech. Eng., Manchester.

Tong, L.S., (1972), "Heat Transfer Mechanisms in Nucleate and Film Boiling", Nuclear Engineering and Design, Vol. 21, No. 1.

Dryout

Training Objectives

The participant will be able to understand:
1   the definitions related to dryout;
2   the dryout correlations;
3   the dryout heat transfer;
4   the problem associated with dryout;

Dryout

Table of Contents

1.　　Mechanisms of Burnout

An understanding of the mechanism of burnout is useful firstly in the development of improved correlation and prediction methods, and secondly in devising means for avoiding the occurrence of the phenomenon.

1.1　　Burnout mechanisms and regions of operation

A large number of alternative mechanisms for burnout have been proposed but the four which appear to have been reasonably well established experimentally are as follows:

(a) Formation of hot spot under growing bubble (Figure 1.1). When a bubble grows at the heated wall, a dry patch forms underneath the bubble as the micro-layer of liquid under the bubble evaporates. In this dry zone, the wall temperature rises due to the reduction in heat transfer coefficient. When the bubble departs, the dry patch may be rewetted and the process repeats itself. However, if the temperature of the dry patch becomes too high, then rewetting cannot take place and local over heating occurs.
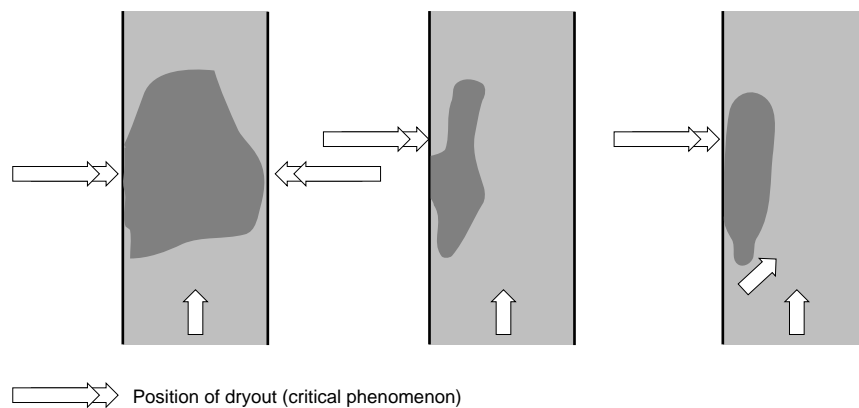
Figure 1.1

Hotspot under growing bubble
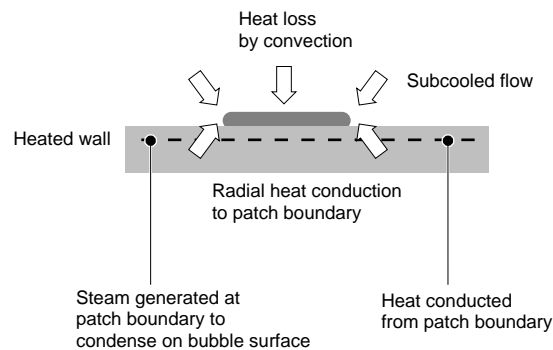
(b) Near-wall bubble crowding and inhibition of vapour release (Figure 1.2). Here, a "bubble boundary layer" builds up on the surface and vapour generated by boiling at the surface must escape through this boundary layer. When the boundary layer becomes too crowded with bubbles, vapour escape is impossible and the surface becomes dry and overheats.

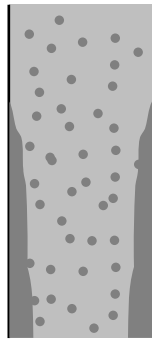*Figure 1.2*
Near wall bubble crowding

Critical
Phenomenon
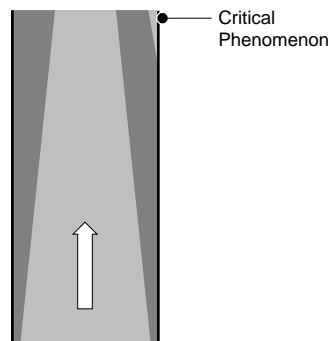
(c) Dryout under a slug or vapour clot as shown in Figure 1.3. In plug flow, the thin film surrounding the large bubble may dry out giving rise to localised overheating. Alternatively, a stationary vapour slug may be formed on the wall with a thin film of liquid separating it from the wall; in this case, localised drying out of this film gives rise to overheating.

Figure 1.3
Dryout under a slug or vapour clot

Position of dryout (critical phenomenon)

(d) Film dryout in annular flow (Figure 1.4). Here, in annular flow, the liquid film dries out due to evaporation and due to the partial entrainment of the liquid in the form of droplets in the vapour core. This mechanism is discussed in more detail below.

Figure 1.4
Film dryout in annular flow

A tentative map of the regions of operation of the above mechanisms was suggested by Semeria & Hewitt (1974) and is illustrated in Figure 1.5. The regions of operation of the respective mechanisms being shown as a function of mass flux G and quality x.

Figure 1.5
*Tentative map of regions of operation of various critical heat flux mechanisims*
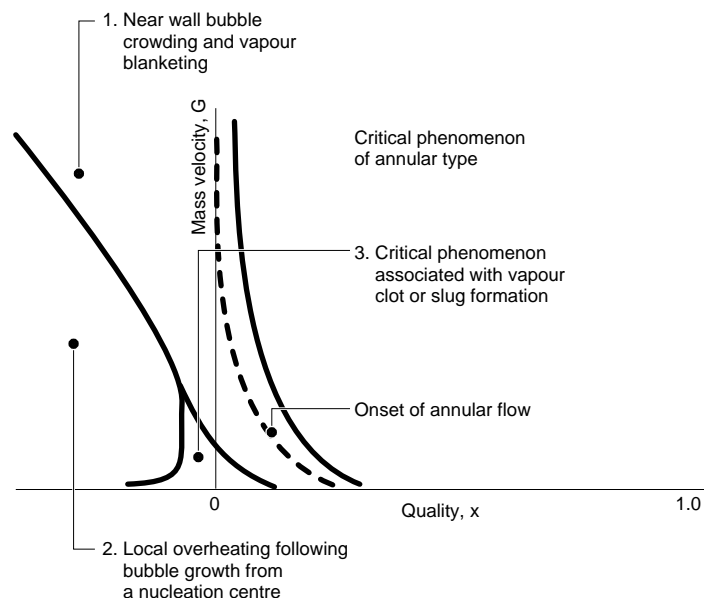
1.2   Burnout mechanism in annular flow

Burnout in annular flow is the most important mechanism from a practical point of view since, for channels of reasonable length, the first occurrence of burnout is likely to occur in this region. Perhaps the most important tool in investigating annular flow burnout is the measurement of film flow rate. This is achieved by extracting the liquid film through a porous wall section; the entrained droplets are not extracted though, to achieve complete separation, some of the vapour must also be withdrawn. Film flow rate measurements have been used to investigate burnout mechanisms in two different ways:

(1) Measurement of the film flow rate at the end of a heated channel as a

function of power input to the channel. Results obtained using this approach are exemplified in Figure 1.6. As will be seen, the film flow rate at the end of the channel decreases with increasing power and the onset of burnout corresponds quite closely to the point at which the film flow rate becomes zero. This confirms the film evaporation (as distinct from a film boiling, for instance) mechanism for burnout.

Figure 1.6

Variation of film flow with input power at the end of a uniformly heated round tube in which water is being evaporated at 70 bars
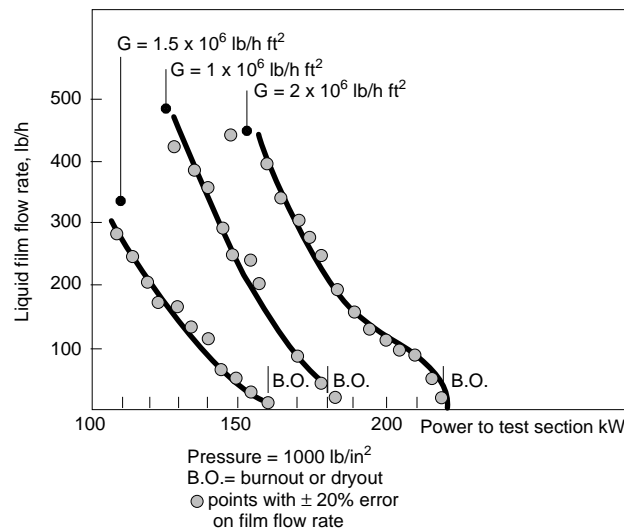
(2) Although measurements of film flow rate at the end of the test section are useful in demonstrating the mechanism, they do not demonstrate the conditions *along the test section* which have led to the occurrence of the burnout phenomenon. To achieve this, measurements of film flow rate may be made along the test section for a heat flux corresponding to the burnout heat flux. This is achieved by first determining the burnout heat flux and then, for constant inlet conditions, and for the known burnout heat flux, making measurements of the film flow rate at the end of channels of various heated lengths, less than the length of the channel for which the burnout conditions had been determined. Results of this form are illustrated in Figure 1.7; for channels with uniform heating, the film flow rate decreases along the channel length, going to zero at the end of the channel where burnout occurs. Also shown on Figure 1.7 are the results for variation of film flow rate with distance for cases where zones ("cold patches") exist along the channel where the heat flux is zero. As will be seen from Figure 1.7, the rate of change of film flow rate with length is different in these zones and can even change in sign (when the unheated zone is near the end of the test section). An explanation of these effects follows from a replot of the data shown in Figure 1.7 in the form of entrained liquid flow rate against local quality. This plot is shown in Figure 1.8. The dotted line represents the

condition of "hydrodynamic equilibrium" where the rate of entrainment of droplets are equal and opposite to the rate of deposition. This hydrodynamic equilibrium is only achieved in very long tubes at constant quality. As will be seen from Figure 1.8, systems in which the quality is changing (ie with evaporation) do not usually have hydrodynamic equilibrium conditions. In the lower part of the channel, the entrained liquid flow rate is less than that for equilibrium and in the upper part of the channel it is greater. Burnout corresponds to the point at which the entrained liquid flow is equal to the total liquid flow, with the film flow being zero. On Figure 1.8, the "cold patch" data show an approach towards the equilibrium at constant quality, the entrained flow increasing at the lower qualities or decreasing at the higher quality as shown. This leads to the situation in which the quality for burnout can be actually greater if part of the tube is unheated. This occurs when there is net deposition in the cold patch zone.

Figure 1.7

Variation of film flow rate with distance uniformly and non uniformly heated round tube.

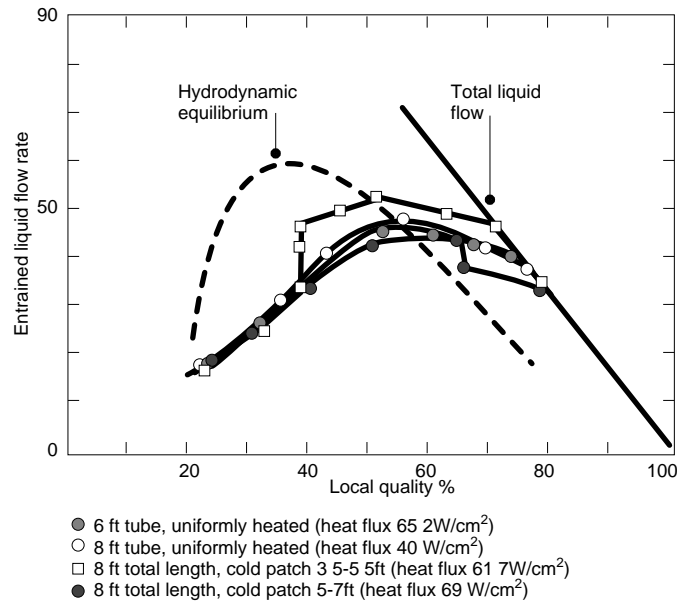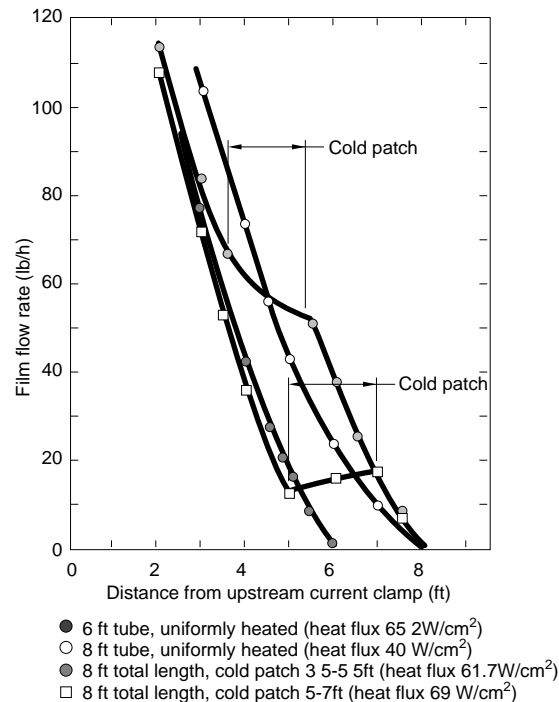*Water evaporation at low pressure. Burnout condition occurring at the end of the tube in each case*

● 6 ft tube, uniformly heated (heat flux 65 2W/cm^2)
○ 8 ft tube, uniformly heated (heat flux 40 W/cm^2)
□ 8 ft total length, cold patch 3 5-5 5ft (heat flux 61 7W/cm^2)
● 8 ft total length, cold patch 5-7ft (heat flux 69 W/cm^2)

Figure 1.8
Entrained liquid flow as a function of quality for
the evaporation of water in a tube at low pressure

- ● 6 ft tube, uniformly heated (heat flux 65 2W/cm²)
- ○ 8 ft tube, uniformly heated (heat flux 40 W/cm²)
- ● 8 ft total length, cold patch 3 5-5 5ft (heat flux 61.7W/cm²)
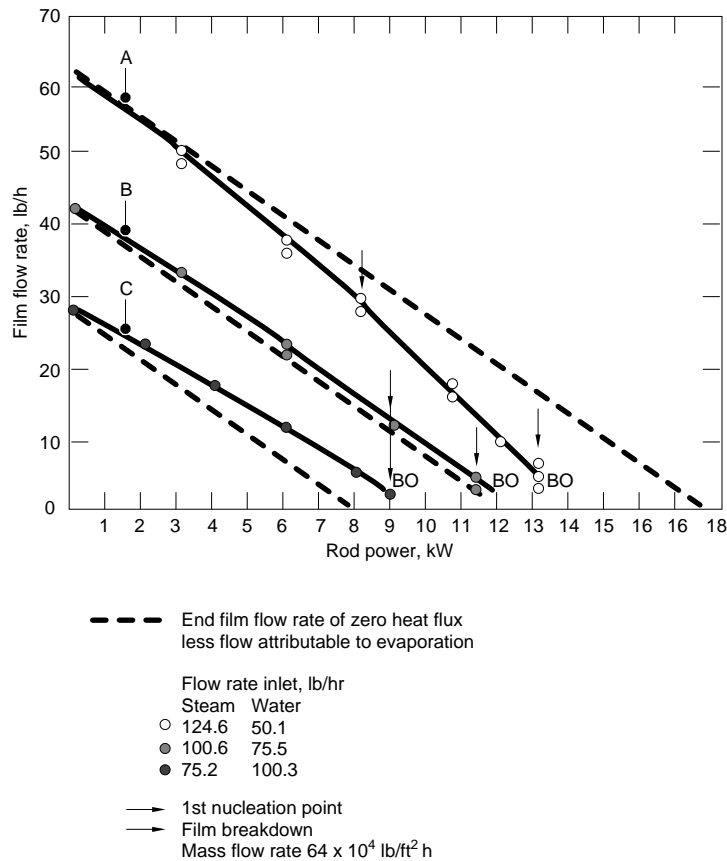- □ 8 ft total length, cold patch 5-7ft (heat flux 69 W/cm²)

1.3   Effect of heat flux on deposition/entrainment

The results illustrated in Figures 1.7 and 1.8 indicate that burnout occurs when the processes of droplet entrainment, droplet deposition and evaporation lead to a condition in which the film flow rate becomes zero. The rate of evaporation can be calculated from the local heat flux, provided the latent heat is known. The important question which arises is whether the rate of entrainment and/or deposition is affected by the presence of a heat flux normal to the surface. The effects which could be caused by a heat flux include:

(1) The effect of nucleate boiling in the film giving rise to additional entrainment due to the bursting of bubbles through the film surface and

(2) The effect of a vapour flux away from the surface inhibiting the deposition onto the surface in the presence of evaporation.

One type of experiment which might throw light on the heat flux effect is that in which a known liquid film flow rate is injected at the start of a heated channel and the film flow rate at the end of the channel measured as a function of the power input. If the film flow rate at the end of the channel falls more rapidly than that expected due to pure evaporation of the film, then it might be deduced that the evaporation is causing enhanced entrainment and vice versa. Results of this type (obtained for a vertical annulus with a film flow on the inner surface) were obtained by Hewitt et al. (1963) and are illustrated in Figure 1.9. Both positive and negative variations with respect to "pure evaporation" were observed, depending on the initial quality.

Figure 1.9

Variation of the film flow with increasing power for the evaporation of a climbing film on the inner surface of an annulus at low pressure

- - - End film flow rate of zero heat flux
      less flow attributable to evaporation

Flow rate inlet, lb/hr
Steam   Water
○ 124.6   50.1
◑ 100.6   75.5
● 75.2   100.3

→ 1st nucleation point
→ Film breakdown
Mass flow rate 64 x 10^4 lb/ft^2 h

A more direct evaluation of the effect of heat flux is obtained by determining the entrained liquid flow rate as a function of length in a channel, the first part of which is heated and the second part unheated. Any variation of the net rate of entrainment with heat flux would be detected in a plot of entrained flow rate versus length. Experiments of this type are reported by Bennett et al. (1966) and the results are illustrated in Figure 1.10. Depending on the point at which the unheated zone started, the entrained liquid flow rate could either continue to increase, remain approximately constant or continue to decrease in the unheated zone. In no case were there a marked change in the net rate of deposition or entrainment.

Figure 1.10
Effect of heat flux on rate of change on entrained liquid flow with length
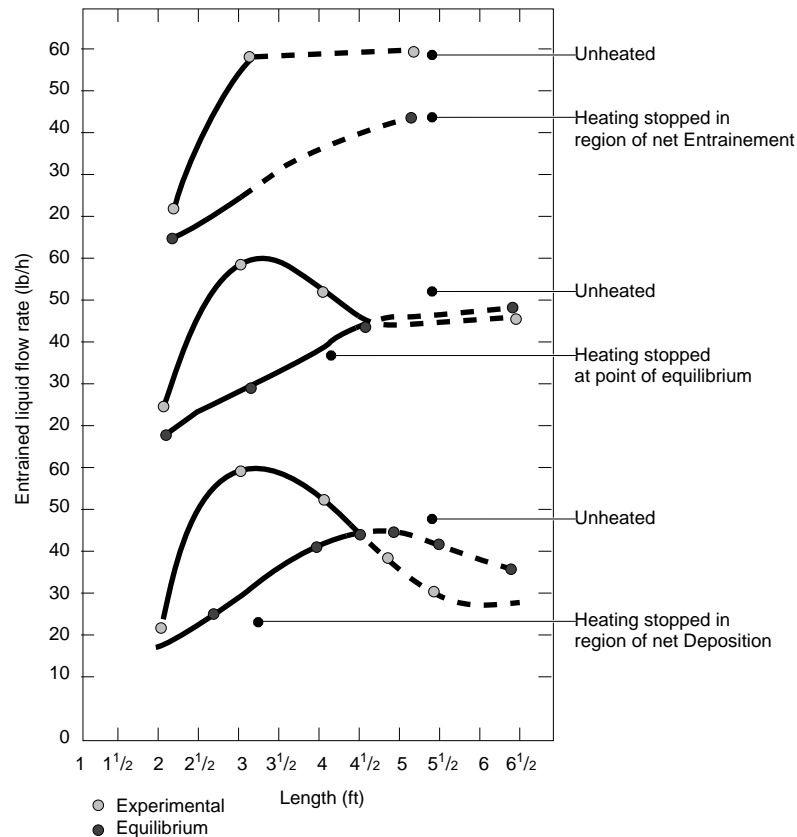
1.4 Burnout mechanisms in horizontal channels

Mechanisms in horizontal channels are discussed by Fisher et al. (1978). Based on studies over a wide range of pressures and qualities, it was concluded that there are three principal modes of burnout.

(a) At very low qualities, a relatively stable stratification of the flow occurs with the formation of "ribbons" of vapour at the upper part of the channel, leading to over heating in that region.

(b) At low and intermediate qualities a "Frothy surge" passes along the channel and wets the upper surface of the tube. The film thus deposited drains away and (in the case of the heated tubes) is also evaporated. If the drainage and evaporation are such that complete film removal (dryout) occurs before the arrival of the next frothy surge than an intermittent dryout and over heating (and subsequent corrosion) can occur.

(c) At high qualities, annular flow occurs but, for horizontal tubes, the liquid tends to concentrate at the bottom of the tube, the films at the upper surface being much thinner. Thus, dryout occurs at much lower heat fluxes.

2.   Boiling Crisis and Burnout

The whole of the curve of Figure 2.1 could be obtained if the temperature of the heating surface were closely controlled. In most practice, however, such as if the heating surface were that of a nuclear fuel element, it is the heat flux that is controlled.

Figure 2.1
Boiling regimes: below point a, liquid natural convection ; a to b, mixed;
b to c, Nucleate boiling; c to d, mixed; d to e, film boiling; e to f, film boiling and radiation
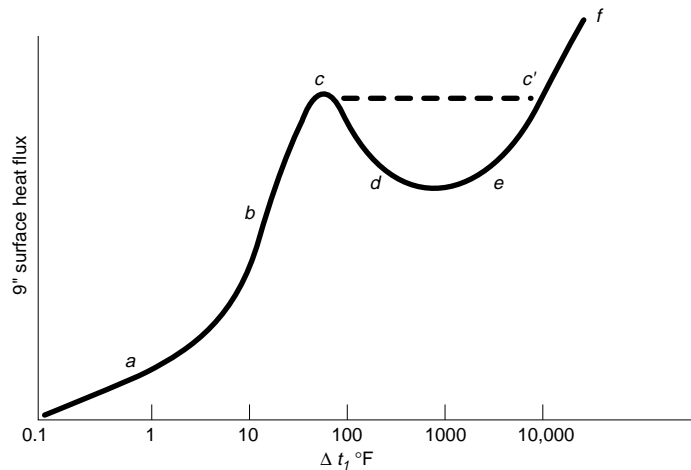
Thus heat flux (the ordinate in Figure 2.1) really becomes the independent variable and temperature difference (the abscissa) becomes the dependent variable. In this case, when the critical heat flux at c and the corresponding temperature are reached, a further increase in heat flux results in a sudden jump from c to c' into the film-radiation regime e-f. This causes the temperature difference to change abruptly from that at c to c'. The heating-surface temperature at c' is so high that it most likely exceeds safe limits. The surface in such a case is said to burn out.

Burnout in a nuclear fuel element may result in fuel-cladding rupture, accompanied by the release into the coolant of large quantities of radioactive gases and solids. In any case, the heat flux corresponding to the surface temperature at burnout is called the burnout heat flux. This may be the flux corresponding to points c and c' but not necessarily so; that is, burnout may occur at any point on the curve, depending upon the material of the heating surface and the operating conditions. In most cases, however, burnout occurs when the heat flux at c called the critical heat flux q_c'' is exceeded. Critical and burnout heat fluxes are often used to describe the same heat flux at c.

Besides critical and burnout heat flux, the conditions at c have also been called

departure from nucleate boiling, DNB, and, more recently, the hydrodynamic crisis and the boiling crisis.

The flow boiling crisis occurs in the general manner shown by Figure 2.2 [88]. Curve A shows the fluid bulk temperature versus channel length, from subcooled inlet conditions, through the two-phase region (where it remains constant), and rising again in the superheat region. Curve B shows the channel wall temperature at low heat fluxes, where burnout is not likely to occur. This curve begins moderately above that of the fluid because of the high heat-transfer coefficients associated with nucleate boiling, but rises at higher vapor qualities where film boiling begins to take place and in the superheat region, where gas heat transfer coefficients are low. Curve C shows the wall temperature at high heat fluxes. The point of departure from nucleate boiling (DNB) occurs suddenly rather than gradually, resulting in a jump in channel wall temperatures that may cause burnout. Downstream of this point, the wall temperature comes down to values comparable to nucleate boiling.

Figure 2.2
Film boiling crisis curve
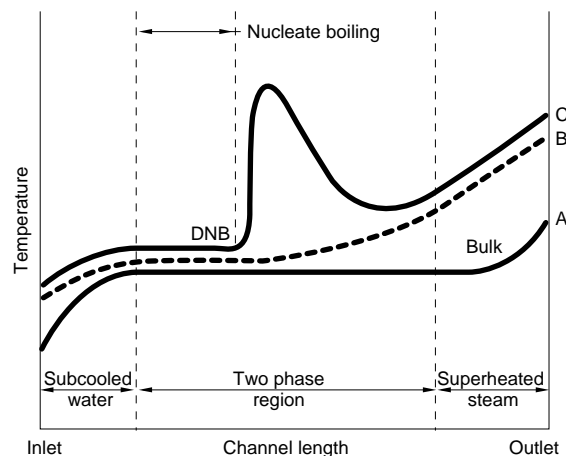
3.   Critical Heat Flux

One of the features of a CANDU reactor is the capability of refuelling the reactor while operating at full power. This normal operation perturbs the reactor and the heat transport system on a daily basis. The Regional Overpower Protection (ROP) system protects the reactor against overpowers in the fuel that could arise from various perturbations in the power shape or during a loss-of-reactivity control. The basic safety design requirement for this system is that the integrity of the heat transport system be maintained if an overpower condition were to occur. Then, in the event of fuel failure, any released radioactivity is retained

within the heat transport system, thus preventing any possibility of a release to the environment. This functional objective can be achieved by limiting the channel powers to Critical Channel Power (CCP) chosen to limit fuel sheath temperature increases resulting from sheath dryout. The CCP results are used to establish the neutron flux detector trip settings for the ROP system of the reactor.

3.1 Definitions of critical conditions

In general, when a heated surface dries out in forced convective boiling, the surface heat transfer deteriorates and the surface temperature increases in order to transfer the same amount of heat to the coolant.

The sudden surface temperature rise that occurs in a heated surface indicates that a change in the heat transfer mechanism between the surface and the fluid has taken place. This phenomenon has received different definitions such as boiling crisis, critical heat flux, dryout, burnout, DNB, etc.

The term burnout is strictly used for those situations leading to the actual meltdown of the heater, i.e., under subcooled or very low quality the surface heat flux required to get a temperature excursion is so high that it could lead to heater failure due to excessive temperature.
For high fluid enthalpies, the critical condition is a suppression of nucleation and the term used is "dryout". In fact the steam bubbles do not escape the sheath surface as in nucleate boiling. Similarly, in an annular type flow regime, the critical condition implies that the liquid film has dryout and causes the temperature rise.

For safety considerations, a necessary condition in the assessment of the CCP is to ensure the integrity of the fuel channel. And, for economic considerations, the fuel bundle has to be re-usable after returning to normal from the critical conditions. Two thermal limits or definitions of the critical conditions were derived from the U-1 CHF test data, the onset of intermittent dryout and the onset of dry sheath.

3.1.1 Onset of Intermittent Dryout

At the onset of intermittent dryout, the heat transfer mode changes from the efficient pre-dryout one (i.e., nucleate boiling/forced convection evaporation) to transition boiling but with some liquid-wall contact still occurring. This critical condition corresponds to the first indication of sheath temperature increases from the completely wetted sheath temperature. This is the conventional definition of dryout used for regional overpower design.

3.1.2 Onset of Dry Sheath (ODS)

The onset of dry sheath conditions correspond to the sheath temperature reaching the minimum film boiling temperature. The minimum film boiling

temperature depends mainly on the system pressure. At 9 MPa pressure, the minimum film boiling temperature predicted by the correlation of Groeneveld and Stewart (Reference 12) is 375°C. This limiting sheath temperature is called the Sheath Temperature Criterion (STC).

At higher sheath temperatures, besides the heat transfer, other physical phenomena - such as element bowing, sheath strain, pressure tube integrity - have to be assessed. An accurate prediction of fuel and sheath temperatures beyond dryout requires reliable models to calculate the sheath-to-coolant heat transfer coefficient, the spreading of the drypatch in the axial direction as well as the fuel element mechanical behaviour in post dryout conditions. In the absence of accurate models and data, a conservative estimate is used.

3.2   CCP and CCF calculations

In CANDU safety analysis, CCP is predicted assuming constant reference header-to-header pressure drop (ΔP_{HH}), inlet header temperature (T_{RIH}) and outlet header pressure (P_{ROH}). Since ΔP_{HH} is kept constant, this means that the channel flow is a power-dependent parameter and, therefore, must be recalculated at every power level. This definition of CCP is realistic for slow Loss of Regulation (LOR) in a reactor having multiple parallel channels. Nevertheless, critical channel powers calculated at constant header boundary conditions are generally corrected by assessing the effect of bulk power increase up to the expected overpower at trip setpoints. The ratio of critical channel power and the reference nominal channel power is called the Critical Power Ratio (CPR).

Another parameter that is sometimes required is the Critical Flow Ratio (CFR) and is defined as the ratio between the Critical Channel Flow (CCF) and the reference nominal channel flow. The critical channel flow is defined as the channel flow required to reach the critical condition (i.e., onset of intermittent dryout or sheath temperature criterion) at constant channel power, outlet header pressure and inlet header temperature. The critical flow ratio is required for events such as operation with only one pump per loop or flow blockages.

The steady-state thermalhydraulic code NUCIRC is used to calculate critical channel powers and critical channel flows.

4.   CHF Correlations

4.1   General

The technological importance of the dryout phenomenon has led to the development of a very large number of alternative dryout correlation methods. Although rod bundle geometries are more complex than tubes, the dryout phenomenology is very similar. The alternative dryout correlation methods can be brought into perspective by briefly summarizing first the types of correlations adapted for dryout in tubes. These alternatives generally fall under two types of

correlation (Reference 13) referred to system parameters driven or local conditions driven.

a) System parameters

$$CHF = [C_1 \, P^{C2} \, G^{C3} + C_4 \, P^{C5} \, G^{C6} \, H] \, A_h$$

and

b) Local conditions

$$CHF = C_1 \, P^{C2} \, G^{C3} + C_4 \, P^{C5} \, G^{C6} \, X_{Do}$$

Where the C_i are constants experimentally determined.

For a given mass flux, fluid physical properties (pressure), tube diameter and for uniform heat flux, it is found that the data for a range of tube length and inlet subcoolings can be represented approximately by a single curve of dryout heat flux ϕ_{DO} against dryout quality X_{DO}. The superficial implication of the relationship between dryout flux and quality at dryout is that the local quality conditions govern the magnitude of the dryout heat flux at that location; this is termed the "local conditions hypothesis" (Reference 13).

c) Critical Quality-Boiling Length

The critical boiling length can be expressed in terms of dryout quality such as:

$$X_{DO} = \frac{F_1 L_{BL}}{F_2 + L_{BL}}$$

An equivalent boiling length average CHF correlation is obtained by applying the heat balance equation:

$$(CHF)_{BL} = \frac{G \, A_C \left(F_1 - X_{DO} \right) H_{FG}}{F_2 - P_h}$$

The same data can also be represented in terms of dryout quality X_{DO} and "boiling length" at dryout $(L_b)_{DO}$.

The boiling length is defined as the distance from the point in the channel at which bulk saturation (zero thermodynamic quality) conditions are attained. This representation can be regarded as indicating a relationship between the fraction evaporated at dryout (X_{DO}) as a function of the boiling length to dryout, indicating the possibility of some integral rather than local phenomenon (Reference 13).

The ϕ_{DO} - X_{DO} relationship can easily be transformed into the X_{DO} - L_B relationship; a heat balance obtains the boiling length in a tube as (Reference 13):

$$L_B = \frac{d_O \, G \left(\lambda \, X + H_f^{X_{DO}} - H_f^{X=0} \right)}{4\phi}$$

where

d_o	=	tube diameter
G	=	mass flux
λ	=	latent heat of evaporation
X	=	local quality
ϕ	=	heat flux (BLA; equals local heat flux for uniform distribution)
$H_f^{X=0}$	=	fluid enthalpy at the onset of bulk boiling location
$H_f^{H_{DO}}$	=	fluid enthalpy at dryout location

If the dryout flux is related to the dryout quality by the expression:

$$\Phi_{DO} = F_1 \left(X_{DO} \right)$$

then

$$\left(L_B \right)_{DO} = \frac{d_O \, G \left(\lambda \, X_{DO} + H_f^{X_{DO}} - H_f^{X=0} \right)}{4 F_1 \left(X_{DO} \right)}$$

For a given tube diameter and mass flux, it follows, therefore, that:

$$X_{DO} = F_2 \left(\left(L_B \right)_{DO} \right)$$

The vast majority of correlations for dryout fall either into the ϕ - X or the X - L_B categories.

Although the ϕ - X and X - L_B correlations are equivalent for uniformly heated channels, they give quite different results when the heat flux is non-uniform.

The "F-factor" method, in conjunction with the ϕ - X representation of dryout, has been developed for the prediction of dryout flux in non-uniformly heated channels (Reference 13). The flux to dryout $\phi_{BO}(z)_{nu}$ for the non-uniform axial heat flux is calculated by multiplying $\phi_{BO}(z)_u$ for the uniform axial heat flux by the F-factor defined as:

$$F = \frac{\phi_{BO}\left(z \right)_{nu}}{\phi_{BO}\left(z \right)_u}$$

The F-factor method is generally the best approach for low-quality ($x \le 10\%$) situations.

The X - L_B approach fits both non-uniform and uniform heat flux data for higher qualities and is generally considered the best approach for calculating dryout conditions for non-uniform heating by applying the X - L_B form of correlation on a local basis (Reference 13).

It is possible to correlate data for dryout in rod bundle geometries by using overall, mixed flow, types of correlations such as that used in NUCIRC. More precise predictions can be made by using correlations based on "sub-channel analysis" such as that used in the ASSERT code, in which the rod bundle is sub-divided into flow zones or sub-channels and conditions are calculated for these individual sub-channels, taking account cross-mixing between adjacent channels and cross-flows generated by pressure differences between the sub-channels.

The CCP or CCF is the channel power or channel flow respectively, at which, with reference to Figure 4.1:

Figure 4.1
Axial heat and quality at onset of dryout
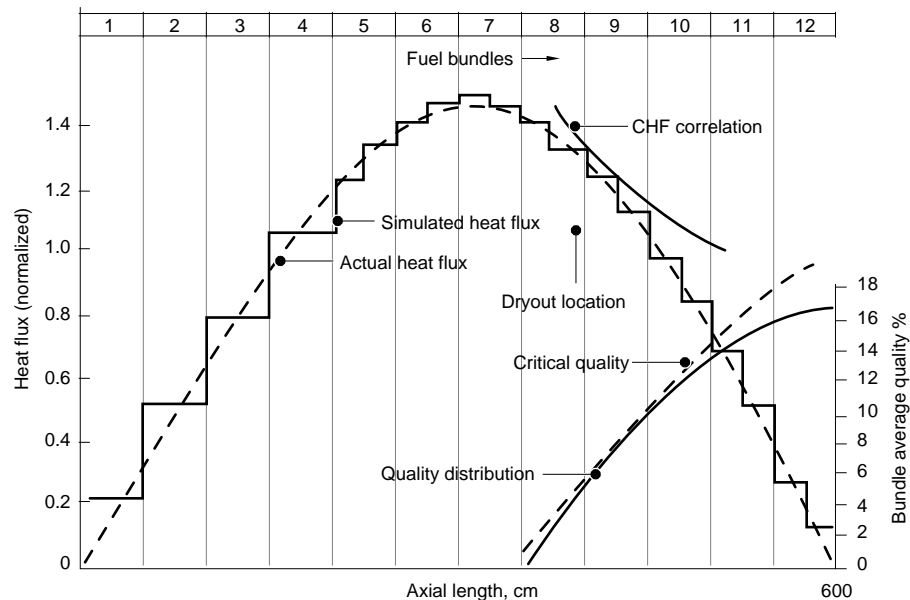
- The critical heat flux curve is tangent to the local heat flux curve or that the Critical Heat Flux Ratio (CHFR) is equal to one. The same definition applies for the boiling length averaged (BLA) heat flux. A local conditions CHF approach is shown in Figure 4.1.
- The critical quality curve is tangent to the local quality curve or that the critical quality ratio reaches the value of one.

The critical condition for the fuel bundle is defined by the CCP or CCF which is evaluated using Critical Heat Flux (CHF) correlations derived from full-scale experimental data in non-crept pressure tubes.

4.2 CHF correlation in NUCIRC

There are four CHF correlations available in NUCIRC for 37-element fuel bundles.

4.2.1 U-111 lower bound critical heat flux correlation

In-reactor critical heat flux experiments were performed in light water on 36-element fuel strings in vertical positions (Reference 14). A correlation which was a lower bound to the data was derived for use in safety analyses.

The lower-bound correlation for the prediction of onset and axial spreading of sheath dryout is:

$$CHF = 1.595 \times 10^6 \exp(-3.2819X)$$

where CHF is the local bundle average critical heat flux (W/m^2)
X is the bundle average (fractional) quality

4.2.2 Local Conditions CHF Correlation

Dryout powers are assessed using a correlation (Reference 15) fitted to critical heat flux data from CRL tests with a 6 metre long 37-element segmented bundle with a uniform Axial Flux Distribution (AFD) in the U-1 water test facility (Reference 16). The test results were converted to D_2O equivalents using Ahmad's modelling criteria (Reference 17) and were fitted with a rms error of ± 5.7%.

This correlation is "design-centre" and is based on U-1 tests uniform axial power distribution. An allowance of -5% ± 2.5% on CCP (at constant flow) was made for the effects of non-uniform axial power distribution in the reactor. This allowance was later increased to 13% after preliminary tests were completed in the U-1 facility for cosine AFD.

The (bundle average) CHF correlation exists in the following form:

$$CHF = \frac{(F_1 - F_2 X) C}{F_3}$$

where
X   =   bundle average quality (fraction)
CHF   =   local bundle average critical heat flux

and F1 to F3 are the following expressions:

$$F_1 = 1.0185 \ 10^{-4} \ P^{.212488} \ G^{1.932441}$$
$$F_2 = 1.2264 \ 10^{-11} \ P^{1.656134} \ G^{2.32355}$$
$$F_3 = 1 + .53917 \ 10^{-5} \ P^{-.17342} \ G^{1.7776}$$

P   =   Pressure (kPa)
G   =   Mass Flux (kg/m^2-s)

The term C in the previous equation is a CHF correction factor for the effect of non-uniform AFD, which is expressed as:

$$C = \frac{\eta}{1 - \frac{(1 - \eta)\Delta X}{X - \frac{F_1}{F_2}}}$$

Where η is a 13% penalty factor ($\eta = 0.87$) to CCP at constant flow which accounts for the effect of axial heat flux distribution, and

ΔX is the quality increase (from inlet) based on local conditions:

$$\Delta X = \frac{h_{outlet} - h_{inlet}}{h_{fg}}$$

4.2.3   Critical quality/boiling length correlations for OID and STC

The OID and STC critical quality-boiling length correlations are D$_2$O equivalent, based on the CRL U-1 loop CHF experimental data, i.e., 3 m uniform, 6 m uniform and 6 m cosine (both 1982 and 1983 data).

Unlike the local conditions CHF correlation, these new correlations use the boiling length hypothesis which can better correlate non-uniform CHF data with dryout location.

The OID and STC X_C - Boiling Length correlations are "best-estimate" correlations and have the same functional form:

$$X_c = \frac{C_1 * P^{C_2} * G^{C_3} * BL}{C_4 * P^{C_5} * G^{C_6} * BL}$$

where
X_c =   critical quality (fraction) (bundle average)
P   =   pressure at channel node (MPa)
G   =   channel mass flux (t . m^{-2} . s^{-1})
BL   =   boiling length at channel node, m

4.2.4 CHF look-up table for 37-element bundles

A 37-element bundle-CHF look-up table for heavy water in conjunction with the boiling-length average heat-flux approach is available as a general CHF prediction method for a string of horizontal, CANDU natural uranium 37-element bundles.

The CHF database compiled at CRL consists of over 30,000 steady-state CHF data points obtained from Canadian, American, Russian, German and French sources.

The CHF data points consist primarily of H_2O vertical flow tube data with some H_2O and freon bundle data. The bundle-CHF look-up table was derived based on:

- the parametric trends of the tube-CHF look-up table,
- water-cooled bundle-CHF data,
- freon-cooled bundle-CHF data,
- correction factor to account for flow stratification.

The bundle-CHF look-up table for heavy water which is presented in Reference 2. The bundle-CHF look-up table for heavy water covers the following range of conditions:

Pressure: 7 to 12 MPa
Mass Flux: 1,000 to 7,000 $kg \bullet m^{-2} \bullet s^{-1}$
Dryout Quality: -0.15 to 0.50

The evaluation of CHF, based on the local cross-sectional average condition, employs the same procedure as that used for the CHF correlations. Since both the dryout location and power are unknown, an iteration procedure is required to find the incipient dryout. The local heat flux and equilibrium quality (for a given axial-flux distribution) and pressure drop are calculated at each node along the fuel string. The CHF is predicted from the table at each node and compared against either the local heat flux (for thermodynamic quality less than 0) or the boiling-length average heat flux (for thermodynamic quality equal to or above 0). Boiling is assumed to start at the point where the cross-sectional average equilibrium quality, X_e, equals 0.

A critical heat flux ratio is defined as:

$$CHFR = \frac{ACHF}{\bar{q}_{BL}} k_{rfd}$$

where

ACHF = CHF value interpolated from the 37-element
          bundle-CHF look-up table for heavy water

$\bar{q}_{BL}$ = local heat flux if $X_e < 0$
      = boiling-length average heat flux if $X_e \geq 0$

k_{rfd} = correction factor to account for the effect
          of bundle radial flux distribution
      = 1.0 for natural uranium
      = 0.84 for enriched fuel

CHF and consequently the determination of CCP will occur at that point where CHFR = 1.

---

5.   Post Dryout Modelling

5.1   Definitions

When the local heat flux exceeds the CHF (or the local quality exceeds the critical quality) then the fuel elements are assumed to be under post-dryout (PDO) conditions. In the boiling curve, the region beyond CHF is called the "film boiling region" or "liquid deficient region". The flow pattern in this region would basically be an annular vapour film with a central liquid core (saturated film boiling region). At higher qualities the flow pattern changes to liquid droplets dispersed in a high velocity vapour core. The experimental data shows a surface temperature as illustrated in Figures 5.1 and 5.2:

Figure 5.1

Heating surface temperature at and above the critical heat flux
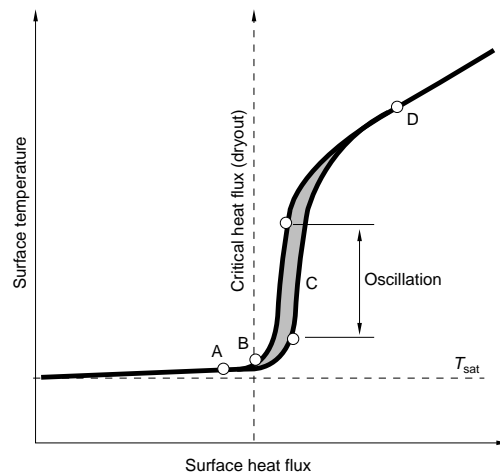
Figure 5.2

Typical heater surface temperature plot obtained during a dryout test
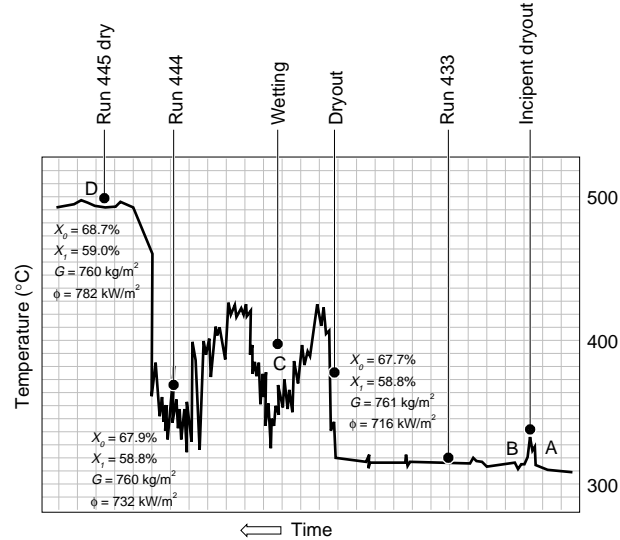
- At A the local heat flux is below the CHF and the surface temperature is steady.
- As the CHF value is reached (point B) small oscillations in the surface temperature are observed. These small temperature oscillations denote the onset of the dryout condition where the liquid film covering the heated surface starts to break up, and a drypatch starts to form.
- A further increase in the surface heat flux (to point C) results in temperature oscillations of considerable magnitude. These oscillations would appear to be the result of the surface being alternatively in contact with steam or rewetted by the available liquid droplets or breaking liquid film.
- Finally, a further increase in heat flux (to point D) results in surface temperatures considerably above the saturation temperature but one which is steady. The heating surface would now appear to be totally "dry".

Post dryout modelling is required because:
- Several accident scenarios lead to fuel dryout as in all large LOCAs.
- Fuel and sheath temperatures must be calculated at and beyond the onset of dryout.
- The limits for fuel and channel integrity must be established.

The prediction of fuel and sheath temperatures at and beyond dryout onset requires reliable models to calculate the sheath-to-coolant heat transfer coefficient and the spreading of the drypatch in the axial direction as well as around the element circumference.

5.2 Heat transfer in liquid deficient region

Three types of correlations can be found in the literature:

a) Empirical correlations, where no attempt is made to explain mechanisms but just define a functional relationship between h_{LD} and the chosen independent variables. Reference 19 gives correlations of this type.

b) Correlations that recognize the departure from thermodynamic equilibrium condition and attempt to calculate the true vapour quality and vapour temperature. The Groeneveld Delorme correlation (Reference 20) belongs to this category.

c) Semi-theoretical models attempting to write down the equations for the various individual hydrodynamic and heat transfer processes occurring in the heated channel. Reference 21 describes one of these models. These type of models are generally only applicable to a well defined flow regime or pattern and/or geometry.

5.2.1 Groeneveld Delorme correlation

The Groeneveld-Delorme correlation (Reference 20) is the one chosen to assess h_{LD}. This correlation has the following functional form:

$$h_{G-D} = .008348 \frac{k_{vf}}{De} \left[\mathrm{Re}_{vf} \left[X_a + \frac{\rho_v \, (1 - X_a)}{\rho_f} \right] \right]^{.8774} \left(\mathrm{Pr}_{v_f} \right)^{.6112}$$

where

$$\rho_v = vapour \, density \, at \, T_{va}$$

$$X_a = \frac{h_{fg} \, X}{h_{va} - h_f}$$

$$h_{va} = h_{ve} + h_{fg} \exp \left(- \tan \Psi \right)$$

(Note: $h_{ve} = h_g$ when $x_e \leq 1.0$)

T_{va}= vapour temperature corresponding to enthalpy h_{va}.

$$\mathrm{Re}_{vf} = \frac{G \, D_e}{\mu_{vf}}$$

$$\Psi = .13864 \, \mathrm{Pr}_g^{.2031} \left[\mathrm{Re}_g \, \rho_g \left(\frac{X}{\rho_g} + \frac{1 - X}{\rho_f} \right) \right]^{.20006} x$$

$$\left[\frac{q \, D_e \, C_{Pg}}{k_g \, h_{fg}} \right]^{.09232} \left(1.3073 - 1.0833 \, X + .8455 \, X^2 \right)$$

The Groeneveld-Delorme correlation is strictly a film boiling correlation for tubes and, therefore, would overpredict surface temperatures in the vicinity of the dryout onset in more complex geometries. This has been confirmed when this correlation was used to predict the measured surface temperatures obtained during the U-1 CHF experiments (see Reference 22). Reference 22 describes a correction to the Groeneveld-Delorme correlation that brings its predictions

more in line with the U-1 loop experimental measurements. The PDO heat transfer coefficient for bundles recommended in this reference is as follows:

OVP = overpower beyond dryout onset

The parametric trends of mass flux (G), pressure (P), heat flux (q) and bundle correction (C) are summarized in Figures 5.3 to 5.6 (Reference 2). One parameter is varied through a wide range of values, while the rest are held constant at the reference conditions. The resulting sets of curves are plotted as (T_W - T_{sat}) versus quality. The reference conditions are:

G = 4,500 kg.m^{-2}.s^{-1}
P = 10,000 kPa
q = 1,000 kW.m^{-2}
C = 1 (overpower = 0.165)

Figure 5.3
Wall superheat vs quality for various overpowers
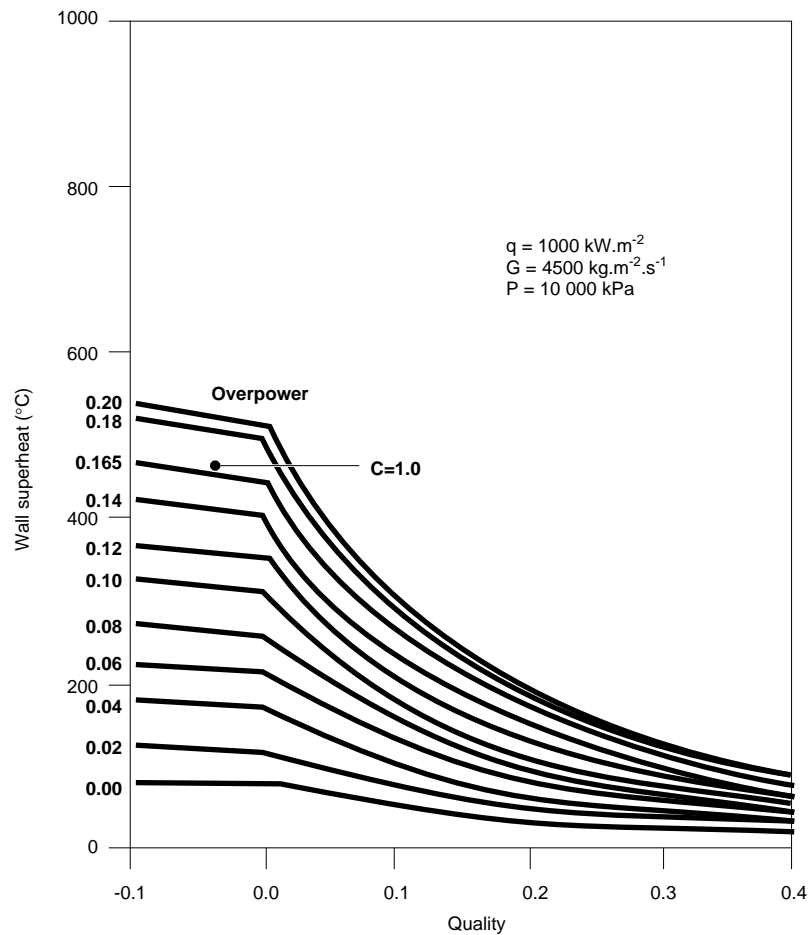
Figure 5.4
Wall superheat vs quality for various heat fluxes

December 1995
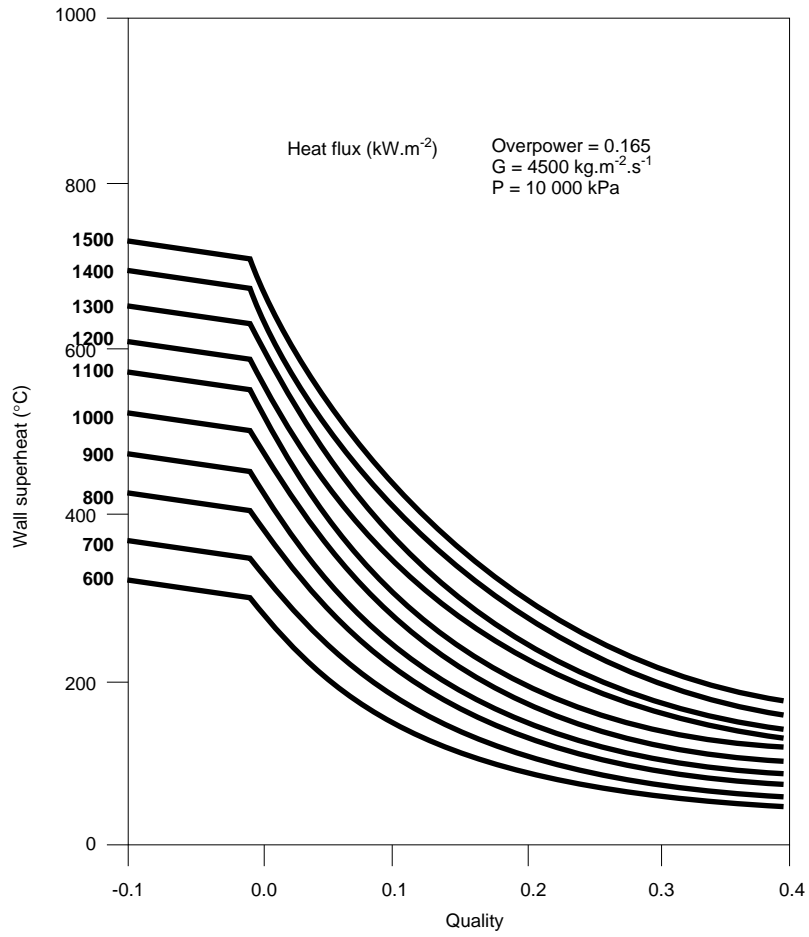
Figure 5.5
Wall superheat vs quality for various mass fluxes
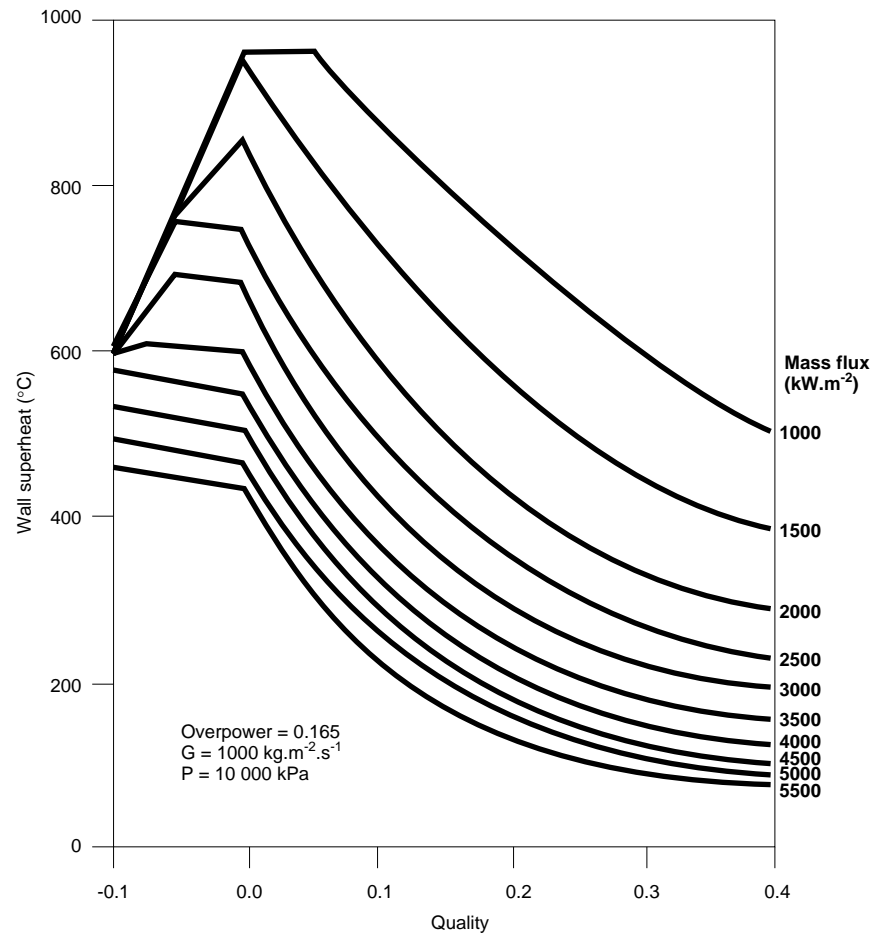
Figure 5.6

Wall superheat vs quality for various pressures
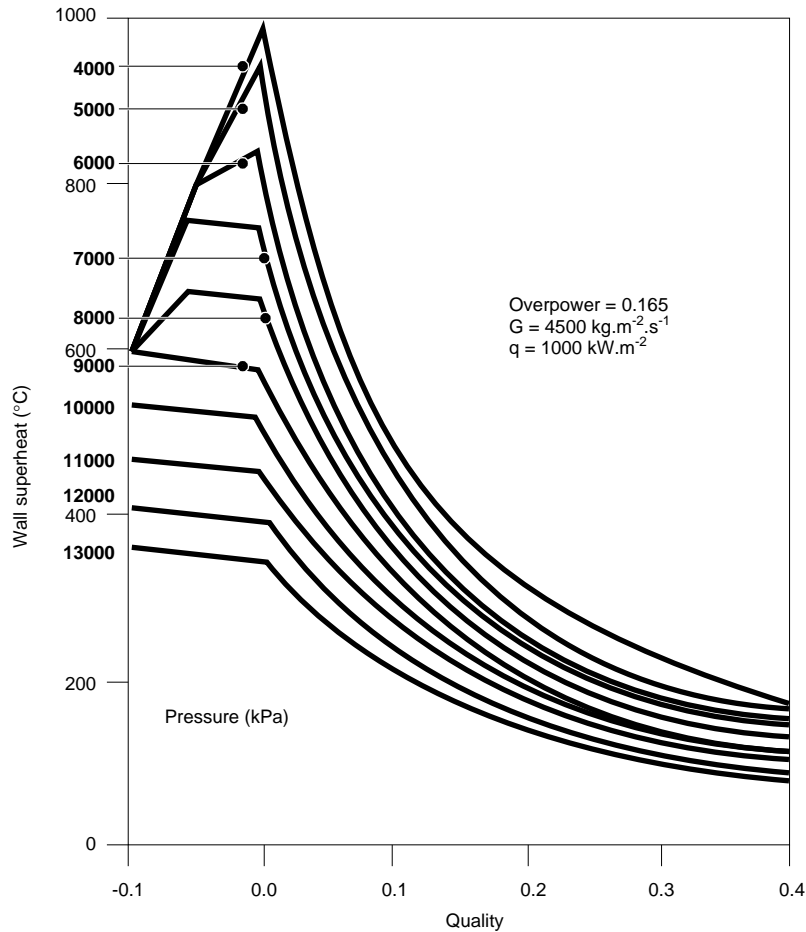
Figures 5.3 to 5.6 show a smooth variation of the parameters, even outside the range of development. Figures 5.4 to 5.6 show the trends of the film-boiling correlation since the bundle-correction factor is held constant (C = 1). Figure 5.3 indicates the effect of the bundle correction factor (C) for various overpowers on the wall temperature. Note that for overpowers greater than 0.165, C equals 1.

Reference 23 gives the value of C as function of the "over-heat-flux ratio" (OHFR), as follows:

$$C = \min\left[\left(4 * OHFR + .4\right), 1\right]$$

where

$$OHFR = \frac{local\ heat\ flux - local\ CHF}{local\ CHF}$$

Both models for the prediction of the correlation factor C could be used when we are assessing critical channel powers. However, the OHFR option must be used when dealing with dryout at constant power, i.e., assessment of critical flow.

5.2.2 Berenson correlation

The Groeneveld-Delorme correlation would be too conservative for relatively low flows as well for subcooled or low quality dryout. Reference 22 recommends that a modified version of Berenson correlation (Reference 24) be also used as follows:

$$h_{bundle} = \frac{h_{LD}}{C}$$

where

$$h_{LD} = h_{G-D} \text{ or } h = h_{Ber-mod}$$

and selected according to the minimum surface temperature:

$$T = \min(T_{G-D}, T_{Ber-mod})$$

The modified Berenson correlation has the following functional form:

$$h_{Ber} = .425 \left[\frac{k_{vf}^3 (9.81)^{\frac{3}{2}} \rho_{vf} (\rho_f - \rho_{vf})^{\frac{3}{2}} (h_{vf} - h_f)}{\mu_{vf} (T_W - T_{sat}) (\sigma_f)^{\frac{1}{2}}} \right]^{\frac{1}{4}}$$

and

$$h_{Ber-mod} = h_{Ber} \left[1 + 25.2 \frac{T_{sat} - T_b}{T_b} \right]$$

Note, the vapour film properties (subscript vf) are evaluated at:

$$T_{vf} = \frac{T_W + T_{sat}}{2}$$

The post-dryout heat transfer coefficient must also be assessed for conditions leading to superheated steam and laminar flow, as well as to include the radiation heat transfer component.

5.2.3 Superheated Steam

A superheated steam coolant is a single-phase regime and several correlations are available in the literature such as Heineman's (Reference 25), Hadaller's (Reference 26), Miropolskiy's (Reference 29), etc. However, in the NUCIRC code the Groeneveld-Delorme correlation is used in the film boiling regime in post dryout and this correlation uses the Hadaller's superheated steam one, meaning that, for continuity reasons, Hadaller's correlation has been chosen to asses h under superheated steam cooling conditions in the NUCIRC code. This correlation has the following functional form:

$$h_{Had} = .008348 \frac{k_{vf}}{D_e} Re_{vf}^{.8774} Pr_{vf}^{.6112} \text{ and } h_{Hein} = .00133 \frac{k_g}{D} Re_g^{.84} Pr_g^{1/3}$$

5.2.4 Laminar flow

Under laminar flow conditions, with a number of Reynolds less than 3,000, and most probably having heat transferred by superheated steam, the heat transfer

coefficient correlations previously mentioned (including Hadaller's) will predict h values that would be too conservative. Therefore and for Re < 3,000, the heat transfer coefficient must also be evaluated for this flow condition. The modelling given in Reference 28 is used and this laminar flow h has the following functional form:

$$\frac{P_e D_e}{\Delta \ell} > 12$$

the heat transfer coefficient is given by:

$$h_{LAM} = 1.61 \frac{k_g}{De} \left[\frac{P_e \cdot D_e}{\Delta \ell} \right]^{\frac{1}{3}}$$

for

$$\frac{P_e D_e}{\Delta \ell} \leq 12$$

$$h_{LAM} = 3.66 \frac{k_g}{De}$$

The higher value of h_{LD} or h_{LAM} is used.

5.2.5 Radiation heat transfer

If the heated surface temperature exceeds 800°C, then the radiative heat transfer mechanism becomes important. To calculate the radiation heat transfer component we need to know (besides temperatures) the following:
- heat source and heat sink emissivities
- geometrical or view factors.

For CCP assessment a simplified modelling for the radiation heat transfer coefficient is used in the NUCIRC code. This model lumps together the emissivity and view factors in a parameter called radiation interchange factor. The function form of this heat transfer coefficient is as follows:

$$h_{rad} = \frac{\sigma c \left[\left(T_g + 460 \right)^4 - \left(T_c + 460 \right)^4 \right]}{\left(T_g - T_c \right) \cdot 3600}$$

where
σ = the Stefan-Boltzmann constant
c = radiation interchange factor
T_s = sheath temperature (°F)
T_c = coolant temperature (°F).

The radiation h_{rad} value is added to the h_{LD} coefficient mentioned before.

5.3 Drypatch spreading

The drypatch spreading is defined as the heated area that goes into dryout as the channel power is increased beyond the CCP (or as the channel flow is decreased beyond its critical value at constant power). The drypatch spreading in a fuel

element must then be calculated for both the axial and circumferential directions. The following methodology is used in the NUCIRC code:

a) The axial spreading of the drypatch is assumed to be controlled by the chosen CHF correlation. This is a conservative assumption because the experimental evidence is that significantly more power is required downstream of the end plate or spacer than upstream of these flow obstructions.

b) The circumferential spreading of the drypatch, i.e., spreading fraction, is calculated by the method described in Reference 30, as follows:

CDF = $18.7 * COR^2 - 32.5 * COR + 13.8$

CDF = circumferential drypatch fraction

COR = critical overpower ratio

$$COR = \frac{Power}{(Power)_{OID}}$$

CDF = 1.0 of COR > 1.135

CDF = 1.0 if COR > 1.135

For critical flow assessment where dryout caused by flow reduction at constant channel power, COR is defined as:

$$COR = \frac{Flow}{(Flow)_{OID}}$$

6.   Fuel Temperature Modelling

The CCP assessment requires to evaluate fuel and sheath temperatures in order to prove that fuel integrity is not in jeopardy at the predicted critical power, i.e., dryout $\rightarrow$ bowing $\rightarrow$ fission gas releases $\rightarrow$ fuel melting, etc.

For CCP, only steady state fuel and sheath temperatures are required and, consequently, the NUCIRC code has built in a fuel temperature evaluation model for this purpose. Furthermore, the NUCIRC model solves the heat conduction equation for a cylindrical geometry, i.e., r, θ, but with uniform parameters in the θ direction such as heat generation per unit volume and sheath-to-coolant heat transfer coefficient. However, there may be circumstances where a more sophisticated fuel temperature model is required, i.e., sheath surface is partially in dryout; for this case, codes like the ones described in References 31 and 32 could be used.

a. Fuel-to-Sheath Gap Heat Transfer Coefficient
The fuel-to-sheath gap heat transfer coefficient (h_{gap}) model used in the NUCIRC code is a simplified version of the model used in the ELESIM code (Reference 33). Basically, h_{gap} is made up by three components:

$$h_{gap} = h_{solid} + h_{gas} + h_{radiation}$$

b   Fuel Temperatures
The model used in the NUCIRC code solves the steady state heat conduction equation for cylindrical geometry (r, θ) and accounting for non-uniform heat generation in the pellet and temperature dependent fuel conductivity. The required formulation can be found in Reference 33.

7.   References

1   Ozisik, M.N., "Basic Heat Transfer", McGraw-Hill Book Company, 1977.
2   Groeneveld, D.C. and Leung, L.K.H., "Compendium of Thermalhydraulic Correlations and Fluid Properties", Version 1991, Rev. 0, COG-90-86 (ARD-TD-243), 1990 December.
3   Bergles, A.E. and Rohsenow, W.M., "The Determination of Forced Convection Surface Boiling Heat Transfer, ASME, paper 63-HT-22, 1963.
4   Bowring, R.W., "Physical Model Based on Bubble Detachment and Calculation of Steam Voidage in the Subcooled Region of a Heated Channel, HPR-10, 1962.
5   Collier, J.G., "Convective Boiling and Condensation", McGraw-Hill, 1981.
6   Tong, L.S., "Boiling Heat Transfer and Two-Phase Flow", John Wiley and Sons, Inc., N.Y., 1965.
7   Wallis, G.B., "One Dimensional Two-Phase Flow, McGraw-Hill, 1969.
8   Hewitt, G.F. and Taylor, N.S., "Annular Two-Phase Flow", Pergamon Press, 1970.
9   Schrock, V.E. and Grossmann, L.M., "Forced Convection Boiling Studies-Forced Convection Vaporization Project", TID-14632, 1959.
10 Chen, J.C., "A Correlation for Boiling Heat Transfer to Saturated Fluids in Convective Flows", ASME 63-HT-34, 1963.
11 Groeneveld, D.C., "The Onset of Dry Sheath Condition - A New Definition of Dryout", Nuclear Engineering and Design, 92, pp. 135-140, 1986.
12 Groeneveld, D.C. and J.C. Stewart, "The Minimum Film Boiling Temperature for Water During Film Boiling Collapse", Proceedings 7th International Heat Transfer Conference, Munich, West Germany, Volume 4, pp. 393-399, 1982 September 6-10.
13 Bergles, A.F., Collier, J.G., Delhaye, J.M., Hewett, G.F. and Mayinger, F., "Two-Phase Flow and Heat Transfer in the Power and Process Industries", Hemisphere Publishing Corporation, 1981.
14 Groeneveld, D.G.and McPherson, G.D., "In-Reactor Post-Dryout Experiments with 36-Element Fuel Bundles", AECL-4705, 1973.

15 Boruvka, L. and Merlo, E.E., "Gentilly-2: Critical Power Assessment", TTR-78, 1982 December.
16 McDonald, A.G., "Critical Heat Flux in a 37-Element, 6-Meter Long Segmented Rod Bundle Geometry", CRNL-2065, 1980 May.
17 Ahmad, S.Y., "Fluid-to-Fluid Modelling of Critical Heat Flux: A Compensated Distortion Model", International Journal Heat Mass Transfer,

Volume 16, pp. 641-622, 1972; also AECL-3663, 1971.

18 Merlo, E.E. and Chan, A., "Critical Channel Power Assessment: Gentilly-2 and Point Lepreau", TTR-289, Part 2, 1991 April.

19 Groeneveld, D.C., "Post-Dryout Heat Transfer at Reactor Operating Conditions", AECL-4513, 1973.

20 Groeneveld, D.C. and Delorme, G.G.J., "Prediction of the Thermal Non-Equilibrium in the Post-Dryout Regime", Nucl. Eng. and Des., Vol. 36, pp. 17-26, 1976; also AECL-5280, 1975.

21 Bennett, A.W., et al., "Heat Transfer to Steam-Water Mixtures Flowing in Uniformly Heated Tubes in Which the Critical Heat Flux has been Exceeded", AERE-R` 5573, 1967.

22 Schneider, G.R., et al., "Post-Dryout Analysis of the U-1 Segmented-Cosine Bundle Data", CRNL-2728, CANDEV-86-07, 1987 December.

23 Snoek, C.W., "Post-Dryout Drypatch Spreading and Temperature Prediction in 37-Element CANDU Fuel", RC-290, COG-89-98, 1989 October.

24 Berenson, P.J., "Film Boiling Heat Transfer from a Horizontal Surface", ASME, J. of Heat Transfer, pp. 351-358, 1961.

25 Heineman, J.B., "An Experimental Investigation of Heat Transfer to Superheated Steam in Round Tubes and Rectangular Channels", ANL-6213, 1960 September.

26 Hadaller, G. and Benerjee, S., "Heat Transfer to Superheated Steam in Round Tubes", WDI-147, 1969.

27 Groeneveld, D.C., "Forced Convective Heat Transfer to Superheated Steam in Rod Bundles", AECL-4450, 1973 April.

28 Kutateladze, S.S. and Borishanskii, V.M., "A Concise Encyclopedia of Heat Transfer", Pergamon Press, 1966.

29 Misopolsky, Z.L., "Heat Transfer in Film Boiling of a Steam Water Mixture in Steam Generating Tubes", Teploenergetika, 10, #5, 1963.

30 Snoek, C.W., "The Cosine CHF Test Bundle Experiment - Post-Dryout Temperature Contours and Drypatch Spreading", APRP-AE-67, 1984 February.

31 Tayal, M., "Modelling CANDU Fuel Under Normal Operating Conditions: ELESTRES Code Description", AECL-9331, 1987.

32 Tayal, M., "A Non-Linear, Finite Element Heat Conduction Code to Calculate Temperatures in Solids of Arbitrary Geometry", Thirteenth Annual Reactor Simulation Symposium, CNS, CRNL, 1987 April 27-28.

33 Notley, M.J.F., "ELESIM: A Computer Code for Predicting the Performance of Nuclear Fuel Elements", Nuclear Technology, Vol. 44, 1979 August.

Reactor Materials

Training Objectives

The participant will be able to describe or understand:
1   importance of material selection
2   reactor material requirements
3   irradiation effects on material properties
4   reactor materials properties
5   CANDU reactor components materials

Reactor Materials

Table of Contents

1 Introduction

The materials selection is directed by the material ability to withstand the severe environmental conditions that would exist in a given reactor concept such as: high temperatures, large temperature gradients and intense radiations fields. Even if structural materials with suitable physical and mechanical properties are available, they must also satisfy, for certain process systems, the requirement of having low neutron capture cross section.

The importance of the behaviour of the material cannot be over emphasized. The system's integrity has to be maintained at all costs to ensure complete safety of workers and public. Another important aspect is that the right choices have to be made in order to minimize costs and delays and eventually further research effort and expense.

The requirements of materials' properties in nuclear reactors can be divided in two main categories: the general properties and the special properties. The general properties are very similar to the conventional engineering properties of materials required in most engineering designs. The general properties are listed in Table 1.1 and are explained in greater detail in section 2.

Table 1.1:

General Properties of Nuclear Reactor Materials

Mechanical strength	Ductility
Structural integrity	*Fabricability, machinability*
Corrosion resistance	Heat transfer properties
Thermal stability	*Compatibility*
Availability	Costs

The structural materials which are not exposed to radiation or to the primary coolant system fall into this category.

The special properties arise from nuclear radiation, as material can suffer change under severe radiation exposure. The effect of radiation on nuclear reactor materials are treated in section 3.

Material requirements can vary widely depending on the particular design. In all cases, fuel materials, cladding, moderator and structural material must be selected to meet the appropriate requirements. This lesson is intended to present the general properties and requirements of the reactor materials. The specific case of the CANDU reactor will be treated in greater detail. The material properties used in CANDU system will be described as well as the specific material requirements for the various CANDU reactor components.

2 General Reactor Materials Properties and Requirements

This section intends to briefly explain the general requirements listed in Table 1.1.

2.1 Mechanical properties

Mechanical strength is the ability of a mechanical element to withstand stresses imposed by external or service loading. In general, the mechanical strength must be adequate under any service or operating condition of a nuclear reactor. A measurement of mechanical strength is the stress produced by service loading.

Ductility is a mechanical property that allows material yield and permanent deformation before fracture, or ultimate failure in tension occurs. There is no absolute measure of ductility, but the percentage of elongation and the percentage of reduction in cross section are commonly used as indices. The greater theses indices, the more ductile a material is. Ductility is the opposite of *brittleness* as illustrated on Figure 2.1.

Figure 2.1:
Difference between a ductile breaking and a brittle breaking

Ductile Cracking   Brittle Cracking

Toughness is the capability of material to withstand shock loading, mechanical or thermal, without failure. Impact strength, even though not an absolute measure, evaluates toughness. Sometimes, the combined effect of mechanical strength and ductility is referred to as toughness of material.

Structural integrity is the mechanical stability of a structure, such as integrity of fuel element and control rod in a nuclear reactor. A structure can maintain its integrity when it has adequate mechanical strength, ductility (or toughness), and strong mechanical stability to withstand severe operating conditions.

2.2 Fabricability, Machinability and Corrosion Resistance

Fabricability is a measure of the feasibility of fabricating pieces of material together by the standard processes of forming, joining, welding, riveting and so on.

Machinability is a material's susceptibility to the machine operation of cutting, milling, rolling, and hammering. A reactor structural component can be constructed after the fabricability and machinability of nuclear materials are proved.

Corrosion, which can effect all metallic parts in contact with corrosive fluids (liquid or gas coolants) should always be taken into consideration for material selection. The degree of *corrosion resistance* depends mainly on the service conditions. This aspect is treated in greater detail in Chemical Aspects of Nuclear Power Plant Operations.

2.3 Heat transfer properties, thermal stability, and materials compatibility

Heat transfer considerations have been reviewed in earlier modules. However, thermal conductivity should usually be high and the coefficient of thermal expansion low or well matched with that of other adjacent material.

Thermal stability is an important property for materials that usually operate at elevated temperature. In most practical cases, the mechanical strength, structural integrity and corrosion resistance of the structure and piping materials decrease with increasing temperature. Particularly, thermal conductivities of uranium and plutonium oxides decrease severely near their melting point temperatures. Thus, high thermal stability is essential for the safe operation of nuclear reactors.

Material compatibility is a major criterion that requires all elements and all components in a given system to be compatible. In other words, the materials selected for each element or component of the system must function properly and consistently. In a light water reactor, for instance, the material of a pressure vessel must be compatible with the coolant. The cladding material must be compatible with both the coolant and the fuel. The corrosion resistance of the vessel or cladding material must be sufficiently high, so that the structural material and the coolant are compatible and function properly while the reactor is operating.

3.0 Radiations Effects on Materials

3.1 Fundamental effects

The unique characteristic of the reactor environment is the presence of intense radiation. The radiations in a nuclear reactor consist of alpha and beta particles, gamma rays, neutrons, fissions fragments, and possibly protons. Although fission fragments are not strictly nuclear radiations, their behaviour is generally similar to that of alpha particles and protons. There are, however, differences in degree arising from much greater mass of fission fragments. In addition, the gaseous fission products, e.g., krypton and xenon, introduce many problems of a different kind in connection with solid fuel materials. An important effect on fuel exposed to high burnup is the swelling due to volume enlargement caused by the accumulation of gaseous fission products within the fuel structure.
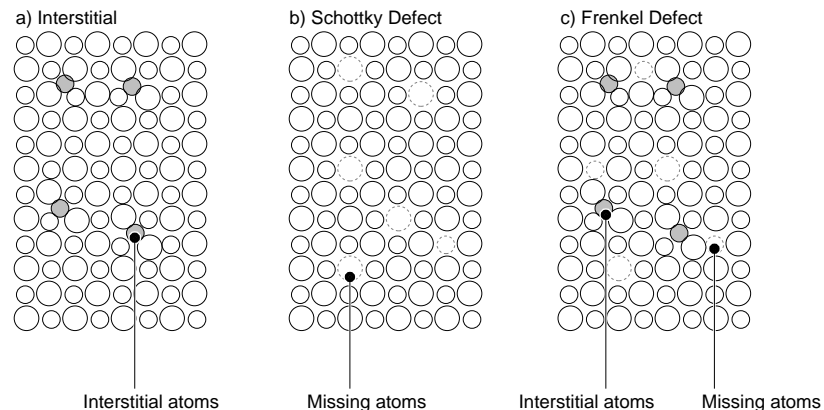
The effect of radiation on crystalline solids depends on the structural type and on the nature of the radiation. The interaction of fundamental radiation with matter are given in Table 3.1. Ionization and electronic excitation, for example, produced by beta particles and gamma rays cause very little permanent change in metals. The reason is that in a metal the electrons in the conduction band are able to accept very small amounts of excitation energy, and so a considerable proportion of the energy of the radiation is absorbed in causing electronic excitation. Because of the large number of empty energy states available, the excited electrons rapidly lose their excess energy, this is taken by the atoms of the metal and appears in the form of heat, i.e., as vibrational energy of the nuclei.

Table 3.1:

Interaction of fundamental radiation with matter

Fundamental particle	Primary effect (or damage)	Secondary effect (or damage)
Electron	Ionization	Displacement (at high energy)
Photon (γ ray)	Ionization	Displacement (at high energy)
α-particle (^{4}He)	Ionization	Displacement (at high energy)
Proton (p)	Ionization and displacement	Displacement (subsequent)
Neutron (n)	Atomic displacement	Ionization

Heavier particles, such as protons, alpha particles and fission fragments do produce significant changes in the properties of metals. As a result of elastic collisions, these particles may transfer appreciable energy to the nuclei of a solid. If the amount of energy transferred is sufficient to cause the nuclei to be displaced from their normal (or equilibrium) positions in the space lattice, physical changes of an essentially permanent character will be observed in the metal. The atomic displacements are illustrated in Figure 3.1.

Figure 3.1:

Point imperfections or defects in crystals

a) Interstitial   b) Schottky Defect   c) Frenkel Defect

Interstitial atoms   Missing atoms   Interstitial atoms   Missing atoms

If, as a result of an elastic collision between the relatively heavy nuclear particle and an atomic nucleus, the energy transferred to the latter exceeds a certain minimum value (around 25 eV for a metal), the struck ("knocked-on") atom may be displaced from its equilibrium position in the solid lattice. If several atoms in close proximity are displaced in this manner, some will be merely transferred from one equilibrium position to another in the lattice. However, if a knocked-on atom is unable to find a vacant equilibrium site, its final location will be a non-equilibrium position. An atom of this kind is said to occupy an *interstitial site* and is known as an *interstitial atom*. For each interstitial atom produced by the action of radiation, there must be a corresponding vacant site in the lattice, possibly at some distance away. The net result is thus more or less permanent defect in the solid, which, if sufficiently common, may be accompanied by a change in physical properties.

In ionic and covalent (organic) compound, both solid and liquid, the effect of radiation is generally greater than in metals. With organic material and water, for example, even gamma rays and beta particles can bring about chemical changes. The ionizing radiations cause damage by breaking chemical (covalent) bonds with, in some cases, the formation of free radicals which results in various molecular rearrangement, e.g., polymerization. The effect of neutrons arise mainly from collisions with hydrogen atoms; the damage is then caused by secondary excitation produced by the recoil protons. Figure 3.2 shows the increase in viscosity with radiation exposure for three organic compounds which might be considered for use as reactor moderator and coolant.

Figure 3.2:
Effect of γ radiation on three different types of hydro-carbon
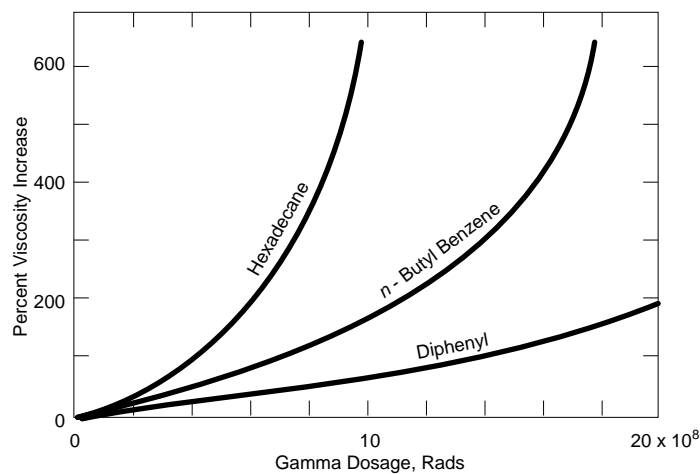
3.2 Radiation effects on material properties

3.2.1 Irradiation effect on physical properties
The irradiation effect on the basic physical properties of nuclear fission material consists primarily of electric resistivity (reciprocal of conductivity), magnetoresistivity, and the Hall effect of electromagnetic field. In general, the

electric resistivity increases with the integrated neutron flux or irradiation time, while the magnetoresistivity and the Hall effect decrease with the integrated neutron flux due to radiation effect or damage in the crystal structure.

### 3.2.2   Irradiation effect on mechanical properties

Most of the mechanical properties are associated with the fuel and structural material which constitute the most important components of a nuclear reactor. This section will discuss the irradiation effect on change in strength, ductility, hardness, creep, fatigue, cracking and other mechanical properties using examples from experimental results.

Mechanical strength

Figure 3.3 presents the irradiation effect in tangential yield stress due to simple tests for specimens of Zircaloy 2 and Zr-2.5 wt% Nb alloy. The stress increases with thermal neutron flux. The present CANDU reactor pressure tubes are made out of Zr-2.5 wt% Nb alloy.

Figure 3.3:

Tangential yield stress versus thermal neutron flux for Zircaloy-2 and Zr-2.5 wt.% Nb at 315°C
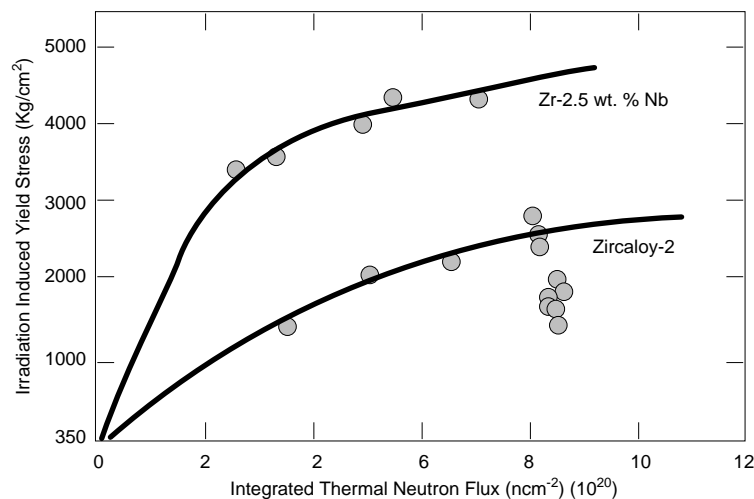

The increase in the yield and ultimate stresses of the structural materials is accompanied by an increase in their hardness during fast and thermal neutron irradiation. In the meantime, the ductility of the structural materials irradiated will be decreased.

Mechanical ductility

Ductility is a very important mechanical property that allows a structural material (carbon steel, stainless steel, or zirconium alloy) to undergo yield and permanent deformation before failure. Figure 3.4 gives the irradiation effect on change in uniform elongation and reduction in area of uranium-aluminium alloys as the integrated neutron flux increases.

Figure 3.4:
Elongation of uranium-aluminium alloys versus neutron flux at 300°C
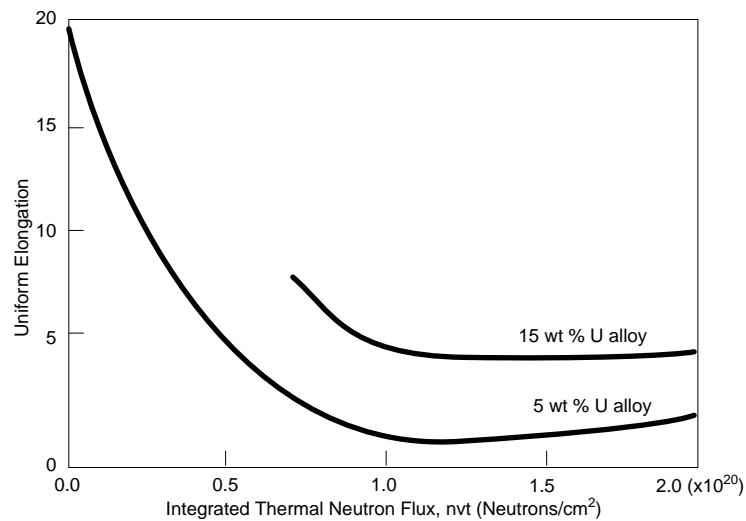
In general, the decreased ductility and increased mechanical strength in nuclear materials, particularly structural materials for fuel element cladding, pressure vessel, control rods produced by the neutron flux can give rise to a number of problems in power reactor design, operation, performance and safety.

Irradiation hardening and embrittlement
The decrease of ductility in materials is a direct consequence of irradiation hardening and embrittlement. Irradiation hardening can result in an increase of yield and ultimate strength (or stress), but a decrease of ductility. Irradiation embrittlement produced by impurity atoms (He^4, H, N, etc.) of nuclear transmutation, radiation decomposition, and other effects can cause a fracture failure of reactor primary components. The irradiation hardening and embrittlement are attributed to the vacancy, interstitial, dislocation and impurity atoms of the basic crystal defects.

Irradiation embrittlement is commonly referred to as *helium embritllement* in stainless steel or *hydrogen embrittlement* in zirconium alloys. The helium production is induced chiefly from nuclear transmutation of (n,α) reactions, and the hydrogen production is mainly from the (n,p) reaction and the radiation decomposition of water in the reactor core. In general, the production of impurity atoms that form voids (as He^4) and interstitials (as H, N) can embrittle the reactor materials.

Creep rate and rupture life
Creep is a slow, plastic and continuous deformation of a solid material under load and, in most cases, at elevated temperature. Figure 3.5 represents a typical creep curve of an unirradiated or irradiated solid metallic material (see Figure 5.7). When the tertiary stage of the creep is reached, fracture of the specimen proceeds, and rupture of the specimen occurs.

Figure 3.5:

Typical creep curve of unirradiated or irradiated solid metallic material
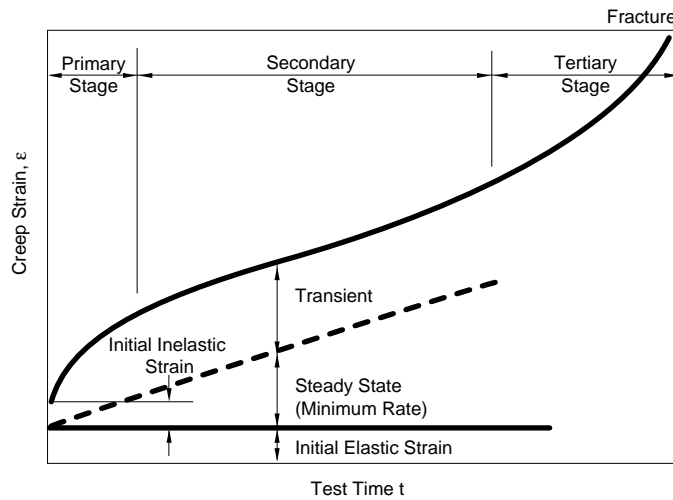
Rupture life is defined as a period of time from the beginning of life of the creep to the end of fracture of the specimen. Figure 3.6 shows the rupture life of Type 316 stainless steel under irradiated and unirradiated conditions at various temperatures. It can be noted from these curves that the rupture life of the irradiated specimen is relatively short in comparison to the unirradiated ones.

Figure 3.6:

Rupture life of Type 316 stainless steel at various temperatures

- - - Unirradiated annealed-controls
—— Irradiated 1.2×10^{22} n/cm^2 EBR-11 E>0.1 Mev
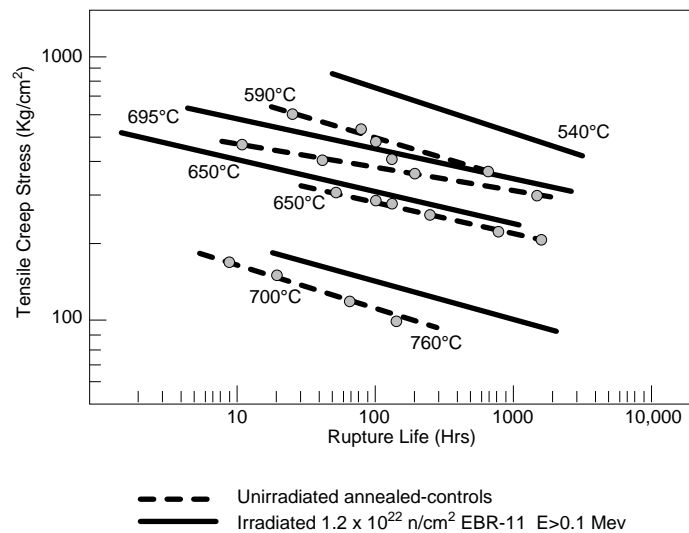
4 Structural Material used for Reactor Components

4.1 General considerations on structural materials

Structural materials provide the physical containment (for fuel protection), mechanical strength, and structural support (framework) for the reactor components. The primary components that use structural material are the fuel cladding, pressure vessel, fuel coolant channels, core support plates, coolant piping system, control element mechanism, among others. The primary

requirements and basic materials of the structural materials are given in Table 4.1.

Although reactor structural materials comprise metals and their alloys, ceramics, and cermets, the most commonly used are those metals and alloys that can function properly as structural materials. Among metal and alloys, beryllium, magnesium, aluminium, zirconium and their alloys have low neutron thermal neutron absorption, high thermal neutron scattering, and good physical, thermal, and mechanical properties, irradiation stability, and corrosion resistance.

Selection of structural materials, based on the primary requirements, varies with different types of nuclear reactors. The pressure vessel material used for light water reactors (LWRs) is carbon (mild) steel. For light water reactors and heavy water reactors, zirconium alloy is used for cladding.

Table 4.1:

Reactor structural materials

Primary requirements	Basic materials
Low neutron absorption (capture)	Zr, Al, Mg, Be
High mechanical strength and ductility	Carbon steels, stainless steels
High thermal stability (heat resistance)	Ni-base superalloys
Great irradiation stability	Refractory metals, Mo, Ti, Ta, W
Low induced radioactivity	Ceramics, BeO, Al_2O_3, MgO, SiO_2
Good heat transfer properties	Cements, $ZrSi_2$, SiC-Al
High-temperature corrosion resistance	Graphite, prestressed concrete

Uranium metal or oxide is readily attacked by air, liquid metal and water which is often employed as a reactor coolant. In fact, metallic and oxide uranium fuels are both corrosive at elevated temperature. Therefore, uranium fuels must be clad with some structural material that is compatible with both fuel and coolant.

4.2 Properties of zirconium alloys, nickel alloys and stainless steel

Zirconium alloys, nickel alloys and stainless steel are the most commonly used materials in light water and heavy water reactors. Their properties will be discussed in greater details in this section.

4.2.1 Zirconium and its alloys

Beryllium, magnesium, aluminium, and zirconium are the only metallic elements that have low thermal neutron absorption cross section and are suitable for use as basic structural materials in thermal reactors. Although beryllium has the lowest thermal neutron absorption cross section and a high melting point (see Table 4.2), the poor ductility, high cost due to scareceness, and toxicity for handling limit its use. Magnesium has the second lowest thermal neutron absorption cross section and compatibility with uranium fuel and carbon dioxide coolant, but a low melting point and poor corrosion resistance to water and steam restrict its use in the gas-cooled reactor. Aluminium has the lowest thermal scattering neutron cross section, high thermal conductivity, and low cost

due to abundance; its low melting point and low thermal strength, however, also limit its use for low temperature operation in thermal research reactors. Only Zirconium, which has the third lowest thermal neutron absorption cross section, high melting point, high mechanical strength at elevated temperatures, good corrosion resistance to water and steam, and reasonable cost and abundance, is widely used as cladding and structural materials in LWRs and HWRs (heavy water reactors).

Table 4.2:

Properties of elements of reactor structural materials

Element	Density (g/cm^3)	Absorption cross section (σ_a) thermal neutron 0.0235 eV (barns)	Scattering cross section (σ_s) thermal neutron 0.0235 eV (barns)	Melting point (°C)
Be	1.85	0.0095	7.0	1283
Mg	1.74	0.063	4.0	650
Zr	6.50	0.180	8.0	1845
Al	2.70	0.235	1.4	660
Nb	8.57	1.100	5.0	2415
Mo	10.20	2.600	7.0	2617

The zirconium alloys used widely as structural or cladding materials in LWRs and HWRs are the family of Zircaloy. Zircaloy-2 is employed in BWRs (boiling water reactors) and HWRs, while Zircaloy-4 is employed in PWRs (pressurized water reactors). Zircaloy-3 was adopted for use in some ship reactors. The composition of the family of Zircaloy, together with some zirconium alloys, is given in Table 4.3.
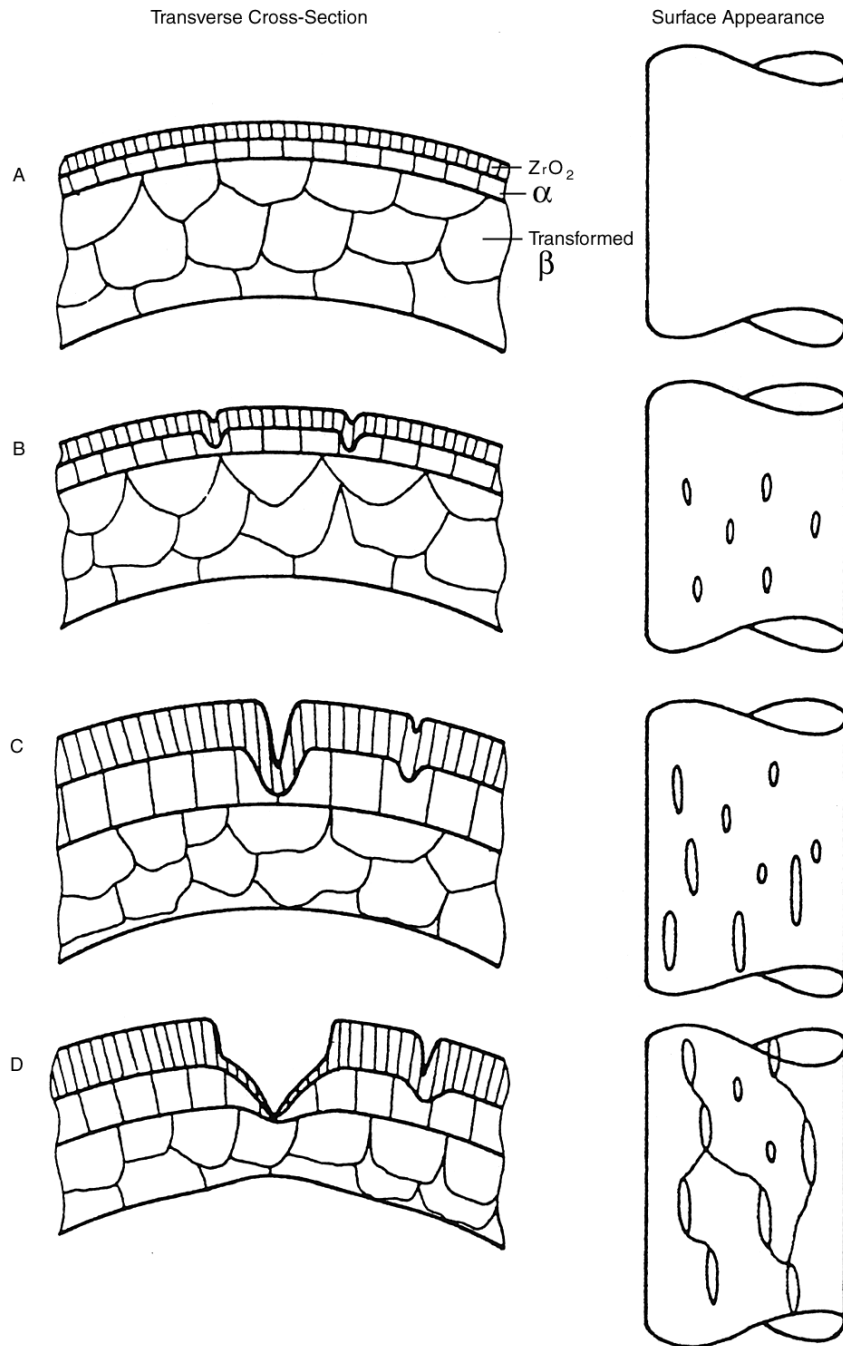
Table 4.3:

Chemical composition of some Zirconium alloys

Element	Zirconium alloy (w/o)			
	Zircaloy 2	Zircaloy 3	Zircaloy 4	Zr-Nb-2.5
Sn	1.2-1.7 (1.5)	0.2-0.3	1.1-1.5 (1.3)	-
Fe	0.07-0.20 (0.14)	0.20-0.30	0.20-0.24 (0.22)	-
Cr	0.05-0.15 (0.09)	-	0.06-0.14 (0.10)	-
Ni	0.03-0.08 (0.05)	-	-	-
N	0.03-0.08 (max)	0.010 (max)	0.010	-
O	0.010 (0.13)	-	0.10-0.16 (0.13)	-
Nb	-	-	-	2.5

These Zirconium alloys, particularly Zircaloys, have consistently good corrosion resistance in water and steam at high temperature (≈ 400°C). This is the uniquely chief requirement of the nuclear structural material being operated in PWR, BWR and pressure-tube type HWR. Figure 4.2 illustrates the propagation of oxide cracking of Zircaloy fuel sheath specimen in steam under temperature ramp condition.

Figure 4.2:

Schematic diagram of oxide cracking in Zircaloy fuel sheath specimen

Transverse Cross-Section   Surface Appearance

In general, the alloying elements selected also improve the mechanical strength and ductility of materials with about the same low thermal-neutron absorption cross-section as zirconium metal.

Table 4.4 presents the advantages and disadvantages of zirconium metal as structural material.

Table 4.4:

Advantages and disadvantages of Zirconium as structural material

Advantages	Disadvantages
Low thermal neutron absorption cross section	Low thermal conductivity
High melting point	
High thermal mechanical strength	Low corrosion resistance at
Good corrosion resistance to water and steam	high temperature (exothermic reaction with steam)
Machinability and fabricability	
Reasonable cost and availability	

4.2.2 Stainless steels

Austenitic stainless steels are iron-base alloys with Chromium and Nickel as primary alloying elements. They are used as structural materials on the basis of their familiar technology, availability, cost, excellent mechanical properties, and excellent corrosion resistance at elevated temperature (below 650°C). In regard to the nuclear properties of an austenitic steel, the absorption and scattering cross sections of fast or thermal neutrons depend on its chemical composition. Stainless steels are attractive as structural material in the fast reactors, thermal reactors (vessel and piping system), radioactive wastes, radioisotopes (container), and other nuclear applications.

However, austenitic steels present some disadvantages such as stress corrosion cracking at the inner surface of fuel cladding and pressure vessel, high thermal stresses due to low thermal conductivity and thermal-cycling fatigue.

4.2.3 Nickel alloys

Nickel alloys, such as Inconel and Hastelloy, have high strength and good corrosion resistance at elevated temperatures. At 650°C, for example, over a long period, the creep rupture strengths of nickel alloys are in the range of 2500-5600 kg/cm^2; the austenitic stainless steels are in the range of 1000-2100 kg/cm^2; and the structural carbon steels (used in LWR pressure vessel) are in the range of 210-450 kg/cm^2.

5 Characteristics of CANDU Reactor Components

This section is intended to outline material requirements for various parts of the CANDU reactor system. The requirements of the CANDU system outside the reactor core bear considerable similarity to those of the PWR series. However, there are certain important design features that dictate significant departures from PWR criteria and particularly for the primary circuit as heavy water is used as coolant compared to light water in PWRs. The important features of the CANDU system from a material point of view are :
- separation of the moderator circuit from the H.T. circuit,

-   use of natural uranium fuel which emphasizes the need for low neutron capture cross section materials as pressure boundary and constructional components in the reactor core,
-   the use of multiple, small sized components, rather than one large vessel with the consequence of having a core structure under irradiation (the pressure tubes holding the fuel), and
-   the use of on-power fuelling.

A simplified flow diagram of the CANDU reactor system is shown in Figure 5.1. The separation of the moderator system from the high temperature, high pressure primary circuit allows the calandria vessel, or the core containment tank, to be a low pressure, low temperature vessel into which reactivity control chemicals can be injected and from which they may be removed without complicating the chemistry control and materials requirements of the primary circuit. The oxygen content and pH of the H.T.circuit can be closely controlled (see lesson on Chemical Aspects), allowing the use of conventional low carbon steel for primary circuit piping.

Figure 5.1:
CANDU nuclear power system: secondary side
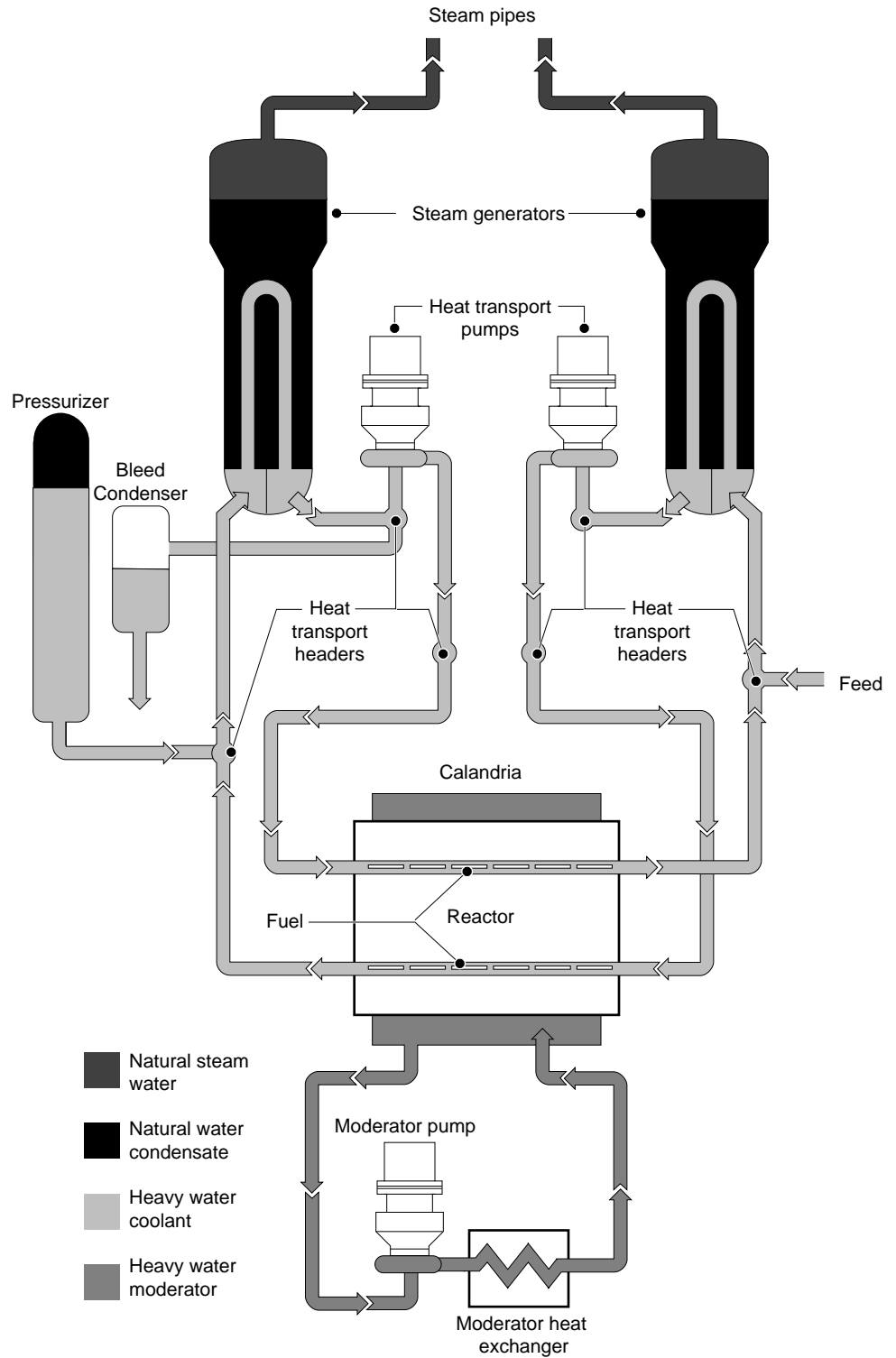
Figure 5.2 shows a schematic of the reactor core. The use of large numbers of smaller sized components has meant the ability to use conventional production line techniques for manufacturing. For example each CANDU 600 reactor uses
380 Pressure Tubes
380 Calandria Tubes
760 End Fittings
760 Feeders
760 Feeder Connections
1520 Annulus Spacers
with each component suitable for fabrication by modern semi-assembly line techniques.

Figure 5.2:
Reactor core schematic
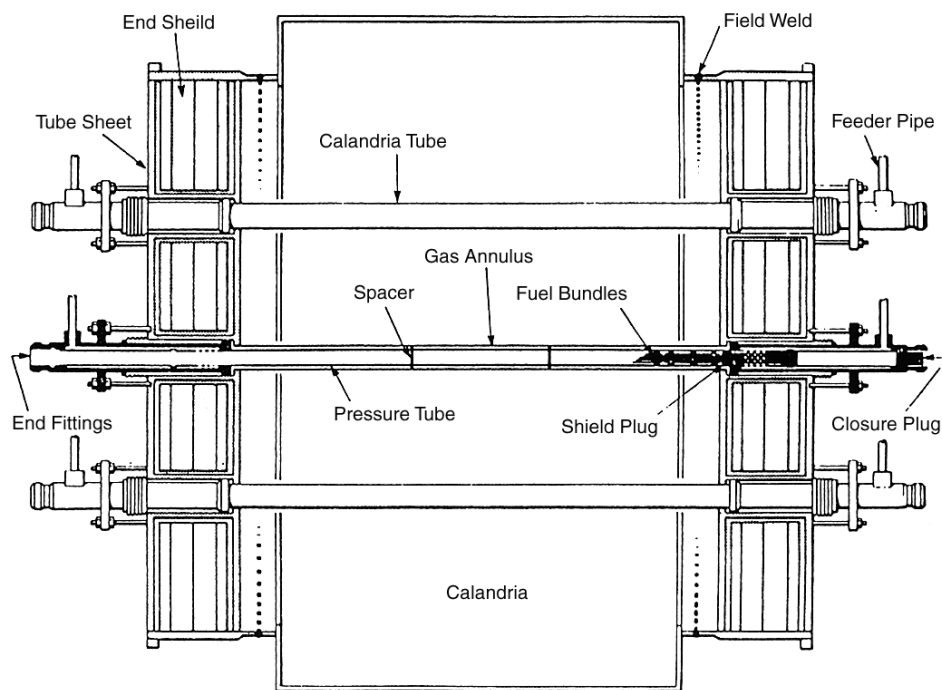
The requirements of low neutron capture cross section, high strength and good corrosion resistance effectively limit the primary circuit core components to zirconium based alloys (see section 4). The technique of cold working has been used in order to achieve the necessary strength levels in the zirconium alloy pressure tubes of the primary circuit. The calandria tubes are made of zirconium alloy in an annealed condition.

The need for on-power fuelling has resulted in the development of suitable alloys which can accept the making and breaking of high temperature seals and the intermittent operation of rotational parts in water at various temperatures as required by the fuelling machine.

Before discussing the components in detail it should be noted that the reactor is designed to the requirements of Section III of the ASME Boiler and Pressure Vessel Code. This Code has been developed for pressure vessels, particularly those of low alloy and carbon steels. Mostly, ASME Code requirements for CANDU components can be met as in general pressure vessel construction, but exception is taken with two sets of components in particular. The pressure tubes and other zirconium alloy components are not ASME Nuclear Code materials but the design requirements follow an ASME Code philosophy. The end fittings, which are of AISI 403 SS, are a code approved material but the condition in which it is used requires a combination of strength and corrosion resistance that dictates the quenched and tempered condition for which Code impact testing requirements can be difficult to meet. Between these two components is a rolled joint which is not an ASME Section III approved joining technique, but which through development and experience has become a reliable and accepted pressure boundary joint.

It can be noted that the safety analysis examine the end fitting failure (rolled joint failure and other mechanisms) and the pressure tube failure scenarios.
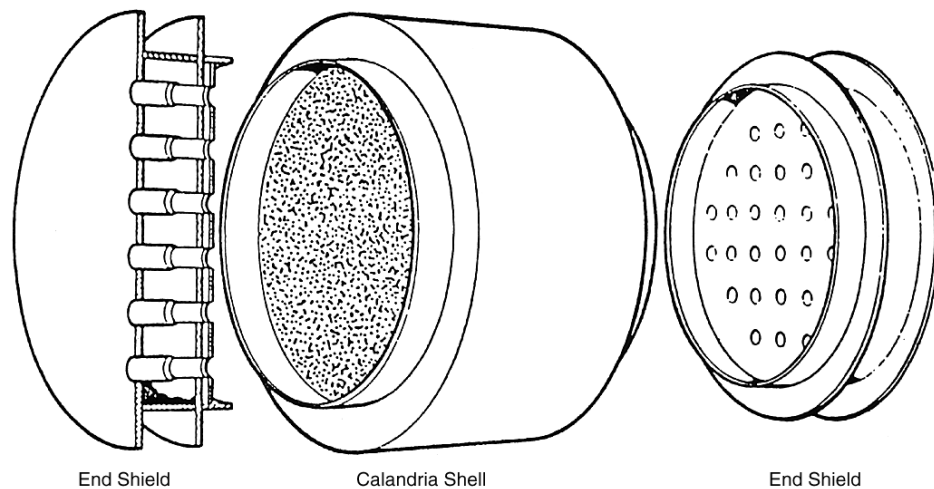
5.1 Calandria Vessel

Figure 5.3 shows a view of a reactor assembly. The calandria vault contains the calandria vessel. Figure 5.4 is an exploded view of the calandria. This is a large cylindrical tank containing the perforated end shields. The end shields are joined together by lattice tubes and are cooled by a light water circuit separate from the moderator circuit. The vessel is made of an ASME grade 304L austenitic stainless steel plate. Use of this grade of stainless steel with compatible welding processes and the lower temperature of operation has avoided the problems that have faced BWR piping with cracking in 304 piping welds.

Figure 5.3:

Reactor assembly
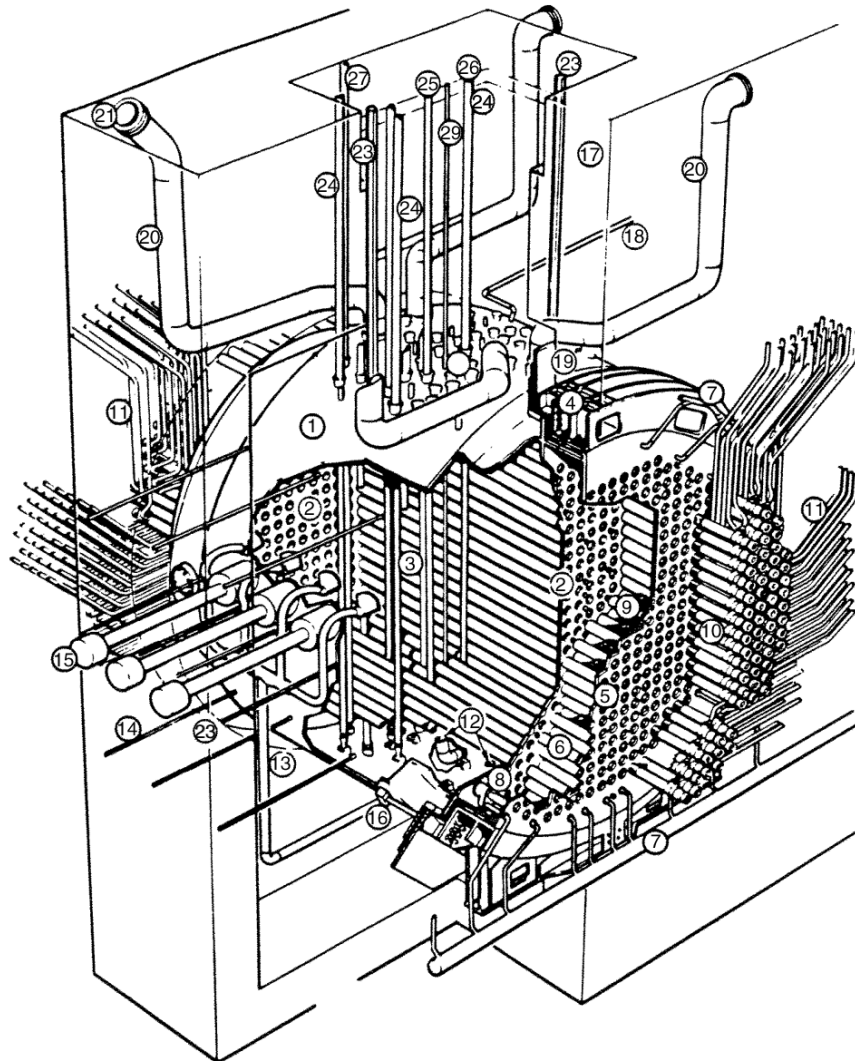
1	Calandria	16	Earthquake Restraint
2	Calandria - Side Tubesheet	17	Calandria Vault Wall
3	Calandria Tubes	18	Moderator Expansion to Heat Tank
4	Embedment Ring	19	Curtain Shielding Slabs
5	Fueling Machine- Side Tubesheet	20	Pressure Relief Pipes
6	End Shield Lattice Tubes	21	Rupture Disc
7	End Shield Cooling Pipes	22	Reactivity Control Units Nozzles
8	Inlet-Outlet Strainer	23	Viewing Port
9	Steel Ball Shielding	24	Shutoff Unit
10	End Fittings	25	Adjuster Unit
11	Feeder Pipes	26	Control Absorber Unit
12	Moderator Outlet	27	Zone Control Unit
13	Moderator Inlet	28	Vertical Flux Detector Unit
14	Horizontal Flux Detector Unit	29	Liquid Injection Shutdown Nozzle
15	Ion Chamber	30	Ball Filling Pipe

Figure 5.4 :
Exploded view of Bruce reactor calandria

End Shield   Calandria Shell   End Shield

In conjunction with the calandria tank, the moderator piping components, as well as the bodies of valves, pumps and heat exchanger vessel components are of stainless steel. The moderator water thus sees stainless steel, the zirconium surfaces of the calandria tubes, and the heat exchanger material which has varied from 70-30 cupro nickel to Incoloy 800, 3RE60 (a ferritic/austenitic stainless steel), and, most recently, Incoloy 825. Table 5.1 gives the moderator heat exchanger materials used in the various CANDU power plant.

Table 5.1:

Moderator heat exchanger materials

Power plant	Material
Douglas Point	70-30 Cu/Ni
Pickering A	70-30 Cu/Ni
Bruce A	Incoloy 800
Pickering B	Incoloy 800 (to be replaced by Incoloy 825)
Gentilly-2	Sandvik 3RE60
Cordoba	Sandvik 3RE60
Point Lepreau	Sandvik 3RE60
Wolsong	Incoloy 800
Cernavoda	Incoloy 800

5.2   Calandria tubes

Figure 5.5 shows some of the components in a fuel channel. Calandria tubes surround and isolate the hot pressure tubes from the cold moderator. The calandria tubes form part of the calandria structure, tying end shields together and supporting the pressure tubes through spacers to limit pressure tube sag.

Figure 5.5:
Fuel channel arrangement
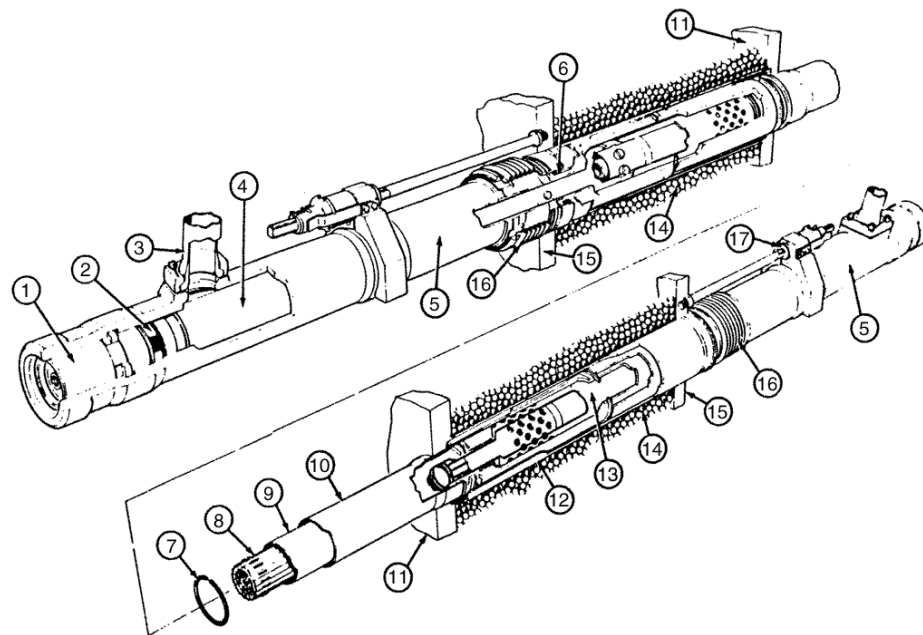
1	Channel Closure	10	Calandria Tube
2	Closure Seal Insert	11	Calandria Side Tube Sheet
3	Feeder Coupling	12	End Shield Lattice Tube
4	Liner Tube	13	Shield Plug
5	End Fitting Body	14	End Shield Shielding Balls
6	End Fitting Bearing	15	Fuelling Machine Side Tube Sheet
7	Tube Spacer	16	Channel Annulus Bellows
8	Fuel Bundle	17	Channel Positioning Assembly
9	Pressure		

Calandria tubes are made from annealed Zircaloy-2 strip. They are made by brakeforming and seam welding with subsequent treatments of the weld zone to give homogeneity. Slight amounts of cold work are put into the tube to size it and this may be followed by a stress relief. The fabrication process is one that results in low irradiation growth in reactor.

Thin-walled, large diameter tubes of diameter to wall thickness ratios of greater than 80 to 1 are difficult to make with small variation in wall thickness by techniques other than starting with strip. The wall thickness variation in the tube wall is limited to a value of not more than 0.05 mm greater than the specified minimum wall.

Examination of a calandria tube removed from Pickering Unit 2 after the G16 pressure tube incident of August 1983, showed the component to be in excellent condition and exhibiting a high degree of irradiation induced strengthening but retaining adequate ductility.

5.3 Fuel channels

5.3.1 Pressure tubes

Table 5.2 summarizes the pressure tube requirements. The pressure tubes must have the capacity to resist deformation from the combination of temperature, pressure and neutron flux to which they are subjected. Also, they must have good resistance to corrosion by the reactor coolant and to wear by sliding fuel bundles. The two alloys that have been used to satisfy these requirements have been cold worked Zircaloy-2 and cold worked Zr-2.5 wt% Nb. The present reactors are tubed with cold worked Zr-2.5 wt% Nb.

Table 5.2:

Pressure tubes requirements
Good corrosion resistance to high temperature water
Good wear and fretting resistance
Withstand coolant pressures of 1500 psi (10.5 MPa)
Withstand neutron fluxes of 2×10^{17} n/m^2/s
Close tolerances in terms of consistent wall thicknesses, consistent ovality, etc.
Good surface finish
Low neutron capture cross section

The pressure tubes are made by a process of extrusion and cold drawing, and the production sequence is shown in Figure 5.6. Present tubes are cold reduced about 25% after extrusion. Zr-2.5 wt% Nb is a two phase alloy as opposed to the single phase Zircaloy-2. The two phase alloy allows flexibility in material conditions and it has been used in both the cold worked and quenched and aged condition. However, the cold worked material has several advantages over the material in the thermally treated condition and has become the standard CANDU pressure tube material.

Figure 5.6:

Pressure tube production sequence
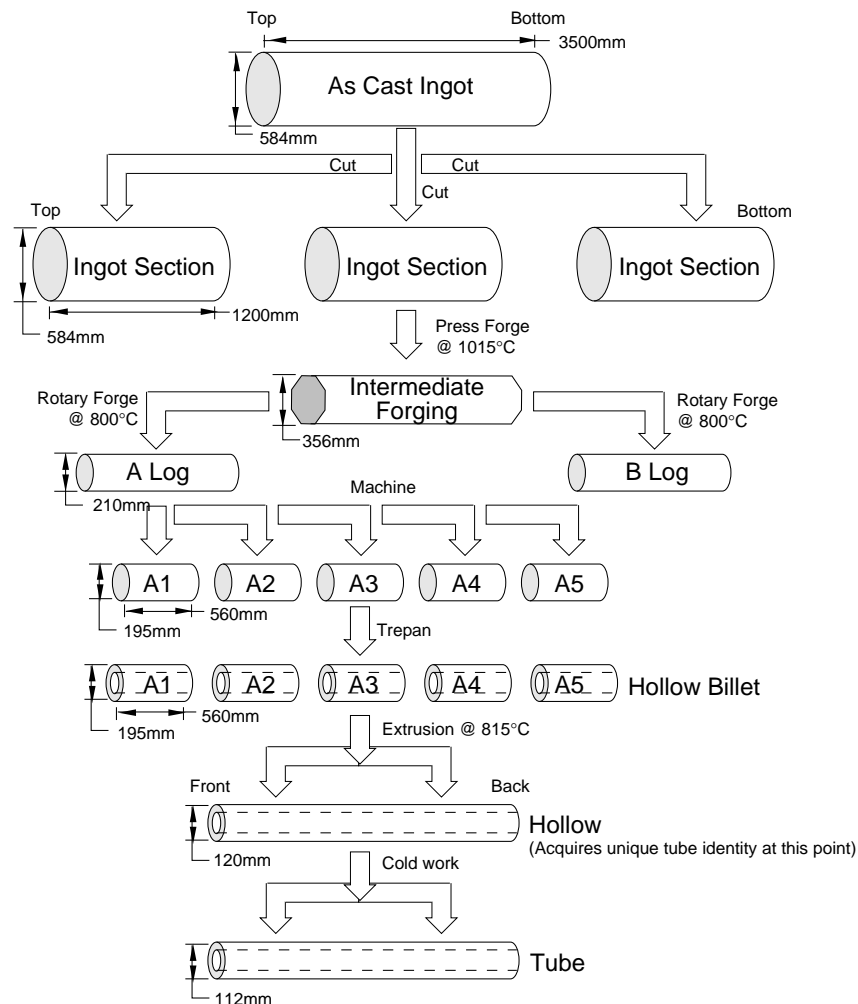
The tubes as installed are 6.3 m long, 100 mm inside diameter and 4 mm wall. Dimensions are closely controlled and defect quality assured by detailed ultrasonic and eddy current inspections. Final treatment of the cold worked tube is a stress relief at 673 K in a steam autoclave which serves to put a protective oxide onto the surface of the tube.

Pressure tubes suffer dimensional change in service as shown in Figure 5.7. They elongate mainly due to irradiation growth. They increase in diameter due mainly to creep and they sag by creep due to the weight of the coolant and the fuel. The tubes are rolled into end fittings which move on bearings to accommodate temperature induced length changes and elongation. The tubes sag until the load is transmitted through garter spring type spacers onto the calandria tube. Diameteral creep continues until approximately 5% diametral creep accumulates after 30-40 reactor years. The channels are designed to allow replacement of pressure tubes and end fittings.

Figure 5.7:
Creep of a tube

Axial Creep   Sag   Diametral Creep
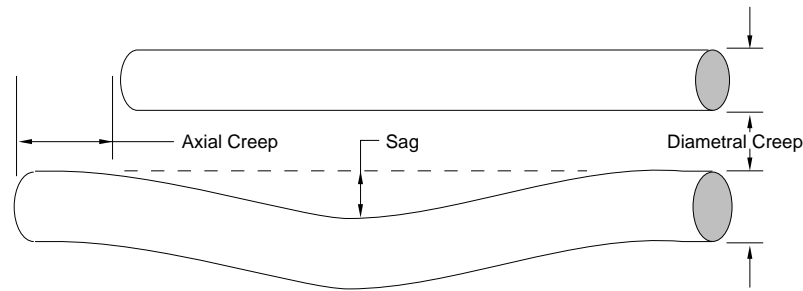
5.3.2   End fittings

End fitting material requirements are the following:
- hardness must be controlled to produce an end fitting to pressure tube hardness ratio which results in a leak tight rolled joint
- hardness requirement must be balanced with requirements for high tensile and impact strengths to
  1.   withstand fuelling machine loads
  2.   withstand temperature and pressure of operational and upset conditions
  3.   retain rolled joint integrity
- irradiation resistance
- corrosion resistance
- capable of retaining highly finished seal faces
- reasonable cost, machinability, capability for plating

The AISI type 403 end fittings are quenched and tempered to provide a material condition that has adequate corrosion resistance and that at the same time is suitable for rolled joint fabrication. Early reactor fabrication used a material condition which could not satisfy the code requirements for impact tests at room temperature in the longitudinal and transverse direction. AECL thus developed an alternative qualification approach which correlated irradiation induced fracture behaviour with low temperature (-50°C) fracture behaviour. This has been followed by low temperature full size burst tests at -50°C to confirm the excellent fracture resistance. Recently, manufacturing developments are producing a material condition that can economically satisfy ASME impact requirements with some recycling heat treatments.

5.3.3   Channel supports or spacers

Channel spacers have been fabricated both in a Zr-2.5 wt% Nb -0.5 wt% Cu alloy (quenched and aged) and in Inconel X-750. The spacers are in the form of a garter spring or toroid which accommodates relative linear motion between the calandria tube and the pressure tube, as well as diametral creep of the pressure tube. The most recent reactor to be tubed has used Inconel X-750 for spacer material. This change was necessitated by the change from a "loose" spacer to a "tight" spacer which will not move under vibration loads.

5.4 Reactivity mechanism

These are substantially zirconium or stainless steel alloys. The Zirconium alloys are a mixture of seam-welded tubes and extruded tubes (< 25 mm diameter). Shut off rods contain cadmium which is considered as a "black" material for the neutrons.

5.5 Primary heat transport components

5.5.1 Feeders and headers

These are carbon steel components generally from extruded and normalized material. The feeders as shown are to ASTM A106B requirements. The headers, also to A106B requirements, are fabricated with pull out nozzles to which the feeder pipes are welded. The feeder and header materials are specified to have a low cobalt content-preferably less than 0.010 wt%. This helps to control the gamma fields produced in the circuit from activated corrosion products. The feeder piping sizes for a 600 MWe reactor vary from 4.32 cm ID and 4.83 cm OD to 9.35 cm ID and 10.16 cm OD. The dimensions of the headers are: 40.6 cm ID and 53.3 cm OD for the outlet header and 37.0 cm ID and 48.3 cm OD for the inlet header. Both headers are approximately 6 m long. Table 5.3 provides information on the material.

Table 5.3:

Properties of feeder and header material

| Material	ASTM A106B		
Cobalt content	Preferably less than 0.010% wt.		
	Yield	UTS	Elongation
Specification minimum	242 MPa	415 MPa	30 %
Average value	315 ± 35 MPa	485 ± 65 MPa	39 ± 20 %

5.5.2 Pumps and valves

The cases, covers and stuffing boxes of the main heat transport pumps and most of the auxiliary pumps are cast or forged carbon steel. Fittings such as discharge and suction spool pieces and elbows are also carbon steel. The rotating elements are of martensitic stainless steel. Wear rings, designed for easy replacement, are of stainless steel or nickel base hard facing alloys. The three stage primary mechanical seals use stainless steel with the rotors and stators being made from graphite and cemented carbides which are chosen for their mechanical stability in order to maintain relative flatness to enhance seal life.

Valve bodies, bonnets and stuffing boxes are of cast or forged carbon steel. Trim materials are nickel base alloys such as Deloro 40/50 or Colmonoy 4/5 (rather than cobalt base alloys such as Stellite 6) in order to reduce activated corrosion products. Stems are of stainless steel and, as with pump shafts, are considered to be pressure retaining materials for purposes of inspection and traceability. Materials for bellows of stem sealed valves are restricted to Inconel type alloys.

5.5.3 Steam generators

Steam generators comprise two main sets of components - the shell components and the tube bundle. The size and pressure loadings of the CANDU steam generators are of a level where construction can be done with carbon steel grades with a minimal use of low alloy steels. This simplifies welding and postweld heat treatment practice. A schematic of a typical CANDU steam generator is shown in Figure 5.9.

Figure 5.9:
Typical steam generator
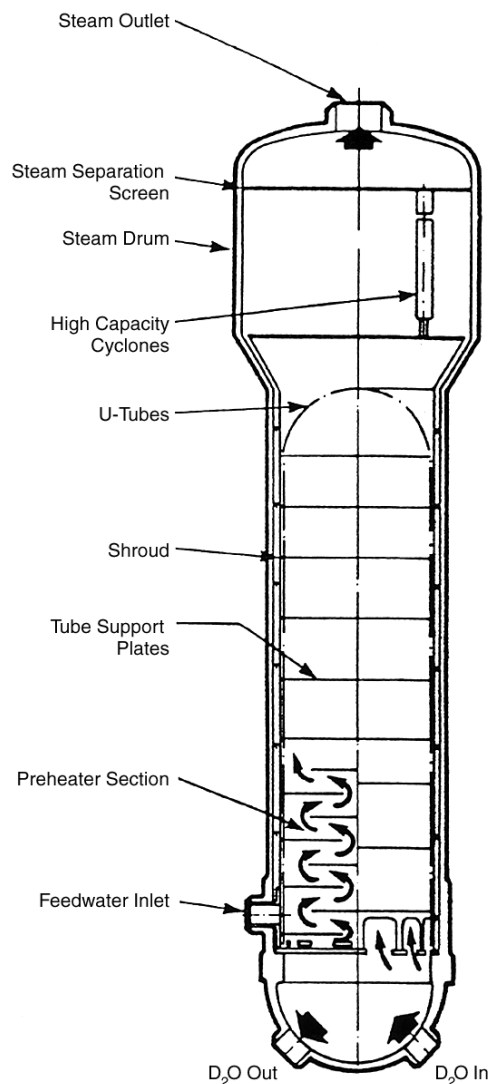
Three alloys have been used for boiler tubing in CANDU reactors, as shown in Table 5.4. Inconel 600 was first used for the NPD reactor but because of cost was replaced by Monel in Douglas Point and Pickering A and B. Although Monel has demonstrated an excellent performance it cannot be used where boiling may occur in the channel due to increased oxidation and circuit activation. Bruce A thus used Inconel 600 in a 610°C/8h aged condition. Concerns about the

stability and ability of Inconel 600 to provide adequate cracking resistance for 30 years lead AECL to pursue the use of Incoloy 800 which has become the standard alloy for CANDU steam generators. A comparison between the relative merits of Inconel 600 and Incoloy 800 is shown in Table 5.5. Recent experience has indicated further concern with Inconel 600 but the secondary side chemistry must also be carefully controlled to achieve adequate performance from Incoloy 800.

Table 5.4:

CANDU steam generator tubing

Monel	Inconel 600	Incoloy 800
Douglas Point	NPD	Gentilly-2
Pickering A	Bruce A	Point Lepreau
Pickering	Bruce B	Cordoba
		Wolsong 1
		Darlington A
		Cernavoda

5.6   Secondary system

Control of the secondary system chemistry has an important influence on the integrity of the steam generator. The secondary side crud buildup is influenced partly by the material of the secondary circuit while the chemistry of the boiler secondary side can be adversely affected by lack of condenser integrity. The material selection for the feedwater systems in CANDU plants has changed over the years. Copper alloys have been substituted for stainless steel and Titanium in the condenser and carbon steel in feedwater heaters has been changed for stainless steel to lower crud levels. The elimination of copper base alloys in the feedtrain allows the use of higher pH values and this in turn leads to lower levels of crud production.

Table 5.5:

Comparison of I600 and I800

I800	Criteria	I600
Not susceptible	Pure water S.C.C.	Susceptible w/o heat treatment
Not susceptible in NaOH below ~ 30 g/l at 300 °C	Caustic S.C.C	In 610 °C aged condition susceptible, will crack in as low as 10 g/l NaOH solutions at 300°C
Pitting attack depends on concentration and oxygen content	Chloride	Pitting attack depending on concentration and oxygen content
Lower Ni concentration than I600 results in less Co58 in corrosion products	Activation	Higher primary circuit field than I800 assuming same level of material cobalt concentration
Relatively resistant to polythionic acid attack	Sulphur compounds	More susceptible to polythionic attack
Carbon concentration controlled to low limits and C-curve effects limited. Better in G28 test.	Heat treatment	Corrosion resistance sensitive to carbon concentration and other microstructural factors
Limited in CANDUs, 10-12 y	Operating	Considerable experience in KWU PWR S/Gs with mill annealed or 610 °C treatment. Limited operating experience with 700 °C/15 h condition
Not quite as good as I600	Thermal conductivity	6 % better than I800
Can accept glass bead surface conditioning	Acceptance of surface conditioning	Use of 700 °C/15 h treatment only since material may not tolerate extra inside surface stresses from glass bead peening
Greater flexibility than I600 for inside surface stresses due to resistance to pure water S.C.C	Tube expansion in tubesheet	Heat treatment or stress modification (kiss roll) techniques required

Condenser integrity is particularly important for steam generator reliability. CANDU plants now use stainless steels for good quality fresh water sites and Titanium tubing for sea water sites. To date the tubes have only been rolled into tubesheets but there have been provisions for leak collection by the use of secondary tube sheets. Welding of tubes would provide more reliability but at a significant increase in cost.

5.7   Example of the cracking of pressure tubes in Pickering A Unit 3

In order to illustrate the causes and consequences of material damage, we will use the example of the cracking of pressure tubes in Pickering A.

In August 1974, Pickering Unit 3 was shutdown for a period of 8 months because of cracks in 17 of the 390 pressure tubes. The cracks were a result of incorrect installation procedures during construction. Improper positioning of the rolling tool used to join the Zr-2.5 wt% Nb pressure tube to the end fitting produced very high residual tensile stresses. High stresses in combination with periods with the tubes cold caused the cracking. Crack propagation was by fracture of hybrides which are brittle when cold.

The pressure tubes of about 6 m length, 4.1 mm wall thickness, and 103 mm inside diameter contain the fuel and heavy water coolant at about 9.0 MPa and 566 K. Cold-worked Zr-2.5 wt% Nb with a design stress of 158 MPa at 573 K is used as pressure tube material. The pressure tubes are horizontal and subject to internal pressure and to bending loads due to weight of fuel and coolant. The end of the pressure tubes are rigidly joined to end-fittings of stainless steel by rolled joints (see Figure 5.10). The end fittings are firmly supported by the end shields. A pressure tube is then a fixed beam subject to a uniformly distributed load and to point loads provided by the central spacers which in turn are supported by the calandria tube. The only discontinuity is where the tube is joined to the end fitting.

Figure 5.10:
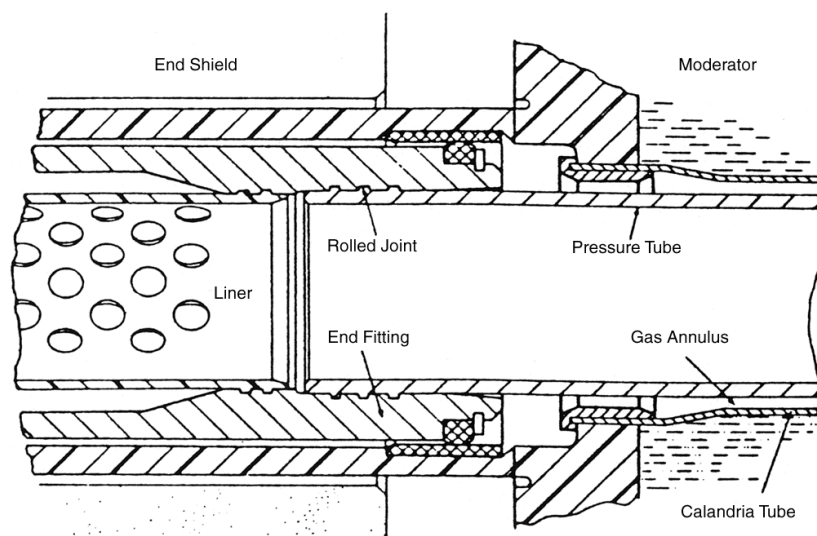*Rolled joint arrangement in Pickering reactor*

Figure 5.10 shows the cross section of a rolled joint. Three grooves are machined in the end fitting bore in the rolled joint area. The pressure tube is inserted into the end fitting covering the grooves. A tube expander is introduced into the pressure through the end fitting (see Figure 5.11). The tube is roll expanded into the end fitting. The tube wall thickness is reduced by 12% to 15% and the grooves in the end fitting are partially filled with tube material. The material in the grooves tends to lock the tube to the end fitting producing satisfactory leak tightness and axial strength. Although the rolled joints themselves have behaved well, improper rolling procedures during construction resulted in cracks close to the rolled joint.

Figure 5.11:
Cross section of a Pickering rolled joint during roll expanding
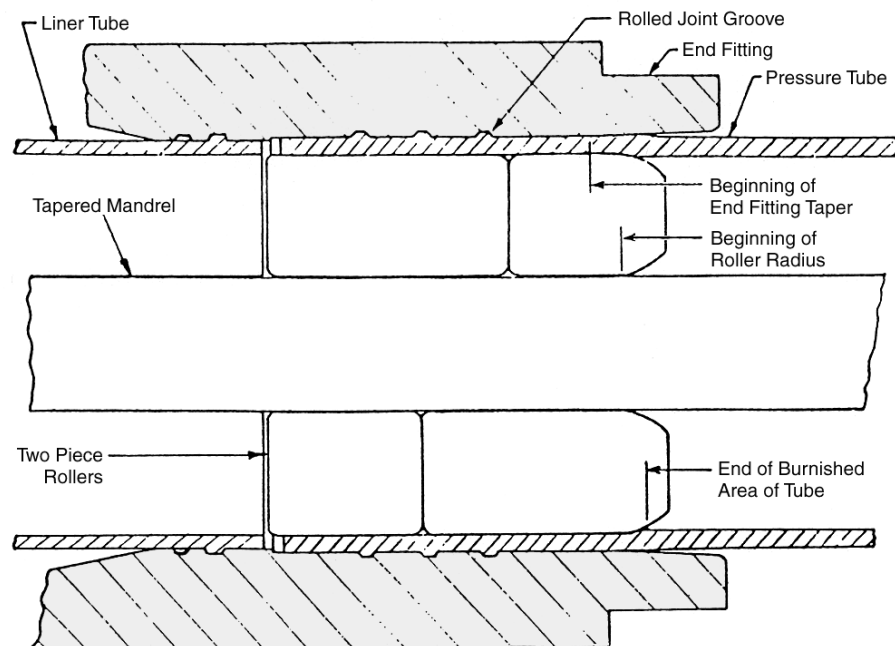
The crack investigation showed that the rolling tools had been inserted about 13 mm too far into the tube during the rolling operation. The rolling tube had thus expanded the pressure tube for about 10 to 15 mm beyond the parallel bore of the end fitting and in a region where the tube has little support (see position of taper and roll in a poor joint, Figure 5.12).

Figure 5.12:

Pickering rolled joint

a. Relative position of rolling tool during installation

Hub

End Fitting

Taper

Pressure Tube

Rolls not extended beyond taper (good joint)

Rolls extended beyond taper (poor joint)

b. Position of radial hydrides and crack in a poor joint

Circumferential Hydride

Radial Hydride

Pressure Tube

Poor Joint

Ends of through wall crack

Poor Joint

Initiation of through wall crack

c. Residual stress distribution on the inner wall of a good and poor joint

Residual Stress Kpsi

MPa

Poor Joint

Good Joint

The cracks were about 15 to 20 mm long and were just inboard of the rolled joints. The crack initiation point was close to the innermost point of contact of the rollers. The cracks had either propagated through the tube wall or had propagated almost through the wall with only a thin web on the outside remaining. The surfaces of the cracks showed that propagation was from the inner wall of the tube and was in three distinct bands. Each band was oxidized at different amount. The first band was heavily oxidized suggesting the crack had been exposed to coolant at temperature for a long time. The last band showed very light oxidation. Electron fractography of the surface of this latter

band showed characteristics found in zirconium alloys that had failed by delayed hydrogen embrittlement.
The event resulted in a eight months shutdown (loss of power production) for one unit of Pickering A and in a change in the rolled joints procedures for the next generation of reactors to be built.

In the next lesson, we will cover the impact of the chemistry control on the materials that have been described in the present lesson.

December 1995

Chemical Aspects of Nuclear Power Plant Operations

Training Objectives

The participant will be able to describe or understand:
1 the chemical induced problems in a nuclear power plant.
2 the chemical parameters for chemistry control.
3 the chemical control methods.
4 The chemical control objectives and methods for the main systems: the heat transport coolant, the moderator, and the steam and feedwater systems.

Chemical Aspects of Nuclear Power Plant Operations

Table of Contents

1 Introduction

The control of chemistry in the many process systems of a nuclear reactor is vital for the wellbeing of the plant. Many operating problems and costly repairs to reactor components around the world can be and have been blamed on inadequate chemistry control.

There are five primary objectives of chemistry control. These may not all apply in a particular system, but when more than one have to be considered, the requirements may conflict. The best chemistry control may therefore be a compromise. The objectives of chemistry control are to:
a) minimize corrosion to maintain system integrity, to preserve worker and public safety, and to minimize costs;
b) minimize activity transport to provide a healthy work environment and to minimize costs;
c) control reactivity to obtain maximum reactor efficiency and to preserve worker and public safety;
d) minimize radiolysis to maintain system integrity and to preserve worker and public safety; and
e) minimize surface fouling to minimize heat transfer inefficiencies and costs and to preserve system integrity.

It is important to realize that to have its maximum effect, chemistry control must be considered from the concept stage of the plant through to the end of plant life and decommissioning.

The diversity of the materials in any one system and their different reactions to the environment clearly necessitate careful control of chemistry for optimum performance.

A review of chemistry basics is given at the beginning of this lesson. The chemical control of the various process systems, namely, the heat transport system, the moderator system, the feedwater/condensate system and the recirculating water system, of a typical CANDU reactor are treated in details.

Figure 1.1:
CANDU nuclear power systems
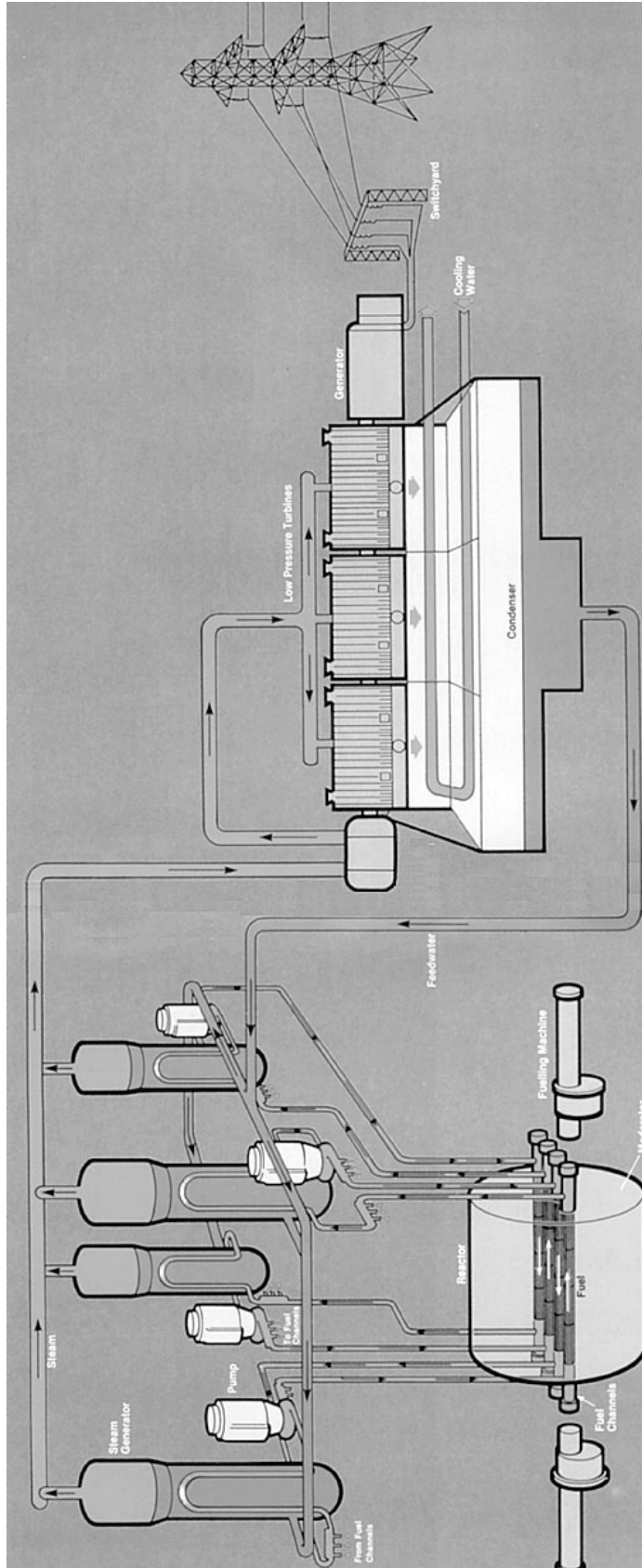
2 Review of Chemistry Basics

2.1 Definition of pH

All aqueous solutions contain both hydrogen ions [H$^+$] and hydroxyl or hydroxide ions [OH$^-$]. The concentration of [H$^+$] multiplied by the concentration of [OH$^-$] equals 10^{-14} at 25°C. The relative proportion of hydrogen and hydroxyl ions determines whether the solution is acidic, neutral, or basic (alkaline):

- if [H$^+$] and [OH$^-$] ion concentrations are both 10^{-7} moles/litre, the solution is neutral.
- if [H$^+$] ion concentration < 10^{-7} moles/litre then the [OH$^-$] is > 10^{-7} moles/litre, and the solution is alkaline or basic. The term caustic may be used to indicate a very strongly alkaline solution.
- if [H$^+$] concentration > 10^{-7} moles/litre then the [OH$^-$] ion concentration is < 10^{-7} moles per litre, and the solution is acidic.

The conventional definition of pH is the negative logarithm of the hydrogen ion concentration, in moles per litre at 25°C.

The pH is used to indicate the relative acidity or alkalinity of a solution, as shown in Figure 2.1. Since the pH scale is logarithmic, a unit change in pH reflects a factor of ten change in [H$^+$] concentration.

Figure 2.1:

*Relationship of the pH scale and [H$^+$] concentration*
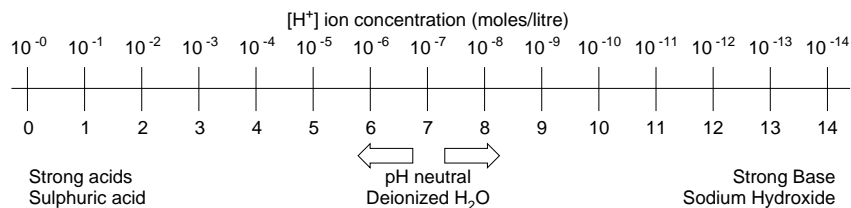
Monitoring pH, i.e., [H$^+$] ion concentration, is an important aspect of chemical control in CANDU systems. For example:

- Acid attack results in corrosion of metals and is a consequence of [H$^+$] ions in solution. Minimizing this attack is commonly a matter of pH control.
- If the pH of the moderator system rises significantly above 7, any gadolinium nitrate poison in solution in the moderator will precipitate out as gadolinium.
- The HTS (Heat Transport System) is held at 10.3 - 10.7 to minimize corrosion by [D$^+$] and [OD$^-$] and to maintain a protective magnetite layer on the carbon steel.
- Very low levels of [H$^+$] and the corresponding very high [OH$^-$] levels. i.e., a high pH, can be a concern if they cause metal wastage or promote caustic embrittlement which is a form of stress corrosion cracking in an alkaline medium.

2.2 Conductivity

The conductivity, $K°$, of a solution is a measure of its ability to conduct an electrical current. The SI unit is the millisiemen per metre, mS/m. It is the ions in the solution that allow it to conduct. Figure 2.2 shows typical conductivities for various aqueous solutions.

Figure 2.2:
Conductivity factors of aqueous solutions
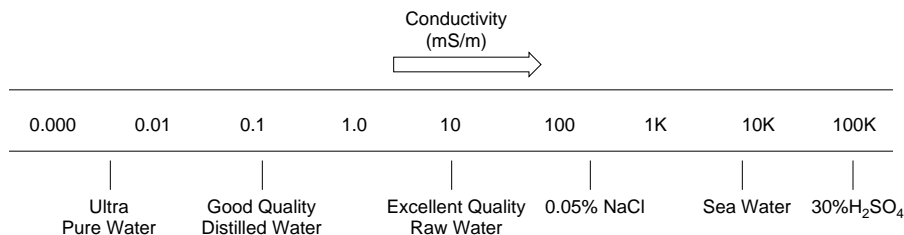
The conductivity of a solution is determined by the total ionic concentration. Note the difference between pH, which is $[H^+]$-ion specific and conductivity which is non-ion specific.

A change in the pH of a solution will always change its conductivity, whereas a conductivity change may or may not alter the solution pH. For example, adding common salt, NaCl, to water increases its conductivity but has no effect on its pH.

Pure deionized water has very low conductivity,i.e., a high electrical resistance. Any substance that dissociates into ions in water will increase the electrical conductivity of the water.

The following examples illustrate the importance of electrical conductivity in a nuclear plant:
- Boiler water conductivity measurements may be used to monitor the effectiveness of boiler blowdowns.
- Moderator D_2O conductivity is kept As Low As Reasonably Achievable (ALARA) to minimize radiolysis.
- Corrosion can be an electrochemical process. Water containing dissociated ions can form an electrolyte which promotes corrosion.
- Stator cooling water must have a very low conductivity in order to act as an electrical insulator.

2.3 Radiolysis

The bonds holding the atoms together in a covalent molecule are produced by the sharing of electron pairs between adjacent atoms. Ionizing radiation is able to transfer energy to these electrons, which destroys the bond between atoms, causing the molecule to break down. Although the mechanism is different (nucleus interaction), neutron irradiation also causes molecules to break down. This chemical decomposition caused by radiation is called radiolysis.

Materials affected by radiolysis in the CANDU system include D_2O, air and polymers. The radiolytes (radiolytic fragments) invariably form new compounds. Radiolysis reaction of deuterium follows the equation:

$$2D_2O \rightarrow 2D_2 + O_2$$
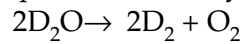
This produces both deuterium and oxygen molecules. Radiolysis of D_2O is increased by many impurities.

There are concerns relating to radiolysis in the CANDU system which are:

- Deuterium and oxygen present an explosion hazard when they migrate to the helium cover gas of the moderator. Passing the cover gas through the recombination units to recombine the D_2 and O_2 into D_2O is required to alleviate this problem.
- O_2 formed by radiolysis in the heat transport system (HTS) presents a serious corrosion problem for carbon steel and its protective magnetite layer. O_2 is scavenged from the HTS by adding H_2 to react with it, producing H_2O. The high operating pressure (≈ 9 MPa) keeps most of the D_2 and other gases in solution; therefore, D_2 does not present an explosion hazard in the HTS.

2.4 Recombination units

As previously mentioned, moderator radiolysis can produce explosive mixture of deuterium (D_2) and oxygen (O_2) in the helium cover gas system. During normal plant operation, the recombination units are capable of maintaining safe levels of D_2 and O_2 in the cover gas by promoting the reforming of heavy water from its gaseous component.

The following chemical equation depicts the recombination reaction of D_2 and O_2:

$$2D_2 + O_2 \rightarrow 2D_2O$$
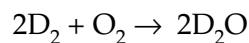
The palladium catalyst in the recombination units makes the reaction possible at low concentrations. Therefore:

- The D_2 and O_2 recombine at a lower temperature and below the lower explosive concentration.
- Low concentrations produce less heat because the amount of heat given off is proportional to the quantity of gases recombining.
- The reaction is described as proceeding quietly, i.e., without an explosion or combustion.

Without a catalyst, recombination will only occur by combustion. If radiolysis proceeds more rapidly than recombination, the levels of D_2 and O_2 in the cover gas will increase. Deuterium in excess of 8% by volume in the helium is potentially explosive, and therefore running a unit at greater than 4% in D_2 is not permitted.

The flame arresters on the inlet and outlet of the units are added protection

because the metal gauze dissipates heat from the reaction and reduces probability of igniting the D_2/O_2 mixture outside the recombination units.

2.5 Ion exchange resins

Ion exchange is a chemical adsorption process which entails an interchange of ions in solution to produce a different chemical compound through the use of an ion exchange resin. The focus of the process is not on the compound formed, but rather upon the effect on the solution resulting from this interchange of ions; an undesirable ion is removed from solution and is replaced by a desirable one.

Resins are manufactured as tiny plastic beads of organic polymers. They are classed as "strong" or "weak". A weak resin is effective for removing strongly ionized substances such as gadolinium nitrate. A strong resin is effective for removing both strongly ionized and slightly ionized substances. An example of a slightly ionized substance is boric acid.

The applications of ion exchange resins are:
- Water treatment plant (WTP): The deionized water conductivity must be low enough to be an effective electrical insulator in the generator stator cooling system. Deionized water is also required as boiler feedwater to minimize corrosion and the buildup of sludge in the boiler.
- Heat transport system: Lithium deuteroxide (LiOD) in the resins are displaced as impurities are absorbed and contribute to alkalinity and to protection from corrosion.
- Moderator system: Ion exchange resins are used to remove acids that may form as a result of radiolysis of air. Any other ions, e.g., added neutron absorbing poisons, are also removed from the moderator by the ion exchange columns.
- Auxiliary systems: Various other systems utilize ion exchange resins for on-going purification. These include end shield cooling, liquid zone control, recirculated cooling water, irradiated fuel bay cooling and stator cooling water.

2.6 Filtration

Filtration is the process of passing a fluid containing suspended matter through a suitable porous material in such a manner as to effectively remove the suspended matter from the fluid. The filtering process may be via mechanical blockage of particles larger than the pores of the filter, or by adsorption.

Filtration is an important step of the water treatment plant where high purity water is prepared for a number of nuclear plant applications. Sand and activated charcoal filters are used in this application.

In heavy water applications, insoluble corrosion products are removed by cartridge filters in the purification circuit. Here, the primary objective of the

filtration process is to remove activated and potentially active particles from the heavy water, thus reducing radiation hazard from their deposition on system surfaces.

2.7 Corrosion

Corrosion is the process of metal wastage produced by chemical action (oxidation). Corrosion of metals is caused by oxidizing agents, acids bases or galvanic action.

The effect of solution pH on the rate of corrosion depends on the metals involved. For example:
- A pH range of 10 - 12 minimizes the corrosion of iron; the corrosion rate rises outside this range.
- Metals with oxidation potentials greater than 0 are vulnerable to simple acid (low pH) attack.
- Zirconium alloys have high corrosion resistance to both acidic solutions, and alkaline solutions up to pH 13.
- A neutral pH is best for stainless steel and copper alloys and is absolutely essential for aluminium.
- Nickel alloys such as monel and inconel demand a high pH environment.

The major types of corrosion are uniform corrosion, galvanic corrosion, stress corrosion cracking, corrosion fatigue, erosion corrosion and microbiologically induced corrosion.

2.7.1 Uniform corrosion

This common form of corrosion is characterized by uniform attack over the entire exposed surface. Corrosion products may form a protective layer on the metal that decreases the rate of corrosion, for example, magnetite on the carbon steel in the HTS. The original design criteria normally account for the extent of material wastage. Chemical control and the use of protective coatings are the most commonly used protection against uniform corrosion.
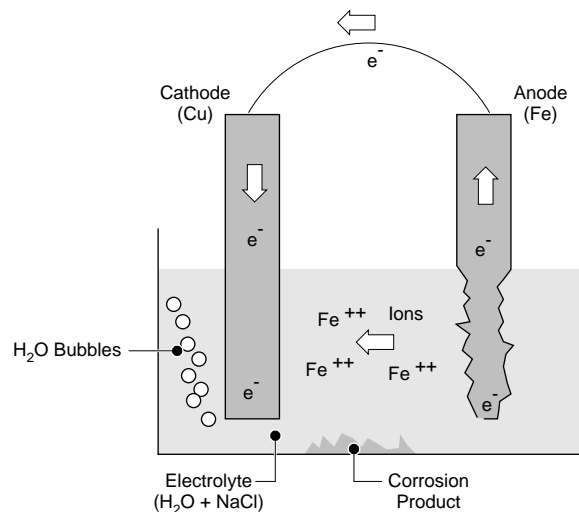
2.7.2 Galvanic corrosion

A galvanic cell consists of two dissimilar metals in an electrolyte and also having external electrical contact with each other. At least one of the metals must have a positive oxidation potential (measured in volts, oxidation potential represents the ease with which metals loose their outer electrons. The greater the oxidation potential, the more reactive is the metal). A potential difference due to the different oxidation potential of the metals causes electrons to flow in the circuit. Oxidation (corrosion) occurs at the anode where metal is removed. Reduction (of electrolyte) occurs at the cathode as shown in Figure 2.3.
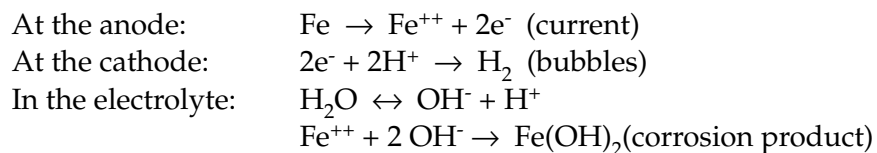
The determination of anode and cathode in a galvanic cell depends upon the oxidation potentials of the two metals. The anode always has a higher oxidation potential than the cathode.

Figure 2.3:

A typical galvanic cell

Reactions

At the anode:	$Fe \rightarrow Fe^{++} + 2e^{-}$ (current)
At the cathode:	$2e^{-} + 2H^{+} \rightarrow H_2$ (bubbles)
In the electrolyte:	$H_2O \leftrightarrow OH^{-} + H^{+}$
	$Fe^{++} + 2\,OH^{-} \rightarrow Fe(OH)_2$ (corrosion product)

Galvanic corrosion occurs when two dissimilar metals are in electrical contact in an electrolytic solution. Recall that the anode, i.e., the metal having the highest oxidation potential, always corrodes. Also, if the cathode metal surface area is large compared to the anode, the rate of corrosion of the anode increases in order to accommodate the increases current flow resulting from increased cathode area. Galvanic corrosion is therefore minimized by selecting metal couples having similar oxidation potentials, by isolating dissimilar metals from each other, and also by isolating the anodic metal from the electrolyte. An example of isolating dissimilar metals from each other is the use of plastic isolating bushing in a fitting which joins two types of metal pipe, e.g., copper and steel. An example of isolating the anodic metal from the electrolyte is the formation of an impervious magnetite layer on the surface of carbon steel pipe in the HTS. Also, if all moisture is removed, there is no electrolyte and a galvanic cell cannot exist.

2.7.3   Stress corrosion cracking

Stress corrosion cracking is the formation of cracks where localized corrosion has combined with steady tensile stresses in the metal to cause the damage. This effect has been seen in low pressure turbine disks and blade roots and also in boiler tubes. The hostile electrolytic environment can attack particular metals or alloys, for example, chloride and stainless steels. Excessive CC can cause failure, typically sudden and without warning.

The source of tensile stresses may originate during manufacture or from in-service conditions. Lowering tensile stress by decreasing applied load, stress

relieving or introducing residual compressive stress through procedures will minimize CC.

Corrosion cracking is also minimized through chemical control of the water in the system, or applying coatings to reduce or eliminate contact between the metal and the hostile ion.

2.7.4 Corrosion fatigue

Corrosion fatigue is characterized by a wedge-shaped crack in an area subjected to cycling stresses in a corrosive environment. The crack usually begins at a pit or surface irregularity and propagates transgranularly. Metal failure occurs at a lower stress level and after fewer cycles than for non-corrosive conditions. The combined effect of corrosion and fatigue is greater than the sum of their individual damages.

2.7.5 Erosion corrosion

Erosion corrosion is the acceleration of corrosion owing to relative movement of the corrosive fluid and the metal surface.

It is characterized by grooves, waves and valleys in the metal surface, and short time periods to unexpected failures. Erosion corrosion is promoted by high fluid velocity, turbulent flow and the impingement of these high-velocity fluids on metal surfaces, for example, at elbows in pipelines.

Erosion corrosion is obviously minimized by reducing fluid velocities, promoting less turbulent flow and by the avoidance of sharp changes in flow direction.

2.7.6 Microbiologically induced corrosion (MIC)

This is corrosion involving the action of bacteria on metal surfaces, most commonly in stagnant water. Slime-forming bacteria are aerobic and thrive in most cooling-water systems. As they metabolize dissolved oxygen from the water, they create an anaerobic environment at the metal surface. Anaerobic bacteria can then attack the metal surface.

Some bacteria can oxidize or reduce metal species directly, for example Fe^{II} to Fe^{III}. The ferric compounds precipitate in pipes. Concentration gradients form under these deposits, resulting in corrosion. Other bacteria can reduce ferric iron to the more soluble ferrous form. This strips off the ferric compounds which normally stabilize the surface of mild steel, leaving it reactive. Corrosion is thus accelerated. Other bacteria can metabolize chromium, thereby corroding stainless steels.

A major factor in minimizing MIC is the elimination of stagnant water. A clean metal surface with sufficiently high fluid velocities will also prevent bacteria from establishing a foothold.

2.7.7 Corrosion control

Three corrosion control methods used in nuclear generating stations are:
(a) Coatings
(b) Chemical Control
(c) Control of MIC

a) Coatings

Coatings are widely used for corrosion control, with the general approach being to isolate the metal from the electrolyte. Paint and a wide variety of synthetic coatings (epoxy, resins, plastics) are applied directly.

b) Chemical Control

The objective of chemical control is to promote and maintain a desirable environment which minimizes corrosion. This involves:

• Removing corrosives before they enter the system

    The water treatment plant removes a major proportion of ions such as chloride, sulphate, silica, calcium and magnesium which are hostile to the feedwater circuit. Nitrogen blanketing is used to minimize oxidation by excluding air and oxygen from systems such as the ECI when posed, or the HTS when drained.

• Eliminating corrosives which gain access to the system or are generated within it.

    Oxygen which enters the feedwater circuit through air in-leakage or dissolved in fresh makeup is removed using both physical techniques such as deaerators and chemical techniques such as scavenging with hydrazine. Boiler blowdown is used to remove both dissolved and suspended solids from the boiler. Removal of the former lowers the concentration of undesirable ions in the boiler. Unfortunately, however, removal of suspended solids is very inefficient. This leads to the major objective on the secondary side of minimizing corrosion, and transport of corrosion products to the boiler.

    Acids of nitrogen generated via radiolysis within the moderator cover gas system are removed from the moderator D_2O by ion exchange, to prevent corrosion and especially to prevent enhanced radiolysis.

• Inhibiting corrosion by adding chemicals which react with the corrosive agent

    Neutralizing amines (morpholine or ammonia) are added to the condensate return to neutralize the acidity produced by any ingress of carbon dioxide, in addition to provide an alkaline medium which minimizes corrosion of the system metals.

    A further example of a desirable chemical environment is the alkalinity level

maintained in the heat transport system. Its careful control minimizes dissolution of the magnetite layer on carbon steel surfaces, as well as corrosion of system metals.

c)   Control of Microbiologically Induced Corrosion

A major factor in controlling MIC is to prevent it by eliminating the conditions which encourage the growth of bacteria. Raw water in populated areas is a particularly good medium for bacteria growth. Raw water must therefore be chemically treated to kill existing bacteria. It must also be filtered to reduce available nutrients. Metal surfaces must be kept clean.

Where water is being recirculated, e.g., through heat exchangers, a pH greater than 10.5, and the exclusion of air help minimize bacteria growth. High velocity flows also prevent bacteria from settling out and forming colonies.

Large tanks of stagnant water, e.g., the irradiated fuel bays of the demineralized water tanks, are very prone to bacteria growth. Control is by chemical treatment and filtration.

If bacteria colonies become established in a system, either mechanical cleaning or very strong chemical treatment is required to remove them.

3   Heat Transport System (HTS)

The heat transport system is a heavy water system that is in a radiation flux only while the water is passing through the reactor core. It is a closed system with temperature and pressure approaching 9 MPa and 300°C, respectively. The flow rate in a large reactor is ≈ 25kg/s per channel. The pressure in the reactor outlet headers is controlled by a pressurizer connected to the outlet headers at one end of the reactor.

Figure 3.1:
Heat transport pressure and inventory control system
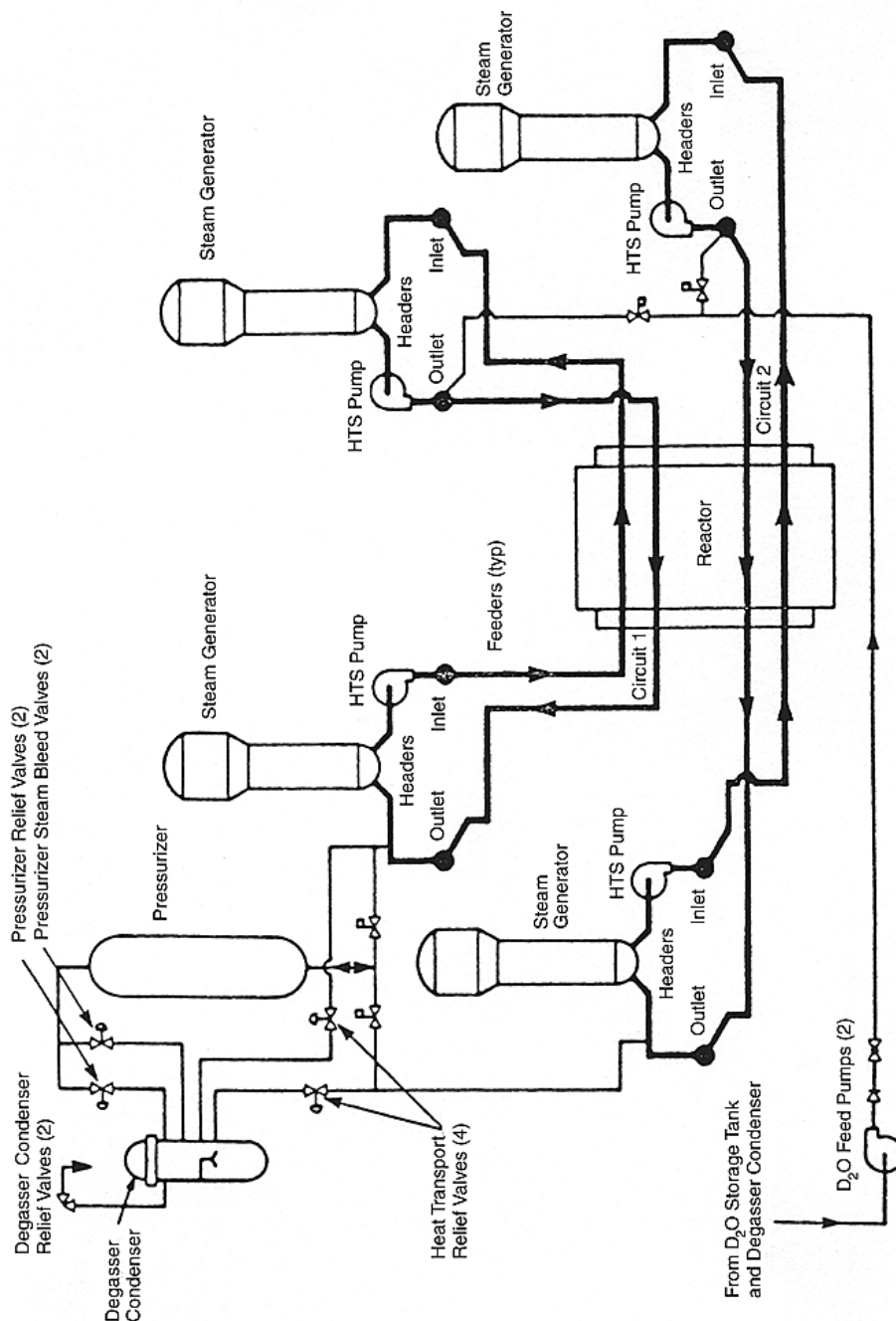
3.1   Objectives of chemical control of the HTS

The primary objective of chemical control of the HTS is to minimize the corrosion of the various system components including:
*   zirconium alloy pressure tubes and fuel sheath,
*   carbon steel piping, feeders, headers and pressurizer and
*   monel, inconel or incoloy boiler tubes.

Carbon steel is used for reason of high strength and economy, but it is vulnerable to corrosion. Its use demands careful control of the HTS D_2O.

Chemical control of the HTS has two other major objectives. The first of which is to control radiation fields in the HTS. This is achieved by minimizing corrosion and therefore minimizing the amount of suspended and dissolved corrosion products subject to neutron activation. Also, by reducing the likelihood of fuel sheaths failure, the possibility of fission products such as I-131 escaping into the water are minimized. Another objective is to eliminate the condition which can give rise to zirconium hydride formation. This objective is reached by controlling the amount of dissolved deuterium.
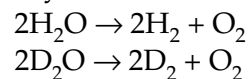
Figure 3.2:
*An overview of heat transport system chemistry*
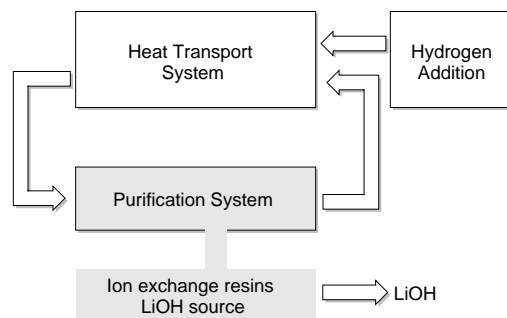
3.2 Dissolved gases

The corrosion rate of the zirconium alloy core materials is very dependent on the oxygen content of the coolant in-reactor. Water (and heavy water) undergo radiolysis in the core according to the following reaction:

$$2H_2O \rightarrow 2H_2 + O_2$$
$$2D_2O \rightarrow 2D_2 + O_2$$

yielding oxygen. Therefore it is very important to control this oxygen production and at the same time to control the corrosion and hydriding of the zirconium alloys.

In CANDUs, radiolytic production of oxygen is countered by maintaining 3-10 cm^3 D_2/kg D_2O as dissolved gas in the coolant. Note that this is done conveniently by adding hydrogen gas. Because of the neutron flux, H_2 in the water carried into the reactor exchanges very quickly with the Deuterium of D_2O according to the following equation:

$$H_2 + 2D_2O \rightarrow D_2 + 2HOD$$
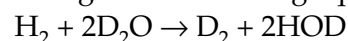
This does not create any chemical problems and the economic penalty associated with downgrading is less than the cost of obtaining D_2 for hydrogen addition. The addition of too much H_2 would increase the risk of hydriding in the fuel sheath and pressure tubes.

The analysis for dissolved D_2 is less difficult than the analysis for dissolved O_2. Therefore, there is no specification for dissolved O_2.

Since the purpose of the dissolved D_2 is to scavenge O_2, the result of too little dissolved D_2 is too much dissolved O_2. Oxygen corrodes both zirconium and carbon steel, and can convert protective oxide layers into porous oxide layers. This allows attack of the underlying metals by the water, producing oxides and deuterium ($Zr + 2D_2O \rightarrow 2D_2 + ZrO_2$). In the case of the zirconium alloys, some of the D_2 resulting from this corrosion can diffuse into the metal, forming brittle zirconium hydride. This in turn can lead to hydride cracking of the metal.

3.3 Alkalinity

At reactor operating temperatures, the pH of the water has a greater effect on corrosion of out-core materials than on corrosion of in-core zirconium alloys, though the effect is slight as far as integrity of components is concerned. The effect of pH on corrosion becomes more important at lower temperatures, with general corrosion of carbon steel becoming unacceptable at neutral or acidic conditions at temperatures below 150°C. Hence, the pH should be kept above 10 at all temperatures, and especially when the reactor is shut down.

Beside being essential for controlling corrosion, alkalinity is important for minimizing activity transport. Corrosion in the HTS leads to dissolved or suspended products which become activated. Early on in the CANDU development program, experiments in the loops in the NRX reactor and elsewhere demonstrated how crud deposited on fuel sheaths; levels of crud suspended in the coolant and deposits on fuel were kept low when the pH was maintained above about 10. More recent experiments have identified the solubility of magnetite (Fe_3O_4), the principal constituent of crud in CANDUs, as the controlling parameter in activity transport. Above pH 9.8 the solubility of magnetite increases with temperature over the range of temperature of an operating CANDU as shown in Figure 3.3. Thus, crud deposited on fuel will tend to dissolve as the coolant is heated during its passage through the core. Because the dissolution keeps deposits thin, the production rate of radioactivity in the core is kept low, and the removal by dissolution and subsequent distribution around the circuit is minimized. If the high pH coolant boils in the core, the resulting increase in alkalinity at boiling sites on the surface of the fuel sheaths is another mechanism for promoting dissolution of crud and therefore thin deposits.

Figure 3.3:
Solubility of magnetite versus temperature for different pH (25°C) values
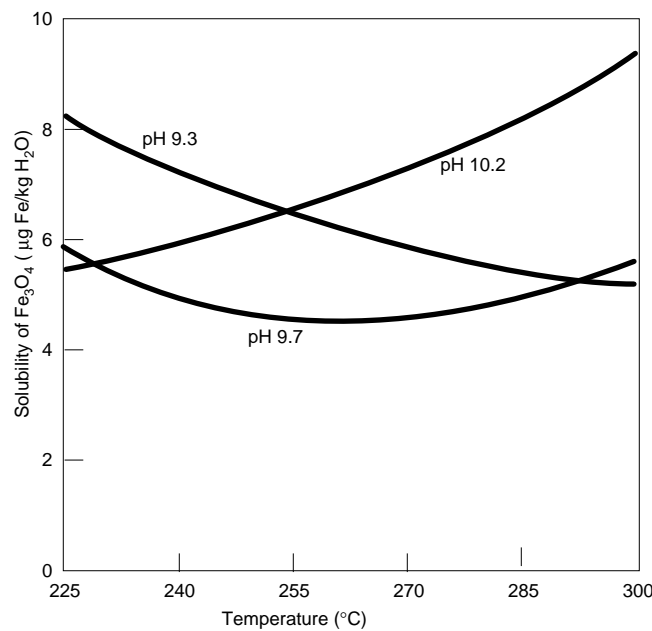
The effects of the alkalinity of the coolant on out-core surfaces also are important for activity transport. A high pH minimizes corrosion rates and, therefore, crud production rates, while the corrosion rate and oxide solubility are directly related to the activation rate of surfaces. On carbon steel piping the corrosion rate controls the activation rate, while on boiler tubing the precipitation of magnetite by cooling controls the activation rate.

The bases that could be used for chemistry control are the hydroxides of Li, Na, K and NH_3. Li is preferred because it transmutes in-core to tritium at innocuous levels compared with those produced by the direct neutron capture of the deuterium, whereas Na and K form undesirable radionuclides. The source of lithium deuteroxide is the ion exchange resins of the water purification circuit supplemented if necessary by LiOH (in D_2O) additions. NH_3 is a weaker base than Li and would have to be used in large quantities in the deuterated form, though it does have the advantage of suppressing radiolysis at the same time, particularly in boiling cores.

The recommended apparent pH range for the heavy water coolant of CANDU 600 reactors is 10.2 - 10.8. Note that the corresponding specifications for the lithium concentrations are 0.35 - 1.4 mg/kg, and the corresponding conductivities are 0.9 - 3.6 ms/m. If impurities are present, the correspondence of these parameters may be upset. For example, dissolved CO_2 will tend to reduce both the pH and the conductivity making the maintenance of the required alkalinity range difficult.

3.4   Impurities

Ionic impurities are controlled by their removal by the ion exchange resin. The main impurities are:

- **Chloride ions**. They can induce stress corrosion cracking of stainless steel components and also lead to pitting. Their source is generally the ion exchange resin, especially when hot water passes through it. The use of "low chloride" ion exchange anion resins is therefore recommended.
- **Fluoride ions.** They can induce rapid corrosion of zirconium alloys. A potential source could be teflon valve packings or sealing tapes.
- **Carbonate ions**. They reduce the effectiveness of the alkalinity control. Their source is organic material (e.g. oil, ion exchange resins and temporary protective coatings) which forms carbon dioxide when irradiated in the presence of water.

Since crud levels in the coolant contribute directly to the production of radiation fields around the circuit, it is important to keep them low. This is accomplished by:

- Continuous steady operation with no thermal hydraulic or chemical transients within the HTS, thus preventing crud bursts in the system.
- Operating at a high pH (10.2 - 10.8). This also minimizes the corrosion rate and deposition of corrosion products in the reactor core.
- Using the maximum possible purification flow when crud concentrations are high, for example during transient conditions of operation.

Fission products contribute directly to system radioactivity and therefore the radiation fields and occupational doses of radiation. Their concentrations are reduced by:

- The location and removal of the defective fuel bundles.
- Purification by ion exchange which will remove and control soluble fission products (for example, iodine and cesium). Most other fission products deposit rapidly on crud and system surfaces. Their control is the same as for radioactive crud control.

Table 3.1:

Chemistry control parameters of the PHT circuit

Parameter	Permissible Range (Optimum Values)	Notes
pH (25°C) (apparent pH of D_2O)	10.2 to 10.8	Controls corrosion and activity transport
Li mg Li/kg D_2O	0.35 to 1.4 (> 0.35)	
Conductivity mS/m (25°C)	0.9 to 3.6 (> 0.9)	Conductivity, pH and Li must be considered together for effective control
D_2 mL (STP)/kg D_2O	3 to 10 (as low as possible within range to meet low dissolved O_2)	Oxidizing conditions if too low; possible hydriding of Zr alloys if too low or too high
O_2 μg/kg D_2O	< 10 (undetectable)	Controlled by level of dissolved D_2
Cl^- mg/kg D_2O	< 0.2 (< 0.05)	Could cause stress corrosion cracking of austenitic materials - hot operation not permitted at greater than 3 mg/kg D_2O
F^- mg/kg D_2O	< 0.1	Aggressive to Zr alloys - unlikely to be found
CO_2 mL (STP)/kg D_2O	< 0.5	Formed from organic impurities
Crud mg/kg D_2O	< 0.1 (< 0.001)	High crud levels increase activity transport
Fission products	< 7 mCiI-131/kg D_2O (< 10 μCiI-131/kg D_2O)	Regulatory limit Typical Operation Limit

4   The Moderator

Whenever there are liquids and gases in contact with metals, as in the moderator system, corrosion and other chemistry related concerns will exist. Figure 4.1 illustrates that there may be corrosion concerns for the calandria body, calandria tubes, reactivity mechanisms, liquid zone tubes, cleanup circuits, heat exchangers, and any other metal surfaces exposed to the moderator.

Figure 4.1:
Chemistry concerns in the moderator circuit
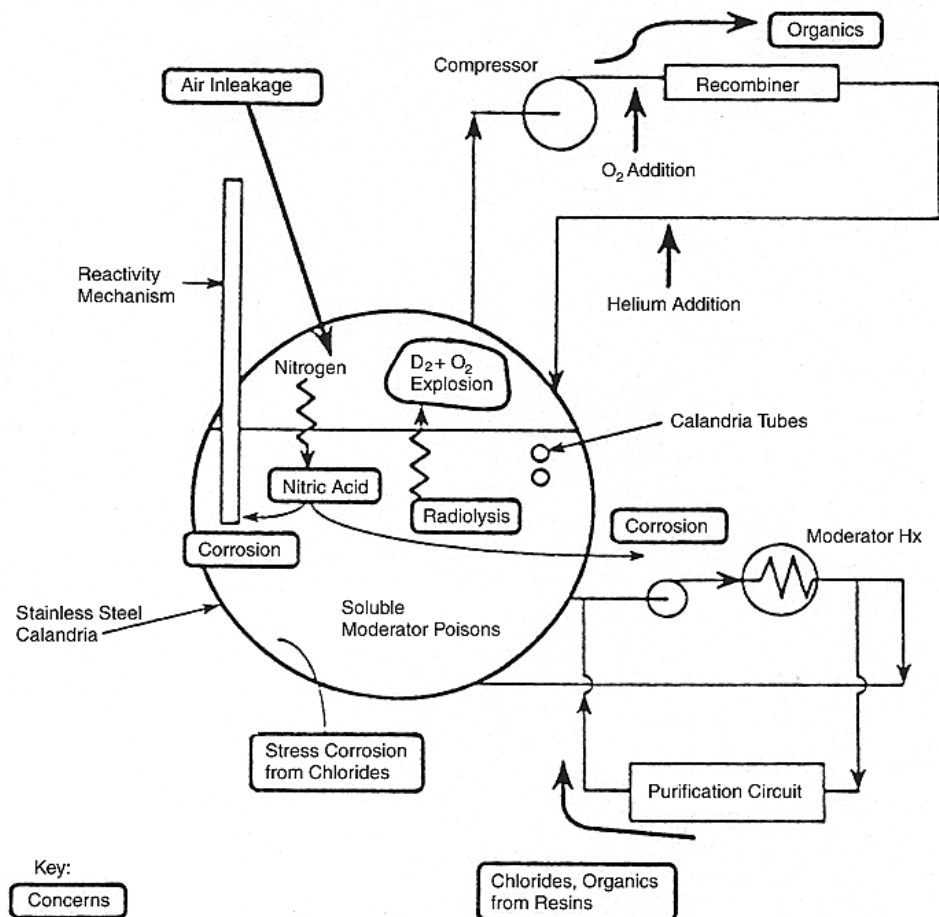
The moderator system is also a concern because of the gas space above it. The high radiation fields within the calandria can cause the moderator D_2O molecules to decompose into D_2 and O_2 gases. Note that the bulk of the moderator is exposed to radiation fields all of the time the unit is in operation, and to some continuing gamma fields after shutdown. In the correct proportions, D_2 and O_2 form an explosive mixture. In the case of the moderator cover gas, the risk of explosion is of more concern than the effects of corrosion.

4.1   Objectives of chemical control of the moderator circuit

The primary objective of chemical control of the moderator is to minimize the radiolysis of D_2O. This is essential in order to minimize the production of gaseous D_2 and O_2 and thereby prevent any possibility of a D_2/O_2 explosion in the moderator cover gas.
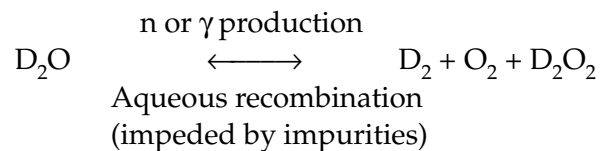
Preventing corrosion of system components is another objective of chemical control of the moderator system. Since the calandria is stainless steel, and is therefore relatively immune to corrosion, the main concern is with respect to

corrosion of the heat exchangers (if copper alloys were used in their construction) and associated equipment, e.g., pipes, pumps, valves. The major source of corrosion is nitric acid formed from the oxides of nitrogen produced by radiolysis of nitrogen from air which has entered the system. The nitric acid lowers the pH of the moderator, promoting corrosion, and worst of all, also enhances the radiolysis of the D_2O.

Minimizing corrosion also minimizes the creation and spread of activated corrosion products which can cause high radiation fields around moderator system equipment.
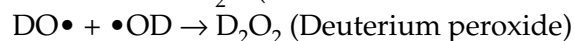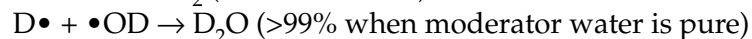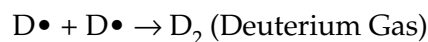
4.2 Radiolysis in the moderator

Radiolysis is the chemical decomposition of molecules by gamma rays (γ) and fast neutrons (n). Since the moderator is continually bombarded by this radiation, radiolysis of the moderator D_2O cannot be prevented. The following unbalanced equation simplifies and summarizes what is actually a complex sequence of intermediate reactions involving molecules, atoms, ions, electrons and free radicals. Note that it also shows that aqueous recombination occurs and is impeded by impurities in the moderator.

$$D_2O \quad \overset{\text{n or } \gamma \text{ production}}{\underset{\substack{\text{Aqueous recombination} \\ \text{(impeded by impurities)}}}{\longleftrightarrow}} \quad D_2 + O_2 + D_2O_2$$

Free radicals are groups of atoms containing an unpaired electron; they are very reactive. The free radical is shown by the element symbol and a raised dot, e.g., $D\bullet$, $\bullet OD$. The raised dot represents the single (unpaired) electron of the free radical. Thus $D\bullet$ is a deuterium atom, $\bullet OD$ is a deuteroxyl radical and both are free radicals.

These free radicals can combine in any of three ways:
  $D\bullet + D\bullet \rightarrow D_2$ (Deuterium Gas)
  $D\bullet + \bullet OD \rightarrow D_2O$ (>99% when moderator water is pure)
  $DO\bullet + \bullet OD \rightarrow D_2O_2$ (Deuterium peroxide)

D_2O_2 is a concern because it is an oxidizing agent which can attack the organic resins in the ion exchange columns.

Figure 4.2 illustrates radiolysis in the moderator/cover gas system. D_2 and O_2 gases can stay dissolved or can come out of solution into the cover gas. Alternatively, $D\bullet$ and $\bullet OD$ radicals can recombine spontaneously in the moderator to form D_2O. This is called "aqueous recombination" and is also illustrated in Figure 4.2. Some impurities in the moderator interfere with aqueous recombination.

Figure 4.2:
Radiolysis in the moderator system
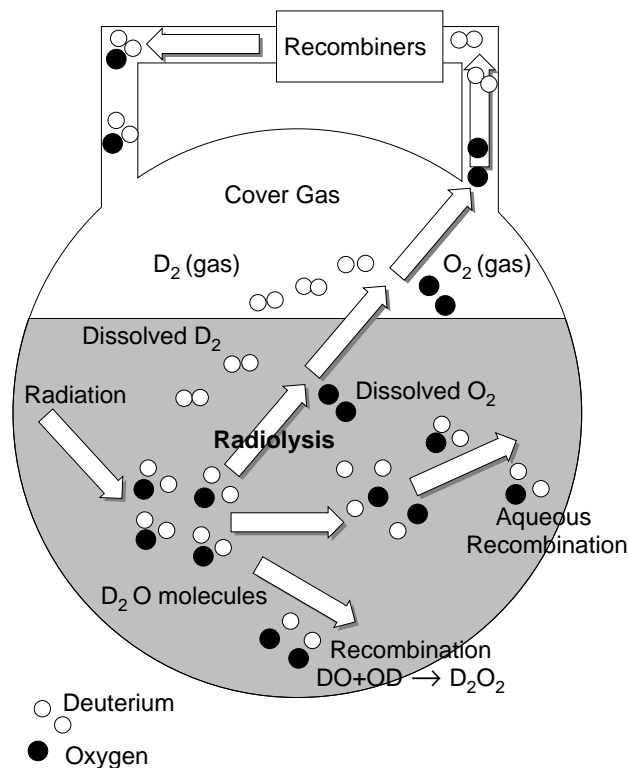
The presence of excessive amounts of D_2 (and O_2) in the cover gas is a cover gas deuterium excursion, commonly called a deuterium excursion. Such excursions can occur very quickly.

An important feature to note about deuterium excursions is that they can occur not only from an increase in the radiolysis rate, but also from a decrease in the aqueous recombination process. Deuterium excursions can also occur if some other factor changes to cause the gasses dissolved in the moderator to come out of solution more rapidly than before.

At steady power, equilibrium is reached between the production and recombination of D_2 and O_2 in the moderator. During power increases, recombination may be less than production of D_2 and O_2 and a cover gas deuterium excursion may occur.

4.3 Chemical controlled parameters

The purity of the moderator water is controlled by ion exchange and is monitored using on-line conductivity meters and routine grab samples.

Figure 4.3:
Main moderator system
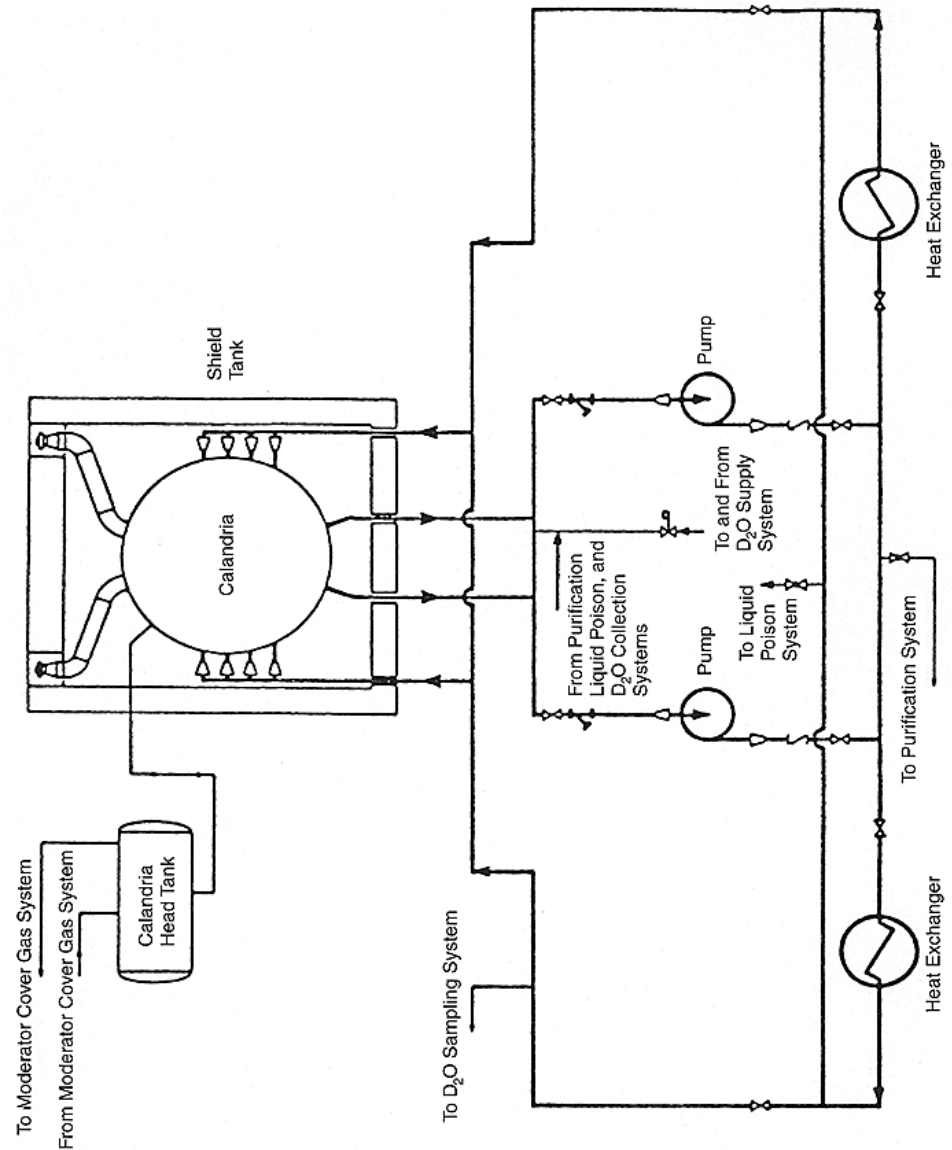
The cover gas D_2 and O_2 concentration is controlled by recombiners, oxygen addition, control of radiolysis, and purging, if necessary, with helium. D_2, O_2 and N_2 concentrations are monitored at the inlet and outlet of the recombination units, via on-line gas chromatographs.

Figure 4.4:
Moderator cover gas system
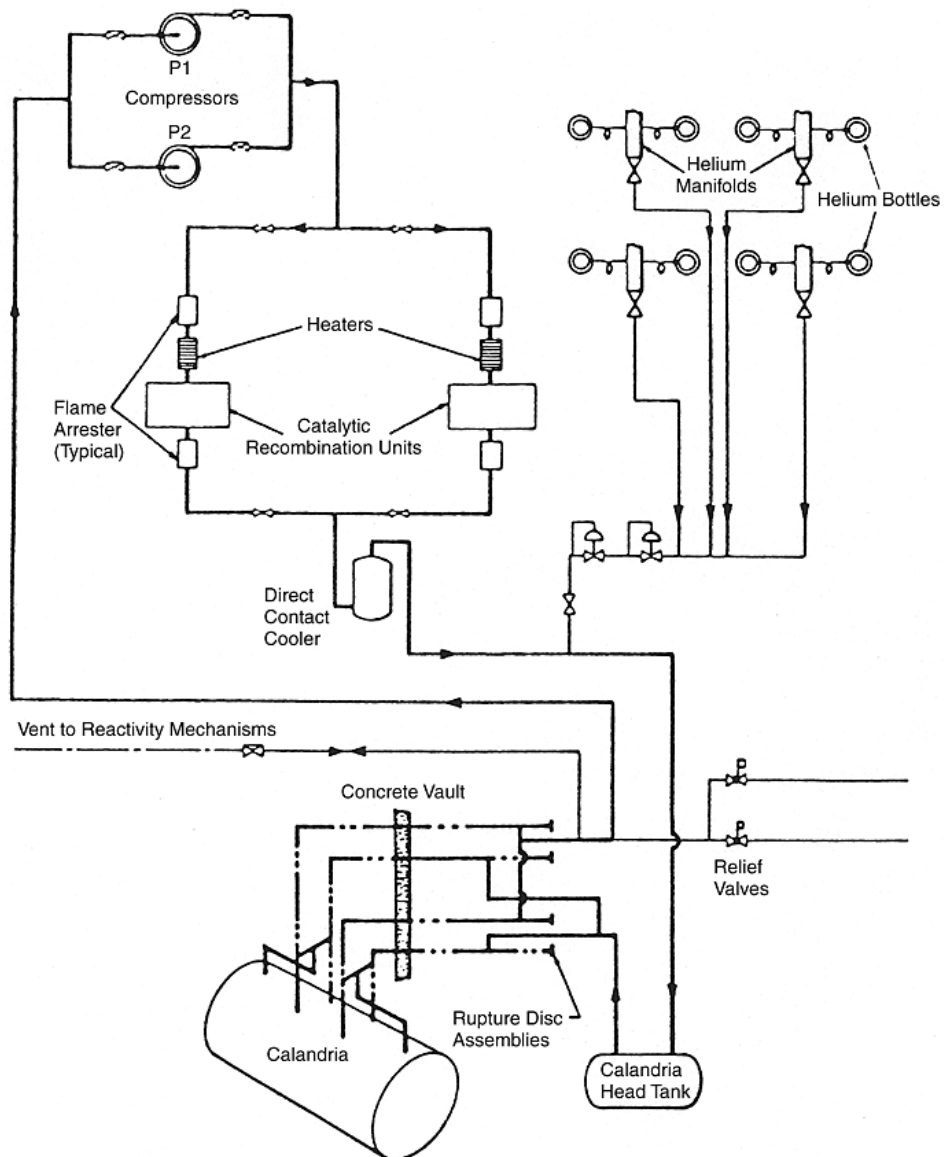
4.3.1   Moderator conductivity

The desired operating condition for moderator conductivity is ALARA (As Low As Reasonably Acceptable), because a low conductivity indicates high moderator water purity, which in turn will minimize the production of D_2 and O_2 radiolysis.

Many soluble impurities interfere with aqueous recombination, and thereby have the effect of accelerating radiolysis. Most water impurities in a power station are ionic. Thus conductivity is usually a good indication of water purity; for the moderator it is in fact excellent.

The situation with respect to moderator poisons is as follows:

boron:

boric acid contributes little to conductivity, and not at all to the radiolysis of water.

gadolinium:

although the gadolinium ion does not affect radiolysis, nitrate does. The relationship between salt concentration and conductivity is linear.

Moderator conductivity is the only control variable of the moderator. It is controlled, using ion exchange columns, to a specification of ≤ 0.1 mS/m.

4.3.2 Moderator pH

Conductivity increases as the pH of the moderator moves away from neutral, in either direction. Consequently, the desired operating condition to minimize conductivity, and therefore radiolysis, would be close to pH 7. A neutral pH is also desirable to minimize corrosion of moderator system components such as pumps and heat exchangers.

Moderator pH is controlled only in conjunction with conductivity using ion exchange columns to remove impurity ions, and replace them with OD^- and D^+ ions, i.e., D_2O. If the conductivity of the moderator is held very low it consists of essentially pure D_2O which ionizes very slightly. Therefore, because of the lack of ions, the pH meter will read erratically although the moderator is essentially neutral, i.e., no OD^- or D^+ ions present. Thus when the moderator conductivity is very low, the pH meter is unusable but the pH is accepted as 7. Therefore, pH is analyzed on power only for troubleshooting high conductivity.

Again, an exception to the above occurs whenever gadolinium nitrate is present in the moderator D_2O. Gadolinium nitrate is the salt of a strong acid and a weak base and therefore a solution containing it has an acidic pH, i.e., less than 7. The pH specification during the guaranteed shutdown state is 4 - 6.

4.3.3 Other parameters

Free deuterium in the moderator cover gas appears first dissolved in the moderator. Deuterium excursions occur when D_2 migrates quickly into the cover gas. If the **dissolved D_2** concentration is low (typically 3 cc/kg D_2O), the likelihood of an excursion is small.

Table 4.1:

Chemistry control parameters in the moderator circuit

Parameter	Permissible range (Optimum value)	Notes
pH (25°C) (apparent pH of D_2O)	4.5 to 7.0 (< 7.0)	System corrosion if low, Gd precipitation is high
Conductivity (mS/m)	0.3 (< 0.2 depending on poison concentration)	High values indicate impure moderator and rise of D_2 excursions
D_2 (mL(STP)/kg)	5 (< 2)	Dissolved D_2 promotes cover gas excursions
Cl^- (mg/kg)	0.2 (< 0.1)	Chlorides promote stress corrosion cracking of stainless steel
F^- (mg/kg)	0.1 (< 0.1)	Fluorides corrode zirconium alloys rapidly

The concentration of D_2 in the moderator must be kept as low as possible. The alarm level is 2% (see table 4.1). At a concentration of 6% D_2 and 3% O_2, a burn occur if there is a spark. Based on H_2 measurements, there is 100% probability of a burn at 8% D_2, 4% O_2 should an ignition source exist. The production of D_2 is controlled by minimizing radiolysis. Also D_2 is removed from the cover gas by recombining it with O_2 in the recombination units (Figure 4.4). Oxygen is added to the cover gas for this purpose. D_2 may also be removed by purging with helium.

The desired **oxygen** content in the moderator cover gas is no more than that required to combine with D_2, i.e., one oxygen molecule per two deuterium molecules. Control of oxygen is by addition of small batches of oxygen to the cover gas at the recombiners inlets.

Any **chlorides** in the moderator will be removed by fresh ion exchange resins. Control of **nitrates** is also achieved by removing them using ion exchange resins.

Fluoride is an impurity in the gadolinium nitrate poison. Fluorides ions cannot be removed by ion exchange because they are smaller than hydroxyl ions, but are removed by the on-line upgrader distillation towers.

5   Steam/Feedwater System

The steam/feedwater system comprises the boiler, turbine, condenser, condensate extraction pump, LP feedheaters, deaerator, boiler feedpumps and HP feedheaters as shown in Figure 5.1.

Figure 5.1:

The condensate, boiler and feedwater system
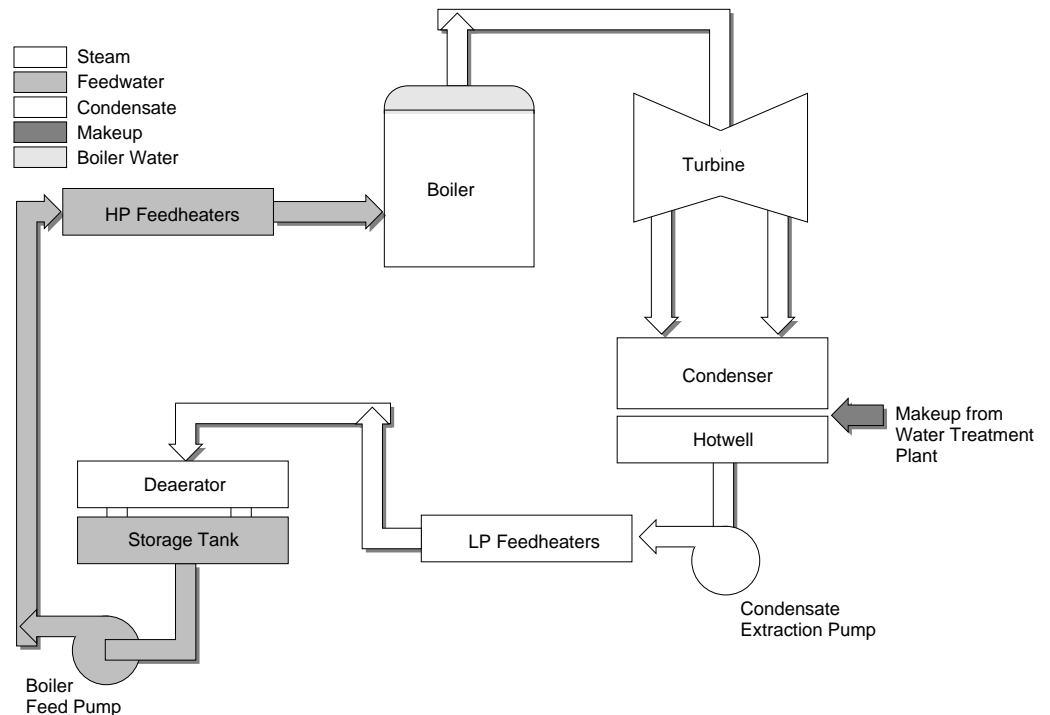
Good chemical control of the steam/feedwater system ensures minimum corrosion of the system hardware, the boiler tubes being the most critical. It also impacts directly on the control of other operational concerns of this system, e.g., boiler tube scale, and tubesheet and tube support plate sludge and deposits.

This control commences with the use of makeup water prepared to a high purity standard in the water treatment plant (WTP). Makeup describes the WTP product which enters the circuit at the condenser to replenish losses and maintain the proper fluid balance in the circuit. At the point of addition to the circuit and elsewhere, chemical additives are introduced to establish operational parameters best suited to the chemical control objectives of the system. An in-line chemical monitoring system, supported by chemical control laboratory grab sample analysis, ensure these operating conditions are optimized.

5.1 Objectives of chemical control

The primary objective of chemical control of the secondary heat transport system is to minimize corrosion of the entire system by controlling pH and the concentration of oxygen and dissolved ionic impurities. In addition to component wastage, such corrosion is undesirable because of the resultant transport of corrosion products to the boilers.

Another major objective of chemical control is to minimize sludge and scale formation in the boiler.

In the following, the three sub-system areas of Figure 5.1 are examined in regard to corrosion, scaling, and sludge buildup.

Condensate

The objective of chemistry control of the condensate system, Figure 5.2, is to minimize corrosion of the entire boiler steam and water system by maintaining a suitable pH and removing O_2. Oxygen enters the condensate via air in-leakage to the subatmospheric parts of the turbine/condenser, and via the makeup water.
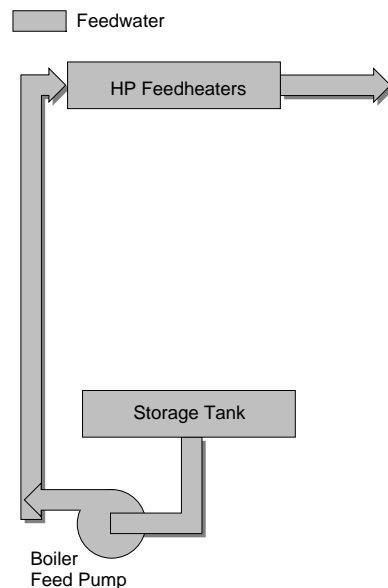
Figure 5.2:

Condensate sub-system
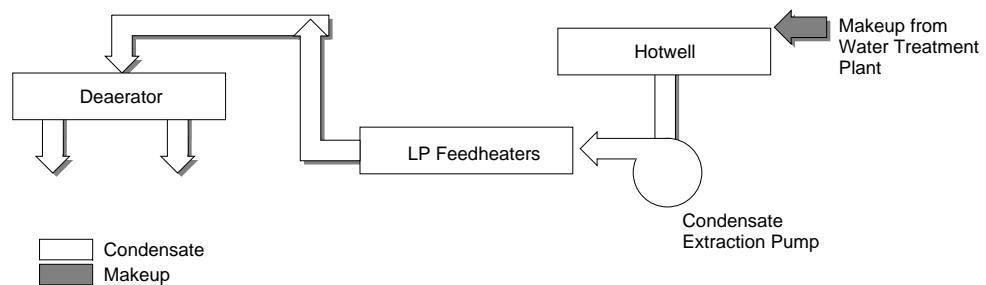
Feedwater

The objective of chemistry control of the feedwater system, Figure 5.3, is to continue to provide protection against corrosion, particularly in the boiler, by maintaining low dissolved oxygen and low impurity levels, minimizing corrosion reduces the quantity of corrosion products entering the boiler. This is very important, because the buildup of sludge can lead to under-deposit boiler tube corrosion at the tubesheet and tube support plates and also impairs heat transfer.
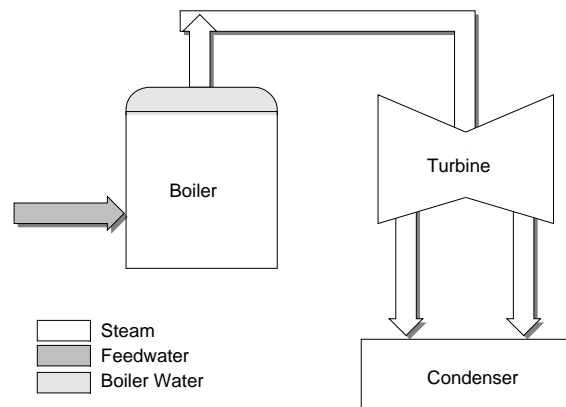
Figure 5.3:

Feedwater sub-system

Boiler

The objective of chemistry control in the boiler system, Figure 5.4, is to minimize the corrosion of boiler tubing and other structural materials. To meet this objective the pH is maintained alkaline and impurity concentrations are kept low.
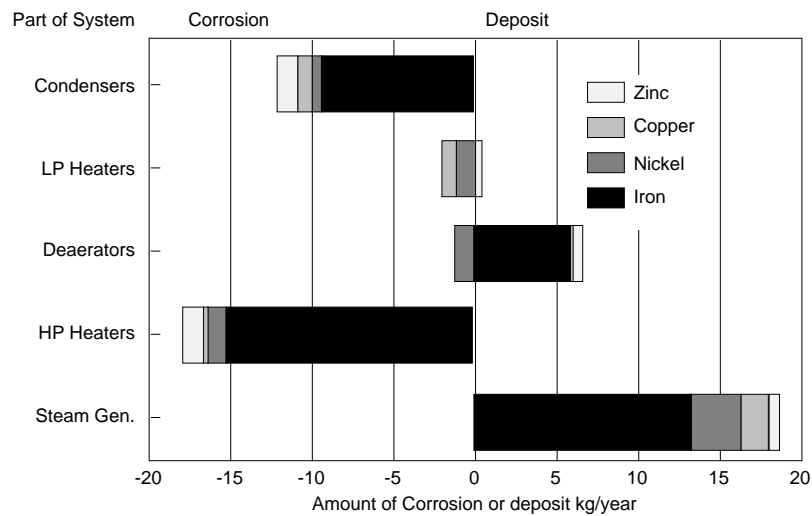
Figure 5.4:

Boiler sub-system

Several problems can arise due to impurities in the boiler water. In particular, sodium, chloride and sulphate above specification can result in tube corrosion. Silica is kept at low concentrations to minimize contribution to scale and sludge in the boiler. Ca^{++} and Mg^{++} ions (which can enter the condensate from the condenser cooling system if condenser tube leaks occur) are another prime contributor to scale and sludge.

The buildup of sludge and corrosion products on boiler tubesheets is also of particular concern, and especially so in the event of condenser in-leakage of WTP upsets. This is because ions such as OH^-, CI^-, Na^+ and SO_4^- can concentrate in the sludge pile or any crevice, by factors of 10^4 to 10^5, thereby further increasing the risk of corrosion of the boiler tubes.

Figure 5.5:

Total transport of corrosion products in G-2 secondary heat transport system

5.2   Sludge and scale formation

The problem due to the presence of sludge and scale is closely associated with the concern for corrosion in boiler water chemical control. As shown in Figure 5.6, boiler scale is the layer of foreign material adhering to the outside of the boiler tubes.

Figure 5.6:

Boiler tube scale and tubesheet deposits
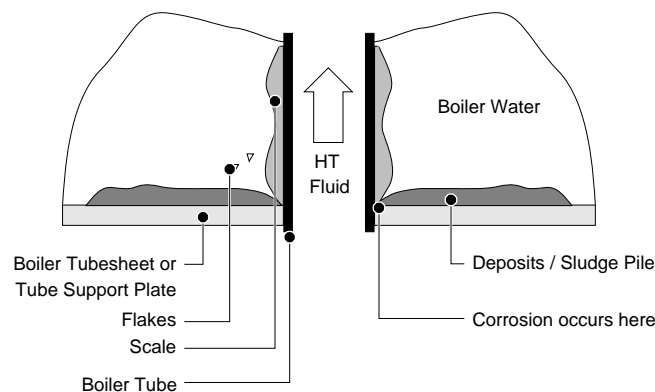
Deposits comprise the particulate material which generally settles in low flow areas of the boiler such as the tubesheet or tube support plate surfaces. Often what was initially scale flakes off boiler tubes to add to these deposits. Deposits and corrosion are closely interrelated, since much of this material originates as corrosion products elsewhere in the feedwater train.

There are two general types of sludge and scale forming substances:
- suspended inorganic solids (particulates) and
- dissolved inorganic material.

5.2.1 Suspended inorganic solids

A major source of this material are the particulates that develop throughout the boiler steam and feedwater circuit from various corrosion processes. Much smaller quantities enter the circuit in fresh makeup, but they do become significant if allowed to accumulate in the boiler. Finally, an acute source of suspended solids is raw water ingress from main condenser tube failures. These are mainly silicates of calcium and magnesium.

The makeup water is normally very pure. Therefore, a high percentage of suspended boiler solids consist of corrosion products, mostly iron oxides and copper metal, transported from pre-boiler locations into the boiler. The copper corrosion products originate from the copper alloy tubes used in the condensers and feedheaters in early CANDU stations only (BNGS-A and PNGS).

5.2.2 Dissolved inorganic materials

Four general categories of dissolved solids found in boiler water are:

(i)   Calcium and Magnesium Salts (Water Hardness)
If there are no condenser tube leaks there should be no calcium or magnesium salts entering the boiler. However, if there are condenser tube leaks, raw water containing these salts, which are primarily bicarbonates of calcium and magnesium, will be drawn into the condensate stream. They will tend to concentrate in the boiler water. Calcium sulphate and magnesium carbonate demonstrate inverse solubility (solubility decreases as temperature increases) and eventually may precipitate. They will collect in the sludge pile or bake onto the boiler tubes. Other calcium and magnesium species, particularly silicates, also occur.

One reaction for this scale formation occurs in the boundary layer surrounding the tubes where the hotter environment promotes bicarbonate decomposition and subsequent deposition of calcium and magnesium carbonate on the tube walls. The following equation is an example of this reaction ; an analogous reaction occurs for magnesium bicarbonate:

$$Ca(HCO_3) \xrightarrow{\text{Heat}} CaCO_3 + H_2O + CO_2$$

Calcium   Scale
Bicarbonate
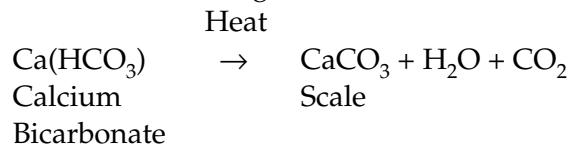
(ii)   Silica
Silica is present in trace quantities in makeup water. On rare occasions, it may also be present as a result of a WTP ion exchanger breakthrough or a condenser tube leak. Silica contributes to tubesheet deposits and boiler scale.

(iii)   Sodium, chloride and Sulphate Ions
These ions enter the system as trace contaminants in the makeup water or as a result of a condenser tube leak. On rare occasions, Na^+ may also be present because of a WTP ion exchange column breakthrough. Sulphate ions form scale,

and all three concentrate in the sludge pile creating a corrosive environment for the boiler tubes.

Figure 5.7:
Steam generator sodium limits during normal operation
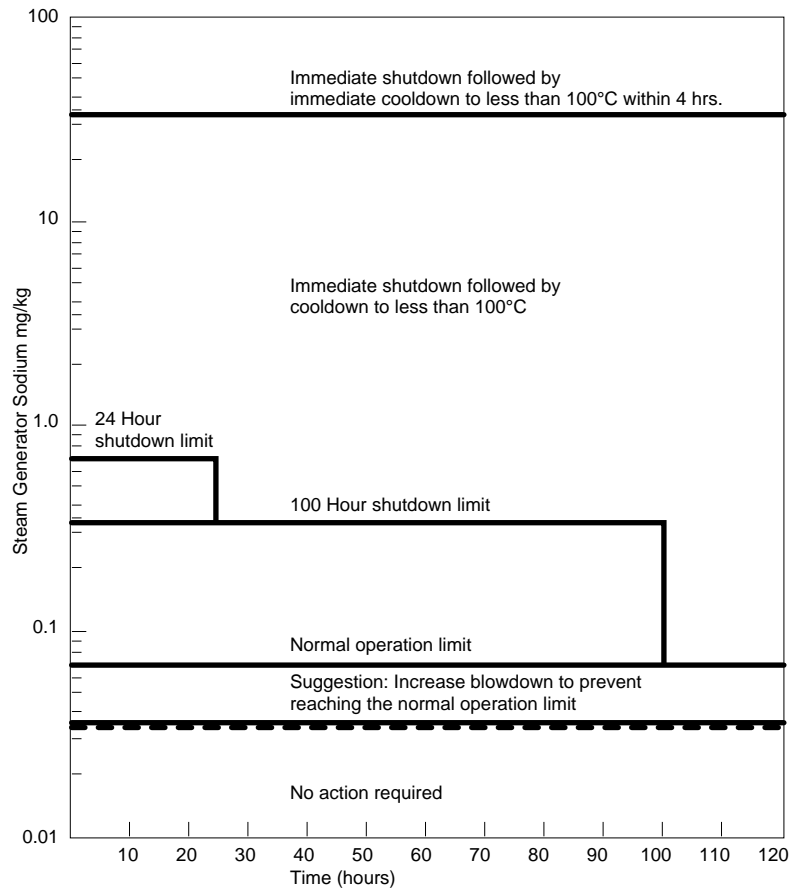
(iv)   Corrosion Products
Dissolved corrosion product species comprise mostly iron and copper compounds, reflecting the materials of construction. Some come out of solution to contribute to sludge piles and scale. Also, oxidizing species such as Cu^{++} and Fe^{++} can aggravate corrosion by elevating galvanic cell voltages.

If main condenser tube leaks develop and raw water enters the system, all categories of dissolved solids become acute, significant contaminants.

Table 5.1:

Sludge and scale-forming substances and their sources

Type		Sources
Suspended Inorganic Solids (Particulates)		Corrosion in boiler steam and feed water system. Ingress of raw water via condenser tube leaks.
Dissolved Inorganics Materials	Ca & Mg Bicarbonates	Raw water via condenser tube leaks.
	Silica	Traces in makeup. WTP IX breakthrough. Condenser tube leaks.
	Na^+, Cl^-, SO_4^{--} Ions	Traces in makeup. Condenser tube leaks. Na^+ from WTP IX breakthrough.
	Corrosion Products	Feed train corrosion.

5.2.3 Dissolved and Suspended Organic Material

A malfunctioning turbine gland seal can permit turbine lubricating oil to enter the condensate, feedwater and boiler system. Raw water entering the system via condenser tube leaks may contain organics. Bacteria growth in the demineralized water system can also contribute to organics addition to the makeup water. Organics may cause corrosion by breaking down into acids such as formic and acetic.

5.2.4 Adverse Effects of Sludge and Scale

If deposits, sludge, scale or entrained particles accumulate in particular areas of the boiler, the probability of further problems due to higher concentrations of certain ions is increased.

One example is under-deposit corrosion (i.e., corrosion occurring under the sludge or any deposit) where a localized high concentration of chloride at the base of boiler tubes leads to pitting of the tubes. Similarly, hydroxyl (e.g., NaOH) buildup can promote caustic attack of the boiler tubes.

Any scale on boiler tubes reduces heat transfer efficiency and therefore forces heat transport system temperature upwards. Large deposits on the tube support plates of the boilers may also cause problems with boiler level control.

Particles entrained in the boiler water contribute to erosion of components and can also settle out form deposits that present sites for under-deposit corrosion.

Any of the above forms of corrosion or erosion can cause shortened boiler tube life, leading to heat transport leaks into the boiler if through wall corrosion occurs.

5.3 Methods to control the purity of water

5.3.1 Blowdown
Blowdown is the method employed to maintain boiler water impurity levels within chemical specification. In this procedure, a portion of the boiler water is discharged to the condenser circulating water (CCW) outfall, and the fluid level in the system is restored using high purity makeup. Although this process also removes some suspended solids, it is not an efficient method for reducing the suspended solids content of the boiler.

The use of blowdown reduces scaling on boiler tubes and the concentration of undesirable ions in tubesheet deposits by removing dissolved solids, and at the same time helps reduce tubesheet deposit buildup by removing some suspended solids.

5.3.2 Makeup water quality monitoring
The traces of non-volatile impurities, e.g., Ca^{++}, CI^-, SO_4^-, in makeup water are almost all ionic. Therefore conductivity measurements, which reflect total dissolved ion content, provide an accurate indication of overall purity, except for sodium and silica which are monitored by on-line analysis.

Direct pH measurement of the very low conductivity makeup water is not used because of its inherent inaccuracy in the essentially non-ionized water. Recall that pH measurements respond only on $[H^+]$ ions.

Sodium and silica have individual specifications because:
- They are the most likely species to break through ion exchange resins.
- The sodium specification is so low that it can be exceeded without causing the conductivity specification to be exceeded.
- Silica is ionized only slightly, thus imparting very little conductivity to the water.

5.4 Chemical control parameters
Figure 5.8 provides an overview of the control and monitoring of the secondary heat transport system, and shows that:
- dissolved oxygen is reduced by the deaerator and by the addition of hydrazine,
- pH is controlled by adding ammonia or morpholine downstream from the CEP discharge,
- dissolved an suspended solids are reduced by blowdown,
- cation conductivity, oxygen, hydrazine, pH and sodium analyzers provide on-line monitoring information that is also verified by the analysis of periodic grab samples.

Figure 5.8:

Condensate, feedwater and boiler system chemical control
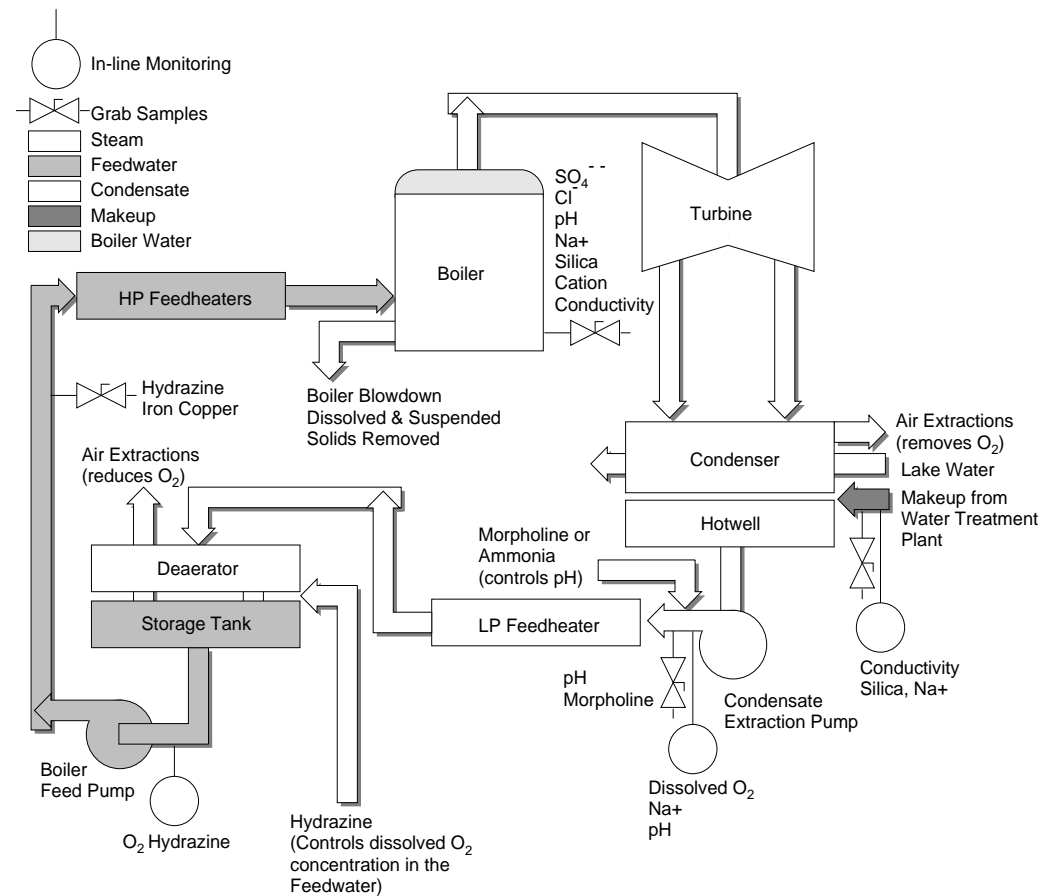
5.4.1   Boiler Water pH Control

The pH of the water is controlled via chemical additions downstream of the CEP discharge. On-line pH measurements are made in this area, prior to the LP feedheaters. Thus boiler water pH is controlled by maintaining the feedwater at the correct pH. Although the value of the desired operating pH depends on the materials used in the vessels and piping, it is always alkaline.

In the newer Ontario-Hydro CANDU stations, e.g., BNGS-B and DNGS-A, the condenser and feedheater tubes are made of stainless steel, and the piping and most other components are of carbon steel. Thus the steam/feedwater system is essentially "all-ferrous". In the older station, e.g., PNGS and BNGS-A, copper alloy tubing is used in the condensers and feedheaters, while carbon steel piping and components are used elsewhere. This mix of materials creates a chemical control problem in that the optimum pH for copper alloys is 6 - 9, whereas for carbon steel it is 10 - 12. Therefore the chemical control of copper/ferrous systems differs from that of all-ferrous systems.

Copper/Ferrous Systems

For those stations with mixed copper/ferrous materials, a compromise is required and the desired condensate pH is 9.1. The pH is controlled using the amine morpholine (C_4H_9NO). This pH is the best compromise for protection of both metals in the system. While more alkaline conditions would be better for both the iron and the magnetite on the ferrous piping, the higher alkalinity would be harmful to the copper alloy condenser and feedheater tubes. Maintaining the above desired condensate pH keeps the boiler water pH at the desired value of 9.1.

The use of ammonia is undesirable because it promotes the oxidation of copper and zinc when oxygen is present.

All-Ferrous Systems

The desired condensate pH is 9.8. The pH is maintained at station with all-ferrous feed trains by the addition of ammonia. The use of morpholine has been demonstrated to result in reduced corrosion product transport in the feedwater, and reduced erosion/corrosion in two phase (wet steam) regions. For this reason morpholine use is also specified at the stations with all-ferrous feed trains. It is not intended that morpholine will be used to maintain the pH, although it will certainly contribute. Both additives are volatile and thus impart alkalinity to the condensate. Maintaining the above desired condensate pH keeps the boiler water pH at the desired value of 9.6.

Figure 5.9:

Steam generator pH limits during normal operations
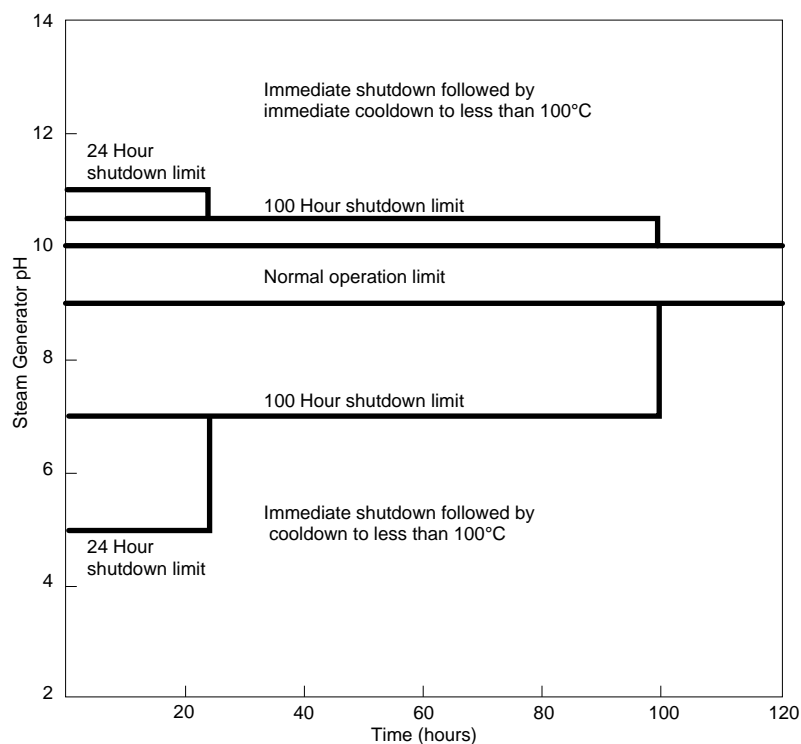
5.4.2 Boiler Water Cation Conductivity

Boiler water has a high background conductivity ($K°$) because of pH additives (morpholine, ammonia) and traces of water salts and dissolved corrosion products. Hence, ordinary (specific) conductivity is not sensitive enough to be used as a control parameter. Therefore a sample of boiler water is passed through a cation exchange column, which replaces all cations (including those of morpholine, ammonia and hydrazine) with the much more conductive H^+ ion. Also, the conductive hydroxides formed by the morpholine or ammonia have been replaced by non-conductive water. This heightens the sensitivity for the presence of anions (normally Cl^- and/or SO_4^{--}, because HCl and H_2SO_4 are more conductive than any other salts. The conductivity of a sample thus treated is called cation conductivity. The desired cation conductivity specification for boiler water is less than 0.3 mS/m.

The use of very low conductivity makeup water from the WTP is a major factor in maintaining a low conductivity of the boiler water. Continuous blowdown controls the boiler water conductivity by constantly removing impurities from the system. Cation conductivity of the boiler water is monitored by continuous analysis, with grab sample verification, and is a shutdown control parameter. Maintaining cation conductivity within the specification limits protects against boiler tube corrosion.

5.4.3 Dissolved Oxygen

Because oxygen is a strong oxidizer, dissolved O_2 is the most harmful impurity in system. The desired concentration of dissolved O_2 are less or equal to 10 µg/kg for the condensate and less or equal to 5 µg/kg for the feedwater.

Dissolved oxygen control is achieved in three stages following the condenser air extraction system. Since the main source of oxygen is from air leaking into sub-atmospheric parts of the turbine/condenser/extraction steam lines, a program to locate and seal air in-leakage is a major control factor.

Dissolved oxygen is removed from the condensate by the deaerator which contains sprays and cascade trays over which the hot water tumbles. The combination of heat and large surface area imparted to the water provides very efficient stripping of dissolved gases. Oxygen is reduced to less than 10 µg/kg and nitrogen is also removed. This efficient stripping action reduces the consumption of hydrazine.

The final stage of dissolved oxygen removal is by the injection of hydrazine, (N_2H_4), between the deaerator and the deaerator storage tank, to chemically react with the remaining oxygen. It is injected at this point to:
- provide adequate temperature for reaction,
- provide hold up time in the deaerator storage tank and
- ensure it will not be removed by the deaerator.

The chemical reaction is:

$$O_2 + N_2H_4 \rightarrow N_2 + 2H_2O$$
$$\text{Hydrazine}$$
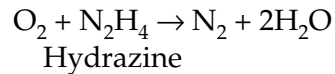
The nitrogen formed is non-corrosive.

A modest excess of hydrazine is required to control the dissolved O_2 concentration of the boiler feedwater to $\leq 5\ \mu g/kg$. This excess will gradually cause a slight pH elevation owing to ammonia (NH_3) formation from hydrazine decomposition. In ferrous-brass tubed systems the excess must be closely controlled to prevent copper dissolution.

Table 5.2:

Chemical control parameters of the secondary heat transport system

| System	On-Line Monitoring	Grab Sample Analysis
WTP (product)	Conductivity Na+, Silica	
Secondary Heat Transport System - Condensate	Dissolved O_2, Na^+, pH	Morpholine, Ammonia
Secondary Heat Transport System - Feedwater	Dissolved O_2, Hydrazine	Iron, Copper
Secondary Heat Transport System - Boiler water		Cation conductivity, Tritium, Silica, Na^+, Cl^-, SO_4^{--}, pH

6   Auxiliary Systems

6.1   Annulus gas system

The objectives of the chemical control of the carbon dioxide filled annulus gas system are:
- To minimize corrosion of the materials of construction.
- To maintain a deuterium impermeable oxide layer on the outer surface of pressure tubes.
- To prevent the development of high radiation fields, or high concentrations of undesirable radionuclides.
- To detect the in-leakage of D_2O from either the heat transport system or the moderator system.
- To minimize the production of condensible organic materials.

Figure 6.1:

Annulus gas system
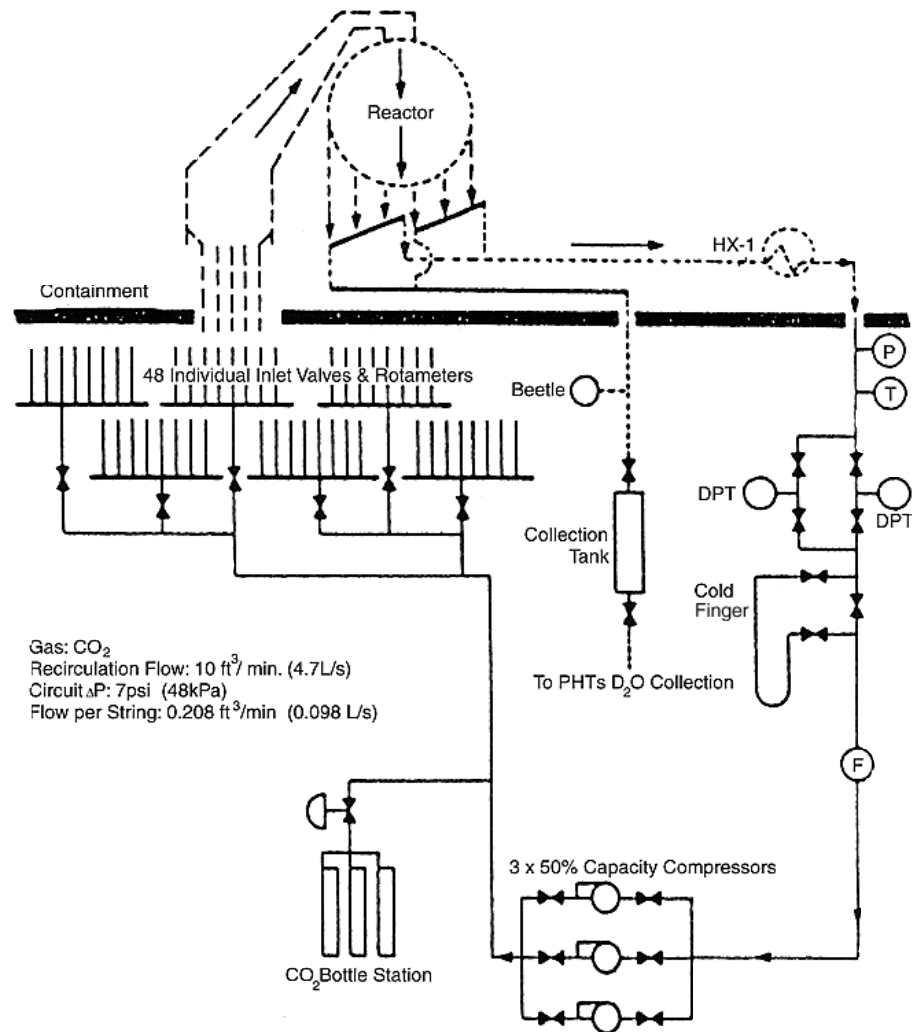
6.1.1   Corrosion control

The corrosion of the construction materials is minimized by:

• Reducing to a minimum the concentration of impurities in the annulus gas which, in the radiation flux, could form compounds that are corrosive.

For example, moist air may form nitric acid which is very corrosive towards Inconel. The presence of such impurities is controlled by the early detection of air in-leakage and by purging with fresh carbon dioxide when necessary.

At the same time a low oxygen concentration is to be maintained in the annular gas. The oxygen must be present to maintain and replenish the oxide layer on the outside of the pressure tube. Oxygen may be added to maintain 0.5 to 5%.

It has been found that the normal low impurity level in the carbon dioxide

provides oxygen. Normal concentrations are 0.01 to 0.1%.
- Maintaining a low system moisture content; higher than specified maximum moisture levels may enhance the formation of nitric acid and the consequent corrosion.

6.1.2   Maintaining an oxide layer

Analysis of pressure tubes from Pickering A, where nitrogen was the annulus gas, indicated that some of the deuterium present in the pressure tubes had entered from the annulus gas system. The deuterium gets into the annulus gas system by diffusion through the end fittings. Pressure tube surface oxide measurements have indicated that the regions of high deuterium coincided with imperfections in the oxide layer on the outer surface of the pressure tubes.

6.1.3   Radiation fields control

Any air in-leakage will carry argon into the system. On activation Ar-41 will form. Control is achieved by early detection of air in-leakage and carbon dioxide purging. Note also that the use of carbon dioxide instead of nitrogen as the annulus gas essentially eliminates the production of carbon-14 in the fuel channel annuli.

Table 6.1:
Chemical specifications for the annulus gas system

Parameter	Sampling Point	Sampling Frequency	Permissible Range (Desired Value)	Action Limits Time	Corrective Actions	Notes
Oxygen	Calandria outlet	1/week or as required (see note 1)	0.5 to 5% (0.5 to 2%)	≥ 0.1% 8 hrs.	1. Resample and repeat analysis 2. Purge by fresh CO_2 at a rate of 4.7 L/sec (10 scfm) if the result is confirmed.	1. More frequent analyses are required if air ingress is suspected or if high Ar-41 fields occur. 2. Analytical method if unable to distinguish between H_2 and D_2. High D_2 may cause hydriding of Zircaloy-2 calandria tubes. Penalty: Corrosion of system and possible hydriding of zircaloy-2 calandria tubes. 3. If moisture content shows a consistent tendency to rise: a. Check H-3 level of system. If consistently high over several samples, purge system at the maximum rate 7.0 L.s (15 scfm) continuously. b. Estimate the D_2O leakage rate. c. If necessary, the source of D_2O leakage can be located by a temperature scan of the tubing at the reactor face after shutdown.
Deuterium	Calandria outlet	1/week or as required (see note 1)	< 0.1% (see note 2)	≥ 0.1% 8 hrs.	1. Resample and repeat analysis. 2. Purge by fresh CO_2 at a rate of 4.7 L/sec (10 scfm) if the result is confirmed.	
Moisture	Calandria outlet	1/week or as required	Dewpoint < 0°C	> 0°C 8 hrs.	1. Resample and confirm analysis 2. Purge by fresh CO_2 at a rate of 4.7 L/sec (10 scfm) if the result is confirmed. See note 3)	
Tritium	Calandria outlet	1/week or as required				

6.1.4   D$_2$O in-leakage controls

Such in-leakage would be costly and dangerous, and it must be detected at a very early stage. Normal moisture analysis should indicate such in-leakage from the consequent rise in moisture and tritium levels.

### 6.1.5   Production of condensible organics

Although there are several suggested sources for these materials, it is generally agreed that the presence of 0.5 to 2.0 vol. percent of oxygen in the annulus gas will prevent their formation.

6.2   Recirculated service water

The system is filled with demineralized water from the make-up water treatment plant and it is dosed with a strong base (such as lithium hydroxide) and hydrazine. The design intent is to maintain a pH of above 10 when measured at 25°C and to maintain a hydrazine concentration which is at least twice the dissolved oxygen concentration. The initial hydrazine concentration should therefore be at least 25 mg N$_2$H$_2$/kg H$_2$O.

Figure 6.2:

Circulating water, Raw service water and recirculated water
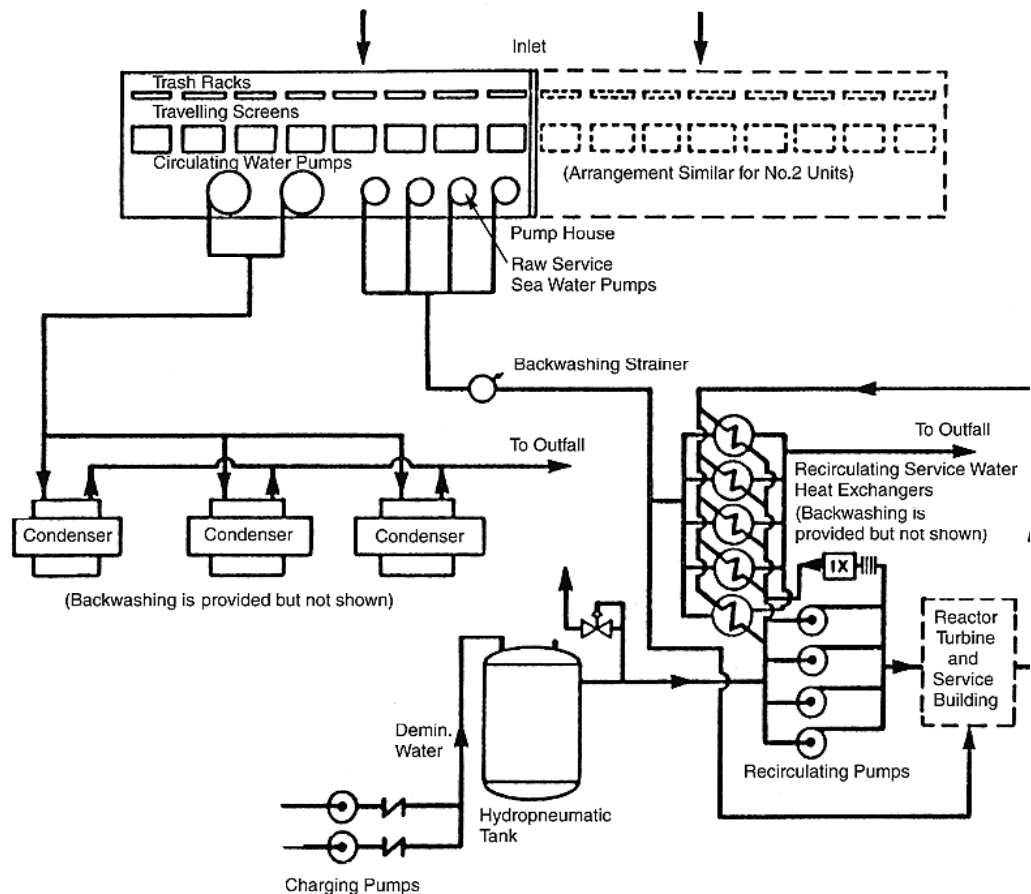
7   Glossary of Chemical Terminology

Acid   A compound which either contains $[H^+]$ ions or will produce $[H^+]$ ions when dissolved in water.

Activation   The conversion of a substance into a radioactive substance through neutron bombardment.

Adsorption   The process of being attracted and adhering to a surface.

Aerobic   Able to live or grow only where free oxygen is present.

Anaerobic   Able to live or grow where there is no free oxygen present.

Anion   An ion (having a negative charge) that migrates through the electrolyte toward the anode under a potential gradient.

Anode   The positive electrode in an electro-chemical cell, where oxidation or corrosion occurs. Metal ions enter solution and electrons flow away from the anode in the external circuit.

Base   A compound which either contains $[OH^+]$ ions or will produce $[OH^-]$ ions when dissolved in water.

Blowdown   The process of removing water from the lower area of a boiler while allowing its replacement with clean makeup water. This serves to remove dissolved and suspended impurities which accumulate in the boiler water.

Cathode   The negative electrode in an electro-chemical cell, where reduction occurs. Electrons are released from the cathode to the substance being reduced.

Cathodic protection   Preventing corrosion of a component by deliberately making it the cathode in an electrolytic cell.

Cation   An ion (having a positive charge) that migrates through the electrolyte toward the cathode under a potential gradient.

Compound   A substance containing only one type of molecule and at least two elements.

Conductivity The ability to transmit or conduct electric current. (In chemistry this normally refers to WATER in a process system).

Corrosion	The process of metal wastage or oxidation produced by chemical action.
Covalent bond	A linkage between two atoms produced by sharing electron pair(s) orbiting both atoms.
Covalent molecule	A molecule in which atoms are bonded together by shared pairs of electrons.
Crud	Undissolved solids in a water system, usually on the primary (D_2O) side.
Dedeuteration	Recovering D^+, OD^- and D_2O from a spent or saturated ion exchange column resin.
Deuterium	The isotope of hydrogen containing one neutron in the nucleus (symbol D).
D^+	A deuterium ion.
$D\bullet$	A free radical of deuterium.
D_2O	Heavy water (deuterium oxide).
Deuteration	Replacing $[H^+]$, $[OH^-]$ and H_2O in new ion exchange resins with $[D^+]$, $[OD^-]$ and D_2O, in preparation for service in a heavy water system.
Electrochemical cell	A general term applied to cells of both the galvanic and electrolytic type.
Electrolyte	A liquid containing ions, and thus able to allow electric current to flow through it.
Electrolytic cell	A device which used electric current to produce a chemical reaction.
Element	A substance consisting of atoms of one type only.
Erosion	The wastage or wearing away of a surface by the abrasive action of moving fluids. Erosion is usually accelerated by solid particles in suspension.
Fe_2O_3	Rust (Hematite) - a porous form of iron oxide.

Fe_3O_4	Magnetite - a relatively impervious form of iron oxide.
Free radical	A group of atoms containing an unpaired electron. Very reactive.
Galvanic cell	A device which employs a chemical reaction to produce an electric current.
H^+	A hydrogen ion.
$H\bullet$	A free radical of hydrogen.
Heterogeneous	Refers to a mixture containing different components, visually distinguishable from each other.
Homogeneous	Refers to a substance or solution having the same composition throughout; there is no visible distinction between components.
Inverse Solubility	The solubility of the solute in the solvent decreases as the solvent temperature rises.
Ion	An atom or molecule possessing a charge.
Isotopes	Atoms of the same element which differ only in the number of neutrons they contain.
Magnetite	A chemical compound ($F3_3O_4$) produced on the inner surfaces of the carbon steel piping of the HTS system to protect the metal from corrosion.
Molecule	The smallest particle of a compound or polyatomic element that can exist in a free state and still retain the characteristics of the element or compound.
Non-volatile	Does not evaporate or vaporize.
OD^-	A deuteroxyl ion (deuteroxide).
$\bullet OD$	A deuteroxyl free radical.
OH-	A hydroxyl ion (hydroxide).
$\bullet OH$	A hydroxyl free radical.

Oxidation	The loss of electron(s) by an atom or group of atoms.
Oxidation potential	A measure in volts of the tendency of an atom to lose (an) electron(s).
pH	A scale for expressing the acidity of alkalinity of a liquid.
Polymer	A substance made up of very large molecules containing recurring units.
Products	The substances produced during a chemical reaction.
Radical	An atom of group of atoms containing an unpaired electron (Radicals are very reactive).
Radioactive	Emitting radiant energy in the form of particles or rays as alpha, beta or gamma rays by unstable atomic nuclei.
Radiolysis	The decomposition of a substance by radiation.
Radiolytes	The radiolytic fragments formed when a substance is decomposed by radiolysis.
Reduction	The gain of electron(s) by an atom or group of atoms.
Scale	Undissolved solids which have plated out onto metal surfaces in a non-active water system.
Silica	Technically silica is silicon dioxide, SiO_2. In power plants, "silica" refers to the silicon-containing species found in raw water. These include free or "reactive" silica (hydrated silica, $SiO_2 \bullet nH_2O$), and unreactive silicates, particularly of calcium and magnesium. Silica in raw water may be dissolved (mostly reactive) or suspended (mostly silicates).
Solubility	A measure of the amount of a substance which will dissolve in a given amount of solvent.
Solute	A substance which is dissolved in a solvent.
Solvent	The liquid in which a solute is dissolved.
Tritium	The radioactive isotope of hydrogen. It contains two neutrons in its nucleus.
Volatile	Evaporates or vaporizes readily.